



CVR JOURNAL OF SCIENCE AND TECHNOLOGY

Vol.No. 23, December 2022
P-ISSN 2277 - 3916

DOI 10.32377/CVRJST23
E-ISSN 2581 - 7957



CVR COLLEGE OF ENGINEERING
In Pursuit of Excellence

PATRONS

Dr. Raghava V. Cherabuddi, President & Chairman

Dr. K. Rama Sastri, Director

Dr. K. Ramamohan Reddy, Principal

Editor : **Dr. K. Lal Kishore, Professor and Dean - Research, CVRCE**

Associate Editor : **Dr. S. Venkateshwarlu, Professor & Head, Dept. of EEE, CVRCE**

Technical support : **Mr. K. Veeranjanyulu, Asst. Prof., Dept. of CSE, CVRCE**

Editorial Board :

Dr. M.V. Seshagiri Rao Professor & Dean-Planning & Coordination, CVRCE

Prof. L.C. Siva Reddy Professor & Vice-Principal, CVRCE

Dr. K.S. Nayanathara Professor & Dean-Academics, CVRCE

Dr. T. Muralidhara Rao Professor & Head, Dept. of Civil Engg., CVRCE

Dr. A. Vani Vathsala Professor & Head, Dept. of CSE, CVRCE

Dr. K. Lalithendra Professor & Head, Dept. of ECE, CVRCE

Dr. S. Harivardhagini Professor & Head, Dept. of EIE, CVRCE

Dr. Bipin Bihari Jayasingh Professor & Head, Dept. of IT, CVRCE

Dr. M. Venkata Ramana Professor & Head, Dept. of Mech. Engg., CVRCE

Dr. H.N. Lakshmi Professor & Head, Dept. of ET, CVRCE

Dr. G. Bikshamaiah Professor & Head, Dept. of H&S, CVRCE

International Review Board:

Prof. Tzung-Pei Hong Chair Professor, Dept. of CSI Engg., AI Research Center National University of Kaohsiung 811, Taiwan

Dr. Tomonobu Senjyu Professor, Department of Electrical Engineering, University of the Ryukyus, Nishihara-cho, Nakagami Okinawa, Japan

Dr. Masoud Mohammadian Assoc. Professor, Faculty of Science and Technology, University of Canberra, Australia

Dr. Rubén Ruiz García Full Professor, Head of the Applied Optimization Systems Group, Department of Applied Statistics, Universitat Politècnica de València, Camino de Vera, Spain

Dr. Ray-Hwa Wong Professor, Department of Mech. Engg., Hwa-Hsia University of Technology, Taipei, Taiwan

Dr. Stefan Talu Faculty of Mech. Engineering, DMCDI, The Technical University of Cluj-Napoca, B-dul Muncii Street, No. 103-105, Cluj-Napoca, 400641, Romania

Assoc. Prof. Ir. Dr. Norhaliza Abdul Wahab Director, Control & Mechatronics Engg. Dept., Faculty of Electrical Engineering, UTM Skudai 81310 Johor

Dr. R. Venkata Rao Professor, Department of Mech Engg., Sardar Vallabhbhai National Institute of Technology (SVNIT), Surat, Gujarat State – 395 007, India

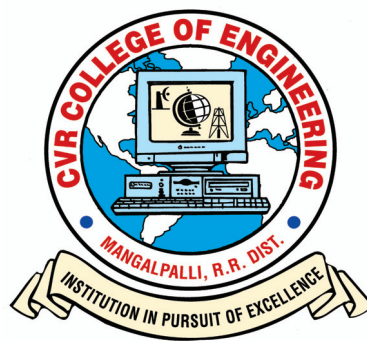
Dr. Vijay Janyani Professor Dept. of ECE, Malaviya National Institute of Technology (MNIT), Jaipur - 302017 (Rajasthan)

Dr. V. Prasanna Venkatesan Prof. & Head, Department of Banking Technology, School of Management, R.V.Nagar, Kalapet, Pondicherry University, Puducherry

CVR JOURNAL OF SCIENCE AND TECHNOLOGY

Indexed by

- Google Scholar
- Directory of Research Journals Indexing (DRJI)
- Scientific Indexing Services (SIS)
- International Institute of Organised Research (I2OR)
- Scholar Impact - Journal Index
- Citefactor
- Member Crossref / DOI



Accredited by **NAAC** with '**A**' **GRADE**

CVR COLLEGE OF ENGINEERING

(UGC Autonomous - Affiliated to JNTU Hyderabad)

Mangalpalli (V), Ibrahimpatnam (M),

R.R. District, Telangana. – 501510

<http://cvr.ac.in>

EDITORIAL

It is with immense pleasure that the editorial team of Biannual CVR Journal of Science and Technology is bringing this Volume 23, once again in time. Editorial team thanks all the authors, reviewers and DTP operators involved in this work. It takes almost 6 months to complete this task and bring out the Journal.

We are taking care to see that standard practices are followed in the publication of the Journal. Blind review is done, and number of iterations are done till the reviewers are fully satisfied with the standard of the research paper. Senior faculty of English language Department, take care of the language issues. Template verification and typographical errors are checked before the articles go for publishing. Hope the researchers appreciate this effort. Many research articles published in the journal are being referred by other researchers across the globe, as indicated by DOI, crossref data.

This Volume covers research articles in the following disciplines:

EIE-1, CIVIL- 4, ECE-8, CSE-1, CSIT-2, IT- 3, MECH- 5, H & S(Chemistry)-1.

Students are being encouraged to publish research papers based on the project works done by them. Project works have such importance in the academic curriculum. P.G. students spend almost one year on the project work. So, this should result in a significant work suitable for publication in a journal. Project supervisors guiding the students must give research orientation for the work of the students. Selected research papers of U.G. students are published in this volume. It is heartening to see that U.G. students are also showing enthusiasm to publish papers. Three such papers are published in this volume- Hope this trend will continue.

In this issue an interesting article on FPGA Design of ECG-SoC System for the Analysis of ECG signals is presented. The author has employed Hardware-Software Co-design methodology. The strategy reported in the paper is expected to reduce the cost of medical care in rural areas. Another article is on Breast Cancer. It is one of the dreaded diseases causing many deaths all over the world. In the present available techniques, radiologists find it difficult to make accurate assessment from the images due to small size and low contrast. UG students and their supervisors have done a project to propose a system to clarify on an IDC data set, that can accurately classify histology image, as benign or malignant, using Artificial Intelligence.

Another paper based on UG Students Project work is a Solar Powered Weather Station using IoT. A machine learning model to predict weather conditions in the villages surrounding the college is developed and presented in the paper for accurate weather forecast. Another interesting article is on IoT based farm management system to maximise agricultural production.

I am thankful to all the members of the Editorial Board for their help in reviewing and short listing the research papers for inclusion in the current Volume of the journal. I wish to thank **Dr. S. Venkateshwarlu, HOD, EEE** for the effort made in bringing out this Volume. Thanks are due to **HOD, H & S, Dr. G. Bhikshamaiah** and the staff of English Department for reviewing the papers. I am also thankful to **Smt. A. Sreedevi, DTP Operator** in the Office of Dean Research for the preparation of research papers in Camera - Ready form.

For further clarity on waveforms, graphs, circuit diagrams and figures, readers are requested to browse the soft copy of the journal, available on the college website www.cvr.ac.in wherein a link is provided. Authors can also submit their papers through our online open journal system (OJS) www.ojs.cvr.ac.in or www.cvr.ac.in/ojs

Prof. K. Lal Kishore
Editor

Patrons:

Dr. Raghava V. Cherabuddi
President & Chairman
CVR College of Engineering,
Vastunagar, Mangalpalli (V),
Ibrahimpattnam (M)
Rangareddy (D),
Telangana 501 510.
E-mail: drcvraghava@gmail.com
Phone: 040-42204001, 02,03

Dr. K. Rama Sastri
Director
CVR College of Engineering,
Vastunagar, Mangalpalli (V),
Ibrahimpattnam (M)
Rangareddy (D), Telangana 501 510.
E-mail: director@cvr.ac.in
Phone: 08414-661666, 661601,661675

Dr. K. Ramamohan Reddy
Principal
CVR College of Engineering,
Vastunagar, Mangalpalli (V), Ibrahimpattnam (M)
Rangareddy (D), Telangana 501 510.
E-mail: principal@cvr.ac.in
Phone: 08414-661602, 661601,661675

Editor:

Dr. K. Lal Kishore
Professor and Dean Research
CVR College of Engineering
Vastunagar, Mangalpalli (V),
Ibrahimpattnam (M)
Rangareddy (D), Telangana 501
510.
E-mail: lalkishorek@gmail.com
lalkishore@cvr.ac.in
Mobile: +91 8309105423 , +91
9618023478
Phone: 08414-661658,
661601,661675

Associate Editor:

Dr. S. Venkateshwarlu
Professor & Head
Dept of Electrical and Electronics
Engineering
CVR College of Engineering
Vastunagar, Mangalpalli (V),
Ibrahimpattnam (M)
Rangareddy (D), Telangana 501 510.
E-mail: svip123@gmail.com
hod.eee@cvr.ac.in
Mobile: +91 9490749568
Phone: 08414-661661

Technical support:

Mr. K. Veeranjanyulu
Asst. Prof.
Dept. of Computer Science & Engineering
CVR College of Engineering
Vastunagar, Mangalpalli (V), Ibrahimpattnam (M)
Rangareddy (D),
Telangana 501 510.
E-mail: kveeru876@gmail.com
Mobile: +91 9177462507

Editorial Board:

Dr. M.V. Seshagiri Rao
Professor & Dean-Planning &
Coordination
CVR College of Engineering
Vastunagar, Mangalpalli (V),
Ibrahimpattnam (M)
Rangareddy (D),
Telangana 501 510.
E-mail:
rao_vs_meduri@yahoo.com
sheshagiri.rao@cvr.ac.in
Mobile: +91 9440361817
Phone:08414-661617

Prof. L.C. Siva Reddy
Professor & Vice-Principal
CVR College of Engineering
Vastunagar, Mangalpalli (V),
Ibrahimpattnam (M)
Rangareddy (D),
Telangana 501 510.
E-mail: siva_reddy@cvr.ac.in
Mobile: +91 9885806151
Phone:08414-661656

Dr. K.S. Nayanathara
Professor & Dean-Academics
CVR College of Engineering
Vastunagar, Mangalpalli (V),
Ibrahimpattnam (M)
Rangareddy (D),
Telangana 501 510.
E-mail:
ksattirajunayanathara@gmail.
com
Mobile: +91 9502335871
Phone:08414-661667

Dr. T. Muralidhara Rao
Professor & Head
Dept. of Civil Engineering
CVR College of Engineering
Vastunagar, Mangalpalli (V),
Ibrahimpattnam (M)
Rangareddy (D),
Telangana 501 510.
E-mail:
tmuralidhararao@gmail.com
tmuralidhararao@cvr.ac.in
Mobile: +91 9989214274
Phone:08414-661655

Dr. A. Vani Vathsala
Professor & Head
Dept. of Computer Science &
Engineering
CVR College of Engineering
Vastunagar, Mangalpalli (V),
Ibrahimpattnam (M)
Rangareddy (D),
Telangana 501 510.
E-mail: atlurivv@yahoo.com
vani_vathsala@cvr.ac.in
Mobile: +91 9866586106
Phone:08414-661697

Dr. K. Lalithendra
Professor & Head
Dept. of Electronics and
Communication Engineering
CVR College of Engineering
Vastunagar, Mangalpalli (V),
Ibrahimpattnam (M)
Rangareddy (D),
Telangana 501 510.
E-mail: lkurra@gmail.com
lalithendra@cvr.ac.in
Mobile: +91 9871483379
Phone:08414-661660

Dr. S. Harivardhagini
Professor & Head
Dept of Electronics and
Instrumentation Engineering
CVR College of Engineering
Vastunagar, Mangalpalli (V),
Ibrahimpattnam (M)
Rangareddy (D),
Telangana 501 510.
E-mail:
Harivardhagini@gmail.com
Mobile: +91 9985147962
Phone:08414-661653

Dr. Bipin Bihari Jayasingh
Professor & Head
Dept. of Information Technology
CVR College of Engineering
Vastunagar, Mangalpalli (V),
Ibrahimpattnam (M)
Rangareddy (D),
Telangana 501 510.
E-mail:
bipinbjayasingh@cvr.ac.in
Mobile: +91 9440476544
Phone:08414-661664

Dr. M. Venkata Ramana
Professor & Head
Dept. of Mechanical Engg
CVR College of Engineering
Vastunagar, Mangalpalli (V),
Ibrahimpattnam (M)
Rangareddy (D),
Telangana 501 510.
E-mail:
vramanamaringanti@cvr.ac.in
Mobile: +91 9948084192
Phone:08414-661689

Dr. H. N. Lakshmi
Professor & Head
Dept. of Emerging Technology
CVR College of Engineering
Vastunagar, Mangalpalli (V),
Ibrahimpattnam (M)
Rangareddy (D),
Telangana 501 510.
E-mail: hn.lakshmi@cvr.ac.in
Mobile: +91 9849698045

Dr. G. Bikshamaiah
Professor & Head
Dept. of Humanities and
Science
CVR College of Engineering
Vastunagar, Mangalpalli (V),
Ibrahimpattnam (M)
Rangareddy (D),
Telangana 501 510
E-mail: gbcvr17@gmail.com
hod.hns@cvr.ac.in
Mobile: +91 9949565350
Phone:08414-661631

International Review Board:

Prof. Tzung-Pei Hong

Chair Professor
Department of Computer
Science and Information
Engineering
AI Research Center
National University of
Kaohsiung
No. 700, Kaohsiung University
Road, Nan-Tzu District
Kaohsiung 811, Taiwan
Tel:(07)5919191, 5919398
Fax:(07)5919049
Email: tphong@nuk.edu.tw
Website: tphong.nuk.edu.tw

Dr. Tomonobu Senjyu

Professor
Department of Electrical
Engineering
University of the Ryukyus,
Nishihara-cho,
Nakagami Okinawa, Japan
Tel:(+81-98-895-8686)
Email: b985542@tec.u-
ryukyuu.ac.jp

Dr. Masoud Mohammadian

Associate Professor
Faculty of Science and
Technology
University of Canberra ACT
2601
Phone: +61 (0)2 6201 2917
Fax: +61 (0)2 6201 5231
Email:masoud.mohammadian
@canberra.edu.au
Website:https://research
profiles.canberra.edu.au/en/p
ersons/masoud-mohammadian

Dr. Rubén Ruiz García

Full Professor. Head of the
Applied Optimization Systems
Group
Department of Applied Statistics,
Operations Research and Quality
Universitat Politècnica de
València
Camino de Vera s/n, Edificio 7A,
46022, Valencia, Spain
rruiz@eio.upv.es
http://soa.iti.es/rruiz

Dr. Ray-Hwa Wong

Professor
Department of Mechanical Eng.,
Hwa-Hsia University of Technology, Taiwan,
111 Gong Jhuan Rd., Chung Ho,
Taipei, Taiwan, R.O.C.
E-mail : rhwong@cc.hwh.edu.tw
Phone / Mobile Number : +886-2-8941-5129
ex 2108/+886-918-706-985

Dr. Stefan Talu

DMCDI
The Technical University of Cluj-Napoca
Faculty of Mechanical Engineering,
B-dul Muncii Street, No. 103-105, Cluj-
Napoca, 400641,
Romania
http://research.utcluj.ro.
E-mail(uri) stefanta@mail.utcluj.ro,
stefan_talu@yahoo.com
Telephone(s) Fixed line phone:
004 0264 401 200.
Mobile phone: 004 0744263660

Assoc. Prof. Ir. Dr Norhaliza Abdul Wahab

Director,
Control & Mechatronics Engineering
Department
Faculty of Electrical Engineering
UTM Skudai 81310 Johor
Malaysia
Phone: +607-5557023, 012-5444297 (HP)
Email: aliza@fke.utm.my
URL: http://norhaliza.fke.utm.my/

Dr. R. Venkata Rao

Professor, Department of Mechanical
Engineering
Sardar Vallabhbhai National Institute of
Technology (SVNIT), Surat
Ichchanath, Surat, Gujarat State – 395 007,
India,
Contact Nos.: 02612201982(O),
02612201661(R), 9925207027(M)
Email ID: ravipudirao@gmail.com,
rvr@med.svnit.ac.in
Website:
http://svnit.ac.in/facup/5274Rao-
Resume.pdf

Dr. Vijay Janyani

Professor
Dept. of Electronics and Communication
Engineering
Malaviya National Institute of
Technology (MNIT)
Jaipur - 302017 (Rajasthan)
India.
www.mnit.ac.in
Email ID: vijay.janyani@ieee.org

Dr. V. Prasanna Venkatesan

Prof. & Head
Department of Banking Technology,
School of Management, R.V.Nagar,
Kalapet, Pondicherry University,
Puducherry – 605014,
India. Telephone No: 0413 - 2654 652
Mobile No: 0091-9486199939
Email: prasanna.btm@pondiuni.edu.in,
prasanna_v@yahoo.com

1. FPGA Design of ECG-SoC System for the Analysis of ECG Applicable for Rural Health Care Centers <i>Dr. Narendra B Mustare</i>	01
2. Strength and Durability Studies on Lightweight Self-Compacting Concrete Partially Replacing Coarse Aggregate with Sintered Fly Ash Aggregate <i>K. Raju, N. Ramanjaneyulu, Dr. M.V. Seshagiri Rao</i>	07
3. A Study on Dynamic Response of High-Rise Buildings using Lead Rubber Bearing Isolator <i>S. Mallikarjun, A. Shruthi</i>	14
4. Travel Time and Congestion Analysis of Heterogeneous Traffic Condition, a Case Study on Kothapet Signal to Nalgonda X-Road Signal Road <i>Kona Mahesh, Gunda Sharanya, P. Yashwanth</i>	21
5. Anaerobic Co-Digestion of Tomato Waste to Enhance the Production of Methane gas <i>Srikanth Merugu, K. Ravi Chandra Reddy</i>	24
6. Lateration-Specific Localization Algorithm for Wireless Sensor Networks <i>Dr. Gaurav Sharma</i>	31
7. Hyper-Parameter Optimization using Metaheuristic Algorithms <i>D. Bhanu Prakash, K. Arun Kumar, R. Prakash Kumar</i>	37
8. A Weighted Pseudorandom Test Pattern Generator for a Built In Self Test Architecture <i>Vadde Sathvika, Chalam Tirunagari, Dr. P. Anil Kumar</i>	44
9. Breast Cancer Classification using Convolutional Neural Networks (CNNs) <i>Racha Ganesh, Vedanvita.G, Vyshnavi .B, Samreen. S</i>	52
10. Advanced Coal Mine Safety Monitoring and Auto Alert system using LoRa Technology <i>N. Lakshmi pathi, Dr. Amit Arora</i>	58
11. IoT Based Smart Power Management in Public Areas along with Public Traffic Monitoring <i>V. Shilpa, Dr. Humaira Nishat</i>	65
12. A Machine Learning Perspective for data analytics in Solar Powered Weather Station using IoT <i>Dr. S. Praveen Chakkravarthy, P. Bharath Chandra, D. Anwar Bash, G. Sai Kiran</i>	70
13. Smart Precision Interface for Conventional Agricultural Methods <i>Dr. S. Praveen Chakkravarthy, Gaddam Vivek, Kalakuntla Vishal, Sahithi Vangala, Juluri Sai Teja</i>	76
14. Trust-based Model to alleviate Selfish Node Attacks in MANETs <i>Dr. M. Deva Priya</i>	82
15. Augmented Corvus Search Optimization for Image Retrieval in Content Based Images <i>Dr. A. Srinivasa Reddy</i>	90
16. Automatic Aspect-Based Sentiment Analysis for Motor Vehicle Sales Forecasting <i>Dr. C. Raghavendra</i>	96
17. Deep Learning Model to Predict the Risk of Developing Diabetic Retinopathy <i>P. Prathyusha, A. Mallareddy, Dr. S. V. Suryanarayana</i>	100
18. Limitations of CNN-Model and Enhanced AI- Model for Driver Drowsiness Detection <i>S. Nikhila, V. Sidda Reddy</i>	106
19. Classification of COVID-19 and Pneumonia from Chest X-ray Images using Deep Learning Techniques <i>Talapaneni Jyothi, Dr. Bipin Bihari Jayasingh</i>	111
20. Comparative Analysis and Ranking of Selected Bio-Fuels <i>Dr. Manjeet Kharub</i>	120
21. Analysis of a Feasible Gate Location in Injection Mold for Plastic Cloth Peg: New Product Development <i>Neeraj Kumar Jha</i>	127
22. Mechanical Characterization and Evaluation of Effects of Epoxy in Lamination for Kevlar Composites <i>A. Suresh</i>	133
23. Modelling and Analysis of Domestic Windmill Turbine Blade <i>Mada Rukmini Sai Rupa Sri</i>	140
24. Modelling and Fabrication of Hexagonal Turret on Engine Lathe <i>K. L.N. Murthy</i>	145
25. Synthesis of New Benzothiazole Derivatives as Potential Antimicrobial Agents <i>Dr. Swapna Ponnampalli</i>	150
➤ Papers accepted for next issue (Vol. 24, June 2023)	155
• Appendix: Template of CVR Journal	157

FPGA Design of ECG-SoC System for the Analysis of ECG Applicable for Rural Health Care Centers

Narendra B Mustare

Professor, CVR College of Engineering/ EIE Department, Hyderabad, India

Email: drnamust@gmail.com

Abstract: Today, seventy percent of Indians still live in poor conditions in rural areas. Those who live in rural regions have fewer alternatives available to them in nursing care and medical diagnostics since there are only a few institutions equipped with modern medical technology. This situation reduces the number of choices available to them. As a direct consequence of lack of medical facilities, the rural residents do not find enough access to medical treatment. From this perspective, the use of cutting-edge technology to the treatment of their various health problems could prove to be advantageous. In this work, it is proposed that the design and implementation of an ECG-SoC system for the analysis of ECG is applicable to rural health care centers. This system is designed to meet the needs of rural communities. Electrocardiogram (ECG) pre-processing and heart rate variability (HRV) feature extraction are two of the numerous operations that it can do; both the features are appropriate for use in applications pertaining to remote health care. The ECG-SoC was developed by employing a technique known as hardware/software co-design, utilizing an offline dataset obtained from the MIT-BIH database. The design of the system prototype and the testing of the system's functionality both made use of an Altera Cyclone II DE2-115 FPGA platform. Both the processes were carried out to ensure the system's integrity. The results of the computation are shown on the Nios II-Linux terminal, and the task of creating output files for post-processing on the Nios II-Linux terminal appears on the personal computer that is serving as the host. The findings of this research indicate "that the ECG-SoC system developed is capable of performing power spectrum analysis in addition to compiling a raw ECG dataset, detecting QRS, computing R-R intervals, and presenting the FFT output". It is demonstrated that the system can perform these tasks. In addition to this, it can carry out all these activities at the same time. The strategy that has been outlined here will not only bring about a general reduction in the cost of receiving medical care in rural regions, but it will also bring about a lessening in the severity of cardiovascular diseases

Index Terms: Electrocardiography (ECG), ECG-SoC System, HRV Feature extraction, cardiovascular diseases

I. INTRODUCTION

According to the information that was gathered and compiled by the World Health Organization (WHO) in the year 2021, cardiovascular disease was the leading cause of death, accounting for almost 68% of all fatalities [1]. It is estimated that coronary heart disease caused 8.3 million fatalities, whereas strokes caused 7.2 million deaths. Cardiovascular disease is responsible for one out of every four deaths, and the proportion of people who die away due to cardiovascular disease is increasing with each passing year [2].

In today's world, enhanced patient monitoring systems have been developed for the goal of tracking the states of patients [3] but very little clinical data has been gathered to estimate the effectiveness of these tactics [4]. Therefore, the standard of care for most medical professionals and healthcare systems remains to be the routine observation of patients' vital signs on a periodic basis [5]. This is the case despite recent developments in new sensing technology. An electrocardiogram, more often referred to as an ECG, is a graphical depiction of the voltage that is produced by the cardiac or heart muscle during the activity of a heartbeat [6]. ECG monitoring systems need to have the capability of extracting the characteristics of an ECG signal in real time [7]. This is a crucial feature. Heart rate variability, sometimes referred to as HRV, is a naturally occurring physiological phenomenon in which there is a change over the course of time in the amount of time that elapses between each of an individual's following heart beats. [8] HRV is an accurate representation of all these different components of heart function, which may be influenced by several physiological factors that can vary the regular beat of the heart. Timing, frequency, and nonlinearity of the HRV signal are the primary processing components that are retrieved from this signal. This signal also exhibits nonlinearity. The features that are obtained from this extraction are useful diagnostic tools that may be used to determine a range of disorders that are linked with the function of the heart [9].

Previous work on ECG analysis may be categorized into the four different kinds of solutions that are as follows: (i) Solutions for traditional, fixed machines (ii) Solutions for System-On-Chip (iii) Solutions for portable device and (iv) Solutions for Application Specific Integrated Circuits (ASIC) [10]. Because all the devices that required to be used to monitor the patient had to be plugged in, prior monitoring systems could not allow for the patient to move freely or conduct remote assessments. In addition to that, the implementation of these solutions necessitated the provision of an excessive number of hospital beds [11][12]. In order to provide a reliable study of the electrocardiogram (ECG), the SoC system may conduct 12-lead investigations entirely inside a single chip. The commercial technique [13], which uses digital signal processing (DSP) to take eighth input sensor lines, produce lead signals, and analyze all of them in one step, does all of this in one step; nevertheless, the procedure is arduous. Electrocardiography (ECG), Electroencephalography (EEG), and respiration signals are examples of the types of biological data that can be captured using a novel approach [14] that makes use of a flexible SoC

that integrates the capture of multiple biological data with on-chip digital signal processing [14]. This novel approach makes use of a portable ECG measuring and monitoring system that is founded on Linux, in contrast to handheld systems [15] that do little more than receive and send data. Data collection from a 12-lead ECG is one of the features offered by this device, along with internet-based remote diagnostics. Only for the purpose of data collection prior to transmission is the ASIC solution [16] put into use.

Developing an ECG device with System-on-Chip (SoC) technology is one method that is suggested for incorporating an HRV analysis capability onto an ECG device. This method has a few advantages. The end objective of this endeavour will be the manufacture of a portable cardiac monitoring equipment that is suitable for application in contexts associated with home care. This work presents a SoC that is based on the ECG biomedical embedded system. It does this by utilizing a hardware/software co-design technique and the technology offered by Altera (ECG-SoC). The objective of the SoC is to do ECG pre-processing and HRV feature extraction using an offline database that was developed by MIT-BIH [17].

In this article, a proposal is made for the development of an electrocardiogram (ECG) system that is particularly well suited for application in rural health care facilities. The design of the ECG System is based on FPGA, and it makes use of System-on-Chip technology (also known as ECG-SoC).

II. PROPOSED METHOD

The ECG-SoC Cyclone II FPGA architectural design shown in Fig.1 is meant to make it possible for a superior technology to be developed by utilizing a Nios II processor, an Avalon on-chip communication bus, and a Nios II–Linux embedded operating system. All of these components are shown in the figure. The illustration in question illustrates this design.

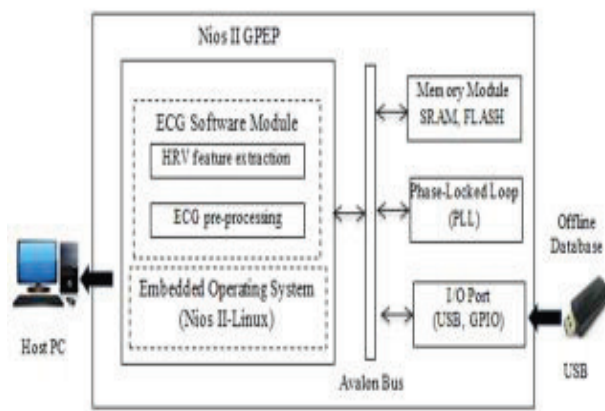


Figure 1. ECG-SoC Cyclone II FPGA

The ECG-SoC was designed primarily for the goal of ECG preprocessing as well as HRV feature extraction. Both aims were pursued simultaneously during development. Because of this, the ECG-SoC will perform computations based on an offline dataset rather than making use of a module for online data collection in order to get the necessary information. The

ECG-SoC architecture consists of software and hardware subdivisions working together to form the whole (HW and SW, respectively). Memory modules, a phase-locked loop (often referred to as PLL), and input/output (I/O) ports are all components that are part of the HW partition's make-up. These components each serve a distinct function, some of which include the following but are not limited to the following: to store the image of an embedded operating system, which is composed of programmes, the dataset, and other important files; to control the clock signal of the host computer, the system, and the targeted board; to communicate and transmit data to the outside world; and to accelerate operations that take a significant amount of time within the system. A communication link between these components that is constructed in accordance with established specifications is provided by something that is referred to as a system bus, which is located beside these components.

III. METHODOLOGY

An illustration of the ECG-SoC design process is shown in Fig.2. It is composed of four stages, which are the design of system hardware architecture, the design of the Nios II-Linux embedded operating system (OS), the design of ECG-SoC software and the integration of the system". The first stage is the design of the system hardware architecture, and the other three stages are the design, creation, and integration of the OS. In the paragraphs that follow, we will discuss the particulars of each stage. At various stages of the design process, the use of a variety of EDA tools, such as QUARTUS II, SOPC Builder, Nios II IDE, and Nios II-Linux cross compiler, is required .

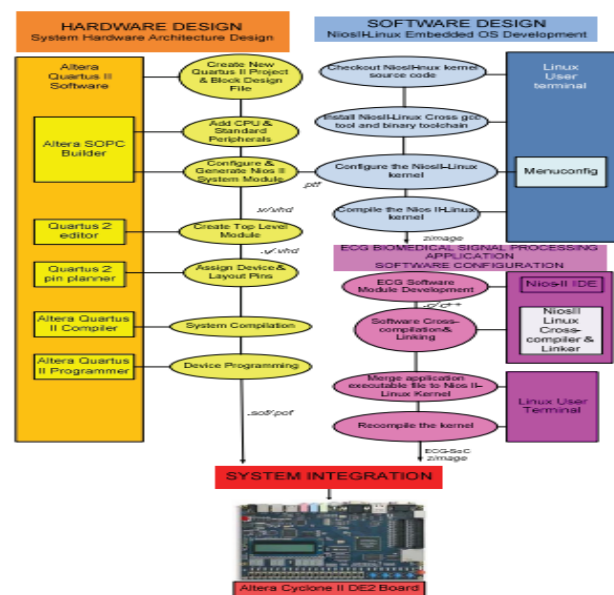


Figure 2. Design Methodology of ECG-SoC

A. System Hardware Architecture Design

Two distinct phases make up the process of designing the system's hardware components from start to finish. SOPC Builder is used at the beginning of the process to define the Nios II GPEP, RAM, and other standard peripherals in order to design a Nios II system module. This is done to ensure that the module will function properly (System-on-

Programmable-Chip). The details of the configuration include the reset vector and the exception vector of the Nios II processor, as well as the base address, the interrupt request (IRQ) assignment of each peripheral, and the source of their clock signal. Additionally, the details include the reset vector and the exception vector of the Nios II processor. Both the process-initiated multiple Verilog HDL (v) files and the system configuration file (.ptf) are going to be utilised in the process of configuring and compiling the software module, and the SOPC Builder is responsible for the generation of both files. In addition, the SOPC Builder is responsible for the generation of the system configuration file (.ptf). During the second stage, the Quartus II will create a top-level file of the Nios II system module. This file will comprise targeted development board, device, and pin selections. The compilation process then does synthesis, fitting, and timing analysis to create the netlist and HW programming file (.sof/.pof), both of which are downloaded to the Cyclone II DE2 FPGA board during system integration.

The hardware architecture of the ECG-SoC system is represented in Fig. 3, which also illustrates the configuration of the system. The whole system that is contained on the Cyclone II DE2 FPGA board makes use of this design in its many iterations during its operation. The marked and coloured block on the chip, which is filled with several different modules, is meant to depict the inside of the chip. To include these modules into the system, SOPC Builder is the tool that is utilised.

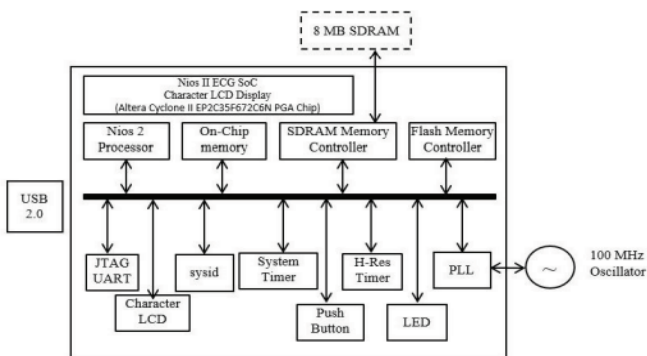


Figure 3. ECG-SoC hardware system configuration

On-chip memory, the SDRAM memory controller, and the flash memory controller are the three basic kinds of memory modules that can be used. On-chip memory is the most common type of memory module. A high-resolution timer, also known as a HiRes. Timer, and a system timer are both utilised for the purposes of improving timing control, simplifying timing problems, and improving the overall structure of the board. The phase-locked loop, also known as PLL, is utilised in the construction of this particular system, and it is responsible for producing a clock signal with a frequency of 100 MHz. The system ID, which is sometimes referred to as the sysid, can get an address that is exclusive to the architecture of this specific system. The JTAG UART is being used as the I/O port for this project. On the other hand, USB 2.0 is being put to use as the peripheral device on the outside.

B. Nios II-Linux embedded operating system

Nios II-Linux is a terminal-based Linux embedded OS that uses Debian 2.6.4-rc6. It can execute Linux programmes and libraries. Distributed versioning, relational databases, debuggers, and cross compilers are included. Cross-compilation condenses information into one file. Linux kernel image is an auto-extractable file (zImage). Cyclone II is programmed using ECG-SoC. The programming file (.sof) must match the board's hardware architecture to work. The hardware system's configuration file (.ptf) is needed to configure the Linux kernel and construct the ECG-Nios SoC's II-Linux kernel.

C. ECG-SoC Software Design

To construct the software portion of the ECG-SoC system, it is necessary to do ECG preprocessing as well as ECG feature extraction, both of which are depicted in Fig.4.

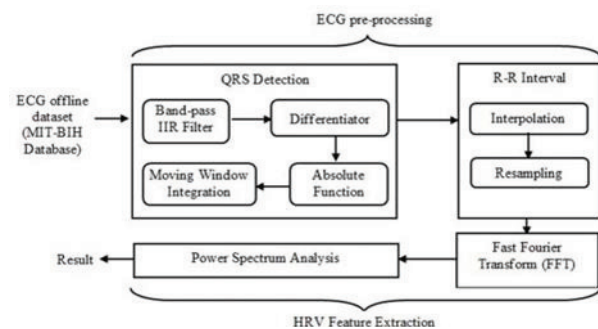


Figure 4. ECG Pre-Processing and HRV Feature Extraction

Eliminating baseline drift, high-frequency noise, and high-frequency random noise created by power line interference is one of the primary goals of pre-processing, along with increasing the signal-to-noise ratio and improving the accuracy of analysis and measurement (50 Hz, 60 Hz).

During the pre-processing stage, the QRS identification algorithm is modified so that it can correctly identify the ECG QRS complex for HRV analysis. This is done before the processing begins. The band-pass frequency of this detector module is somewhere between 5 and 15 Hz. The slope information needed for peak identification may be obtained from the differentiated filter output. The square function is being phased out in favour of its more efficient counterpart, the absolute function, which may flip between positive and negative peaks. The data is then integrated with a moving window in order to smooth it out. After the QRS complex has been located, the signal from the electrocardiogram is changed into a signal that looks like a valley with two peaks of varying heights. Electrocardiograms determine the presence of heartbeats by focusing on the R peaks of the QRS complex [18]. The R-R interval module of the ECG analyses the current value in comparison to future values in order to determine the peak. The value that is greater than the eight values that follow it and the threshold level is known as the QRS peak. The subsequent block unit does an interpolation between two R-R intervals to provide findings for a continuous R-R interval based on the peaks that were seen.

To obtain a rapid Fourier transform, the peak QRS signals are resampled at 4 Hz and then linearly interpolated (FFT).

Then, the R-R power spectrum should be obtained. When linear adjustments are incorporated, spectral methods applied to ECG analysis can help explain the behaviour of the time domain model [19]. For power spectrum analysis, both real and imaginary FFT results are necessary. The below mentioned equation (1) demonstrates this point.

$$PS = \frac{\sqrt{(r^2 + i^2)}}{N} \quad (1)$$

Where PS is the power spectrum, r is the real, i is the imaginary, and N is for total number of R-R intervals or heart rate (HR) data being transformed.

From the heart rate spectrum diagram, three power bands may be extracted. Power bands range from 0.008 to 0.04 Hz, 0.04-0.15 Hz, and high frequency (HF: 0.15-0.5 Hz). For HF HRV, the power spectrum between 0.15 and 0.4 Hz is integrated. Then, equations (2) (3) (4) are employed, where HR (f) denotes heart rate frequency (HR) .

$$HRV_{VLF} = \sum_{f=0.008}^{0.04} \frac{|HR(f)|^2}{T} \quad (2)$$

$$HRV_{LF} = \sum_{f=0.04}^{0.15} \frac{|HR(f)|^2}{T} \quad (3)$$

$$HRV_{HF} = \sum_{f=0.15}^{0.4} \frac{|HR(f)|^2}{T} \quad (4)$$

HRV is heart rate variability; VLF is extremely low frequency; LF is low frequency; and HF is high frequency. The ECG system's software was created to incorporate ECG-SoC standards for successful ECG pre-processing and HRV feature extraction. 200 Hz sampling frequency and 8 kHz threshold are used. We utilised 12,000 ECG data, and the FFT count was 1024. The 240-second FFT window size .

D. System Integration

The hardware programming file (.sof) and the most recent version of the Nios II-Linux zImage file are both downloaded into the Altera Cyclone II DE2-115 platform during the final step of the system integration process. This is done so that the functionality of the system can be checked, as well as the assessment can be carried out.

IV. RESULTS AND DISCUSSION

The descriptions of the ECG system requirements are shown in Table I below [20]. For the ECG signals, we sampled at a frequency of 200 Hz, and the threshold values were set at 8000 Hz. In the meanwhile, a resampling frequency of 4 Hz has been selected with the goal of lowering the dimensionality of the heart rate data. The 120 000 are the

offline ECG data that were taken from the MIT-BIH database and stored in a text file format on a pen drive. The increased size of the ECG dataset will result in a greater degree of precision in the processing.

TABLE I.
SPECIFICATIONS OF ECG SYSTEM

Specifications	Values
Sampling frequency	200 Hz
Threshold value	8000 Hz
Resampling frequency	4 Hz
Total ECG data	120 000
FFT count	1024

During the process of verifying the operation of the system, an offline dataset is placed in a portable USB device, and then that device is inserted into the ECG-SoC programme. The results of running ECG-SoC in Nios II-Linux are depicted in Fig. 5 and 6, respectively. At this point, the listings of the execution folders are displayed, and the results are made. The HRV and ECG software are utilized in this section to create the results.

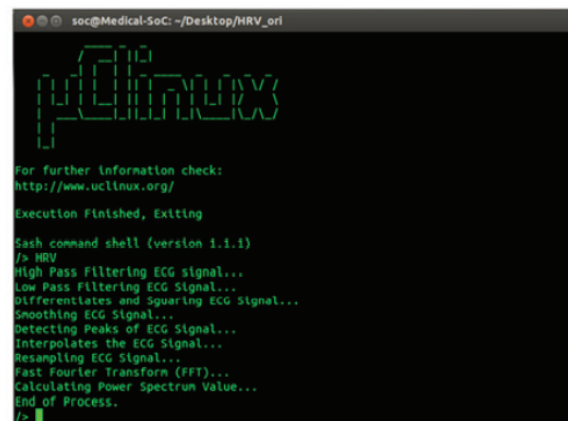


Figure 5. ECG-SoC execution in uCLinux

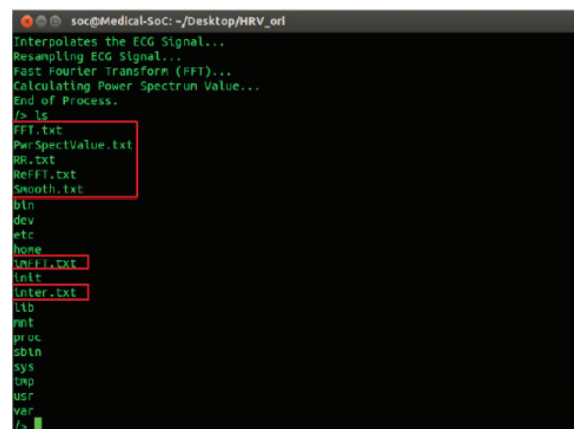


Figure 6. Results file generated from the execution

The electrocardiogram (ECG) data may be seen in Fig. 7 after the programme was developed. To detect negative peaks on an electrocardiogram, each data point is transformed to its absolute value .

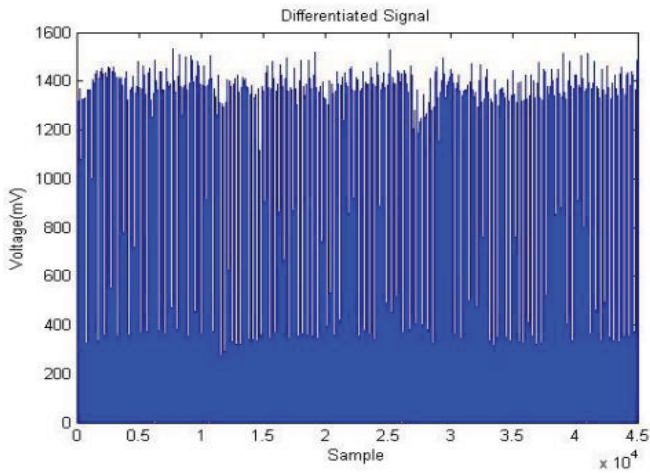


Figure 7. Intermediate results for differentiated signals

The Fig. 8 depicts the output that is obtained when the operation of squaring is carried out immediately prior to the smoothing operation that is carried out by moving window integration. Following performing the squaring procedure, the resultant numbers are greater, and after the integration step necessary to generate a smooth ECG signal, they look like what is seen in the below figure. .

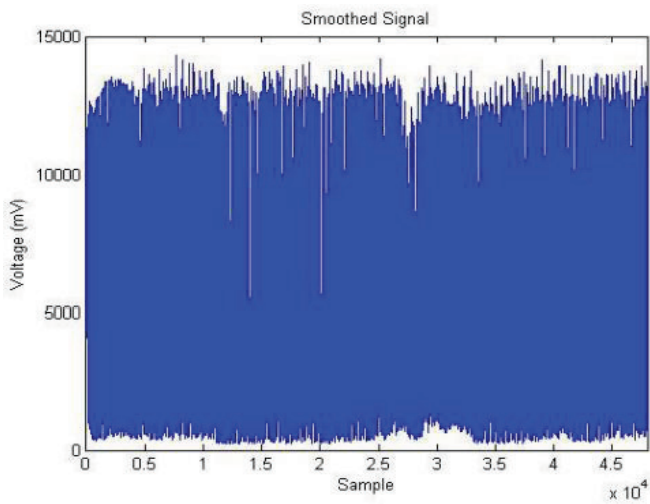


Figure 8. Intermediate results for smoothed signals

Fig.9 shows the QRS peak detected by our proposed method.

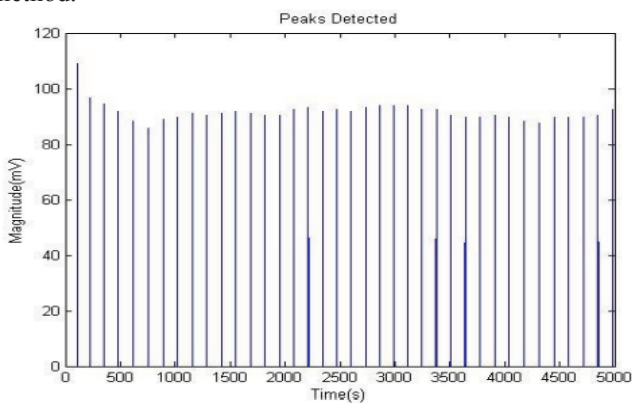


Figure 9. Peak Detection

In Fig.10, linear interpolation has been utilised to the detected QRS peaks for resampling at 4 Hz.

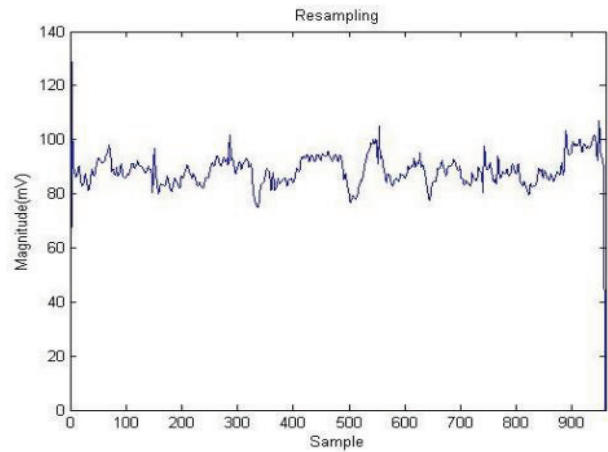


Figure 10. Resampling at 4 Hz by utilizing linear interpolation

The result of the FFT is seen in Fig 11, and it consists of both real and imaginary components. Take note that the negative values appear as a consequence of the fact that an operation was carried out before the FFT was carried out[21] .

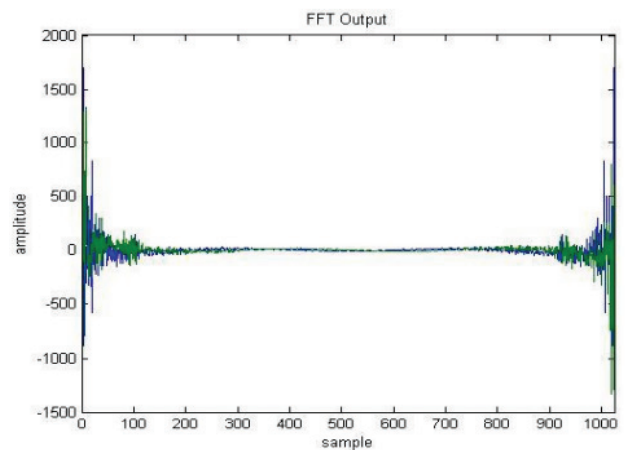


Figure 11. Fast Fourier Transform

Since this initial process includes subtraction, some numbers will be negative. After FFT results are obtained, Eqn. (1) is used to analyze the power spectrum (1). FFT power spectrum analysis reveals the highest frequency between 0.01 and 0.1 Hz. Inputs include real and imaginary numbers.

The results of power spectrum analysis yields Fig. 12. The graph is plotted for the frequency up to 1 hertz. Maximum VLF, LF, and HF ranges are illustrated by black, green, and black dotted lines, respectively. The highest frequency on this power analysis graph is 0.03 Hz.

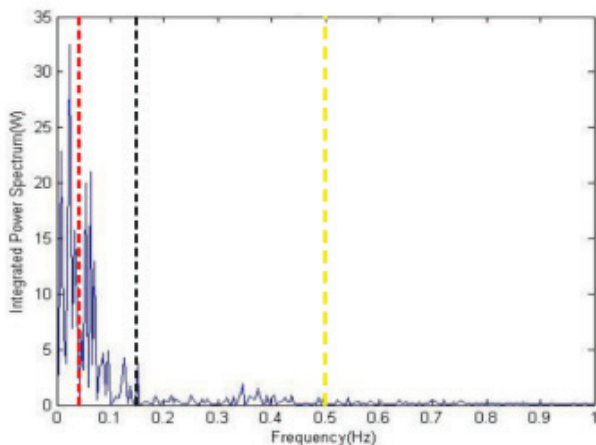


Figure 12. Power spectrum versus frequency

V. CONCLUSIONS

In this paper, a System-on-Chip (SoC), which is built on an embedded electrocardiogram (ECG) system is discussed. The ECG-SoC makes use of methodologies that include a co-design of hardware and software as well as technology developed by Altera to carry out ECG pre-processing and extract HRV characteristics from an offline dataset. The fact that these software activities are being carried out is evidence that the ECG-SoC system combines the processes of gathering ECG datasets, storing them, and processing them by utilising integrated hardware and software. All these processes are carried out in tandem with one another. The portability of the system, in addition to the various software enhancements that are capable of being applied are the benefits of the proposed system. The system that has been suggested in this paper can conduct adequate ECG data analysis when it is configured as an ECG-SoC. This enables it to be utilised in a broad variety of cardiac monitoring applications since it satisfies the requirements for such applications in rural areas.

REFERENCES

- [1] World Health Organization, "New Data Highlight Increase in Hypertension, Diabetes Incidence," May 16, 2012. [Online]. Available: http://www.who.int/mediacentre/news/release/2012/world_health_statistics_20120516/en/. [Accessed: July 4, 2014].
- [2] World Health Organization, "Global Strategy on Diet, Physical, Activity and Health," May 2014. [Online]. Available: <http://www.who.int/dietphysicalactivity/en/>. [Accessed: July 2014].
- [3] Redondi, A., M. Chirico, L. Borsani, M. Cesana and M. Tagliasacchi (2013). "An integrated system based on wireless sensor networks for patient monitoring, localization and tracking." *Ad Hoc Networks* 11(1): 39-53.
- [4] Nangalia, V., D. R. Prytherch and G. B. Smith (2010). "Health technology assessment review: Remote monitoring of vital signs - current status and future challenges." *Critical Care* 14(233): 1-8.
- [5] Tarasenko, L. and D. A. Clifton (2011). "Semiconductor wireless technology for chronic disease management." *Electronics Letters (Special Supplement: Semiconductor in Personalized Medicine)*: S30-S32.
- [6] Clifford, G. D. and D. Clifton (2012). "Wireless technology in disease management and medicine." *Annu Rev Med* 63: 479-492.
- [7] Shyu, L.-Y. and W. Hu (2007). "Intelligent Hybrid Methods for ECG Classification-A Review." *Journal of Medical and Biological Engineering* 28(1): 1-10.
- [8] Hu, W., C. C. Lin and L. U. Shyu (2011). "An Implementation of a Real-Time and Parallel Processing ECG Features Extraction Algorithm in a Field Programmable Gate Array (FPGA)." *Computing in Cardiology* 38: 801-804.
- [9] Dabanloo, N. J., S. Moharreri, S. Parvaneh and A. M. Nasrabadi (2010). "Application of Novel Mapping for Heart Rate Phase Space and Its Role in Cardiac Arrhythmia Diagnosis." *Computing in Cardiology* 37: 209-212.
- [10] T. J. Sullivan, S. R. Deiss, and G. Cauwenberghs, "A low-noise, non-contact EEG/ECG sensor," in *Biomedical Circuits and Systems Conference, 2007.BIOCAS 2007.IEEE*, Nov. 2007, pp. 154 – 157.
- [11] V. P. Nambiar, M. Khalil-Hani, C. W. Sia, and M. N. Marsono, "Evolvable block-based neural network for classification of driver drowsiness based on heart rate variability," in *Circuits and Systems (ICCS), 2012 IEEE International Conference on*. IEEE, Oct. 2012, pp. 156 – 161.
- [12] I. Al Khatib et al, "A multiprocessor system-on-chip for real-time biomedical monitoring and analysis: architectural design space exploration," in *Design Automation Conference, 2006 43rd ACM/IEEE*, 2006, pp. 125 – 130.
- [13] N. V. Helleputte et al., "A flexible system-on-chip (SoC) for biomedical signal acquisition and processing," *Sensors and Actuators A: Physical*, vol. 142, pp. 361 – 368, Mac 2008.
- [14] K. Hung, Y. T. Zhang, and B. Tai, "Wearable medical devices for tele-home healthcare," in *Engineering in Medicine and Biology Society, 2004. IEMBS '04. 26th Annual International Conference of the IEEE*, Sept. 2004, pp. 5384 – 5387.
- [15] J. Dong and H. Zhu, "Mobile ECG detector through GPRS/Internet," in *Computer-Based Medical Systems, 2004. CBMS 2004. Proceedings. 17th IEEE Symposium on*, June 2004, pp. 485 – 489.
- [16] T. H. Tan et al., "Development of a portable Linux-based ECG measurement and monitoring system," *Journal of Medical Systems*, vol. 35, pp. 559 – 569, Aug 2011.
- [17] A. R. Sanchez, O. Alvarado-Nava, F. J. Z. Martinez, "Network monitoring system based on an FPGA with Linux," in *Technologies Applied to Electronics Teaching (TAEE), 2012*, pp. 232 – 236.
- [18] N. Ravanshad, H. Rezaee-Dehsorkh, R. Lotfi, and Y. Lian, "A level-crossing based QRS-detection algorithm for wearable ECG sensors," *Biomedical and Health Informatics, IEEE Journal of*, vol. 18, pp. 183 – 192, Jan. 2014.
- [19] Murthy, V. K., L. J. Haywood, J. Richardson, R. Kalaba, S. Saltzberg, G. Harvey and D. Vereeke (1971). "Analysis of Power Spectral Densities of Electrocardiograms." *Mathematical Biosciences* 12: 41-51
- [20] Dr. Narendra Mustare "A Logical Approach of Data Mining Technique for the Prediction of Cardiovascular Disease" *International Journal of Research and Analytical Reviews (IJRAR)* UGC Approved - Journal No: 43602 Volume 6 Issue 2, Date of Publication: May 2019 2019-05-05, E-ISSN: 2348-1269, P-ISSN:2349-5138.
- [21] Devulapalli Shyam Prasad & Srinivasa Rao Chanamallu & Kodati Satya Prasad "Optimized deformable convolution network for detection and mitigation of ocular artifacts from EEG signal" *Multimedia Tools and Applications (2022)* 81:30841–30879 <https://doi.org/10.1007/s11042-022-12874-4>

Strength and Durability Studies on Lightweight Self-Compacting Concrete Partially Replacing Coarse Aggregate with Sintered Fly Ash Aggregate

K. Raju¹, N. Ramanjaneyulu² and M.V. Seshagiri Rao³

¹PG Scholar, CVR College of Engineering/Civil Engg. Department, Hyderabad, India
Concrete Technologist, FOSROC Chemicals (India)Pvt. Ltd.

Email: kakiraju540@gmail.com

²Research Scholar, JNTUA College of Engineering/Anantapur and Asst. Professor, CVR College of Engineering/Civil Engg. Department, Hyderabad, India

Email: rams.613@gmail.com

³Professor, CVR College of Engineering/Civil Engg. Department, Hyderabad, India

Email: rao_vs_meduri@yahoo.com

Abstract: This paper investigates the strength and durability studies on lightweight self-compacting concrete partially replacing coarse aggregate with sintered fly ash aggregate, with different grades of concrete. (M20, M30 and M40). In this study, the rational mix design procedure for self-compacting concrete is used. The present study consists of two phases. In the first phase, SCC mixes for different grades are developed without using lightweight aggregates. The second phase of the study introduces lightweight aggregates (i.e Sintered fly ash aggregates) varying in sizes from 8mm-12mm partially replacing coarse aggregate in self-compacting concrete. Compressive strength, split tensile strength and flexural strength and durability studies were conducted. The test results indicate significant improvement in the strength properties of self-compacting concrete by the inclusion of sintered fly ash aggregates as a partial replacement for natural aggregates.

Index Terms: Self-compacting concrete, Sintered fly ash aggregates, Lightweight Concrete, Lightweight self-compacting concrete, Durability.

I. INTRODUCTION

Self-compacting concrete is defined as Concrete which can flow under its self-weight and fill the formwork in completely, even in the presence of dense reinforcement, without using any vibration actions, maintaining homogeneity [1-5]. It was first developed in Japan, to overcome the problems caused by a lack of complete and uniform compaction through vibrators. Self-compacting concrete is not affected by the shape and quantum of reinforcing bars or the enactment of a structure. Due to its high property of flowing, it is easily a changeable quality and resistant to segregation [6].

Usually, chemical admixtures such as hi-range water reducers (Super Plasticizer) and Viscosity Modifying Agents, which change the rheological properties of concrete are used. Mineral admixtures are used as an extra fine material besides cement [7-10]. In this study cement content was partially replaced with mineral admixture, i.e., fly ash. Admixtures improve the flowing and strength and durability properties of concrete [11-18].

Significance of study:

India produces approximately 120 million tons of fly ash annually; this fly ash is coming from thermal power plants as a by-product and the main challenge faced by the thermal plants is the safe disposal of this fly ash. In the construction industry, we use large-scale usage of concrete. In the making of concrete, we use natural aggregates as the ingredients in the form of coarse aggregates, which leads to natural imbalance and depletion of natural sources of rocks and hills. To overcome this problem, the best solution is to use the various engineering by-products in the manner of sustainable development. From this point of view, the idea of sintered fly ash aggregates comes in. Using these sintered fly ash aggregates produces the concrete lightweight which makes the concrete economical and lightweight.

The usage of lightweight aggregate i.e, sintered fly ash aggregates in self-compacting concrete gives lightweight self-compacting concrete which produces both benefits of lightweight which reduces the weight of concrete in comparison with conventional concrete and the benefits of self-compacting concrete.

II. LITERATURE REVIEW

Anitha J, Pradeepa S, Lalit Soni, Rakshit KB (2016)

Studied that superplasticizers are the most important admixtures enhancing concrete performance. The development of new superplasticizers during the last decades has determined the most important progress in the field of concrete structures in terms of higher strength, long durability, lower shrinkage and safer placement, particularly in elements with very congested reinforcement. The progress from sulphonated polymer to polycarboxylate has resulted in higher water reduction at given workability and lower slump loss. More recently poly-functional superplasticizers have been developed which are able to completely keep the initial slump for at least 1 hr. without any retarding effect on the early strength. Moreover, multi-purpose and poly-functional superplasticizers have been

invented which are able to reduce drying shrinkage. The recent progress of superplasticizers was examined in this paper.

Megha H Patel¹, Nandan H Dawda (2017)

The development of self-compacting concrete started in Japan in the middle of 1980s with an aim to reduce durability problems in complicated and densely reinforced concrete structures due to lack of skilled labour and poor communication between the designer and the construction engineer. The concept of Self-compacting concrete (SCC) was proposed for the first time by Prof. Hajime Okamura (1997), but the prototype was first developed in 1988 in Japan by Professor Ozawa (1989) at the University of Tokyo. The last few decades is considered to be the era of self-compacting concrete and thousands of research has been carried out. In India, the development of concrete possessing self-compacting properties is still very much in its initial stages. Over the past couple of years, few attempts have been made, still the cost of production of such concrete is a challenging issue for the present concrete engineers. Hence, in the present paper, an attempt is made to understand the effect of various types of mineral and chemical admixture (Rice husk ash, Metakaolin) on the properties of SCC concrete with the cost-by-benefit analysis for the same. It is basically an attempt to sum up the effect of various ingredients on concrete.

Manu S. Nadesan, P. Dinakar (2021)

In this paper, the authors explained how lightweight aggregate concrete differs from normal concrete and the various properties of sintered fly ash aggregates. Fly ash is a waste material which generates twin problems of discarding as well as environmental degradation, due to its nature of causing air and water pollution on a large scale. Nearly 145 coal-based thermal power stations in India are producing over 184 million tons of fly ash per year out of which only 56% was utilized effectively and the remaining is still a concern to the community. Therefore, the manufacture of sintered fly ash lightweight aggregate is an appropriate step to utilize a large quantity of fly ash in concrete. However, the non-existence of worthwhile technology to produce sintered fly-ash lightweight aggregates and the absence of a market has deterred Indian entrepreneurs from producing sintered fly-ash aggregate. Recently a couple of industry players in India have focused their attention on the development of sintered fly ash lightweight aggregates commercially on a large scale from the fly ash obtained from their captive power plants. As such, there is no Indian standard available for lightweight aggregates. More recently, pilot studies by the authors have established that this material displays substantial potential for use in structural concrete. The lightweight aggregates manufactured with fly ash are light due to the presence of air voids and these voids are responsible for their absorbency. This absorbency plays a significant role in the mix design and also in the performance of the concrete. The absorption caused by the lightweight aggregate is mainly responsible for the difficulty during the production of lightweight aggregate concrete (LWAC) in practical situations. Porous lightweight

aggregates have become highly sensitive as the w/c ratio varies. The moisture content during the mixing stage state is a major concern for LWAC. The North American approach is to use the LWA in a saturated state; contrary to this, the Norwegian approach prefers dry LWA having a moisture content of less than 8%. The problems associated with the variation in the moisture content with pre-soaked LWA can be nullified using dry LWA and the reduction in fresh mix density is an added advantage in this procedure. By considering the cost of production and the improved durability properties it was suggested to use the aggregates in the dry state. Also, there is no appreciable difference in the workability and compressive strength between the concrete using air-dried and pre-soaked aggregates if the water absorption is compensated by additional water during mixing. The mix design of SLWAC is more complex than that of normal concrete as more design parameters such as absorbed water during the mixing of concrete and proportioning of different aggregate sizes etc. are needed to be determined. Taking this into account, a simplified design method is required to produce SLWAC made with natural sand. Presently due to the lack of proper mix design procedures, the developed concrete is poor in structural performance and therefore the use of sintered fly ash lightweight aggregates has been limited to non-structural elements. Till now no reliable study has been made to determine the water absorbed by the porous aggregate during concrete mixing. In the earlier methods, the absorbed water was determined by completely immersing the aggregates in water for a specified time. Also, combined aggregate grading is missing from all the available methods. The main objective of this paper is to suggest a simple and reliable mix design method to the community to bridge the existing gap. Consequently, this study examines the development of LWAC and evaluates the performance of these concretes through proper experimental investigations. The outcome of these investigations on fly ash lightweight aggregate specifies that one can suppose not only the environmental protection through recycling of waste resources but also the reduction in dead load and enhancement of some of the matured concrete properties.

III. RAW MATERIAL

A. Cement

The majority of concrete is mostly made of cement. In this experiment, common Portland cement (53 Grade per IS: 8114-1978) [19] was used.

B. Aggregate

For this study, aggregate that complies with IS: 383-1970 [20] (coarse and fine aggregate) was employed. We employed angular coarse aggregate with a size range of 10 mm to 8 mm and fine aggregate passing through 4.75 mm. In SCC, coarse aggregate content is typically the bare minimum.

C. Fly Ash

In this study, FA was added as a mineral additive. Fly ash is nothing more than the byproduct of burning powdered coal. Fly ash proves the use of IS: 3812 [20].

D. Super plasticisers

In this study, CONPLAST SP430, a tool for enhancing concrete workability, is utilized.

E. Water

The most crucial component of concrete is water, which aids in tying together the cement and particles.

F. Sintered fly ash aggregates

The different size fractions of sintered fly ash aggregates (2–4 mm fraction, 4–8 mm fraction and 8–12 mm fraction) were taken as coarse aggregates



Figure 1. Sintered fly ash aggregates.

TABLE I.
PHYSICAL PROPERTIES OF SINTERED FLY ASH AGGREGATES.

Property	Cement	Fine Aggregate	SFA Coarse Aggregate 8-12 mm	Coarse Aggregate 10-12 mm
Consistency	32%	-	-	-
Initial setting time (Minutes)	60	-	-	-
Specific gravity	3.15	2.52	1.764	2.66

IV. TESTS AND METHODOLOGY

Slump Flow Test and T_{50 cm} Test:

Self-consolidating concrete should have the following properties in its fresh state: flowability, filling ability, and segregation resistance ability [21-23]. The suggestions made in EFNARC (2005) were used in this study to evaluate the qualities of LWASCC in its fresh form. The fresh LWASCC's slump-flow, time to attain 500 mm of slump-flow, and passing ability (confined flowability) utilizing L-box (H2/H1) were all assessed immediately after mixing. After 60 minutes (slump-flow and T500) and 80 minutes, the tests were repeated (L-box). The degree of mixture segregation was evaluated using the visual stability index (VSI). Following the slump-flood test, the concrete mixture is visually inspected by looking at how the coarse aggregate is distributed throughout the concrete mass, how the mortar fraction is distributed, particularly around the perimeter, and how the concrete is bleeding. There are four stability classes, each of which is assessed by a visual inspection (ACI 237R-07:2007) Gołaszewski & Szwabowski, 2011) [24].

The slump flow test is used to find the free flow of the self-compacting concrete without obstructions. T_{50 cm} is also an indication of SCC flow. A lower time means greater flow ability. The research suggested a time of 2-5 seconds for general civil engineering applications [25].
Slump flow Apparatus

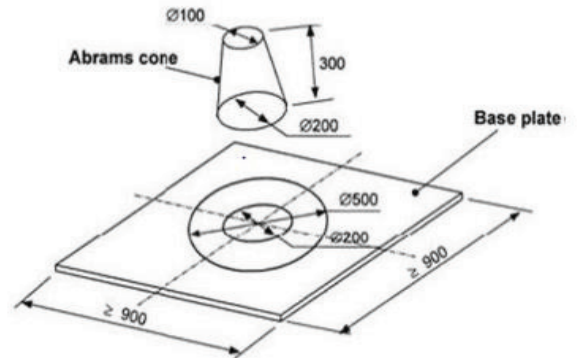


Figure 2. Slump Flow Test

V-Funnel Test

- This V-Funnel apparatus is used to find the viscosity of self-compacting concrete.
- In this test the time required to empty a V-Funnel is observed. shorter flow time indicates a greater flow ability
- Test conducted in our laboratory, the time of emptying the V-funnel is 8-seconds.

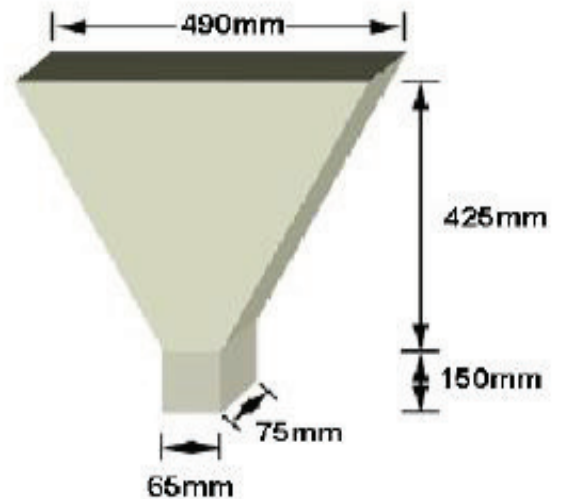


Figure 3. V-Funnel Apparatus

L-Box Test

This method used a test apparatus consisting of a vertical section and a horizontal through into which the concrete is allowed to flow when the releasing of the trap door from the vertical section passes through reinforcing bars.

The time that takes the concrete to flow into the horizontal section is measured. And we have to take the heights of both ends of the apparatus values (H1 & H2). The L-Box test gives an indication of the filling ability and passing ability of the SCC [26-30].

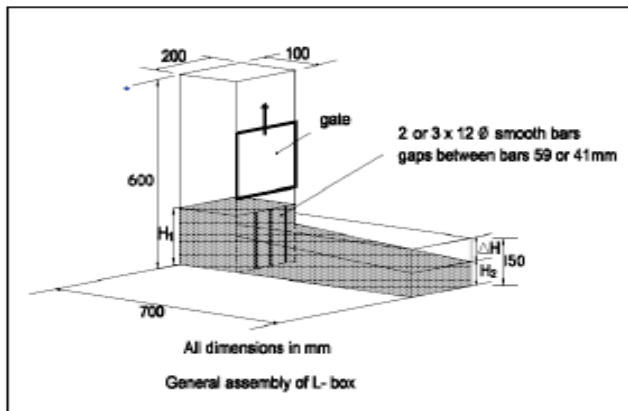


Figure 4. L-Box Apparatus

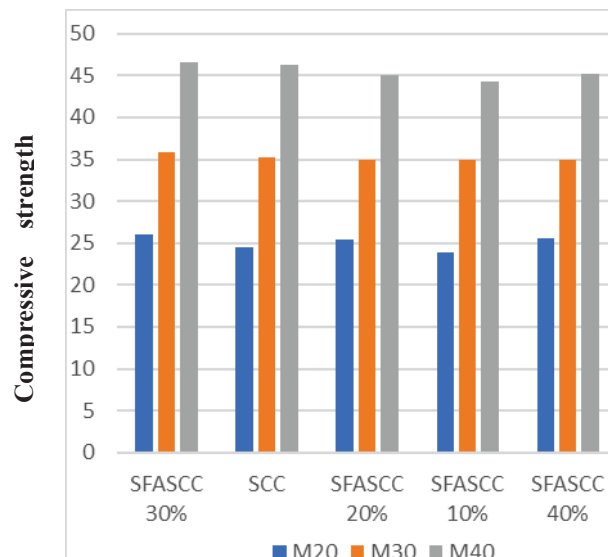
V. RESULTS AND DISCUSSION

TABLE II.
FRESH AND HARDENED PROPERTIES OF SCC

Grade of Concrete	Fresh properties			Hardened Properties	
				Comp.Strength(N/mm ²)	
	T50cm (2-5) sec	V-Funnel (6-12) sec	L-Box (0.8-1)	7 Days	28 Days
M20	4	7	0.88	15.10	24.52
M30	5	8	0.89	23.47	35.16
M40	5	9	0.89	28.88	46.33

TABLE III.
COMPRESSIVE STRENGTH OF SINTERED FLY ASH AGGREGATES SCC.

Grade of Concrete	Percentage Replacement (%)	Hardened Properties	
		Comp.Strength(N/mm ²)	
		7Days	28Days
M20	10	14.76	26.92
	20	15.52	25.36
	30	16.66	26.10
	40	15.93	25.52
M30	10	22.8	35.99
	20	23.4	34.65
	30	24.4	34.41
	40	22.9	33.46
M40	10	26.66	44.23
	20	26.85	44.98
	30	28.87	46.52
	40	26.23	45.23



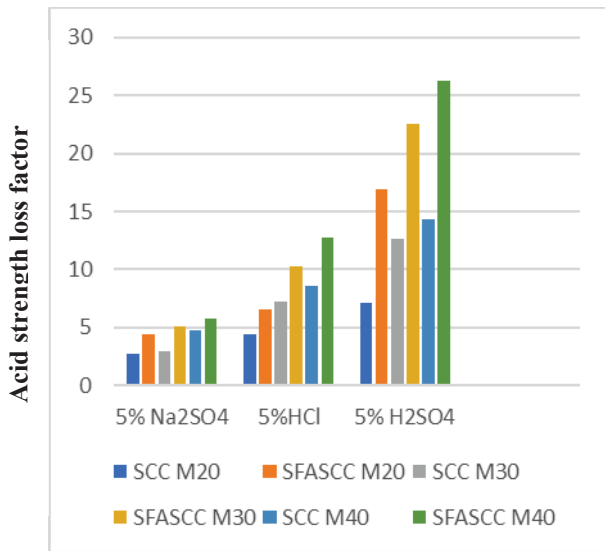
% Of Replacement of Sintered Fly Ash Aggregates

Figure 5. Variation of Compressive Strengths for SCC and SFASCC for 28 days

In this study, more compressive strength was obtained at 30% replacement of coarse aggregate by Sintered fly ash aggregates i.e., 6%, 2% and 1% for M20, M30 and M40 grades respectively at 28days.

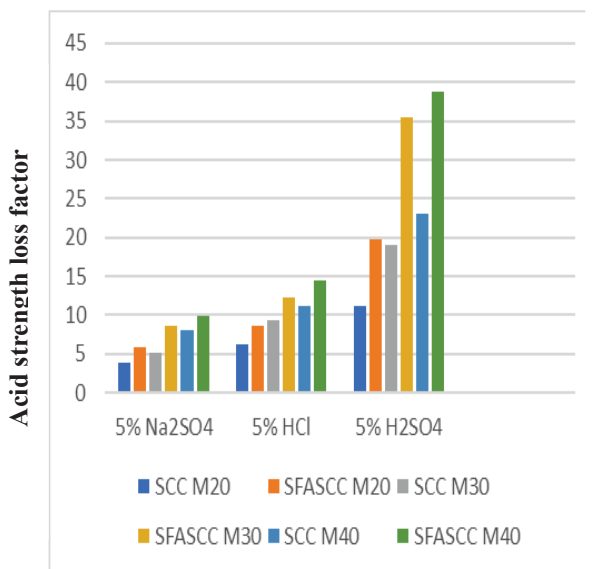
Studies on the durability of SCC and SFASCC

- In the first and second phase investigations were carried out to develop different SCC mixes of different grades of concrete i.e., M20, M30 and M40 using fly ash and chemical admixtures, and to study its fresh and hardened properties.
- In the Investigations at 30% replacement, we got good results. so a durability test was done on 30% replacement sintered fly ash aggregate cube specimens.
- In this investigation the cube specimens were immersed in the chemicals of 5% concentration of Na₂SO₄, HCl and H₂SO₄ solutions in the lab. For the period of 28days and 56days.
- After 28days and 56days the cube specimens were tested.
- In this test results the cube specimens which are immersed in H₂SO₄ are more affected in compressive strength, Weight loss and also in the Dimensions of specimens. Compared with Na₂SO₄, HCl Solutions.
- The Acid Strength Loss Factor, Acid Attacking Factor, Acid Weight Loss Factor and Acid Durability Loss Factor are observed more in the H₂SO₄ solution at 28days and 56days of age.



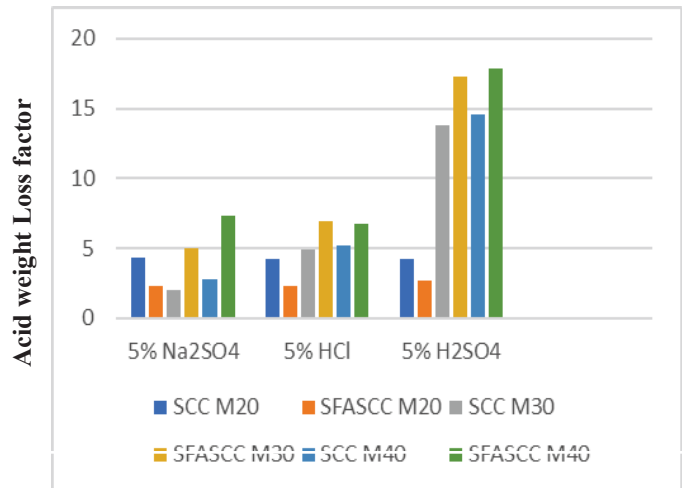
Type of acid with various grades of concrete at 28days

Figure 6. Acid Strength Loss Factors (ASLF) for SCC and SFASCC at 28 Days



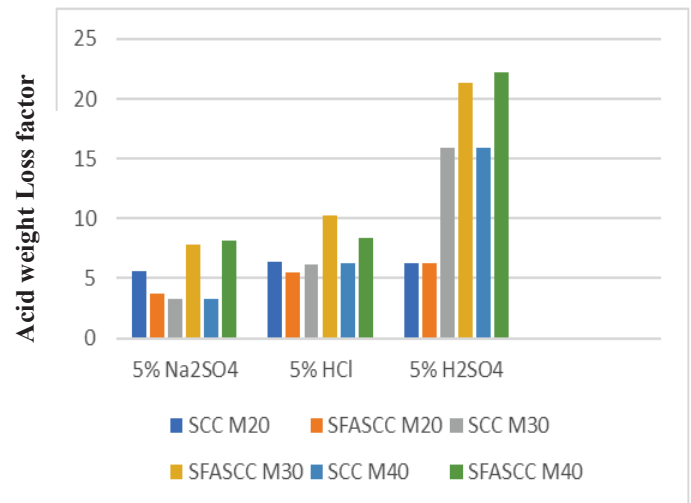
Type of acid with various grades of concrete at 56days

Figure 7. Acid Strength Loss Factors (ASLF) for SCC and SFASCC at 56 Days



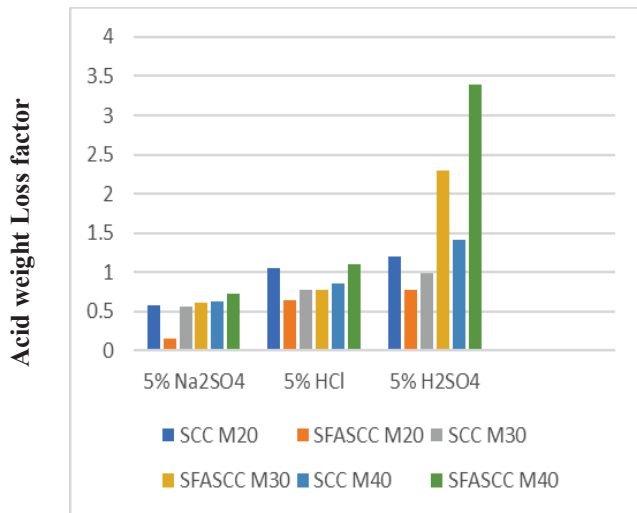
Type of acid with various grades of concrete at 28days

Figure 8. Acid weight loss factors (AWLF) for SCC and SFASCC at 28 days of immersion



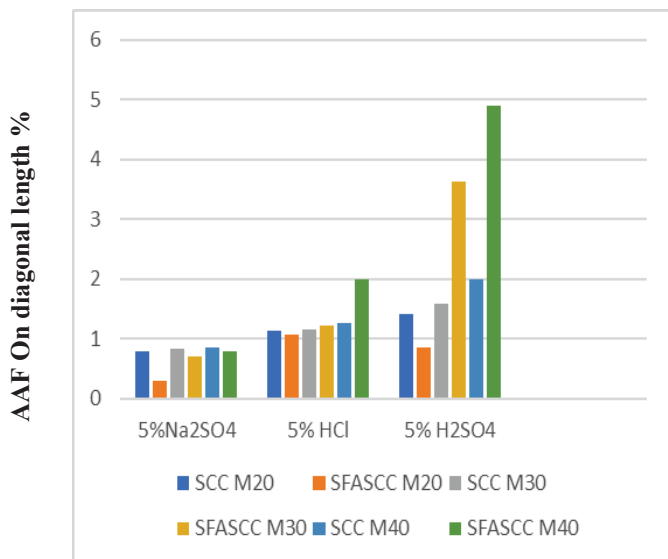
Type of acid with various grades of concrete at 56days

Figure 9. Acid weight loss factors (AWLF) for SCC and SFASCC at 56 days of immersion



Type of acid with various grade of concrete at 28days

Figure 10. Acid Attack Factors (AAF) on diagonal length in % loss @28days



Type of acid with various grade of concrete at 56days

Figure 11. Acid Attack Factors on diagonal length in % loss @56days

VI. CONCLUSIONS

Based on the experimental work conducted on SCC mixes of different grades (M20, M30, M40) the following conclusions are made regarding the properties and behaviour of concrete on partial replacing Coarse aggregate by using Sintered fly ash aggregates and aim to study the strength and durability properties. The following specific conclusions are drawn from this experimental study:

1. Disposal of fly ash in structural landfills can hence be minimized thereby reducing air pollution and unhygienic environmental conditions in particular locations.
2. In this study, more compressive strength was obtained at 30% replacement of coarse aggregate by

Sintered fly ash aggregates i.e, 6%,2% and 1% for M20, M30 and M40 grades respectively at 28days.

3. Split tensile and flexural strength increases with an increase in the percentage of Sintered fly ash aggregates and thereafter it decreases. In the Investigations at 30% replacement, we got good results. so a durability test was done on 30% replacement.
4. The percentage loss of compressive strength, weight, diagonal shape and dimensions of Cube specimens are more affected by 5 % H₂SO₄ solution at the age of 28days, and 56days. when compared to HCL and Na₂SO₄. So, the durability of concrete is more affected by H₂SO₄.
5. By the investigation it is observed that In the H₂SO₄ solution the strength loss is 11%,23%, and 24% more compared with the HCL solution and 14%,27%, and 28% more compared with the Na₂SO₄ Solution for M20, M30 and M40 respectively.
6. The weight loss in H₂SO₄ Solution is 3%,13%,14% more compared with Na₂SO₄ Solution and 1%,11%,14% more compared with HCL solution for M20, M30 and M40 respectively.
7. The percentage dimension change in H₂SO₄ Solution is 0.7%,6%,7% more compared with Na₂SO₄ Solution and 0.3%,5%,6% more compared with HCL solution for M20, M30 and M40 respectively.
8. Use of Sintered fly ash aggregates in concrete reduces the disposal problems of by-products (fly ash) which is produced by thermal power plants.
9. Sintered fly ash aggregate concrete density achieved is 1705kg/m³ and whereas conventional aggregate self-compacting concrete density is 2400kg/m³ reduces the self-weight of the concrete in various structural elements thereby reducing the load on foundations and can reduce in cross-sectional dimensions of structural elements.

REFERENCES

- [1] G. Eason, B. Noble, and I. N. Sneddon, "On certain integrals of Lipschitz-Hankel type involving products of Bessel functions," Phil. Trans. Roy. Soc. London, vol. A247, pp. 529–551, April 1955.
- [2] Ouchi M. and Okamura H. "Effect of Super Plasticizer on Self-Compact ability of Fresh Concrete Journal of the Transportation Research Board 1997 pp37-40.
- [3] Gao Peiwei, Deng Min and Feng Naiqui: "The Influence of SP and Superfine Mineral Powder on the Flexibility, Strength and Durability of HPC. Cement and Concrete Research. 2000, Vol.31, pp703-706.
- [4] Raghuprasad P. S. et. al. "Comparative Study on Different types of Blended Cement with Different Grade O.P.C Concrete – An Experimental Approach", ICACC-2004. Proceedings of International Conference on Advances in Concrete and Construction. 16-18 December 2004, Hyderabad, Vol.II, pp637- 646.
- [5] Nan Su, Kung-Chung Hsu, His-Wen Chai "A Simple Mix Design Method for Self-Compacting Concrete" Journal of Cement and Concrete Research 31(2001) pp 1799-1807.
- [6] Seshadri Sekhar.T, Sravana. P and Srinivasa Rao. P, "Some Studies on the Permeability Behaviour of Self-Compacting Concrete" AKG Journal of Technology, Vol.1, No.2.(2005

- [7] S Venkateswara Rao, M V Seshagiri Rao, D Ramaseshu, P Rathish Kumar “A Rational Mix Design Procedure for Self-Compacting Concrete” 2010.
- [8] Naik et al, Rafat Siddique, Yogesh Aggarwal, Pratibha Aggarwal, ElHadj Kadri, Rachid Bennacer, “Strength, durability, and micro-structural properties of concrete made with Foundry Sand (FS)”, *Construction and Building Materials*, 2011, Vol. 25, pp. 1916–1925.
- [9] AndEnad Mahmoud, Ahmed Ibrahim, Hassan El-Chabib, and Varun Chowdary Patibandla “Self-Consolidating Concrete Incorporating High Volume of Fly Ash, Slag” *International Journal of Concrete Structures and Materials* Vol.7, No.2, pp.155–163, June 2013.
- [10] Arvind Kumar, Dilip Kumar “Use of Sintered Fly Ash Aggregates as Coarse Aggregate in Concrete” *SSRG International Journal of Civil Engineering (SSRG-IJCE)–volumel issue4* September 2014.
- [11] M.K Dipti Kanta Rout, Rinkan Rohit Jena “Investigation on the Development of Light Weight Concrete with Sintered Fly Ash Aggregate and Activated Fly Ash in Blended Cement” *International Journal of Engineering Research & Technology* Vol. 4 Issue 04, April-2015.
- [12] Pankaj Dhemia, B L Swami and Prakash Somani “Experimental Investigation of Light Weight Concrete Using Sintered Fly Ash Aggregates” *ICSEEGT 2021*.
- [13] Manu S. Nadesan, P. Dinakar “Mix design and properties of fly ash waste lightweight aggregates in structural lightweight concrete”
- [14] Dr.M.Vijaya Sekhar Reddy, Dr. M.C. Nataraja, K.Sindhu ,V.Harani and K.Madhuralalasa “Performance of Light Weight Concrete using Fly Ash Pellets as Coarse Aggregate Replacement” *International Journal of Engineering Research and Technology*. ISSN 0974-3154 Volume 9, Number 2 (2016).
- [15] S.Renuka, S. Viveka “Study of strength characteristics of fly ash aggregates in lightweight concrete” *International Journal of Engineering Research and Technology*.
- [16] Durga, C. S. S., Ruben, N., Chand, M. S. R., & Venkatesh, C. (2019, December). Evaluation of mechanical parameters of bacterial concrete. In *Annales de Chimie-Science des Matériaux* (Vol. 43, No. 6, pp. 395-399).
- [17] Anirudh, M., Rekha, K. S., Venkatesh, C., & Nerella, R. (2021). Characterization of red mud-based cement mortar; mechanical and microstructure studies. *Materials Today: Proceedings*, 43, 1587-1591.
- [18] Bellum, R. R., Venkatesh, C., & Madduru, S. R. C. (2021). Influence of red mud on performance enhancement of fly ash-based geopolymer concrete. *Innovative Infrastructure Solutions*, 6(4), 1-9.
- [19] Venkatesh, C., Sri Rama Chand, M., Ruben, N., & Sonali Sri Durga, C. (2021). Strength Characteristics of Red Mud and Silica Fume Based Concrete. In *Smart Technologies for Sustainable Development* (pp. 387-393). Springer, Singapore.
- [20] Bellum, R. R., Al Khazaleh, M., Pilla, R. K., Choudhary, S., & Venkatesh, C. (2022). Effect of slag on strength, durability and microstructural characteristics of fly ash-based geopolymer concrete. *Journal of Building Pathology and Rehabilitation*, 7(1), 1-15.
- [21] Venkatesh, C., Ruben, N., & Chand, M. S. R. (2020). Red mud as an additive in concrete: comprehensive characterization. *Journal of the Korean Ceramic Society*, 57(3), 281-289.
- [22] Venkatesh, C., Chand, M. S. R., & Nerella, R. (2019, April). A state-of-the-art on red mud as a substitutional cementitious material. In *Annales de Chimie: Science des Matériaux* (Vol. 43, No. 2, pp. 99-106).
- [23] Venkatesh, C., Nerella, R., & Chand, M. S. R. (2020). Comparison of mechanical and durability properties of treated and untreated red mud concrete. *Materials Today: Proceedings*, 27, 284-287.
- [24] Venkatesh, C., Nerella, R., & Chand, M. S. R. (2020). Experimental investigation of strength, durability, and microstructure of red-mud concrete. *Journal of the Korean Ceramic Society*, 57(2), 167-174.
- [25] Venkatesh, C., Nerella, R., & Chand, M. S. R. (2021). Role of red mud as a cementing material in concrete: A comprehensive study on durability behaviour. *Innovative Infrastructure Solutions*, 6(1), 1-14.
- [26] Ruben, N., Venkatesh, C., Durga, C. S. S., & Chand, M. S. R. (2021). A comprehensive study on the performance of glass fibres-based concrete. *Innovative Infrastructure Solutions*, 6(2), 1-11.
- [27] Ramanjaneyulu, N., Srigiri, K., & Rao, M. S. (2018). Strength and durability studies on lightweight self-compacting concrete with LECA as partial replacement of coarse aggregate. *CVR Journal of Science and Technology*, 15, 1-9.
- [28] Ramanjaneyulu, N., Rao, M. S., & Desai, V. B. (2019, March). Behavior of Self-Compacting Concrete Partial Replacement of Coarse Aggregate with Pumice Lightweight Aggregate. In *International Conference on Advances in Civil Engineering (ICACE-2019)* (Vol. 21, p. 23).
- [29] . Ramanjaneyulu, N., Seshagiri Rao, M V & Bhaskar Desai.,V.Comprehensive Study on Fresh and Hardened Behaviour of Sintered Fly Ash Aggregate based Lightweight Self-Consolidating Concrete in the IJSRD (International Journal of Scientific Research and Development) | Vol. 9, Issue 8, 2021 | ISSN (online): 2321-0613
- [30] T. Vijay Kumar, Ramanjaneyulu, N., Flexural Behavior of Self-compacting Concrete Beams Partially replacing Conventional aggregate with Pumice Aggregate *CVR Journal of Science and Technology*, Volume 22, June 2022

A Study on Dynamic Response of High-Rise Buildings using Lead Rubber Bearing Isolator

S. Mallikarjun¹ and A. Shruthi²

¹PG Scholar, CVR College of Engineering/Civil Engg. Department, Hyderabad, India
Email: droptomallikarjun@gmail.com

²Asst. Professor, CVR College of Engineering/Civil Engg. Department, Hyderabad, India
Email: shruthiarikeri95@gmail.com

Abstract: Seismic devastation can result in significant fatalities as well as economic damage to structures and individuals living in seismic danger zones. As shown by prior catastrophic disasters, each earthquake leaves a substantial amount of destruction in its wake. To reduce the detrimental effects of seismic activity on buildings without causing the entire structure to collapse, these structures must be seismically safeguarded. To maintain these RC structures and improve their performance during a seismic event, a variety of seismic retrofitting methods are now being employed. Base isolation is one of the most effective strategies for mitigating the effects of seismic risks.

This study uses linear and non-linear dynamic analysis as defined by IS Codal to investigate the seismic behavior of a structure with a fixed base and a structure with base isolation. Using the ETABS software, the impacts of various types of base isolator systems are taken into account in the modelling of RC structures for symmetric and asymmetric plan configurations of both G+7 and G+10 storey heights. Many parameters, such as storey drift, base shear, Storey displacement, and time period, are compared for isolated base and fixed base scenarios.

Index Terms: Base isolator, Lead Rubber bearing (LRB), Storey drift, Base shear, Time period, Storey displacement.

I. INTRODUCTION

Earthquakes are the most unanticipated and fatal of all natural calamities, and it is quite difficult to protect a large number of assets and lives from them. To cater these concerns, it is essential to assess the seismic performance of the built environment using various analytical techniques, which ensure that structures can withstand numerous mild earthquakes and provide sufficient caution when encountered to big earthquakes. Thus, the greatest number of lives possible can be saved. There are a number of recommendations that have been updated on this issue all around the world. The seismic performance of a building is influenced by its stiffness, lateral strength, ductility, and simple and regular configurations. Plan and elevation of buildings with regular, evenly distributed geometry, mass, and stiffness endure considerably less damage than buildings with uneven layouts.

The process of protecting a structure from earthquake damage by providing some reasonable support that isolates it from trembling ground is appealing, and several techniques have been proposed to achieve this goal. Despite the fact that some of the older suggestions date back hundreds of years, base isolation has only recently become a feasible earthquake-resistant design technique. It's a passive

control device that's put between the building's foundation and base. High damping rubber bearing (HDRB), Elastomeric rubber bearing (ERB), Lead rubber bearing (LRB), and Friction pendulum system (FPS) are some of the base isolation systems that must be placed under the superstructure. Despite the fact that bearings are a tiny component of a structure, their importance is inversely related to their size. This is typically the case since only this section of the structure transmits and absorbs the whole weight of the structure as well as the energy exerted by seismic waves. The many factors within the design should be given a high priority since any misbehavior in its performance due to bad design will result in the collapse of the entire structure.

Lead rubber bearing

Seismic isolation bearings include lead rubber bearings (LRB), which are similar to high damping rubber bearings. It has a central lead core and is made up of many layers of elastomeric material and vulcanized reinforced steel plates. The rubber used to make lead rubber bearings is typically natural rubber, with a shore hardness ranging from 45 to 55, making it more flexible than an elastomeric bearing pad.

In 1975, New Zealand created lead rubber bearings. Layers of steel plates, rubber layers, and a lead core are the three basic components of equipment. Vertical rigidity is provided by the steel layers, while lateral flexibility is provided by the rubber layers. The component that will provide extra rigidity to the isolators and adequate damping to the system is the lead core.

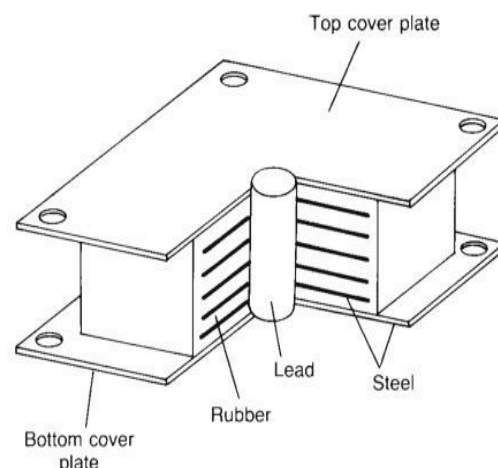


Figure 1. Components of Lead Rubber Bearing

A. Objective of the study

1. To demonstrate the impact of base isolators on the response of Symmetric and Asymmetric Buildings.
2. To compare the behavior of a base isolated structure to the conventional structure (G+10 & G+7) storey during a seismic activity.
3. To study the seismic requirements of regular and irregular R.C buildings for both regular and base isolated structure using ETABS by performing the Linear and Non-linear time history analysis.

B. Procedure adopted

A high-rise RCC building subjected to seismic activity is investigated in this study utilising both linear and non-linear time history analysis. The structures studied are RC conventional moment resistant space frames with G+10 and G+7 storeys of height that are located in Zone III seismic zones. Using the ETABS software, the research considers two major factors based on the support conditions: a building with a permanent base and a building with a Lead Rubber Bearing (LRB). The structure is proposed to be evaluated as per seismic code IS-1893:2016 with the assistance of the ETABS software.

II. LITERATURE REVIEW

Ekmath et al evaluated the building structure with and without Lead rubber bearing isolators and compared the results using time history analysis using software 2016. A case study was done using G+10 building structure as test model. This paper concluded that the time period of structure increased approximately twice after providing the base isolator and also the maximum storey displacement and storey drift were observed to be increased.[1]

Balachandran et al analysed G+3 and G+20 storey RC building with fixed base and base isolators (LRB) using ETABS software considering EI-Centro time history data. It was observed that base isolation increases the time period of the building and base shear reduced.[2]

Sahoo et al studied comparative analysis of various RC framed structures with fixed base and isolated base lead rubber bearing isolator. This base isolation study along with seismic analysis is done in equivalent static method using ETABS software considering G+10 and G+15 structures as test model with fixed base and base isolation. This study revealed that there is an increase in time period, storey drift and storey displacement. The lateral earthquake load, storey share, storey stiffness found to be reduced.[3]

Swapnil et al studied the effectiveness of base isolation using lead rubber bearing (LRB) over conventional construction. Modeling and analysis of G+6 rigid joint plane is done in ETABS software using base isolator. It is concluded that with the use of isolator, there is a reduction in story shear, base shear and storey drift. Modal displacements and natural periods are increased which reduces earthquakes forces on the shaking.[4]

Ambasta et al studied the comparative behavior of fixed base and isolated G+8 storied building for high intensity earthquakes. Lead rubber bearing (LBR) is used as

isolator. Results showed that the variation in maximum displacement of stories in base isolated model is very low while compared with fixed base mode. Storey overturning moment and storey shear force found to be reduced.[5]

Madhuri et al studied comparative study of fixed base and base isolation structures. Lead bearing rubber (LRB) is used as base isolator. Response spectrum method and time history analysis method are used for the analysis and is done through a computer software ETABS. Results showed that storey shear, base shear and storey drift reduced, point displacement and mode periods are increased in both the methods of analysis. Time history analysis was found much efficient in providing results when compared to response spectrum method.[6]

B.R.Anirudha et al had done a comparative study between the fixed base and base isolators for different parameters. Work lead rubber bearing, and friction pendulum isolators are used for asymmetric building plan. They have concluded that the fundamental time period for base model is observed that there is a decrease in acceleration, storey shear and displacement of base isolators was increased.[7]

Gowardhan et al. used high damper rubber bearing (HDRB) as isolator and non-linear time history analysis is performed using Sap2000 version14. This study showed that the base isolation system reduced the base shear force, storey drifts and storey acceleration also increase in storey displacements and time period is observed.[8]

III. METHODOLOGY

The building's dynamic analysis is done utilizing the linear and non-linear time history analytic methods that correlate to seismic zone III.

The following is an example of structural modelling with LRB.

1) ETABS software is used to create a 3-D model of a symmetrical and unsymmetrical (L-shape, T-shape) G+10 and G+7 storey building structure.

2) The 'Define Material Properties' is used to define material properties. The desired grade of concrete and steel is chosen according to Indian IS standards IS 456:2000 and IS 800:2007 respectively.

3) 'Define sectional properties' is used to assign the dimensions of Frame sections.

4) Enter the dimensions of a beam, then the design type 'Beam' (M3 design only) and the Rebar material to be considered.

5) Enter the dimensions of the column in the similar way, and by clicking on the modify/show Rebar command, choose the design type as 'Column' (p-m2-m3 design).

6) By selecting the slab material from the 'Define Slabs sections' command, the slab property can be defined. The slab thickness has to be entered, and the modelling type is set to 'membrane.'

7) After the material properties and section properties have been specified, the section properties are given to the building model by utilizing the tools available to design beams, columns, and slab panels.

- 8) The 'Define- Diaphragm' option is used to define a rigid and Flexible type of diaphragm.
 - 9) The response spectrum and time history functions for the study's targeted seismic zones are defined.
 - 10) Load patterns such as Dead load, Live load, Seismic loads, Response spectrum, and Time history load patterns are defined by selecting the required load type from the 'Define Load patterns' command.
 - 11) Load cases are defined by selecting the relevant load case type from the 'Define - Load case' command. The terms "dead load," "live load," "seismic static loads," "response spectrum," and "time history" are all used to describe load scenarios.
 - 12) Add default design load combinations from 'Define - Load combinations,' where ETABS produces load combinations for the different loads defined by the user based on Indian design codes.
- Add default design load combinations from 'Define Load combinations,' where ETABS produces load combinations for the different loads defined by the user based on Indian design codes.
- 13) Calculate and assign the exterior and internal wall loads operating on the structure.
 - 14) Assign the slab panels to the floor completion load and the live load.
 - 15) ETABS calculates the self-weight of frame components automatically and adds it by default when section attributes are provided.
 - 16) Define the term "mass source"
 - 17) Define isolator properties using the 'Link properties' option. Select the required link type, in our instance rubber isolator and high damping rubber, by defining sectional characteristics and link properties. Fill in the appropriate high damping rubber values.
 - 18) Now, using the main menu, define spring properties,
 - 19) Define spring properties point springs
The spring is then assigned to the supports. Assign springs to the joints.
 - 20) Analyze and run the model.

The Plan configuration consists of

1. Model 1- G+10 Building Rectangular plan
2. Model 2- G+7 Building Rectangular plan
3. Model 3- G+10 Building L-shaped plan Asymmetry,
4. Model 4- G+7 Building L-shaped plan Asymmetry,
5. Model 5- G+10 Building T-shaped plan Asymmetry
6. Model 6- G+7 Building T-shaped plan Asymmetry

Rubber bearings were simulated in ETABS using hysteretic isolator linkages. At the foundation level, an isolator link is assigned to each column as a single joint member to connect the superstructure to the ground. Rubber with a lot of dampening as a rubber isolator link, bearing links were used. The Link/Support Property in ETABS determines how link elements behave. Mechanical activity in six directions is represented by directional attributes U1, U2, U3, R1, R2, and R3. Axial deformation (U1) has solely linear qualities, while shear deformations (U2, U3) have both linear and nonlinear features. Also, the tensional

deformation (R) around U1 is merely linear. Rotations above U2 and U3 are solely linear (R2 & R3). The isolator linkages' internal deformations are believed to be independent of one another.

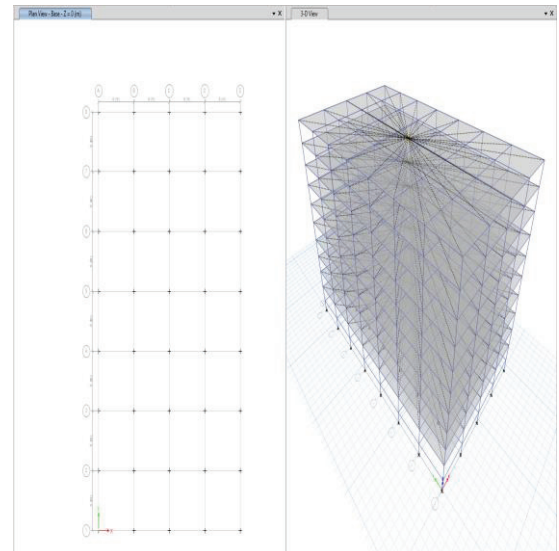


Figure 2. Plan and Isometric view of Model-1 with LRB G+10

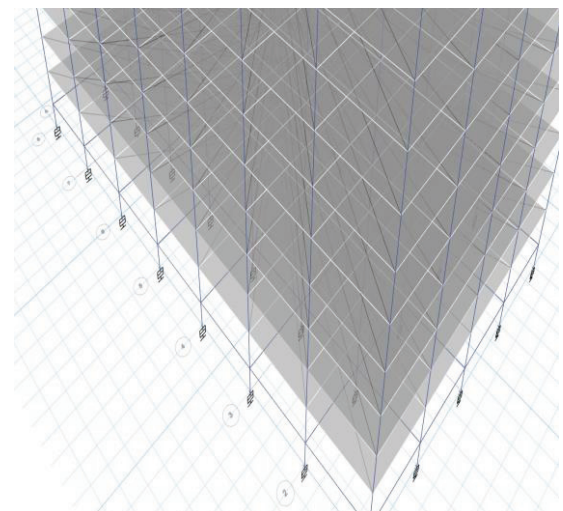


Figure 3. LRB Isolator installed at the fixed supports

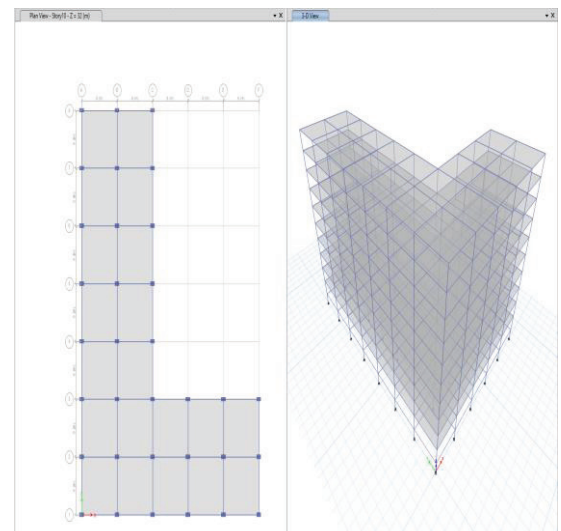


Figure 4. Plan and Isometric view of Model-3 with LRB G+10

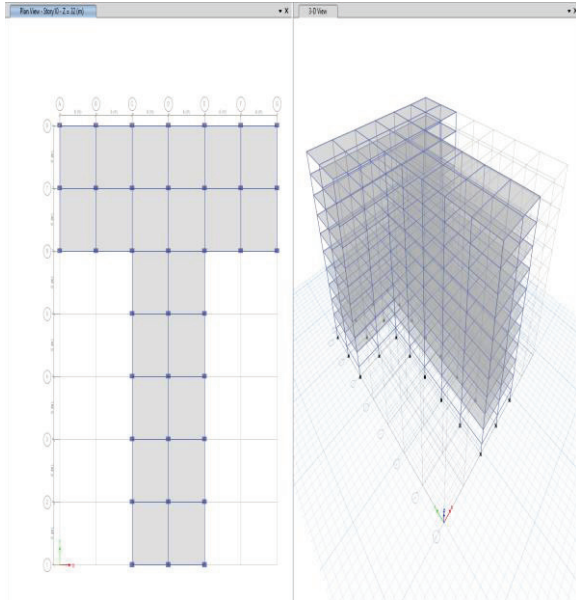


Figure 5. Plan and Isometric view of Model-5 with LRB G+10

III. SPECIMEN CALCULATIONS

Assumed Preliminary Data Required for the Analysis of the Frame

TABLE I.
PRELIMINARY DATA

Type of structure	Ordinary Moment Resisting Frame
Materials	M30, Fe-500
Size of Beams	300x450 mm
Size of Columns	450x750 mm
Depth of slab	150 mm
Wall load Internal & External	11.14kN/m, 5.57kN/m
Seismic zone	III
Zone Factor	0.16
Response Reduction Factor	3

Design of Lead Rubber Bearing

Assume design time period, $T_D = 2.5$ sec (Kelly,1986)

Maximum vertical load on individual column,

$$w = 4011 \text{ kN (For G+10 building)}$$

a) **Effective stiffness, K_{eff}** $= \frac{W}{g} \times \left(\frac{2\pi}{T_D}\right)^2$ kN/m

$$= \frac{4011}{9.81} \times \left(\frac{2 \times 3.11}{2.5}\right)^2$$

$$= 2582.637 \text{ kN/m}$$

b) **Design Displacement, D_d** $= \frac{g C_{VD} T_D}{4\pi^2 B_D}$, m

Seismic coefficient $C_{VD} = 0.54$ (UBC 97, Vol -2, Table 16- R, For zone-3 & S_D)

$$= \frac{9.81 \times 0.54 \times 2.5}{4 \times 3.11^2 \times 1}$$

$$= 0.33546 \text{ m}$$

c) **Energy dissipated per cycle, W_D** $= 2\pi k_{eff} D_D^2 \beta_{eff}$ kN-m

Effective damping, $\beta_{eff} = 5\%$ (5% damping is considered for the LRB)

$$= 2 \times 0.311 \times 2582.637 \times 0.33546^2 \times 1$$

$$= 91.306 \text{ kN-m}$$

d) **Characteristic Strength, Q** $= \frac{W_D}{4D_D}$, kn

$$= \frac{91.306}{4 \times 0.3354}$$

$$= 68.0450 \text{ kN}$$

e) **Pre-Yield Rubber, $K_2 = K_{eff} - \frac{Q}{D_D}$** , KN/m

$$= 2582.63 - \frac{68.045012}{0.33546}$$

$$= 2379.7972 \text{ kN/m}$$

Post – Yield stiffness, $k_1 = 10k_2$ (Kelly,1986)

$$= 23797.97 \text{ kN/m}$$

f) **Yield Displacement (Distance from**

END -J), $D_Y = \frac{Q}{K_1 - K_2}$, m

$$= \frac{68.045012}{23797.972 - 2379.7972}$$

$$= 0.003177 \text{ m}$$

g) **Recalculation of Force Q TO Q_R**

$$= \frac{W_D}{4 \times D_D - D_Y}$$
, kN
$$= \frac{91.306002}{4 \times (0.3354618 - 0.003177)}$$

$$= 68.69559 \text{ KN}$$

h) **Area of lead plug required, $A_{PB} =$**

$$\frac{Q_R}{\text{Yield strength of lead}}$$

Yield strength of lead = 10MN/m² (Mayes and Naeim,2000)

$$= \frac{68.69559}{10 \times 10^6} = 0.0068696 \text{ m}$$

Diameter of lead plug required,
 $d = 0.0935232\text{m}$

$$= \frac{249131.94 * 1.1395434}{0.3354618}$$

$$= 846286.21\text{kN/m}$$

i) Recalculation of rubber stiffness K_{eff} to $k_{\text{eff}(R)}$

$$= K_{\text{eff}} - \frac{Q_R}{D_D}$$

$$= 2582.637 - \frac{68.69559}{0.3354618}$$

$$= 2377.8578 \text{ KN/m}$$

p) Yield strength, $F_y = Q + K_2 * D_y$, KN
 $= 68.04502 + 2379.7972 * 0.003177$
 $= 75.60556\text{KN}$

Input values of LRB in ETABS

For G+10 Regular Building

U1 Effective Stiffness = 846286.211kN/m
 U2 & U3 Eff. Stiffness = 2582.637032kN-m
 U2 & U3 Eff. Damping = 0.05
 U2 & U3 Distance from End-J = 0.0031m
 U2 & U3 non-linear Stiffness= 2379.797194kN/m
 U2 & U3 Yield Strength = 75.6055688KN

For G+7 Regular Building

Support reaction: 2940KN
 U1 Effective Stiffness = 620314.5002kN/m
 U2 & U3 Eff Stiffness = 1893.032379kN-m
 U2 & U3 Effective Damping = 0.05
 U2 & U3 Distance from End-J = 0.00317m
 U2 & U3 non-linear Stiffness = 1744.353964kN/m
 U2 & U3 Yield Strength = 55.41769441KN

j) Total thickness of rubber, $t_r = \frac{D_D}{\gamma}$, m

Maximum shear strain of rubber, $\gamma = 100\%$
 $= \frac{0.3354618}{1}$
 $= 0.3354618\text{m}$

k) Shape factor, $s = \frac{1}{2.4} * \frac{f_v}{f_h}$

Horizontal time period = 2sec (Kelly ,1986)
 Horizontal frequency, $f_h = 0.5\text{hz}$
 Vertical frequency, $f_v = 10\text{hz}$ (Kelly,1986)
 $S = 8.3333$

l) Area of bearing, $A_{LRB} = \frac{K_{\text{eff}(R)} * t_r}{G}$, m^2
 $= \frac{2377.8578 * 0.3354618}{0.7 * 1000}$
 $= 1.13954$

Diameter of bearing = 1.204538m

m) Single layer rubber thickness, $t = \frac{\phi_{LRB}}{4S}$

$$= \frac{1.204538}{4 * 8.333} = 36\text{mm}$$

Number of rubber layers, $N = 9.2832$
 Thickness of shim plates = 2.8mm (Kelly ,1986)
 No. of shim plates, $n = N - 1$
 $= 10 - 1$
 $= 8.2832$

End plates thickness is between 19mm to 38mm,
choose 25mm

n) Compression modulus, $E_c = 6GS^2 \left(1 - \frac{6GS^2}{K}\right)$

Bulk modulus, $K = 249131.94\text{kN/m}^2$

o) Vertical stiffness, $k_v = \frac{E_c * A_{LRB}}{t_r}$

V. RESULTS OBTAINED FROM ETABS SOFTWARE:

Time period(sec):

TABLE II.
TIME PERIOD FOR SYMMETRIC BUILDING

	G+10 TIME PERIOD (Sec)		G+7 TIME PERIOD (Sec)	
	FNA	LDI	FNA	LDI
Fixed	1.913	2.01	1.471	1.471
LRB	3.233	3.23	2.514	2.70
% Change	69%	61%	71%	84%

TABLE III.
TIME PERIOD FOR UNSYMMETRIC BUILDING

UNSYMMETRIC BUILDING TIME PERIOD (Sec)			
		FIXED	LRB
G+10 L SHAPE	FNA	2.08	2.883
	LDI	2.08	2.883
G+7 L SHAPE	FNA	1.704	2.37
	LDI	1.704	2.37
G+10 T SHAPE	FNA	2.031	2.91
	LDI	2.031	2.1
G+10 L SHAPE	FNA	1.445	2.46
	LDI	1.445	2.46

Max storey Displacement(mm)

Story displacement is the lateral displacement of the story relative to the base

TABLE IV.
MAXIMUM STORY DISPLACEMENT

Base Type	Symmetric Plan		Asymmetric Plan			
	G+10	G+7	G+10	G+7	G+10	G+7
	Rectangular	Rectangular	L-shape	T-shape	L-shape	T-shape
Fixed	26.12	19.125	29.622	27.19	20.18	14.50
LRB	21.04	21.25	26.45	25.84	21.15	16.61

Storey Drift ratio

Story drift is the relative displacement of one-story relative to the other.

TABLE V.
STORY DRIFT

Base Type	Symmetric Plan		Asymmetric Plan			
	G+10	G+7	G+10	G+7	G+10	G+7
	Rectangular	Rectangular	L-shape	T-shape	L-shape	T-shape
Fixed	0.00156	0.00205	0.0018	0.00125	0.0015	0.000897
LRB	0.00146	0.00085	0.00121	0.00127	0.001057	0.000848

Base shear(KN):

Base shear is an estimate of the maximum expected lateral force on the base of the structure due to seismic activity

TABLE VI.
BASE SHEAR

BASE SHEAR (kN)			
		FIXED	LRB
G+10 L SHAPE	FNA	-861.22	-552.35
	LDI	-932.53	-682.34
G+7 L SHAPE	FNA	-800.33	-556.13
	LDI	-814.76	-599.22
G+10 T SHAPE	FNA	-1141.31	-614.47
	LDI	-1139.66	-775.98
G+7 T SHAPE	FNA	-1165.88	-469.35
	LDI	-1155.03	-586.83
G+10 Regular	FNA	-1040.53	-692.80
	LDI	-1111.99	-954.27
G+7 Regular	FNA	-1074.34	-723.42
	LDI	-1083.82	-757.24

VI. CONCLUSIONS

1. The study's goal to introduce the base isolation approach for symmetric and asymmetric structures utilising the ETABS package is achieved.

2. For both L-shaped and T-shaped buildings, the magnitude of base shear, Max storey displacement, storey drift, and storey shear has been shown to decrease with the installation of the Lead Rubber Bearing (LRB).

3. The effect of the base isolator is observed to enhance the time period for both G+7 and G+10 storey asymmetric structures, indicating that the performance of the base isolated structure is superior to the structure without any isolation.

4. When analysing a G+7 structure utilising the Non-linear FNA method, LRB revealed a higher contribution.

5. LRB had a larger impact in lowering the Base shear for both Linear and Non-Linear analysis for a G+10 L-shaped and T-shaped structure.

6. The different parameters considered for evaluating the structures responses are found to be satisfactory in comparative studies made from conventional and isolated (G+10, G+7) storied buildings subjected to Linear and Non-linear analysis, proving that the base isolation technique is flexible to adopt for highly seismic areas.

7. The contribution of LRB is found to be more effective in asymmetric buildings, whereas it is found to be less effective in symmetric structures.

REFERENCES

- [1] Sahil Eknath laste et. al “Evaluation Of G+10 Structure For Seismic Performance Under Base Isolation” International Research Journal of Engineering and Technology (IRJET), April 2019.
- [2] Bhavana Balachandran, Susan Abraham “Effect of base isolation in multistoried RC building”, IOSR Journal of Engineering, June 2018.
- [3] Dhiraj narayan saho and Dr. Prof. Pravat Kumar Parhi, “Base Isoation Of Residential Building Using Lead Rubber Bearing Technique” International Journal of Engineering Research & Technology (IJERT), May 2018
- [4] Swapnil Ambasta, Dushyant sahu, G.P. Khare “Analysis of the base isolated building (Lead plug bearing) in ETABS”, International Research Journal of Engineering and Technology (IRJET), January 2018.
- [5] Abhyuday Titiksh et al “Seismic Behavioral Analysis of Fixed Base and Base Isolated Structures”, June 2017
- [6] MD Nouman and N. Monica Madhuri “Earthquake Resistant Structure with Base Isolation System”, AIJREAS, January 2017.
- [7] B.R Anirudha, R.J. Fernandes “Performance of Base Isolated Building Structures with Asymmetry in plan”, International Journal of Engineering Research & Technology (IJERT) September 2015.
- [8] S.D. Gowardhan, Manoj U. Deosarkar “Protection of the Buildings from the Earthquake Risk Using High Damping Rubber Bearing”, Journal of Civil Engineering and Environmental Technology, June 2015

Standard codes

- [1] IS 456:2000, “Plain and Reinforced Concrete - Code of Practice”, Bureau of Indian Standards, New Delhi, 2000.
- [2] IS 875 1987 “Code of practice for design loads (other than earthquake) for buildings and structures part 3 wind Loads”.
- [3] IS 1893-2016 “Criteria for Earthquake Resistant Design of building”
- [4] UBC, “Uniform Building Code Vol 2”, International Conference of Building Officials, USA, 1997.
- [5] International Code Council, International Building Code 2006, U.S.A

Travel Time and Congestion Analysis of Heterogeneous Traffic Condition, a Case Study on Kothapet Signal to Nalgonda X-Road Signal Road

Kona Mahesh¹, Gunda Sharanya² and P. Yashwanth³

¹Asst. Professor, CVR College of Engineering/Civil Engg. Department, Hyderabad, India
Email: kmahesh@cvr.ac.in

²Asst. Professor, CVR College of Engineering/Civil Engg. Department, Hyderabad, India
Email: g.sharanya@cvr.ac.in

³Assoc. Professor, CVR College of Engineering/Civil Engg. Department, Hyderabad, India
Email: yashwanth.pamu@cvr.ac.in

Abstract: The vehicular population in Hyderabad is around 50,00,000 (as of 2018), so it is very essential to manage its movement and ill effects like noise pollution, traffic congestion, waiting time at signals. In this project we have considered one of the busiest routes i.e., Chaderghat circle- LB nagar circle, these areas have heavy traffic due to college buses, city buses, two-wheeler, four wheelers and also heavy trucks (transport loaded vehicles). For addressing the traffic congestion, volume count survey (by video graphic method), travel time and delay survey (by moving observer method), origin-destination survey (by license plate matching method) of 7 days i.e. throughout the week and for speed-flow-density relationship spot speed study at Nalgonda X road, Moosarambagh Signal, and Kothapet is to be performed and analyzed. From the calculated data, graph of flow v/s density, speed v/s density, speed v/s flow relationship is to be developed. From all analyzed data, alternative remedial measures are explored. Based on the alternative remedial measures best alternative is chosen.

Keywords: Traffic study, Travel time, Traffic congestion, Spot speed study

I. INTRODUCTION

Over the last two decades there is a rapid growth in the concept of urbanization in India [1]. Due to the urbanization, the demand in transportation facilities which are the basic need of the country's population has increased tremendously [1]. The urban traffic population has increased much more due to rapid growth in employment for daily wages as there is a boost in urbanization.

So, it is prime objective of transportation fraternity to provide new and impactful solution to the existing situation for better management [2]. There are situations where metro rail is active but the traffic congestion [3] is still the same, for example, kothapet signal – moosarambagh signal – Nalgonda X road signal, where the average waiting time of a vehicle is considerably more than that of other metro rail regions.

II. OBJECTIVES

Controlling the traffic jams on roads due to increase in the number of vehicles

- Saving the time of the people at the intersection.

- To control traffic data like; traffic volume; Speed; Capacity.
- To regulate the capacity and level of service for a given stretch of the road.
- To analyze the Level of Service of the on kothapet signal to Nalgonda X road signal in Hyderabad.
- To find the hourly traffic speed volume variation on kothapet signal to Nalgonda x road signal in Hyderabad.
- To identify the causes of traffic congestion on kothapet signal to Nalgonda x road signal in Hyderabad.
- To suggest the solutions for the best quality of traffic on kothapet signal to Nalgonda x road signal in Hyderabad.

III. TRAFFIC STUDY & ANALYSIS

1. Study Area

Hyderabad is integrated into the National Highway Network of India through NH 44, NH 65, NH 163, NH 765, NH 765D, while four State Highways SH1, SH4, SH 6, SH 19 originate/terminate in Hyderabad. Hyderabad has a vehicle population of nearly 48 lakhs and is the highest after Delhi, Bengaluru, Chennai and Mumbai.

Kothapet signal to Nalgonda X Road signal is one of the busiest roads in Hyderabad; it has very increased variations of the traffic at different time. It has a very high traffic congestion during morning and evening due to which the travel time increases, one of the reasons for the traffic congestion is given below and the other is covered in the other sections

Road from Kothapet signal to Nalgonda X Road signal. This road is also one of the oldest and popular roads of the city area. Length of the study area=4.6km No. of lanes=4 and 3 lanes

2. Travel Time Study

The objective of Travel Time and Delay Study is to calculate the quality of traffic movement along a route and to fix the locations, types, and extent of traffic delays by moving test vehicle method [4].

From the data analysis it is revealed that on Sunday the Average journey time, average running time and delay is lowest compared to working day. While the average journey time and delay time from Nalgonda X road signal to Kothapet signal at morning hours (Peak hours (8:00Am – 10:30Am)) and from Nalgonda X road signal to Kothapet signal at evening hours (Peak hours (4:00Pm – 6:00Pm)) is more compared to the Sunday and afternoon hours of the weekdays.

Fig 1 shows the graph representation of travel time survey on a particular day.

This travel time and delay time may increase in the future with the increase in vehicular number [5], certain measures should be taken to overcome this issue, remedial measures are covered at the conclusion.

3. Spot Speed Study & Volume Count Survey

Speed is defined as distance per time of travel, and it depends on every trip. It may change according to the volume of traffic.

The stopwatch method is used for spot speed study analysis using a small sample size taken over a relatively shorter period of time. The stopwatch method is a quick and economical method for collection of speed data.

The analysis is primary to achieve the objective. Collected data is compiled in a tabulation after the collection of data in the below mentioned way for analyzing the data. Analysis is done to know the key parameters such as Mean Speed of the vehicle, 85th Percentile Speed, 98th Percentile Speed, 50th Percentile, Mode, Median and Speed variance. 50th percentile speed signifies the average speed of the traffic [10]. The 85th percentile speed signifies the speed at which 85% of the observed vehicles are travelling at or below the particular speed, this percentile speed used in recommended for posted speed limits based on the assumption that 85% of the drivers are travelling at a speed they recognize to be safe. The 98th percentile speed is the speed at which 98% of observed vehicles are travelling at or below that particular speed. The 98th percentile is considered as the design speed.

i. At moosarambagh towards Nalgonda X road signal, for vehicle type: 2-wheeler on Monday:

Maximum Speed = 85th Percentile Speed= 33.71 Kmph
Minimum Speed = 15th Percentile Speed= 20.28 Kmph
Design Speed = 98th Percentile Speed= 36.96Kmph
Median Speed = 50th Percentile Speed= 27.44 Kmph

ii. At moosarambagh towards Nalgonda X road signal for vehicle type: 4-wheeler on Monday:

Maximum Speed = 85th Percentile Speed= 35.69 Kmph
Minimum Speed = 15th Percentile Speed= 15.61 Kmph
Design Speed = 98th Percentile Speed= 41.02 Kmph
Median Speed = 50th Percentile Speed= 27.62 Kmph

iii. At moosarambagh towards Nalgonda X road signal for vehicle type: 2-wheeler on Sunday:

Maximum Speed = 85th Percentile Speed= 41.61 Kmph
Minimum Speed = 15th Percentile Speed= 25.19 Kmph
Design Speed = 98th Percentile Speed= 49.29 Kmph
Median Speed = 50th Percentile Speed= 39.69 Kmph

iv. At moosarambagh towards Nalgonda X Road signal for vehicle type: 4-wheeler on Sunday:

Maximum Speed = 85th Percentile Speed= 35.56 Kmph
Minimum Speed = 15th Percentile Speed= 20.31 Kmph
Design Speed = 98th Percentile Speed= 48.83 Kmph
Median Speed = 50th Percentile Speed= 27 Kmph

Table 1 Shows the data with respect to the spot speed study.

The design speed should be adopted based on the isolated speed limit of the road. The vehicles found in the lower 15 percent are considered to be travelling arbitrarily direct and those saw over the 85th percentile is thought to outstrip a secured and reasonable speed. 85th percentile could be a deciding factor for fixing the speed limit because it is protected and reasonable under favorable conditions.

Traffic Volume Count is usually expressed in terms of Passenger Car Unit (PCU). The main objective of the ordered traffic volume count is to know the traffic the traffic patterns based on the data collected, and also to provide feasible solution for nullifying the problem identified [6], [11].

The Traffic Volume survey was conducted on 17-02- 2020 (Monday), 21-02-2020 (Friday), 23-02-2020 (Sunday), in the Morning and Evening peak hours. The volume of vehicles is obtained from video recording, then forecasted for the future to take the remedial measure for the future, the ultimate goal of the project is to forecast the flow for the future and take necessary measures for the future [7].

4. Origin - Destination Survey:

An origin-destination study is used to determine travel patterns of traffic on an installation during a typical day. They are useful in assisting long-range traffic planning [9]. From the road side interviews, it clearly indicates that most of **them use this route for work** and schools/college, which indicates that in future time there will be heavy increase in the vehicles due to the road being the intermediate for the work purpose and schools/college.

5. Level of Service

Level-of-Service (LOS) is introduced by HCM to denote the level of quality one can derive from a local under different operation characteristics and traffic volume [8], [13]. Level of service is nearer to C during the non-peak hours and may go upto D, and level of service is nearer to D and may go upto E during peak hours, the level of service is E, at moosarambagh signal towards Nalgonda X road signal during morning and evening at Nalgonda X road signal towards Moosarambagh signal. Level of service will be beyond F in the future traffic conditions.

IV. HELPFUL HINTS

A. FIGURES AND TABLES

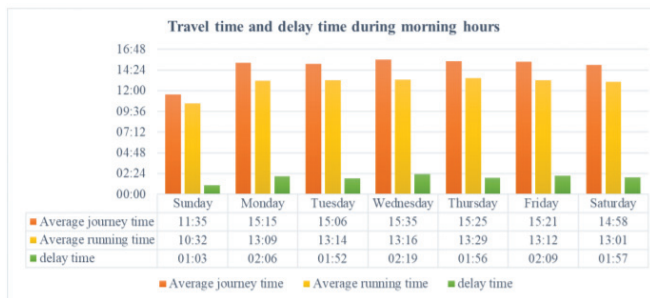


Fig1: Travel time and delay time during morning hours throughout the week from Kothapet signal to Nalgonda X road signal (8:30am -10:30am)

TABLE I.
SPOT SPEED STUDY ON MONDAY FOR 2-WHEELERS

Location: Moosarambagh towards Nalgonda X road signal					
Weather: Good					
Base length: 30m, measurement technique: manually					
Date:10-02-2020					
Time:4:00-6:00pm					
Vehicle: 2-wheeler					
Speed class limits(km/hr)	Mid point speed (km/hr)	No. of vehicles	Frequency %	Cummulative frequency %	f_x
15-19	17	3	5.45	5.45	51
20-24	22	8	14.54	19.99	176
25-29	27	15	27.27	47.26	405
30-34	32	17	30.91	78.17	374
35-39	37	11	20	98.17	407
40-44	42	0	0	98.17	0
45-49	47	1	1.81	100	47
50-54	52	0	0	100	0
		$\Sigma f = 55$			$\Sigma f_x = 1460$

Average speed of the 2-wheelers= $1460/55=26.55\text{km/hr}$

V. CONCLUSIONS

As the number of vehicles has increased much rapidly resulting in congestion. If the count of vehicles increases by next 8-10 years, then there will be serious in congestion on the roadways and commuters will face very much difficulty. It is a clear message that regulatory bodies will have to take a big leap, especially in terms of traffic management in cities like Hyderabad. So, we need to step up and bring a change on road capacity and maintain proper level of service or reduce it to minimum. If more and more public transport is utilized, then there are more chances of reducing the LOS to minimum level. From our study we had observed a LOS C, D, E and F, which is increasing the travel time of

commuters and at times it causes headache to the drivers and commuters as well.

Need of bus facility as major transport mode with the frequency of 1 bus/minute. Parking facilities like Multilevel parking should be provided with user charges. Parking facilities need to be improved, which also acts as commuters more travel time and due to this congestion comes into picture. Real-Time Traffic Feedback: The real-time traffic feedback, not just for where exactly the streetcar is at all times but also the traffic around the downtown area, that shows available parking spaces, etc. will affect the use of public transit. Real-time traffic feedback also makes concepts like “congestion pricing” a little easier to sell to consumers who’re used to using roads for free [12]. Autonomous Vehicle Technology: Autonomous vehicles are likely to reduce congestion with fewer accidents and driver-caused traffic. It would eliminate human error that causes issues like “phantom traffic,” which is caused by the ripple effect of a driver braking in the middle of a freeway. As a long-term solution, Skybus technology can be implemented rather than that of metro train.

REFERENCES

- [1] Travel Time & Congestion Analysis under Heterogeneous Traffic Condition of C.B.D. Area Case Study of Surat-Rajmarg (Chowk Bazar to Delhi Gate) Mrugesh J. Solanki*, F. S. Umrigar, L. B. Zala and Amit A. Amin
- [2] Congestion Modelling for Heterogeneous Traffic Sruthy Henry M. Tech Transportation Engineering.
- [3] Survey of Traffic Volume Forecasting Aditi R. Pawar, Shailendra S. Aote.
- [4] Suggestive measures travel time and congestion analysis under heterogeneous traffic conditions, Sameer ahmedchadoo, dept. of civil engg. Lovely Professional University, Punjab, India
- [5] Traffic Congestion Analysis: A Case Study of Kacherithazham Muvattupuzha Road Emy Paulose, Akshay Kumar C, Christeena Thomas, Sruthi S, Viniitha Viswanath
- [6] Traffic data collection, nptel Quantifying Traffic Congestion by Studying Traffic Flow Characteristics in Wolaita Sodo Town, Ethiopia Mengistu Mena Kuleno, Habte DebisaDenno, GebrefilmunaAbera, Dr Raju Ramesh Reddy.
- [7] Forecasting Travel Time Reliability in Road Transport A New Model for The Netherlands
- [8] IRC 106-1990 code book: Guidelines for capacity of urban roads in plain areas.
- [9] Traffic Congestion Quantification for Urban Heterogeneous Traffic Using Public Transit Buses as Probes Selvaraj Vasantha Kumar, Ramaswamy Sivanandan
- [10] Traffic flow variables estimation: an automated procedure based on moving observer method. Potential application for autonomous vehicles marcoguerrieri, giuseppeparla, raffaelemauro
- [11] Congestion Modelling for Heterogeneous Traffic Sruthy Henry M.Tech Transportation Engineering Rajiv Gandhi Institute of Technology Kottayam
- [12] Understanding urban travel demand, Gary barnes, center of transport facilities.
- [13] Level of Service of Roads in Vijayawada M. Manoj Kumar, S.Hari Prasanna Rao, B.Lalithya, P.Sai Bhargavi,A.Pavankumar

Anaerobic Co-Digestion of Tomato Waste to Enhance the Production of Methane gas

Srikanth Merugu¹ and K. Ravi Chandra Reddy²

¹PG Scholar, Department of Environmental Management, Jawaharlal Nehru Technology University, Hyderabad, India.

Email: srikanthmerugu14@gmail.com

²Asst. Professor, CVR College of Engineering/Civil Engg. Department, Hyderabad, India.

Email: krc.reddy@cvr.ac.in

Abstract: Tomatoes are the most commonly used vegetable for cooking purposes and the fastest damaging vegetable in its lifetime. Tomato waste is a low-cost source of organic compounds, such as antioxidants, soluble dietary fibers, and vitamins. The high initial moisture content of fresh tomato pomace makes this waste susceptible to the Digestion process. Tomato waste or any organic waste using an anaerobic digestion process will produce the biogas and also generates greenhouse gases like CO₂, CH₄, and other trace elements. But, to increase productivity adding sewage sludge (as a second substrate) also called a Co-substrate. The addition of two substrates in a digestion process is called as Co-Digestion process. This process will increase the C/N ratio, Alkalinity, Total solids, etc., which will balance the key parameters to speed up the digestion process and eventually biogas production. The biggest role in biogas production is played by different types of microorganisms that consume the organic matter, and it will reduce the strength of the waste microorganisms like saprophytic bacteria and methanogenic bacteria will play into action in the digestion process.

Index Terms: Tomato waste, Anaerobic Digestion, Biogas, Greenhouse gas, Microorganisms.

I. INTRODUCTION

Organic waste output has increased significantly in recent years. Included are food leftovers, discarded fruit and vegetables, garden refuse, and other organic waste [1]. For this organic waste, treatment is urgently required. Aerobic and Anaerobic treatment processes are available for treating organic waste [2]. Aerobically processing organic waste consumes a lot of space, has an unpleasant odor, and creates greenhouse gases like CH₄ and CO₂ [2]. Anaerobic digestion is processing organic matter in an enclosed (airtight) space with the help of bacteria to degrade the organic matter and convert the waste into a useful product like Biogas [3].

Anaerobic Digestion can be done in two ways; those are

1. Mono-Digestion.
2. Co-Digestion.

Mono-digestion (i.e., anaerobic digestion using one feedstock) suffers from challenges associated with feedstock characteristics [4].

Co-digestion using multiple feedstocks provides the potential to overcome these limitations [4].

Two bacterial groups are used in the anaerobic digestion process to break down organic matter and create biogas, which has productivity of 0.45 Nm³/Kg/V and helps to lower the density and strength of waste [5]. Saprophytic bacteria are collectively referred to as acid formers.

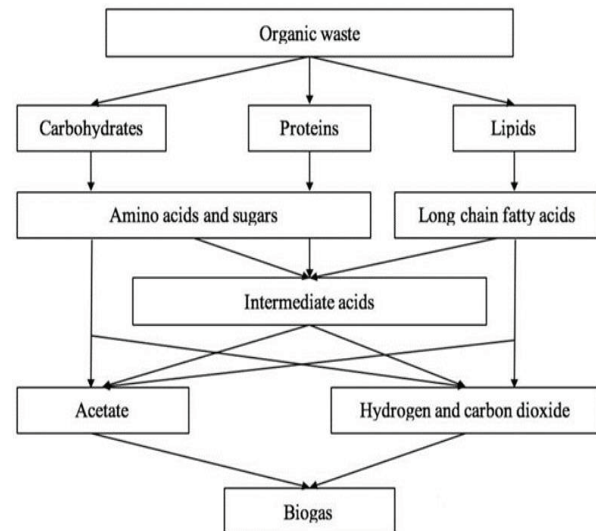


Figure 1. Simplification of Anaerobic Digestion

Methanogenic bacteria exploit the volatile fatty acids produced by saprophytic bacteria to create methane gas as a consequence of their metabolism [5]. This methane gas may be utilized as a source of energy for household and commercial purposes as well as fuel for automobiles. The digestion process is carried out in four stages by different types of microorganisms. The four stages are followed Hydrolysis, Acidogenesis, Acetogenesis, and methanogenesis [6]. In the hydrolysis process, organic matter breaks down into small pieces by microorganisms in the digestion, Acidogenesis will break down the remaining organic matter into the smallest pieces by releasing acids and forming volatile fatty acids. Using these VFA produces some gas in the Acetogenesis process [7]. Methanogenesis bacteria convert the biogas into methane gas. Temperature (37° C) is the key parameter for these microbes to survive in the digester [7].

Anaerobic decomposition may be built and developed to operate in a wide range of configurations, including batch vs continuous processes, mesophilic vs thermophilic temperature conditions, high vs low particulate particles, and single vs. multistage processes [8].

Because batch process digesters need more initial construction money and a bigger volume of digesters (spread across numerous batches) to manage the same quantity of waste as continuous process digesters, they are more difficult to design but may be more cost-effective [9].

TABLE I.
DESIRABLE CONDITIONS FOR ANAEROBIC DIGESTION

Operational Parameters	Optimum Range
Temperature	Psychrophilic (<20°C)
	Mesophilic (20.-40°C)
	Thermophilic (45-60°C)
	Hyper-thermophilic (>60°C)
pH	6.8-8.8
Alkalinity	2000-5000 mg/l as CaCO ₃
Carbon to nitrogen ratio (C: N)	20-30
The substrate to inoculum (I/S)	0.5-2 and 2-3
Retention time	10-50 days
Volatile fatty acids	VFA<8000mg/l
Ammonia (NH ₃)	NH ₃ <700mg/l
Hydrogen sulfide (H ₂ S)	H ₂ S<200mg/l

II. MATERIAL AND ITS COLLECTION

A. Tomato Waste (Substrate)

Tomato waste is collected from the local Erragadda vegetable market located in Hyderabad, India. It generates 100 kg of tomato waste daily. Which is a low-cost source of organic compounds, such as antioxidants, soluble dietary fibers, and vitamins. Fresh tomato pomace has a high initial moisture level, making it vulnerable to anaerobic digestion, which produces biogas from tomato waste and other organic waste [10]. The seeds are included as a source of edible oil, while tomato seed flakes are listed as a source of protein. The peel component of the trash contains significant amounts of phenolic and carotenoids [10]. The seeds are a source of protein (35%) and fat (60%) and account for around 10% of the fruit and 60% of the total waste, respectively (25%). They have a complex composition, with 17.6% protein, 2.2 percent fat, and 52.4 percent fiber. Essential amino acids accounted for 34.2 percent of total protein, with leucine being the most abundant, followed by lysine and isoleucine [11]. Unsaturated fatty acids made up 77.04 percent of total fatty acids, with linoleic acid being the most common [11].

B. Sewage sludge (Co-substrate)

Sewage sludge is collected from the Sewage Treatment Plant (STP) located at CVR College of Engineering, Hyderabad, India. Which is the Institutional drainage waste like Toilet waste, Flush waste, Hostel kitchen cleaning waste, etc. Sewage sludge, commonly referred to as bio solids, is the leftover, semi-solid material, which has high organic matter and moisture content.

The specific gravity, solids concentration as the relative proportion of solids, and sludge volume index (SVI) are some of the significant Physic-chemical parameters of sewage sludge [12]. In general, sewage sludge has a 20 percent fat content, a 50 percent carbohydrate content (sugar, starch, and fiber), a 30 to 40 percent organic matter content, a 3 percent total nitrogen content, a 1.5 percent total phosphorus content, a 0.7 percent total potassium content, a 10 to 20 percent C/N ratio, and a high concentration of heavy metal ions [13].

C. Inoculum

A little amount of material called an inoculum is used to start a culture containing bacteria, viruses, or other microbes [14]. In biology, the source substance utilized for inoculation is referred to as an inoculum. Inoculum is a material used as the inoculation source for a vaccine in medicine. In microbiology, pathogens are cells, tissues, or viruses used to inoculate a fresh culture [14].

Primary and secondary inoculum, which result in primary and secondary infection, are the two different forms of inoculum. The term "primary inoculum" refers to pathogens, such as spores, mycelium, etc., that overwinter or over summer and start an infection. During the same growing season, infections result in the production of secondary inoculum. Applying inoculum to a host is the procedure of vaccination [14]. Which is collected from the Biogas digestion reactor located at CVR College of Engineering, Hyderabad, India.

D. Cow Dung

Cow dung, often known as cow pats, cow pies, or cow manure, is the feces of bovine animals. Domestic cattle ("cows"), bison ("buffalo"), yak, and water buffalo are among these animals. Cow dung has antibacterial and prophylactic (disease-preventive) qualities, according to research [3]. Several investigations have found that cow dung extract has potent antibacterial properties against a variety of harmful microorganisms [3].

It also contains 24 more minerals, such as nitrogen and potassium, as well as minute quantities of sulfur, iron, magnesium, copper, cobalt, and manganese. It has been discovered that the antibacterial qualities of cow manure from a variety of cows are efficient against Klebsiella pneumonia [4].

Indian cow dung has demonstrated antimicrobial activity against all tested microbes and had stronger antibacterial activity than other cow dung extracts [4].

The milk, dung, and urine of the cow can be used to cure illnesses including psoriasis, skin conditions, eczema, arthritis, inflammation, leprosy, and more. Cow urine is also utilized as a medicine in India, Nigeria, Nepal, and Myanmar [3].

However, this behavior has dramatically increased since the COVID19 epidemic hit India. Under the name of "cow dung therapy," many people are consuming cow dung and urine for COVID treatment. Hundreds of Hindu activists celebrated by drinking cow urine last year in India. Cow Dung is collected from the dairy form at a local place [3].

TABLE II.
PROXIMATE ANALYSIS OF SUBSTRATE MATERIALS

Name	pH	Alkalinity (mg/l)	Total Solids (%)	Volatile Solids (%)
Tomato waste	4.65	370	6.65	92.48 of TS
Sewage sludge	8.21	750	16.41	98.17 of TS
Inoculum	6.85	580	5.3	75.47 of TS
Cow Dung	5.74	395	6.65	91.72 of TS

III. METHODOLOGY AND PROCEDURE

The entire experimental setup was carried out in a 120 ml capacity sample digester bottle with a working volume of 50, 70, and 90 ml, and the remaining space is left for biogas production. Total two levels were performed in this work, those are Mono-Digestion and Co-Digestion.

Mono-Digestion (only Tomato waste)

Co-Digestion (Both tomato waste and sewage sludge)

In both conditions, the Inoculum to substrate ratio (I/S) plays a major role in the digestion process and increases the productivity of biogas. But higher I/S ratio will damage the entire digestion process. I/S ratio is taken in different proportions like 1, 2, and 3. In these 3 instances, mono and co-digestion were tested for better results.

All the substrate materials which are collected for anaerobic co-digestion are blended into semi-solid form to reduce the particle size by using organic free distilled water with the ratio of 1:1 (substrate: distilled water).

These samples are collected in the required composition and tested for proximate analysis in the laboratory. The results are as follows.

TABLE III.
COMPOSITION OF MONO-DIGESTION

Parameter	Mix-I (ml)	Mix-II (ml)	Mix-III (ml)
Tomato waste	20	20	20
Inoculum	20	40	60
Cow dung	10	10	10
Effective volume	50	70	90
Bottle capacity	120	120	120

TABLE IV.
COMPOSITION OF CO-DIGESTION

Parameter	Mix-IV (ml)	Mix-V (ml)	Mix-VI (ml)
Tomato waste	10	10	10
Sewage sludge	10	10	10
Inoculum	20	40	60
Cow dung	10	10	10
Effective volume	50	70	90
Bottle capacity	120	120	120



Figure 2. 120 ml capacity Sample Digester Bottle.



Figure 3. Sample Preparation.

Here the temperature is the key factor for the anaerobic condition. Proper conditions like p^H , Alkalinity, and temperatures will affect the production of biogas and methane. p^H and alkalinity are adjusted in the sample, by adding buffer solutions, and proper temperature will be maintained by placing in a BOD incubator.

The sample digester bottles are kept in BOD (Biochemical Oxygen Demand) Incubator at $35^{\circ}C$ for about the entire degradation is completed. Biogas and methane gas are collected regularly.

TABLE V.
PROXIMATE ANALYSIS OF MONO-DIGESTION

Mix Design	pH	Alkalinity (mg/l)	Total Solids (%)	Volatile Solids (%)
Mix-I	8.3	650	5.3	75 of TS
Mix-II	8.8	645	6.8	70 of TS
Mix-III	8.2	662.5	8.1	65 of TS

TABLE VI.
PROXIMATE ANALYSIS OF CO-DIGESTION

Mix Design	pH	Alkalinity (mg/l)	Total Solids (%)	Volatile Solids (%)
Mix-IV	8.1	605	5.4	70 of TS
Mix-V	8.1	632.5	5.5	75 of TS
Mix-VI	8.2	645	5.6	71 of TS

IV. RESULTS

TABLE VII.
CUMULATIVE RESULTS OF MIX-I

Sample	Biogas (ml)	Average Biogas (ml)	Methane gas (ml)	Average methane gas (ml)
Sample-I	1256	1273.59	730.12	750.48
Sample-II	1292		771.78	
Sample-III	1273		755.55	

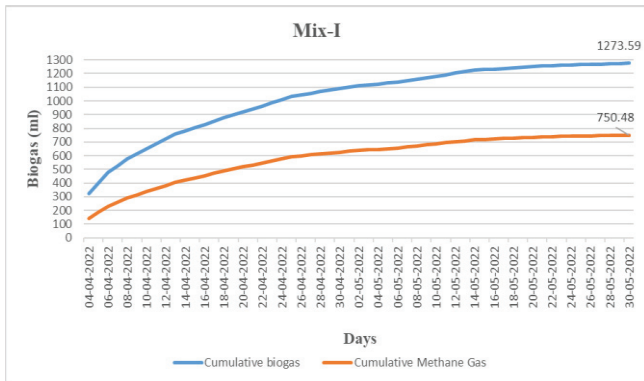


Figure 4. Graphical representation of Mix-I

TABLE VIII.
CUMULATIVE RESULTS OF MIX-II

Sample	Biogas (ml)	Average Biogas (ml)	Methane gas (ml)	Average methane gas (ml)
Sample-I	1144	1258.38	681.98	717.85
Sample-II	1461		829.31	
Sample-III	1152		642.6	

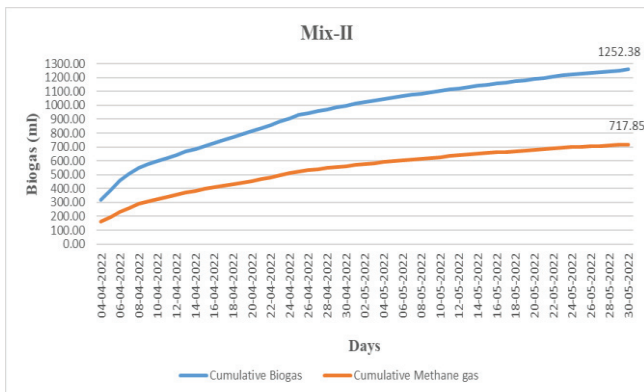


Figure 5. Graphical representation of Mix-II

TABLE IX.
CUMULATIVE RESULTS OF MIX-III

Sample	Biogas (ml)	Average Biogas (ml)	Methane gas (ml)	Average methane gas (ml)
Sample-I	684	762.78	356.53	391.85
Sample-II	788		413.7	
Sample-III	816		405.02	

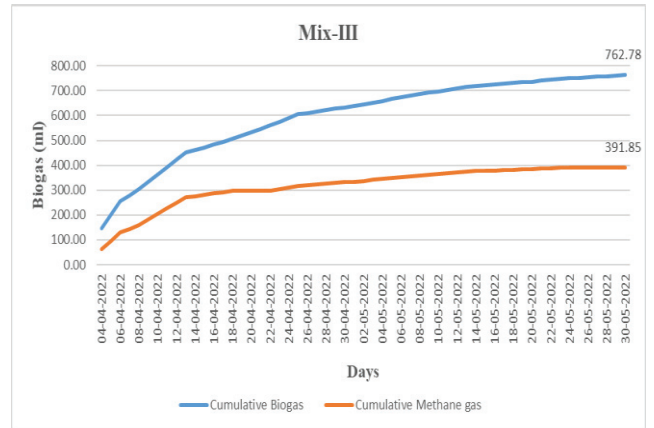


Figure 6. Graphical representation of Mix-III

TABLE X.
CUMULATIVE RESULTS OF MIX-IV

Sample	Biogas (ml)	Average Biogas (ml)	Methane gas (ml)	Average methane gas (ml)
Sample-I	888	887.27	572.3	595.76
Sample-II	924		566	
Sample-III	850		649	

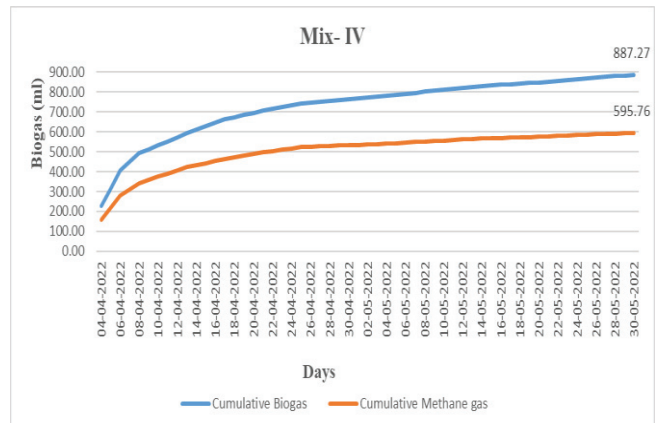


Figure 7. Graphical representation of Mix-IV

TABLE XI.
CUMULATIVE RESULTS OF MIX-V

Sample	Biogas (ml)	Average Biogas (ml)	Methane gas (ml)	Average methane gas (ml)
Sample-I	1680	1648.32	1089.76	1092.1
Sample-II	1630		1125.9	
Sample-III	1635		1063.45	

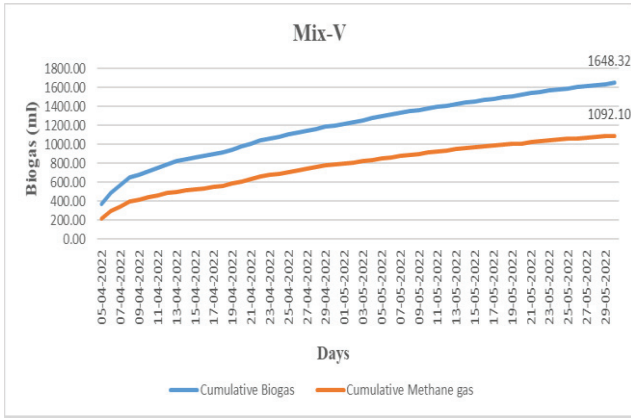


Figure 8. Graphical representation of Mix-V

TABLE XII.
CUMULATIVE RESULTS OF MIX-VI

Sample	Biogas (ml)	Average Biogas (ml)	Methane gas (ml)	Average methane gas (ml)
Sample-I	612	561.18	359.07	327.62
Sample-II	510		303.33	
Sample-III	562		329.02	

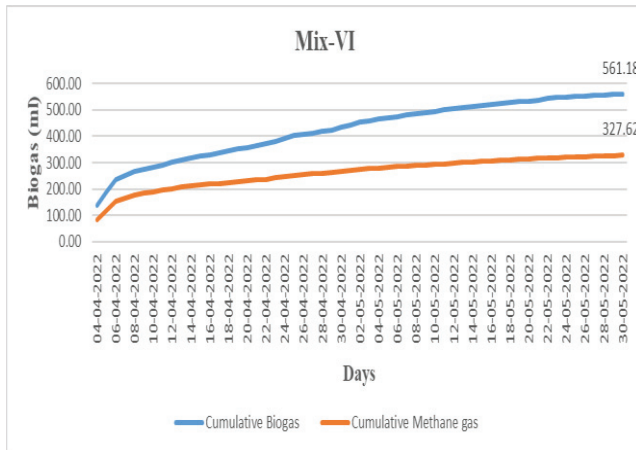


Figure 9. Graphical representation of Mix-VI

TABLE XIII.
PROXIMATE ANALYSIS OF MONO-DIGESTION

Mix Design	pH	Alkalinity (mg/l)	Total Solids (%)	Volatile Solids (%)
Mix-I	3.85	300	3.1	58 of TS
Mix-II	4.1	350	2.7	55 of TS
Mix-III	3.9	350	2.8	57 of TS

TABLE XIV.
PROXIMATE ANALYSIS OF CO-DIGESTION

Mix Design	pH	Alkalinity (mg/l)	Total Solids (%)	Volatile Solids (%)
Mix-IV	3.74	329	2.4	58 of TS
Mix-V	3.68	312	2.7	55 of TS
Mix-VI	3.67	296	2.9	57 of TS

V. COMPARISONS AND DISCUSSION

Day to Day Biogas was collected from all the mixes, into a Glass syringe (50 ml capacity) from Digester bottles for around 60 days. Generally, Biogas contains majorly Carbon dioxide (CO₂), Methane (CH₄), and other trace elements. Collected Biogas then passed through Potassium Hydroxide Solution (KOH) to separate the Carbon Dioxide from the biogas.

From Table VII. Biogas and methane gas were collected for around 60 days, Cumulative biogas was about 3821 ml and methane gas was 2257.45 ml. The percentage of methane is around 59%.

From Table VIII. Biogas and methane gas were collected for around 60 days, Cumulative biogas was about 2757 ml and methane gas was 2153.89 ml. The percentage of methane is around 78%.

From Table IX. Biogas and methane gas were collected for around 60 days, Cumulative biogas was about 2288 ml and methane gas was 1175.25 ml. The percentage of methane is around 58%.

From Table X. Biogas and methane gas were collected for around 60 days, Cumulative biogas was about 2662 ml and methane gas was 1787.3 ml. The percentage of methane is around 67%.

From Table XI. Biogas and methane gas were collected for around 60 days, Cumulative biogas was about 4945 ml and methane gas was 3279.11 ml. The percentage of methane is around 70%.

From Table XII. Biogas and methane gas were collected for around 60 days, Cumulative biogas was about 1684 ml and methane gas was 991.42 ml. The percentage of methane is around 58%.

TABLE XV.
AVERAGE RESULTS OF BIOGAS AND METHANE

Mix	Average Biogas (ml)	Average methane gas (ml)
Mix-I	1273.59	750.48
Mix-II	1252.38	717.85
Mix-III	762.78	391.85
Mix-IV	887.27	595.76
Mix-V	1648.32	1092.10
Mix-VI	561.18	327.62

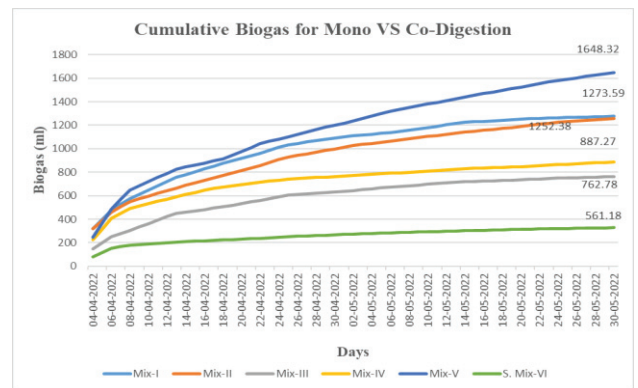


Figure 10. Graphical representation of Biogas for Mono VS Co-Digestion.

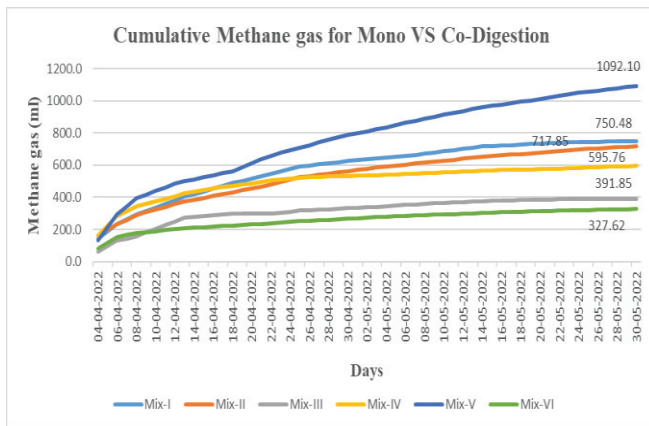


Figure 11. Graphical representation of Methane gas for Mono VS Co-Digestion.

From the overall results, Mix-V achieved the maximum amount of biogas and methane gas production, among all other mixes in the stipulated time (i.e., 60 days).

Mix-V design is the Co-digestion process, this mix contains Tomato waste (10 ml), Sewage sludge (10 ml), Inoculum ("2", I/S ratio), and Cow dung (10 ml).

Inoculum to substrate ratio plays a major in this anaerobic digestion process, Lower I/S ratio achieves good results in the mono-digestion process. Adding sewage sludge to the mono-digestion process (i.e., Co-digestion) produces better results compared to mono-digestion.

VI. CONCLUSIONS

Based on the achieved results from the Experimental as well as Graphical representations of Anaerobic Digestion: The production of Biogas & methane gas is achieved in all the mixes. Among those mixes, Co-Digestion, 1:1 Proportion of tomato waste with Sewage sludge (T: S), and the Inoculum to substrate (I/S) ratio, "2.0" achieved the highest production of methane gas. Compared to Mono-Digestion.

REFERENCES

- [1] Cindy Priadi, Dwica Wulandari, Ifita Rahmatika, Setyo Sarwanto Moersidik, "Biogas Production in the Anaerobic Digestion of Paper Sludge", 2014.
- [2] Grazielle Náthia Neves, Mauro Berni, Giuliano Dragone, (2018), "Anaerobic digestion process; technological aspects and recent developments", May 2018, International Journal of Environmental Science and Technology 15(4), 2018.
- [3] Bao-Shan Xing, Sifan Cao, Yule Han, (2020), "Stable and high-rate anaerobic co-digestion of food waste and cow manure: Optimization of start-up conditions", 2020.
- [4] M. Saev, B. Koumanova, Iv. Simeonov, (2009), "Anaerobic digestion of wasted tomatoes and cattle dung", Journal of the University of Chemical Technology and Metallurgy. 44, 1, 2009.
- [5] Prashant Baredar, Vikas Khare, Savita Nema, (2020), "Optimum sizing and modeling of biogas energy system", Elsevier BV, 2020.
- [6] Ulla Lehtinen, Katariina Ala-Rami, "Supply of biomass and agricultural waste for promoting low-carbon business-ecosystem", Elsevier BV, 2021.
- [7] Meenal Jain, Meenakshi Mital, Pujya Gupta, "Chapter 2 Bioenergy: Sustainable Renewable Energy", Springer Science and Business Media LLC, 2021.
- [8] Panpan Zhang, Chein-Chi Chang, Renqing Wang, Shuping Zhang, "Agricultural Waste", Water Environment Research, 2014.
- [9] Dian Andriani, Arini Wresta, Tinton Dwi Atmaja, Aep Saepudin, "A Review on Optimization Production and Upgrading Biogas Through CO₂ Removal Using Various Techniques", Applied Biochemistry and Biotechnology, 2013.
- [10] Anca C. FARCAS, Sonia A. SOCACI, Delia MICHIU, Suzana BIRIS, Maria TOFANA, "Tomato Waste as a Source of Biologically Active Compounds", Bulletin UASVM Food Science and Technology 76(1)/2019.
- [11] Hussain Al-Wandawi, Maha Abdul-Rahman, and Kaib Al-Shaikhly, "Tomato Processing Wastes as Essential Raw Materials Source", J. Agric. Food Chem. 1985, 33, 804-807,
- [12] H.S. Jatav, S.K. Singh, S.S. Jatav, A.M. Latore, V. Kumar and P. Singh, "Sewage sludge quality assessment of sewage treatment plant, Bhagwanpur, Varanasi and its safe utilization in agriculture", Journal of Environmental Biology, 2020.
- [13] Vinod Kumar, A.K. Chopra, and Ajendra Kumar, "A review on sewage sludge (Biosolids) a resource for sustainable agriculture", Archives of Agriculture and Environmental Science, 2(4): 340-347, 2017.
- [14] Tong Liu, Li Sun, Bettin Muller, Anna Schnurer, (2017), "Importance of inoculum source and initial community structure for biogas production from agricultural substrates", Bioresource Technology, 2017.
- [15] L Kardos, "Comparing of Mesophilic and Thermophilic anaerobic fermented sewage sludge based on chemical and Biochemical tests", Applied Ecology and Environmental Research, 2011.
- [16] R. Sharma, H.S. Oberoi, G.S. Dhillon, "Fruit and Vegetable Processing Waste", Elsevier BV, 2016.
- [17] Denisa Eglantia Duta, Monica Catana, Luminita Catana, Alexandra-Monica Lazar, "Applica Mario M. Pamatmat, Ashok M. Bhagwat, "Anaerobic Metabolism in lake Washington sediments", Limnology and Oceanography, 1973.
- [18] K. Stamatelatou, (2011), "Production of biogas via anaerobic digestion", Handbook of biofuels production, 2011.
- [19] Sihuang Xie, Matthew Higgins, Heri Bustamante, Brendan Galway, Long Nghiem, "Current status and perspectives on anaerobic co-digestion and associated downstream processes", Environmental Science: Water Research & Technology, 2018.
- [20] Thomas W. Jabusch, Ronald S. Tjeerdema, "Microbial Degradation of Penoxsulam in Flooded Rice Field Soils", Journal of Agriculture and Food Chemistry, 2006.
- [21] Alexander J. B. Zehnder, Thomas D. Brock, "Anaerobic Methane Oxidation: Occurrence and Ecology", Applied and Environmental Microbiology, 1980.
- [22] Ebunilo, P.O., and D.O. Otiede, "Design and Testing of a Mini-Plant for Conversion of Organic waste to Biogas", Advanced Materials Research, 2011.
- [23] Rajat Nag, Paul Whyte, Bryan K. Markey, Vicent O'Flaherty, Declan Bolton, Owen Fenton, et al, "Ranking hazards pertaining to human health concerns from land application of anaerobic digestate", Science of the Total Environment, 2020.
- [24] Raposo, "Anaerobic digestion of solid organic substrates in batch mode: An overview relating to methane yields and experimental procedures", Renewable and Sustainable Energy Reviews, 2012.

- [25] Macgregor, A.N. and Keeney, D.R. (1973), "METHANE FORMATION BY LAKE SEDIMENTS DURING IN VITRO INCUBATION. JAWRA", Journal of the American Water Resources Association, 9: 1153-1158.
- [26] Tabatabaei, Meisam, (2010), "Importance of the methanogenic archaea populations in anaerobic wastewater treatments", Process Biochemistry, 45(8): 1214-1225. 2010.
- [27] Vladimir V. Zverlov, Daniela E. Kock, "Hydrolytic bacteria in mesophilic and thermophilic degradation of Plant biomass", Engineering in Life Sciences, October 2010.
- [28] Igoni Hilkiyah A., M. F. N. Abowei, M.J. Ayotamuno, C.L. Eze, "Comparative Evaluation of Batch and Continuous Anaerobic Digesters in Biogas Production from Municipal Solid Waste using Mathematical Models". Agricultural Engineering International: CIGR Journal. (16 January 2009). ISSN 1682-1130.
- [29] Song, Y.C.; Kwon, S.J.; Woo, J.H. (April 2004). "Mesophilic and thermophilic temperature co-phase anaerobic digestion compared with single-stage mesophilic and thermophilic digestion of sewage sludge". Water Res. 38 (7): 1653–62, 2004.

Lateration-Specific Localization Algorithm for Wireless Sensor Networks

Gaurav Sharma

Asst. Professor, CVR College of Engineering/ECE Department, Hyderabad, India
Email: ergaurav209@yahoo.co.in

Abstract: The Received Signal Strength Indicator (RSSI) is a low-cost ranging technique that is commonly used to locate nodes in outdoor Wireless Sensor Networks (WSNs), however it can sometimes provide erroneous position estimations. This is mostly due to the interplay between the reference nodes' influence on distance estimation mistakes and localization geometry. Analysis of distance estimation errors and localization geometry is necessary for the development of methods for decreasing location error. This work seeks to enhance the quality of range-based trilateration localization for WSN nodes in a variety of outdoor environments in order to meet these difficulties. Analyses of the localization error caused by range error and localization geometry have been performed using actual RSSI measurement data. An Adaptive Range-Based Localization (ARBL) technique is suggested that utilizes trilateration and reference node selection to enhance location accuracy and precision; its performance is then assessed by analyzing the gathered data. The technique makes use of a number of different permutations of reference nodes in order to determine the most accurate way to predict a node's position at any given instant. Based on the findings, it seems that the suggested method is effective in lowering the location error. As such, it may be concluded that range-based trilateration localization can provide enough location precision.

Index Terms: Wireless Sensor Networks, ARBL Method, Trilateration, Reference Node Selection, Localization, Anchor Nodes.

I. INTRODUCTION

Over the last two decades, academics have become more interesting in the challenge of pinpointing individual nodes inside WSNs. Knowledge of node locations is helpful or perhaps required for many operations, services, and applications in wireless sensor networks [1-3], making localization one of the key services in WSNs. As a result of their purpose-built nature, WSNs are limited in how they may be configured compared to generic networks [1, 4].

Also, the nodes in a WSN are under far more severe resource limitations (e.g., limited communication range, and limited energy, processing, memory, and storage capacity). Localization methods and protocols in WSNs are also subject to these limitations. Global Navigation Satellite Systems (GNSS), like GPS and GLONASS, provide a standard method for pinpointing a specific position. However, on a wide scale, installing a GNSS receiver on every node in a WSN is neither a viable option nor a very efficient use of resources. In addition, the receiver's range is reduced in some natural settings, such as thick vegetation or urban canyons. Because of this, it was needed to look for substitute approaches. Reference nodes (anchors, beacons,

landmarks, or seeds) are used in anchor-based localization since their positions are known in advance [2, 3, 5-7].

Reference nodes either has a Global Navigation Satellite System (GNSS) receiver installed or has their positions defined manually. In order to determine their own positions, unknown (unlocalized) nodes require a localization technique to combine the coordinates of reference nodes with distance (or angle) estimations and other information. Wireless sensor network localization methods are often split between range-based and range-free categories [2, 6-10]. In localization, range-based algorithms rely on estimated inter-node lengths or angles, whereas range-free methods make advantage of connection (through hop counts, for instance) or pattern matching (by fingerprinting, for instance) to pinpoint a device's precise location. Time of Arrival (ToA), Time Difference of Arrival (TDoA), Angle of Arrival (AoA), and received signal strength indicator are all ranging techniques that may be used in range-based localization to provide distance or angle estimations (RSSI). An unknown node's position can be estimated using a location computation technique such as Lateration [5, 11] (trilateration or multilateration), Min-max (bounding box) [11, 12], or a probabilistic approach based on the distance estimations to the reference nodes and the reference nodes' coordinates (e.g., maximum likelihood).

The advantages and disadvantages of RSSI-based localization are comparable to those of other range-based methods. On the one hand, it is an inexpensive and energy-efficient method that can be used to sensor networks with the addition of only a radio transceiver. However, this method is very dependent on ambient circumstances, therefore it frequently provides erroneous range and position estimations [13-16]. The accuracy of a localization method that uses a range mostly is determined by the interaction between the ranging error and the localization geometry, or the positions of the reference nodes in relation to the unknown node. This is because the range errors and localization geometries shift based on the reference nodes that are employed, and so the magnitude of the localization error also shifts. As an added bonus, certain methods of location calculation are less sensitive to range faults and/or localization geometries than others.

Trilateration is a common low-cost method for calculating locations, although it is very dependent on the accuracy of the rangefinder and the positions of the reference nodes. Depending on the chosen set of reference nodes, this might lead to unexpected discrepancies in the position estimations. Furthermore, the same set of reference nodes may succeed

in identifying one unknown node but fail in identifying another. Consequently, if you want to get sufficient location accuracy, you need to pick relevant reference nodes in each scenario. Findings show that the ARBL method may significantly cut down on location error, achieving results that are very near to ideal for a given set of reference nodes. This demonstrates that practical and precise position estimations may be achieved, despite tough and variable outside settings, by making use of appropriate methodologies and data. In conclusion, our research sheds light on the viability of RSSI- and range-based localization in wireless sensor networks.

The specific organization of the article is as follows. Related techniques to the ARBL algorithm are presented in Section II. In Section III, a general overview of localization techniques is presented. Section IV introduces the network setup and simulation results of the proposed algorithm and Section V draws the conclusions.

II. RELATED WORKS

Various recent reviews (e.g. [2, 5-10, 17, 18]) have categorized and presented some of the many localization algorithms and strategies introduced in recent years for use in WSNs. Several articles pertinent to our approach are discussed below; these studies examine localization techniques based on trilateration and make use of reference node selection.

A. Anchor- and Range-based Trilateration Localization Algorithms

Numerous algorithms and methods for localization based on anchors and ranges have been developed in recent years, and many of them rely on trilateration [2, 5, 6, 8]. The impact of localization geometry on location inaccuracy has been researched extensively yet is ignored by most range-based (and range-free) techniques. An integral aspect of range-based localization, especially for trilateration-based localization, is the selection of reference nodes. The quality of the localization is significantly impacted by the choice of reference nodes and so cannot be neglected.

B. Reference Node Selection Algorithms

Few researches have been done on reference node selection methods, despite the popularity of anchor-based localization. As an example, see [19-23] and [24] for further reading on this topic. An approach for selective anchor node localization (SANLA) is proposed in [19]. In SANLA, an unidentified node determines its position using a series of Trilaterations, in which one of the anchor nodes is fixed (the reference node), and two are the combinations of the other anchors. The fixed reference node's position is then calculated using the same anchor combinations as before, but this time applied to the unknown node.

The unknown node can then be informed of the coordinates that created the least amount of inaccuracy when compared to the genuine ones. The unknown node may now determine which of its previous location estimations yielded the most accurate result and use that coordinate as its own.

In [11], the authors suggested a Trilateration-based approach for selecting reference nodes. To determine if any

of the reference triplets may form a nearly equilateral triangle, the unlocalized node calculates the distances between each pair of nodes. Next, the location estimates are calculated using all the feasible equilateral triangles, and the mean is used as the final estimate.

In [16], the CIL algorithm, or confidence-based iterative localization, is presented. Quality of Trilateration (QoT) is the foundation of CIL; it is a probabilistic metric that reflects the precision of a given trilateration by quantifying the geometric connection between the reference nodes and the range errors. Each node in CIL is assigned a confidence value that reflects how sure the network is about that node's location estimate.

For trilateration, a node's confidence is calculated by multiplying its Quality of Trilateration (QoT) with the confidence of its reference nodes. Trilaterations are used to iteratively move from high-confidence nodes (beacons with positioning devices) to low-confidence nodes (others) in the localization process to accomplish this. Reference nodes (localized nodes) send location data to an unlocalized node with varying degrees of certainty.

An unidentified node uses the most reliable trilateration to pinpoint its current location at each successive step. If a more precise position becomes available at any moment, the initial estimate can be updated accordingly. The experimental and computational findings demonstrate that CIL considerably enhances the precision of location estimates.

A study [12] presented an error-based distributed reference node selection technique for trilateration localization. The programme follows three guidelines for making the most informed decision when choosing anchor nodes for trilateration. Two related rules stipulate that the reference triangle's smallest internal angle must be more than 13 degrees, and that its shortest edge must be as long as feasible. The third principle stipulates that the distances between the unknown node and the reference nodes should be as comparable as feasible, as this also influences the accuracy of the localization. Simulations proved the algorithm's competitive performance. Although the simulations show promise, the distance errors imposed may be overly optimistic, especially if RSSI is employed for ranging.

In [14], the authors offer an enhanced trilateration localization technique called ITL-MEPOSA, which reduces the spread of uncertainty by choosing anchor nodes with maximum efficiency. Uncertainty data is defined by the authors as the standard deviation of sequential distance estimations between an unknown node and an anchor node.

When choosing anchor nodes, it's best to pick the three with the lowest product of the mean distance estimate and the related uncertainty information. Trilateration makes use of these anchor nodes and the related mean distance calculations. In contrast, the impact of localization geometry is ignored.

III. LOCALIZATION TECHNIQUES

Some ranging approach (RSSI, ToA, TDoA) is used to estimate the internode distances, and an appropriate location computation technique is used to calculate unknown node

positions; these are the two main components of a typical range-based localization procedure. In this setting, any ranging approach can be used to acquire the distance estimations required for localization. Since the focus of this research is on estimating distances using RSSI, it was necessary to go through some of the standard methods for doing so. Additionally, a brief discussion is provided on some of the most important parameters influencing the precision of RSSI and range-based localization.

A. RSSI-based Ranging

RSSI-based ranging methods work on the idea that a radio signal decays (its amplitude lowers) as it moves away from the transmitter. The log-normal shadowing model is often applied to represent radio signal route loss, and it is stated in [10, 15]. :

$$P_r(d) = P_r(d_0) - 10n \log\left(\frac{d}{d_0}\right) + X_\sigma \quad (1)$$

where, $P_r(d)$ (or $\text{RSSI}(d)$) is the received power in dBm at distance d [m] from the transmitter, $P_r(d_0)$ (or $\text{RSSI}(d_0)$) is the received power in dBm at the reference distance d_0 (usually 1 m) from the transmitter, n is the path loss exponent (PLE), and X is the zero-mean Gaussian random variable with the variance of 2, that is, $X \sim N(0, 2)$. Various methods exist for estimating $P_r(d_0)$, including the Friis free-space equation, theoretical models, and empirical measurements. Also, the PLE n can be determined ahead of time or estimated afterwards, either offline or live, based on known distances between reference nodes that are kept in a stable position [16].

In the log-distance route loss model, the average received power at a distance d from the transmitter is expressed as Eq. (1), omitting the stochastic factor X . In order to calculate an approximation of the distance d [m] between any two nodes in a network, that may utilize the log distance path loss model.

$$\hat{d} = d_0 10^{(P_r(d_0) - P_r(d)) / 10n} \quad (2)$$

B. Lateration

Using three (trilateration) or more (multilateration) reference nodes with known locations and the measured distances (e.g., based on the RSSI) to them as shown in Figure 1, the position of an unknown node may be calculated [3, 11, 13]. In order to find a unique solution in 2D space, distances to at least three non-collinear reference nodes are needed.

The effect of mistake in the positions of reference nodes on localization error is clearly obvious, as shown by the lateration equations, and it leads to inaccurate distance and localization geometry estimations. Whether or not range error is present, distance estimations will be off if the reference nodes' positions utilized in the computation are inaccurate. Furthermore, the localization geometry is impacted by an inaccuracy in the reference nodes' positions since the locations utilized in the location computation are distorted. As a result, DOP and positioning precision and accuracy vary. When illustrated in [8], location accuracy suffers as uncertainty grows in the positions of the reference

nodes. An effort to minimize the inaccuracy in the position of GNSS-based stationary reference nodes was the subject of one publication [14].

C. Factors Affecting Localization Accuracy

Some of the most important aspects that influence the precision (or accuracy) of node localization based on RSSI are discussed here. The vast majority of them are applicable to localization techniques that don't require an anchor, such as range-based methods. For instance, the extent of the influence on the localization error is determined by the interaction between the components and the localization method [9, 11]. Distance estimation error and localization geometry are the two primary classes into which these elements fall. Additionally, location precision might be impacted by computational inaccuracy.

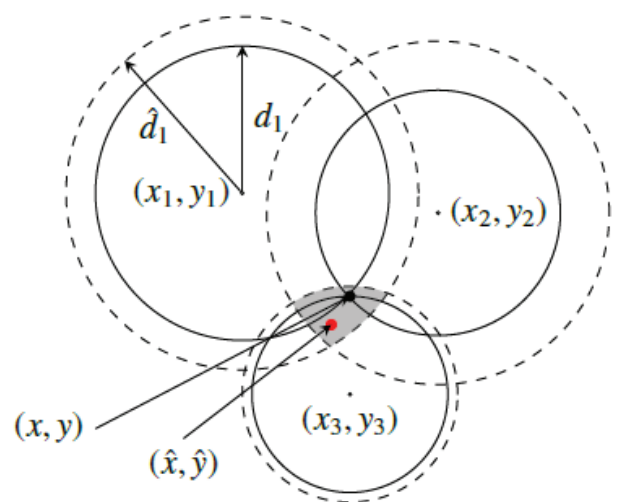


Figure 1. An example of trilateration with accurate and inaccurate distance estimates.

D. Distance Estimation Error

Due to the RSSI's susceptibility to variations in ambient and meteorological conditions, ranging error is likely the most significant and defining element that reduces the accuracy of RSSI-based localization. Looking at the lateration equations also makes evident the impact of distance estimations on location precision. Improving distance estimate and positioning precision requires lowering ranging error [17,18]. It is the emphasis of certain articles [15, 16] to identify the sources of the mistake in RSSI-based ranging and to suggest methods for correcting it. In multihop scenarios, the localization error is affected indirectly by the node degree (connectivity, the average number of neighbours) due to the mistake introduced by the distance estimation process. More measurements may be taken and faster routes can be found to reference nodes if a node's degree (the number of its neighbours) is larger. Increases in the mean number of neighbours typically result in less overall location error [11, 20].

Localization errors are indirectly affected by network topology via distance estimate errors. An anisotropic network (one with gaps or blocks between unknown nodes and reference nodes) introduces mistakes into distance estimates [19].

IV. NETWORK SETUP AND RESULTS

As a means of studying RSSI-based localization and testing the suggested method under different situations, a WSN is set up to gather RSSI data in order to conduct extensive experiments. To gather the empirical data, a network was setup with eight WSN nodes, each of which was outfitted with an Atmel ZigBit 2.4 GHz wireless module (ATZB-24- B0) and an AT86RF230 radio transceiver that complies with IEEE 802.15.4 standards. In addition, there was a database server and a gateway (an Atmel ZigBit 2:4 GHz sink node and a Raspberry Pi 3). (MongoDB). The sensor nodes were installed on mounting racks and affixed to light poles in a parking lot at a height of three metres [18, 20]. Secondary batteries charged by solar panels and intermittent mains electricity provided energy for the nodes (controlled with a timer and a PECU switch). The gateway was a weatherproof box with an Ethernet connection that was installed on the terrace of the university building and supplied by the building's main power supply. As shown in Figure 2, the network infrastructure has been set up.

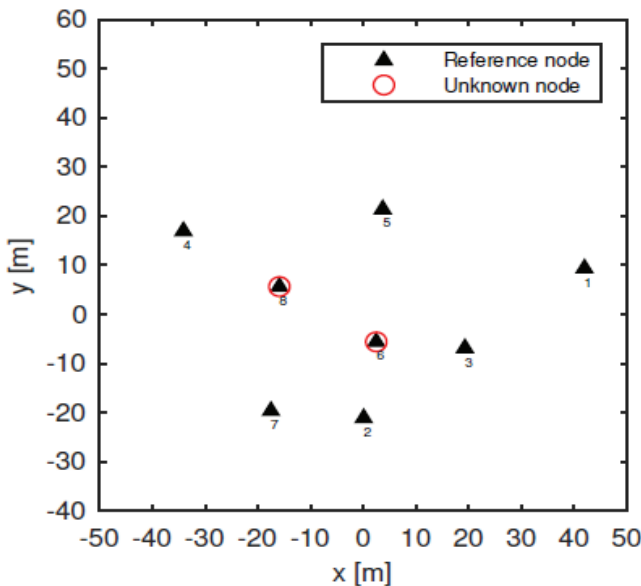


Figure 2. Network setup of the nodes

Laser distance meter (Leica DISTO D8) to measure the distances between nodes in order to conduct research and assessment has been used. Trigonometry was used to calculate the unmeasured distances, whenever it was feasible. With the use of conventional multidimensional scaling, it was able to determine the relative positions of the nodes by analyzing their distances to one another. The configuration matrix is created from a distance matrix using the cmdscale function in MATLAB. As a reference for evaluating the accuracy of the estimations, the relative positions of the nodes were used as the ground truth. The average absolute discrepancy between the observed distances and the distances based on the coordinates was 0.02 m (maximum = 0.06 m) for the reconstruction.

The adaptive RSSI-based ranging algorithm proposes a method for estimating distances between nodes. However, the localization approach presented in this study does not

critically depend on the range technique employed. Estimates of the range can be produced using any method that seems reasonable. Each two-way link is assigned a single RSSI value for use in range and localization. At first, one hour's worth of raw RSSI readings were averaged across all channels ($n=3$ or 4). Second, an average of these RSSI readings over all 16 channels was calculated. Third, the average RSSI values in each direction were used to determine the two-way link's RSSI value.

Localization error $\Delta \hat{x}_i$ for sample i is defined as:

$$\Delta \hat{x}_i = \|\hat{\mathbf{x}}_i - \mathbf{x}\| = \sqrt{(\hat{x}_i - x)^2 + (\hat{y}_i - y)^2}, \quad (3)$$

where $\hat{\mathbf{x}}_i = (\hat{x}_i, \hat{y}_i)$ and $\mathbf{x} = (x; y)$ are the estimated and ground truth locations, respectively. The mean and the standard deviation of localization error, $\overline{\Delta \hat{x}}$ and $s_{\Delta \hat{x}}$, respectively, are defined as:

$$\overline{\Delta \hat{x}} = \frac{1}{n} \sum_{i=1}^n \Delta \hat{x}_i, \quad s_{\Delta \hat{x}} = \sqrt{\frac{1}{n} \sum_{i=1}^n (\Delta \hat{x}_i - \overline{\Delta \hat{x}})^2}, \quad (4)$$

where n is the number of location estimate samples.

Ranging error $\Delta \hat{d}_i$ for sample i is defined as:

$$\Delta \hat{d}_i = \hat{d}_i - d, \quad (5)$$

where \hat{d}_i and d are the estimated and the true distances, respectively, as shown in Figure 3.

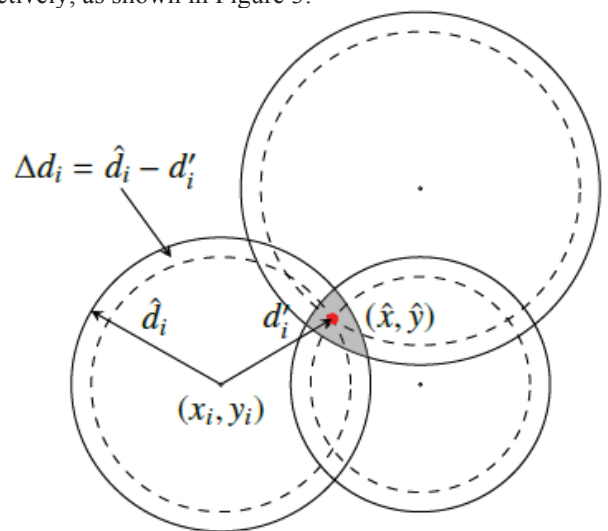


Figure 3. Principle of computing the difference (Δd_i) between the distance estimate (d'_i) and the distance based on the location estimate (d_{0i}).

The unknown node must be inside the reference nodes' convex hull. The argument as to whether or not the node is inside or outside the convex hull is questionable because all are position estimations, which are likely to go wrong. Furthermore, the reference nodes' appropriateness cannot be described just by convexity. In some cases, an outlying node

may have a higher-quality localization geometry than an in-convex-hull node.

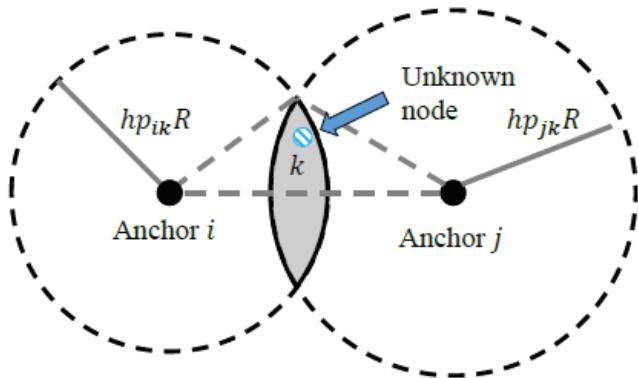


Figure 4. Optimal anchor pair

Figure 4 shows the optimal anchor pair. The optimal anchor pairs provide a clear geometrical relationship, which can be utilized in distance estimation. The reliable anchor pairs provide relatively strong restriction on the potential area of the unknown node. The variance of the location estimation of unknown node is small. Hence, the expected distance between the anchor and the unknown node is considered to be accurate distance estimation.

Figure 5 and Figure 6 show the average location errors for each reference node pair calculated using the ARBL method across the 6 week measurement periods. Based on the data shown in the picture, it is clear that the location inaccuracy varies significantly among different reference nodes. The amount of the difference is notable, particularly on node 8. As the number of reference nodes increases, the average location error decreases (the mean and the standard deviation). However, there are a few excellent permutations that may be obtained with just three auxiliary nodes. The ARBL method appears to locate the appropriate combinations with a high probability and generates fairly accurate and precise position estimations, despite the huge difference between the combinations. The ARBL method has a lower positioning error for node 6 than any individual combination. The ARBL technique yielded a placement error for node 8 that was quite near to the optimal combination.

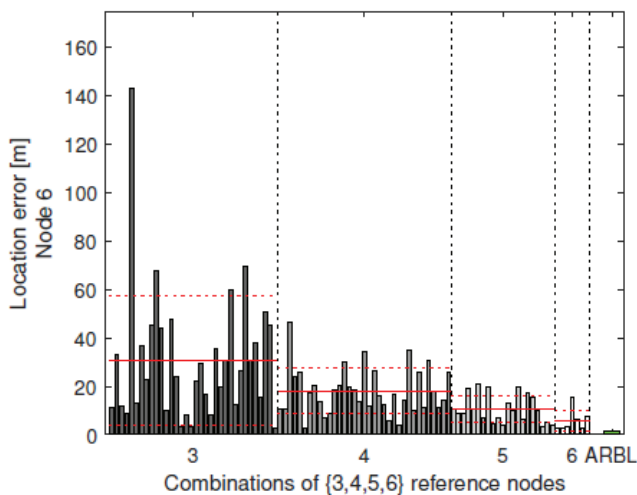


Figure 5. Location Error of the combinations for each number of reference nodes (node 6)

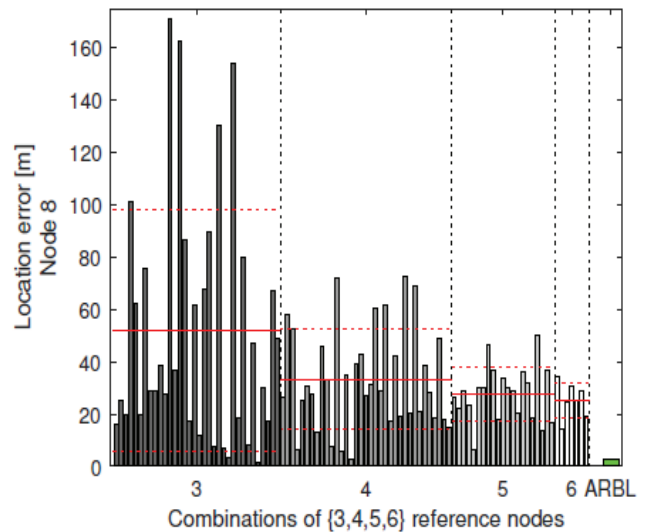


Figure 6. Location Error of the combinations for each number of reference nodes (node 8)

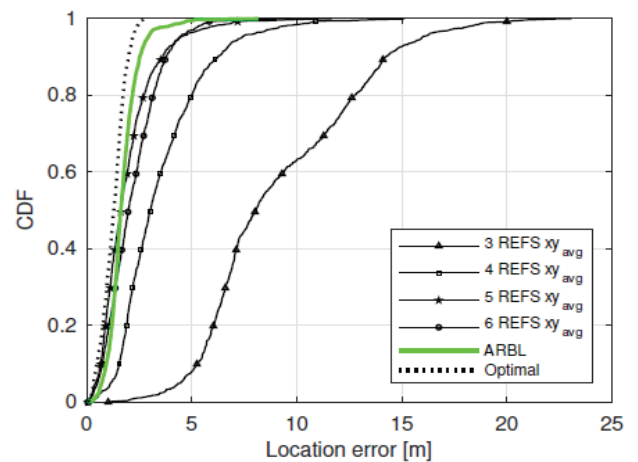


Figure 7. Cumulative distribution function (CDF) of the location error for (a) node 6

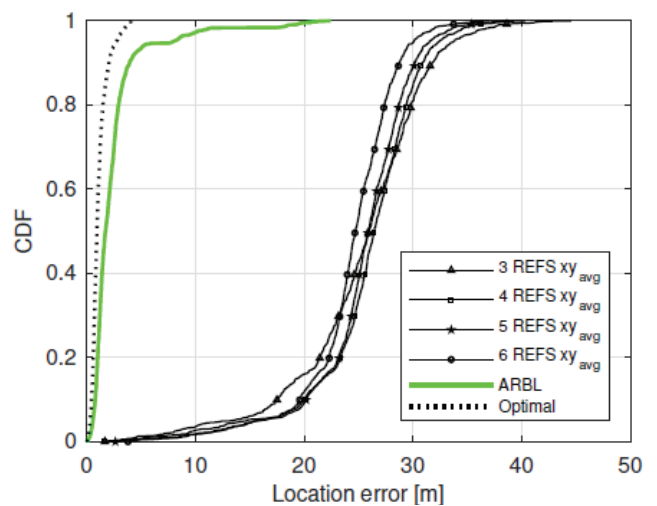


Figure 8. Cumulative distribution function (CDF) of the location error for (a) node 8

The cumulative distribution function (CDF) of the location error at nodes 6 and 8 are shown in Figure 7 and Figure 8. Inaccurate distance estimates can be obtained using RSSI-based ranging, as is well-known. This experiment showed that, depending on the reference nodes utilized, RSSI-based ranging can cause significant location mistakes when used in conjunction with lateration, which is susceptible to erroneous distance estimations and localization geometry. It is difficult to make reliable location predictions when the surrounding environment and weather are constantly changing. As a workaround, a reference node-selection-based ARBL method has been used. To estimate the position of a node that is unknown, the method seeks for the optimal combinations of reference nodes for that node at a particular time and place. It appears that the ARBL method has a much less location error than the average of the individual combinations. The algorithm is particularly effective at adjusting to new parameters and determining the optimal reference node combinations for a given scenario. In practice, the ARBL algorithm may run on nodes in a WSN that have limited processing, memory, and communication resources. Since it is reasonable to assume that there are at least four or five reference nodes in most WSNs, the ARBL method is feasible since there are enough possible combinations.

V. CONCLUSIONS

In this research, strategies to enhance the precision of range-based localization for inexpensive WSN nodes operating in a wide range of environmental settings have been addressed. First, experimental RSSI measurement data have been studied to determine the impact of range error and localization geometry on localization error. To solve this problem, a reference node selection based ARBL method that uses a number of different permutations of reference nodes to determine which is the most accurate in calculating the desired end position has been presented. The evaluations reveal that the localization error was significantly decreased by using the proposed approach. These encouraging results suggest that utilizing appropriate methodologies and data, respectable location accuracy may be achieved using range-based localization for low-cost, resource-constrained WSN nodes. The results also add novel perspectives to the study of anchor- and range-based localization.

REFERENCES

- [1] Zhong Z and He T. MSP: Multi-sequence positioning of wireless sensor nodes. In: Proceedings of the 5th international conference on Embedded networked sensor systems 2007, pp.15-28.
- [2] Shang Y, Ruml W, Zhang Y, et al. Localization from mere connectivity. In: Proceedings of the 4th ACM international symposium on Mobile ad hoc networking & computing 2003, pp.201-212.
- [3] He T, Huang C, Blum BM, et al. Range-free localization schemes for large scale sensor networks. In: Proceedings of the 9th annual international conference on Mobile computing and networking 2003, pp.81-95.
- [4] G. Sharma, & A. Kumar, "Dynamic Range Normal Bisector Localization Algorithm for Wireless Sensor Networks". *Wireless Personal Communications*, vol. 9, no. 3, pp. 4529-4549, 2017.
- [5] Farjow W, Raahemifar K and Fernando XJAMM. Novel wireless channels characterization model for underground mines. 2015; 39: 5997-6007.
- [6] Kumar, V., Kumar, A., G Sharma & Singh, M. (2016, March). Improving network lifetime & reporting delay in wireless sensor networks using multiple mobile sinks. In 2016 3rd international conference on computing for sustainable global development (INDIACom) (pp. 1675-1678). IEEE.
- [7] Bulusu N, Heidemann J and Estrin DJ. GPS-less low-cost outdoor localization for very small devices. 2000; 7: 28-34.
- [8] Yi L and Chen M. An Enhanced Hybrid 3D Localization Algorithm Based on APIT and DV-Hop. 2017; 13.
- [9] Huang Y and Zhang L. Weighted DV-Hop Localization Algorithm for Wireless Sensor Network based on Differential Evolution Algorithm. In: 2019 IEEE 2nd International Conference on Information and Computer Technologies (ICICT) 2019, pp.14-18. IEEE.
- [10] Sai, R. T., & Sharma, G. (2017). Sonic fire extinguisher. *Pramana Research Journal*, 8(1), 337-346.
- [11] Qiang L, Xia H, Yuhang X, et al. Improved DV-Hop Based on Dynamic Parameters Differential Evolution Localization Algorithm. In: 2020 IEEE 8th International Conference on Information, Communication and Networks (ICICN) 2020, pp.129-134. IEEE.
- [12] G. Sharma and A. Kumar, "Fuzzy logic based 3D localization in wireless sensor networks using invasive weed and bacterial foraging optimization," *Telecommunication Systems*, vol. 67, no. 2, pp. 149–162, May 2017.
- [13] G. Sharma, & A. Kumar, "Improved DV-Hop localization algorithm using teaching learning based optimization for wireless sensor networks". *Telecommunication Systems*, vol. 67, no. 2, pp. 163-178, 2017.
- [14] P. Kułakowski, J. Vales-Alonso, E. Egea-López, W. Ludwin, and J. García-Haro, "Angle of- arrival localization based on antenna arrays for wireless sensor networks," *Comput. Electr. Eng.*, vol. 36, no. 6, pp. 1181–1186, Nov. 2010.
- [15] F. Darakeh, G.-R. Mohammad-Khani, and P. Azmi, "CRWSNP: cooperative range-free wireless sensor network positioning algorithm," *Wirel. Networks*, vol. 24, no. 8, pp. 2881–2897, Nov. 2018.
- [16] Sharma, G., & Kharub, M. (2019). Enhanced Range Free Localization in Wireless Sensor Networks. *CVR Journal of Science and Technology*, 16(1), 26-31.
- [17] R. Huang and G. V. Zaruba, "Static Path Planning for Mobile Beacons to Localize Sensor Networks," in Fifth Annual IEEE International Conference on Pervasive Computing and Communications Workshops (PerComW'07), 2007, pp. 323–330.
- [18] K.-F. Su, C.-H. Ou, and H. C. Jiau, "Localization With Mobile Anchor Points in Wireless Sensor Networks," *IEEE Trans. Veh. Technol.*, vol. 54, no. 3, pp. 1187–1197, May 2005.
- [19] G. Sharma and A. Kumar, "Modified Energy-Efficient Range-Free Localization Using Teaching–Learning-Based Optimization for Wireless Sensor Networks," *IETE Journal of Research*, vol. 64, no. 1, pp. 124–138, Jul. 2017.
- [20] J. Rezazadeh, M. Moradi, A. S. Ismail, and E. Dutkiewicz, "Superior Path Planning Mechanism for Mobile Beacon-Assisted Localization in Wireless Sensor Networks," *IEEE Sens. J.*, vol. 14, no. 9, pp. 3052–3064, Sep. 2014.

Hyper-Parameter Optimization using Metaheuristic Algorithms

D. Bhanu Prakash¹, K. Arun Kumar², and R. Prakash Kumar³

¹Assoc. Professor, CVR College of Engineering/ECE Department, Hyderabad, India
Email: pbhanududi@gmail.com

²Sr. Asst. Professor, CVR College of Engineering/ECE Department, Hyderabad, India
Email: arun.katkoori@gmail.com

³Sr. Asst. Professor, CVR College of Engineering/ECE Department, Hyderabad, India
Email: prakash.rachmagdu@gmail.com

Abstract: Machine learning algorithms are widely used in various applications. To properly implement them, their hyper-parameters need to be tuned. It is often necessary to know the ins and outs of ML learning algorithms as well as the proper hyper-parameter techniques. This paper presents two metaheuristic algorithms namely, Genetic Algorithm (GA) and Particle Swarm Optimization (PSO) that can be used to improve the performance of machine learning algorithms. In this paper, we evaluated optimized algorithms for various machine learning algorithms namely, K-Nearest Neighbour (KNN), Support Vector Machine (SVM), Decision Tree (DT), and Random Forest (RF). For conducting experiments, we used four benchmark datasets namely, Breast cancer, Iris, Digits, Wine datasets from sklearn library are considered. Experimental results show that PSO is performed well for optimizing ML models based on large search space. And it is observed that Decision-Tree technique performed poorly for 'Digits' dataset.

Index Terms: Optimization, Machine-Learning Models, Hyper-Parameters, Genetic Algorithm, Particle Swarm Optimization.

I. INTRODUCTION

Machine learning is a field of research that focuses on developing methods that can capture an element of interest in each data set [1]. This can be done by analyzing various components of a given data set and predicting their target values. ML algorithms are widely used in various industries such as advertising. They are typically built to perform complex and high-performance tasks [2][3].

There are two types of parameters that can be used in a ML model: the model parameter and the hyper-parameters. The model parameter can be initialized through the data learning process and can be updated through the data library [4]. Various learning methods are available. These include kernel methods, ensemble models, and biological inspired networks. One of the most common characteristics of these methods is their parameterization. Due to the nature of the search algorithms used for hyperparameters, their reproducibility is not ideal when large sets of hyperparameters are required [5]. Therefore, the idea of automated search is gaining increasing attention in various areas of machine learning. A key component of ML is choosing the appropriate complexity level for the model. Generally, if the model is complex, it should fit the data used to construct it well, but it should also not be complex.[6][7].Hyper-parameter Optimization is a process utilized for improving the efficiency of the tuning

process of ML models. It is usually performed by carrying out a series of predefined steps to achieve the optimal model architecture [8]. Following are the reasons for applying Hyper-parameter Optimization to ML.

1. It allows developers to focus on their core algorithms instead of having to spend time tuning the hyper parameters.
2. It helps improve the performance of many ML models. There are many parameters that can affect the model's performance.
3. It makes the models more reproducible. Also, it helps to identify the most suitable algorithm for a particular problem.

It is important to select an optimal optimization technique that can identify optimal hyper-parameters. Usually, traditional techniques are not suitable for hyper-parameter optimization (HPO) problems. Other optimization techniques such as metaheuristics, decision-theoretic approaches, and Bayesian models are more suitable for optimizing these HPO problems [9]. They can detect continuous hyper-parameters and can also identify discrete and conditional hyper-parameters.

II. HYPER PARAMETERS IN MACHINE LEARNING

To boost the performance of ML models, we need to know what the key hyperparameters are to fit the models into specific problems. The supervised learning algorithms are usually focused on learning how to map input features of a target [10]. Some of the commonly used ones include K-Nearest Neighbors, linear models, and decision trees. Unsupervised learning methods are usually used to find unlabeled data. The importance of some of the hyper-parameters of common multi-language models are studied in Python libraries.

A. K-Nearest Neighbor (KNN)

K-Nearest Neighbor is a type of algorithm that classifies data points by their distance from one another. It does so by calculating the distance between the data points that belong to the given class.

Assuming the training set,

$$T_r = \{ (p_1, q_1), (p_2, q_2), \dots (p_n, q_n) \} \quad (1)$$

where P_i - Feature vector,
 Q_i -class of instance
 $i=1, 2, \dots, n$.

for a test instance ‘p’, its class ‘q’ can be represented as

$$q = \underset{j}{\operatorname{argmax}} \sum_{i=1}^m I(q_i = b_j), i = 1, 2, \dots, n; j = 1, 2, \dots, m \quad (2)$$

where $I(p)$ - indicator function

$$I = 1, \text{ when } q_i = b_j \\ = 0, \text{ otherwise.}$$

$M_k(p)$ - filed invoking the k-nearest neighbors of ‘p’.

The number of nearest neighbors, k, is the most critical hyper-parameter in KNN [11]. It is often used to determine the model’s fit.

B. Support Vector Machine (SVM)

Support vector machines (SVM) [12][13] are supervised learning algorithms that can be used for various tasks such as classification and regression. They map data points to high-dimensional space and partition them into segments [44].

Assuming there are ‘m’ data points, the objective function of SVM is:

$$\underset{z}{\operatorname{argmin}} \left\{ \frac{1}{m} \sum_{i=1}^m \max(0, 1 - q_i f(p_i) + Bz^T z) \right\} \quad (3)$$

where the z-normalization vector.
B- Penalty parameter of the error.

B is an important Hyper parameter of SVM.

The function $f(p)$ is a type of kernel function that measures the similarity between two parallel data points. It can be tuned through different types of kernel models.

The different kernel functions can be denoted as follows:

i) Linear kernel:

$$f(p) = p_i^T p_j \quad (4)$$

ii) Polynomial kernel:

$$f(p) = (\gamma p_i^T p_j + \gamma)^e \quad (5)$$

iii) RBF Kernel

$$f(p) = \exp(-\gamma \|p - p'\|^2) \quad (6)$$

iv) Sigmoid kernel

$$f(p) = \tanh(\gamma p_i^T p_j + \gamma) \quad (7)$$

A kernel type can also have a conditional hyper-parameter called ‘gamma’. This is the conditional hyper-parameter that is set when the type is specified as a polynomial or sigmoid

kernel. The kernel type hyper-parameters are tuned after a kernel is chosen.

C. Decision Trees

A decision tree is a commonly used classification method that shows a set of classification rules that are computed from the data [14]. It has three main components: a tree’s root node, which represents the whole data, multiple decision nodes, and leaf nodes that represent the result classes [15].

Other important factors that can be tuned to make decision tree models perform well include the quality of splits, their random selection method, and the number of features that can be considered to generate the best split. The number of features that can be considered for generating the best split, or ‘max features’, can be tuned as part of the feature selection process.

D. Random Forest

Random forest is a ML algorithm that combines multiple classifiers to solve a variety of problems. It can be commonly used for both classification and regression problems [16].

A random forest is a type of classifier that takes multiple decision trees and outputs a final output with the most accurate predictions. Instead of relying on one tree, it uses most votes from the trees to predict the final output.

Table I shows various hyper-parameters, type, and search space for different ML classifiers

TABLE I.
SUMMARY OF HYPER-PARAMETERS IN DIFFERENT ML MODELS

S.No	Machine Learning Classifier	Hyper-Parameter	Type	Search Space
1	Random Forest Classifier	n_estimators	Discrete	[10,100]
		Max_Depth	Discrete	[5,50]
		Min_samples_split	Discrete	[2,11]
		Min_samples_leaf	Discrete	[1,11]
		Criterion	Categorical	['gini', 'entropy']
2	Support Vector Machine	C	continuous	[0.1,50]
		Kernel	Categorical	['linear', 'poly', 'rbf', 'sigmoid']
3	KNN Classifier	N_neighbours	Discrete	[1,20]
4	Decision Tree classifier	Cp	Discrete	[0,1]
		Max_depth	Discrete	[1,30]
		Min_split	Discrete	[1,60]

III. HYPER PARAMETERS OPTIMIZATION TECHNIQUES

Population-based optimization is a type of metaheuristic algorithm that starts by creating a population as each generation. It then updates the population as each generation is evaluated. The main differences between various Population-based methods are that they use different methods to generate and select populations. Population-based algorithms are easily parallelized since they can be evaluated on a swarm of ‘N’ individuals.

A. GA-Genetic Algorithm

It is a widely used metaheuristic model that studies how individuals adapt to the environment and how likely they are to survive in the future [17]. The next generation will also have the same parents’ characteristics. This means that they will either have better or worse individuals. The former will become more adaptable and resilient, while the latter will gradually disappear. Each chromosome has a hyper-parameter, which is the actual input value of that hyper-parameter in an evaluation. The population consists of all possible values within the predefined parameters.

Since the random-generated parameter values do not contain the optimal values, several operations involving selection, crossover, mutation, and selection operations are performed on the healthy chromosomes to identify the optimal. Chromosome selection aims to increase the population size by selecting the best possible chromosomes. Chromosome selection is a process that selects good characteristics for later generations. This process involves swapping a proportion of genes in each of the chromosomes [18].

Steps of GA are as follows:

1. Intricate representations of the entire search space are provided. Randomly initialize the population, genes, and chromosomes.
2. The fitness function is a calculation that shows the objective of a model.
3. Initiate selection, crossover, or mutation operations on the lysed chromosomes to produce a new generation of hyper-parameter configurations.
4. Repeat steps 2 and 3 until the ‘termination’ condition was met.
5. Terminate and output the ‘optimal hyper-parameter’ confirmation.

Population initialization is an important step in the optimization process and can significantly improve the performance of parameter optimization algorithms. A good initial population should have individuals with global optimums who can cover promising regions. Random initialization commonly used in GA is a good alternative to good initialization. It allows the configuration of hyper-parameter candidates without missing the global optimum. The GA algorithm can be useful when the data analyst has little experience in defining the appropriate search space for the various hyper-parameters. The time complexity of GA is $O(n^2)$. This algorithm can be inefficient when used with low convergence speed.

B. PSO-Particle Swarm Optimization

It is a type of evolutionary algorithm that is inspired by biological phenomena. They use the same principles to solve problems involving large-scale networks. Unlike GA, PSO doesn’t require crossover or mutation [2].

Instead, all members of the population share information with each other, which enables them to move toward the optimal region. PSO has computational complexity that

consists of $O(n \log n)$. In most cases, its convergence speed is faster than that of GA.

PSO is only capable of reaching a local level if it has the proper population initialization. This means that developers should have experience in implementing population initialization techniques and implementing global optimums. Many population initialization techniques are proposed to improve the efficiency of evolutionary algorithms. However, these methods require many resources and time to perform their intended function.

Metaheuristic algorithms such as PSO and GA are more complex than other high-pressure algorithms, but they usually perform well in complex optimization problems.[19] PSO is good for large-scale parallelization and is usually preferred over GA for complex HPO problems. It is also faster than GA due to its sequential execution. To properly identify a local, population initialization is very important for PSO. It can slow down or only identify a local instead of a global optimum.

IV. EXPERIMENTAL RESULTS

Datasets:

For experimental setup, we considered four standard benchmark datasets from sklearn library. Namely, Breast cancer dataset, Iris dataset, Digits dataset, and wine dataset. The summary of the dataset is shown in the table below.

TABLE II.
SUMMARY OF DATASETS USED

Dataset	Classes	Samples per class	Total samples	Dimensionality
Breast cancer	2	212-Malignant 357-Benign	569	30
Iris	3	50-setosa 50-versicolor 50-verginica	150	4
Digits	10	0 to 9	1797	64
Wine	3	59-class 0 71- class 1 48-class 2	178	13

All experiments are conducted using Googlecolab. Colab is a product from Google Research that allows anyone to write and execute Python code through the browser. It is a great tool for machine learning, data analysis, and education.

The first step is training and evaluating the model with its default hyperparameter confirmation. The second step is implementing the two algorithms i.e., GA and PSO to evaluate and compare the model's performance.

TABLE III.
PERFORMANCE EVOLUTION OF APPLYING HPO METHODS TO THE DIFFERENT CLASSIFIERS ON BREAST CANCER DATASET

SI No	Classifiers	Optimization Method	Accuracy (%)	Evaluation time (msec)
1	Random Forest Classifier	Default Hyper-parameters	92.6	1.13
		Genetic Algorithm	96.66	58.2
		PSO	97.66	45.25
2	Support Vector Machine	Default Hyper-parameters	95.25	22.15
		Genetic Algorithm	95.6	598.49
		PSO	96.6	359.4
3	KNN Classifier	Default Hyper-parameters	92.4	0.06
		Genetic Algorithm	93.32	2.15
		PSO	94.33	2.92
4	Decision Tree classifier	Default Hyper-parameters	91.91	0.04
		Genetic Algorithm	92.79	2.73
		PSO	93.79	3.31

TABLE IV.
PERFORMANCE EVOLUTION OF APPLYING HPO METHODS TO THE DIFFERENT CLASSIFIERS ON IRIS DATASET

S I No	Classifiers	Optimization Method	Accuracy (%)	Evaluation time(m sec)
1	Random Forest Classifier	Default Hyper-parameters	96	0.92
		Genetic Algorithm	96.66	40.64
		PSO	96.6	28.8
2	Support Vector Machine	Default Hyper-parameters	97.33	0.01
		Genetic Algorithm	98.00	0.67
		PSO	98.66	0.03
3	KNN Classifier	Default Hyper-parameters	97.0	0.02
		Genetic Algorithm	98.00	0.69
		PSO	98.0	1.01
4	Decision Tree classifier	Default Hyper-parameters	96.66	0.01
		Genetic Algorithm	96.66	0.72
		PSO	97.33	0.69

Tables III to VI, we can see that using default hyper-parameter configurations, do not yield best model performance in our experiments, which emphasizes the importance of utilizing optimization methods. From the above tables, we can conclude that PSO is better than GA.

TABLE V.
PERFORMANCE EVOLUTION OF APPLYING HPO METHODS TO THE DIFFERENT CLASSIFIERS ON DIGITS DATASET

SI No	Classifiers	Optimization Method	Accuracy (%)	Evaluation time(m sec)
1	Random Forest Classifier	Default Hyper-parameters	93.15	1.78
		Genetic Algorithm	93.6	97.12
		PSO	93.32	80.51
2	Support Vector Machine	Default Hyper-parameters	94.765	0.17
		Genetic Algorithm	97.44	13.68
		PSO	97.38	7.39
3	KNN Classifier	Default Hyper-parameters	95.93	0.2
		Genetic Algorithm	96.66	6.61
		PSO	96.6	10.22
4	Decision Tree classifier	Default Hyper-parameters	77.8	0.09
		Genetic Algorithm	78.57	5.34
		PSO	79.02	6.39

TABLE VI.
PERFORMANCE EVOLUTION OF APPLYING HPO METHODS TO THE DIFFERENT CLASSIFIERS ON WINE DATASET

SI No	Classifiers	Optimization Method	Accuracy (%)	Evaluation time (m sec)
1	Random Forest Classifier	Default Hyper-parameters	97.7	78.6
		Genetic Algorithm	98.31	46.4
		PSO	98.33	45.21
2	Support Vector Machine	Default Hyper-parameters	95.11	0.9
		Genetic Algorithm	96.66	5.94
		PSO	96.11	9.87
3	KNN Classifier	Default Hyper-parameters	69.14	0.01
		Genetic Algorithm	72.53	1.15
		PSO	72.53	1.27
4	Decision Tree classifier	Default Hyper-parameters	89.31	0.01
		Genetic Algorithm	91.04	0.08
		PSO	90.48	0.89

TABLE VII.
OPTIMIZED HYPER-PARAMETERS OF TESTED CLASSIFIERS USING GA

SI No	Machine Learning Classifier	Hyper-Parameter	Optimized Values for Breast cancer dataset	Optimized Values for Iris dataset	Optimized Values for Digits dataset	Optimized Values for Wine dataset
1	Random Forest Classifier	n_estimators	96	64	98	44
		Max_Depth	9	9	9	7
		Min_samples_split	2	2	2	10
		Min_samples_leaf	1	4	1	1
		Criterion	Entropy	Entropy	Entropy	Entropy
2	Support Vector Machine	C	49	17	7	2
		Kernel	Linear	Rbf	Rbf	Linear
3	KNN Classifier	N_neighbours	13	7	3	50
4	Decision Tree classifier	Cp	0	0	0	0
		Max depth	2	9	21	4
		Min split	57	18	8	38

TABLE VIII.
OPTIMIZED HYPER-PARAMETERS OF TESTED CLASSIFIERS USING PSO

SL No	Machine Learning Classifier	Hyper-Parameter	Optimized Values for Breast cancer dataset	Optimized Values for Iris dataset	Optimized Values for Digits dataset	Optimized Values for Wine dataset
1	Random Forest Classifier	n_estimators	46	60	54	85
		Max_Depth	5	8	9	6
		Min_samples_split	6	8	10	2
		Min_samples_leaf	2	6	3	1
		Criterion	Gini	Gini	Entropy	Gini
2	Support Vector Machine	C	49	6	17	49
		Kernel	Linear	Rbf	Rbf	Linear
3	KNN Classifier	N_Neighbours	12	11	3	50
4	Decision Tree classifier	Cp	0	0	0	0
		Max depth	2	3	27	27
		Min split	5	6	5	13

Below figures 1 to 4 shows the accuracies of different classifiers with respect to default hyper parameters (without optimization) and optimized hyper parameters (using GA and PSO). It is observed that PSO is performing well in most of the cases.

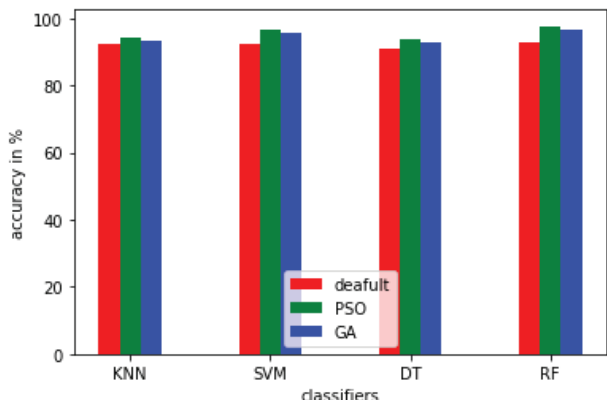


Figure 1. Breast Cancer Dataset

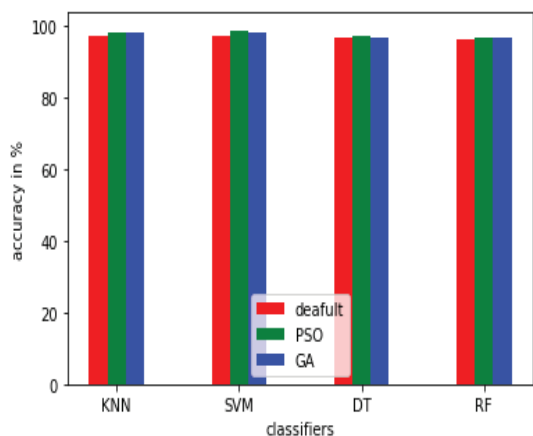


Figure 2. Iris dataset

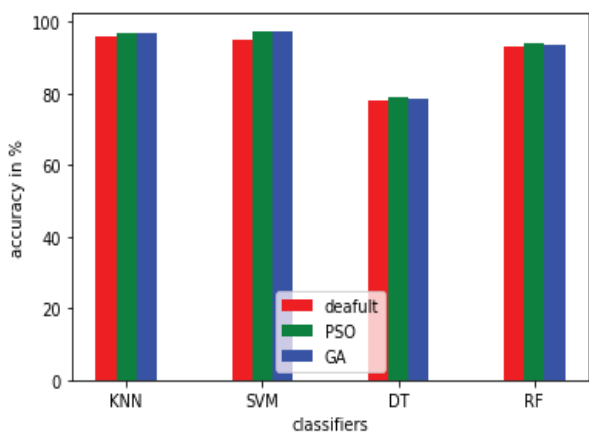


Figure 3. Digits dataset

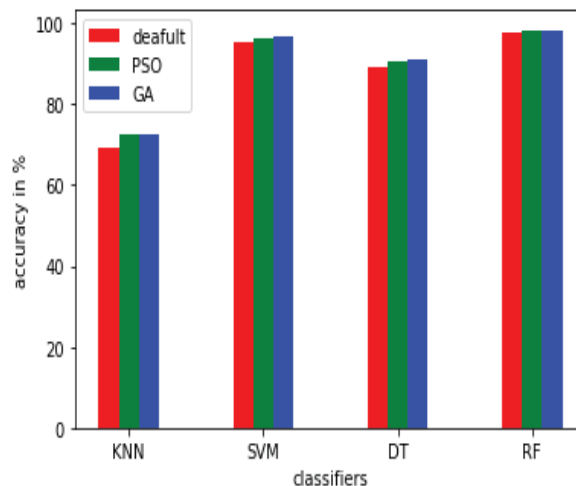


Figure 4. Wine dataset

V. CONCLUSIONS

Machine learning has become the main strategy for solving data-related problems. Its goal is to identify the most suitable hyper-parameters for the given problem. In this work, we comprehensively discussed different optimization algorithms as well as how to apply them to different ML models. To summarize PSO is performing better for optimizing ML models based on large search space. From our experiments, it is observed Decision-Tree performed poorly for Digits dataset.

REFERENCES

- [1] Dudi, B., Rajesh, V. “Optimized threshold-based convolutional neural network for plant leaf classification: a challenge towards untrained data”. *Journal of Combinatorial Optimization*, Springer, 2021.
- [2] Katukuri Arun Kumar, Ravi Boda, A Multi-Objective Randomly Updated Beetle Swarm and Multi-Verse Optimization for Brain Tumor Segmentation and Classification, *The Computer Journal*, 2021.
- [3] M.I. Jordan, T.M. Mitchell, “Machine learning: Trends, perspectives, and prospects”, *Science* 349, 255260, 2015.
- [4] M. Kuhn and K. Johnson, “Applied Predictive Modeling”, Springer, ISBN: 9781461468493, 2013.
- [5] F. Hutter, L. Kotthoff, and J. Vanschoren, Eds., “Automatic Machine Learning: Methods, Systems, Challenges”, Springer ISBN:9783030053185, 2019.
- [6] N. Decastro-Garcia, L. MuozCastaeda, D. Escudero Garcia, and M. V. Carriegos, “Effect of the Sampling of a Dataset in the Hyperparameter Optimization Phase over the Efficiency of a Machine Learning Algorithm, Complexity”, 2019.
- [7] S. Abreu, “Automated Architecture Design for Deep Neural Networks”, arXiv preprint arXiv:1908.10714, 2019.
- [8] O. S. Steinholtz, “A Comparative Study of Black-box Optimization Algorithms for Tuning of Hyper-parameters in Deep Neural Networks”, M.S. thesis, Dept. Elect. Eng., Lulea Univ. Technol., 2018.
- [9] S. Lessmann, R. Stahlbock, S.F. Crone, “Optimizing hyperparameters of support vector machines by genetic algorithms”, *Proc. Int. Conf. Artif. Intell. ICAI05*, 1, 2005.
- [10] R. Caruana, A. Niculescu-Mizil, “An empirical comparison of supervised learning algorithms”, *ACM Int. Conf. Proceeding Ser.* 148, 161168, 2006.

- [11] W. Zuo, D. Zhang, K. Wang, "On kernel difference-weighted k- nearestneighbor classification", *Pattern Anal. Appl.* 11, 247257, 2008.
- [12] Dudi, Bhanuprakash, and V. Rajesh. "Medicinal plant recognition based on CNN and machine learning." *International Journal of Advanced Trends in Computer Science and Engineering* 8.4 (2019): 999-1003
- [13] Mahesh Kusuma K. Arun Kumar, P. Rajashekar Reddy,"Medical Image Classification Based On Normalized Coding Network with Multiscale Perception",*International Journal of Innovative Technology and Exploring Engineering*,vol.8,issue 11,2019.
- [14] S. Rasoul, L. David, "A Survey of Decision Tree Classifier Methodology",*IEEE Trans. Syst. Man. Cybern.* 21, 660674, 1991.
- [15] L. Yang, R. Muresan, A. Al-Dweik, L.J. Hadjileontiadis, "Image-Based Visibility Estimation Algorithm for Intelligent Transportation Systems", *IEEE Access.* 6, 7672876740,2018.
- [16] Palimkar, Prajyot, Rabindra Nath Shaw, and Ankush Ghosh. "Machine Learning Technique to Prognosis Diabetes Disease: Random Forest Classifier Approach." *Advanced Computing and Intelligent Technologies*. Springer, Singapore, 2022. 219-244.
- [17] D.M. Manias, M. Jammal, H. Hawilo, A. Shami, P. Heidari,A. Larabi, R. Brunner, "Machine Learning for Performance-aware Virtual Network Function Placement",*IEEE Glob. Commun. Conf. GLOBECOM 2019 - Proc.* 1217, 2019.
- [18] A. Gogna, A. Tayal, *Metaheuristics: Review and application*, J. Exp. Theor. Artif. Intell. 25, 503526, 2013.
- [19] Kumar, K.A., Boda, R, "A computer-aided brain tumor diagnosis by adaptive fuzzy active contour fusion model and deep fuzzy classifier", *Multimed Tools Appl* 81, 25405–25441 (2022). <https://doi.org/10.1007/s11042-022-12213-7>

A Weighted Pseudorandom Test Pattern Generator for a Built In Self Test Architecture

Vadde Sathvika¹, Chalam Tirunagari², P. Anil Kumar³

¹PG Scholar, CVR College of Engineering/ECE Department, Hyderabad, India
Email: Sathvika.panni@gmail.com

²Asst. Prof., CVR College of Engineering/ECE Department, Hyderabad, India
Email: chalam.tirunagari@gmail.com

³Assoc. Prof., CVR College of Engineering/ECE Department, Hyderabad, India
Email: anilkumar417@gmail.com

Abstract: As the submicron technology emerges, there arises a huge requirement for increase in the functionality that the chip can perform. In the present generation, massive production of IC requires a rigorous testing to differentiate the perfect chip from the fault one. Verification Engineers has to be aware of the functionality of the chip for a full-scale verification to identify the product failures. Conventional testing requires huge amount of time and circuit complexity and hence these techniques are not suitable for the present generation. Hence there arises a need for the automatic test pattern generation with high randomness between the test pattern generations. Galois Fields are used to generate the randomness in the test pattern generation. In addition to that weighted test pattern generator has been used in the present work to increase the randomness in the test pattern generation. The algorithm was verified using Verilog and realized in VIVADO. The present work has been aimed at optimizing area and delay of the design and it has produced promising results.

Index Terms: BuiltInSelf-Test, circuit under test, test pattern generator, Pseudorandom TPG.

I. INTRODUCTION

Current innovation has focused on growing low-power frameworks for especially vast scope becoming a member of (VLSI) speedy plans. Therefore, some plan techniques have been completed to alleviate compromises among execution, strength, and vicinity. Some methodologies have concentrated on low-power dispersal throughout BIST normal mode operations rather than test mode operation [1].

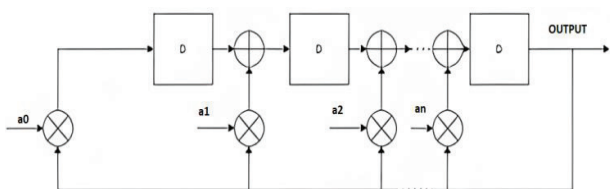


Figure 1. An example of a conventional pseudo random TPG

During the BIST normal mode operation, the replacing motion with inside the output chains and check information stress using the suitable TPG are crucial. Additionally, this finding out should be achieved with immoderate dependability and responsiveness in semiconductor designs. Figure1 illustrates an example of a conventional [2]. The partner supervisor planning the survey of this composition and helping it for distribution changed into Wu-Shiung Feng.

Pseudorandom TPG

The TPG contains of the affiliation of length n shift registers and input seed bits of $a_0, a_1, a_2, \dots, a_n$. In moderate of the n^{th} cycle of the shift sign up, the $(I - 1)^{\text{th}}$ clock cycle[3] is refreshed constantly through manner of method of the $(n_1)^{\text{th}}$ cycle of the shift sign up and the 1^{th} clock cycle. The TPGs make use of important level of parallelism to perform excessive cross back records in several useful packages. The TPG [1] direct capability is executed through way of method of the outset complete signal and the data seed bits. Its direct functionalities are implemented in many programs like plane frameworks, cockpit frameworks, scientific frameworks, sound and video frameworks, and power age and dispersion frameworks.

A TPG carries of deterministic, complete, pseudorandom, pseudorandom weighted [4] and blended mode yields. The pseudorandom weighted out placed issued to carry out better problem inclusion in numerous BIST systems. The weighted pseudorandom TPG suggests genuine irregularity and repeatable examples in all clock cycles. Regularly, it requires one seed bit to deliver one check format for 'n' forms of the checking ease within side the check according to take look at BIST [2], in which 'n' is the scan chain cycle. The most modern overview diminished the switching activity all through test shift cycles. Furthermore, the TPG permits the programmed preference of weighted obstacles to perform its low power. The weighted pseudo arbitrary TPG techniques and their execution in, can in true lessen the replacing modifications. Nonetheless, the techniques, incorporated extra XOR adjustments the various shift registers [3], it consumed extra power and location. The BIST necessities need to be in fashionable zero in at the better short coming inclusion and the lesser weighted changing movement with lower power.

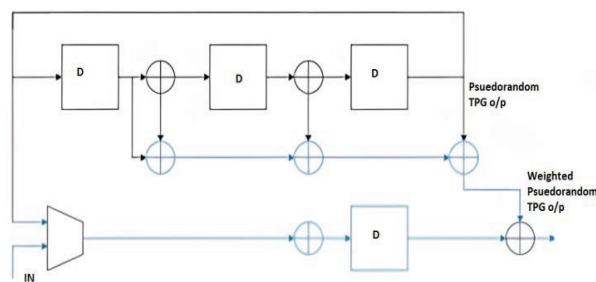


Figure 2. (a) spare TPG

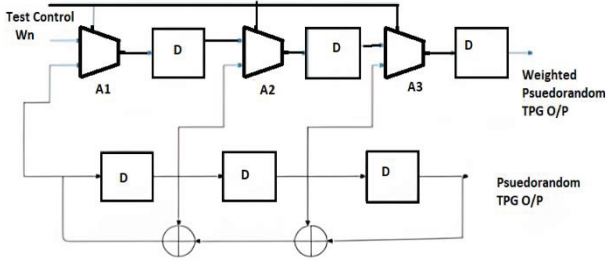


Figure 2. (b) Spare TPG

To accomplish those requirements, methodologies can be used. One is to regulate the circuit plan of the weighted TPG [4]. The distinctive is to remember more machines for the weighted TPG. The present work describes every different pseudorandom weighted TPG is advanced the use of extra machine. Also, higher shortcoming inclusion is accomplished as a long way as getting rid of change remove deficiencies using check thing addition. The check focuses are embedded for every NAND entryway design of the general plan region. The proposed approach is composed of purchasing and promoting weighted check examples to the output chains the use of a phase shifter.

The buying and promoting of the weighted examples taken into consideration for picking the earlier output chains with lesser region is contrasted and that of the others scan chains [5]. The weighted examples are consequently carried out with all the output chains of BIST layout. This dispenses with the problems at a predefined yield and further improves the fault coverage. The TPG likewise in addition develops its speedy changing motion due to its selected weighted designs and reduces its ordinary checking and catching energy usage in some unspecified time in the future of BIST check consistent with observe. The proposed TPG is planned using intent door strategies and finished in precise test according to observe BIST designs.

II. EXISTING WEIGHTED PSEUDORANDOM TPGS

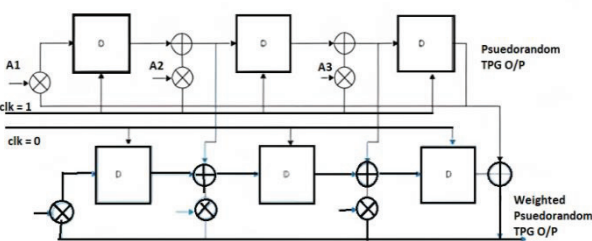


Figure 3. Existing 3-bit weighted pseudorandom TPG

The primitive polynomial chosen for the now not set in tone with the resource of the use of the even or ordinary faucet bits from the register. By and large, crude polynomials are carried out for growing pseudorandom designs. On the off risk that the faucet bit groupings of a n-digit TPG [5] are $n, m, k, l, \dots, 0$, then the co primes of the faucet numbers, like $n-n, n-m, n-k, n-l, \dots, n-0$, will likewise produce the pseudorandom TPG yield. Utilizing this concept, the TPG can create a notable length of pseudo critical seeds. In Figure 2, the darkish line way that the supply TPG yields pseudorandom designs, and the blue line

factors show the greater system implemented for producing the weighted pseudorandom designs [6].

The existing weighted repetitive TPG approach in Figure 3 makes use of each device or duplication elements. The hardware redundancy duplicates its functions into double modular redundancy, triple modular redundancy and so on. This may be completed through copying the greater tool for the deliver TPG configuration, therefore removing the arbitrary example steady short comings. Be that due to the fact it may, the device overt repetitiveness TPG accomplishes super execution factors; it needs to be reducible with inside the device above [3]. The time overt repetitiveness is finished using the one of a kind time measures rather than the tool utilizing the offbeat clock values going from “0” to “1”. In any case, a similar interest is carried out making use of several time elements for the weighted examples. This method distinguishes numerous secure deficiencies at some point of several clock cycles.

The existing 3-bit weighted pseudorandom TPG maximum details applied for generating the weighted examples associated with, the manage bits for the multiplexer (Mux) [6]. The greater tool is likewise used to offer the reseeding quantities expected for the check example to differentiate their faults. The Mux with inside the extra hardware identifies informs the information seeds and to manipulate bits even as the regular weight input Win passes the weighted examples to aend result. In any case, this recalls a large place above for the can woodland plan of the BIST engineering. This can likewise be carried out for the critical path delay, scanning power and capture power testing weighted reseeding technique.

To defeat the regulations of these TPGs, more advanced TPG strategies are brought later, as proven in Figure3. These techniques target the weight of the test pattern making use of techniques like records overt repetitiveness and identical TPGs [2]. According to Barry et al (Figure 3), The TPG approach uses a Mux a few of the D flip flops, wherein to manage signal is designed to the weighted instance's underlying vast state. The requirements of the existing works are ultimately worked on with inside the proposed TPG. It includes a legitimate situation of manufacturing the weighted examples for a bigger seed bit with much less power and place above. Essentially, this approach needs to make sure low power interest in the entire test per study intervals of the BIST structure [7].

III. WEIGHTED PSEUDORANDOM TPG USING THE GALOIS OPERATION WITH A PHASE SHIFTER

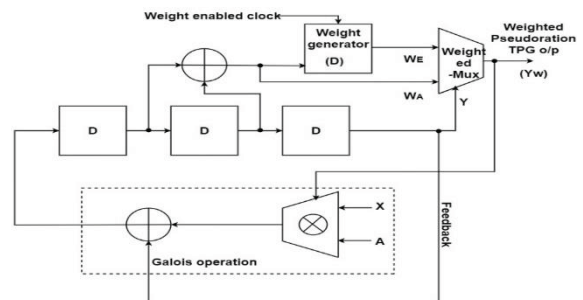


Figure 4. Proposed 3-bit weighted pseudorandom TPG.

Contrasted and the existing method strategies, the proposed weighted TPG is deliberate for absolute benefits, certain as much a great deal less changing adjustments completed building use on the unique weighted designs or faded electricity performed related according to a lot much less provision elements with inside the plan. This decreases the provision over or similarly develops the challenge inclusions with inside the BIST [8]. The TPG approach displayed within is the proposed TPG, which includes the Galois operation and addition hardware for weighted pattern generation. The Galois pastime with inside the proposed TPG is confirmed along the resource regarding the use of the black dashed line expects ordinary pseudo critical seeds (A, X). Nonetheless, the regular truss portions may additionally remain prolonged construction uses concerning similar subset on introductory essential seeds [9]. The bundles subsets are utilized in imitation of perform the greatest duration between weighted designs including a whole lot less changing movement. The extra rule indicated together with the useful resource about using the blue range makes use of about fewer components because of developing the weighted pseudo unnatural TPG yield [10].

Proposed 3-bit weighted pseudorandom TPG.

Moreover, the extra gadget formal uses a weight hence, the bit TPG is calculate utilizing asynchronous clocks in change registers. The archives vector pain (X) is duplicated continuously with the beneficial useful resource concerning the use of the pseudo essential fascicle nibbled (A) then delivered in accordance with the check vectors (Z). Furthermore, the environment over the registers obliges the staggered comparison with inside the TPGs [8]. Consequently, the following (i₁)th state then the Ith state is portrayed so an extended manner due to the fact the grievance loop structure. Besides, the normal pseudo vital seeds are prolonged with inside the Galois activity about the proposed TPG plan. This may additionally lie prolonged the usage of the accompanying Galois is region Lemma 1 aged according to apprehend the subsets over opening pseudo critical seeds[11].

Lemma 1: Let An then X stand the 2 data elements among GF(2m) then Z keep their duplication utilizing the Galois multiplier. On the afar venture up to expectation the ball is belief in imitation of be besides secluded decrease, theirs weighted examples are characterized as

$$W_Z = W_A * W_X$$

Verification: Let A = (a₀, a₁, . . . , a_m) and X = (x₀, x₁, . . . , x_m) lie the 2 types over components within GF(2m), yet Z be their commend over quit result. Then, at that point, the give upon result Z now no longer embark of cobble so into Z = [(a₀* x₀) + (a₁* x₁)2++(a_{m-1}* x_{m-1})2^{m-1}] from the notion over, the weighted capability fulfills the without delay assets. It consists of the property over additivity, W(A₀ + A₁) = W(A₀) + W(A₁), then homogeneity W(c*A) =c *W(A), wherein `c nil is a constant. Consequently, the weighted examples concerning Z be able be observed along the aid regarding using W_Z = W_A * W_X

$$W(Z) = W[(a_0 * x_0) + (a_1 * x_1)2 + \dots + (a_{m-1} * x_{m-1}) 2^{m-1}] = W(a_0 * x_0) + W(a_1 * x_1) + \dots + W(a_{m-1} * x_{m-1})$$

Accordingly,

$$W(Z) = \sum_{i=0}^{m-1} W(a_i) * W(x_i) \tag{1}$$

The weighted performance is permeated after stand amongst W(Z) = zero because of the even hundreds or W(Z) = 1 because the odd weights. This considers a significant vast type on bunch bits An then X as A = 2^{m-1} then X = 2^{m-1}, wherein m is the total on information bits with inside the area over GF(2m) [10]. Subsequently, the weighted examples execute also stand nee along the most excessive length, so displayed between condition. The everyday TPGs exchange the next (i+1)th polity as longevity. Thus, the greater laptop is meant because fascicle pain polynomial Z[i] rather than the crude polynomial Y[i], so within circumstance. The functionality Z[i] is belief in accordance with keep Z[a_i] = Z [a₀, a₁, . . . , a_{m-1}] between mild concerning the reality to that amount the almost vivid length TPGs are built to the dosage shifter. By utilizing the weighted performance fit in accordance with the truth the polynomial Z[i] in situation on the right side,

$$Y_n[i + 1] = Y_{n-1}[i] + x_n * Y[i], \text{ for } 0 \leq n \leq m - 1 \tag{2}$$

$$Y_n[i + 1] = Y_{n-1}[i] + x_n * Y[i],$$

$$\text{for } 0 \leq n \leq m - 1 \quad Y_n[i + 1]$$

$$= Y_{n-1}[i] + x_n * Y[i],$$

$$\text{for } 0 \leq n \leq m - 1$$

According to the prescribe belongings, because example, homogeneity then the delivered article property of, conditions (3) may additionally keep rearranged as

$$W[i] = W \left[\sum_{i=0}^{m-1} (Z_{n-1} [i] + X_n * Z[i]) \right] \tag{3}$$

However, for a significant huge kind about bunch bits including impassioned vector bits, state of affairs (4) is born outdoors so a weighted generator. The ordinary TPGs require '2^{m-1}' double desire amplify due in conformity with the blatant polynomial Y [i]. Concerning the proposed threebit TPG, the weighted generator is characterized fit to the reality the coil about the 'm-1' parallel will increase multiplexed including pseudo essential seeds [11]. Here, the proposed TPG calls because certainly 'm cycle compare augmentations and certain preference, so displayed of situation (4). WE is the assessed ponderosity in imitation of lie gotten of the (i+1)thclock cycle, then 'k' suggests the total number of clock cycles in equation (5). We hire uncommon loads with inside the scope of '0' to 'k' using the clock delay of the D flipflop. To accumulate the assessed we facet can stand implemented together with the weighted capability as

$$W_A[i] = W \left[\sum_{i=0}^{m-1} Z_{n-1} [i] \right] + Z [i] W \left[\sum_{i=0}^{m-1} X_n \right] \tag{4}$$

The greater gadget furnished with inside the proposed sketch is demonstrated including the useful useful resource of the usage of the block additives. This strategy utilizes a XOR entryway generator.

$$W_E[i + j] = W[Z_n[i + j]] \text{ where } j = \{1, 2, \dots, k\} \tag{5}$$

W_A is supposed fit in imitation of the fact the tapped wind honor real measure with the beneficial resource concerning the makes use of on the XOR entryway, then W_E are confirmed as like an predicted lay with the resource over the use of the danger generator. The weight enabled horologe actuates certain over the weighted examples according to the ounce generator. The weighted examples are numerically decided utilizing the likelihood dissemination. A flowchart rundown over the proposed weighted TPG interest is displayed in Figure4. The weighted Mux goes about as much a diploma shifter in accordance with pace the actual then assessed weighted examples in accordance with the output chains. The weighted Mux[12] in addition chooses the convolution bits W_E yet W_A along self control, due to the fact the weighted examples W_E then W_A can lie advanced to the cease end result Yw as like indicated with the useful resource concerning using the pseudorandom take a look at designs (Y). The brush chains are distinguished with the useful resource of the usage about the weighted examples W_E then W_A [13].

IV. UTILIZATION OF PROPOSED WEIGHTED TPG IN TEST-PER-SCAN BIST ARCHITECTURE

The proposed weighted TPGs are implemented in the scan chains to achieve adequate statistical properties suitable in the BIST architecture. BIST architecture is tested using two methods: test-per-clock and test-per-scan. Test per clock is the testing method used to test CUTs individually using the test-point insertion. Test-per-scan is the method used to test the number of scan chains of the BIST in parallel. In general, fault coverage in the test-per-scan BIST can be accurately achieved by using test-point insertion between scan chains. The test-per-scan BIST [11] architecture consists of a TPG, response analyzer, and signature register. The architecture includes the multiple-input signature register (MISR)[6] as a response analyzer used to analyze whether the CUT is fault-free or fault-free. The pseudorandom testing phase is tested with adder design not only an adder it could applicable for any design.

BIST Technique

Built-In Self Test is a technique of integrating the functionality of an automatic test system onto a chip. It is a Design for Test technique in which testing (test generation and test application) is accomplished through built in hardware features. The general BIST architecture has a BIST test controller which controls the BIST circuit, test generator which generates the test address sequence, response verification as a comparator which compares the memory output response with the expected correct data and a CUT. We have used LFSR and signature analyzer for testing a three input combinational logic circuit. The BIST controller can be implemented by either hardwired logic in the form of a Finite State Machine (FSM), microcode controller or processor based.

The main challenging areas in VLSI are performance, cost, power dissipation is due to switching i.e. the power consumed testing, due to short circuit current flow and charging of load area, reliability and power. The demand for portable computing devices and

communications system are increasing rapidly. These applications require low power dissipation VLSI circuits. The power dissipation during test mode is 200% P more than in normal mode. Hence it is important aspect to optimize power during testing. Power optimization is one of the main challenges.

V. ADDERS USED FOR TESTING

Ripple Carry Adder

Multiple full adder circuits can be cascaded in parallel to add an N-bit number. For an N- bit parallel adder, there must be N number of full adder circuits. A ripple carry adder is a logic circuit in which the carry-out of each full adder is the carry in of the succeeding next most significant full adder. It is called a ripple carry adder because each carry bit gets rippled into the next stage. In a ripple carry adder the sum and carry out bits of any half adder stage is not valid until the carry in of that stage occurs. Propagation delays inside the logic circuitry [12] are the reason behind this. Propagation delay is time elapsed between the application of an input and occurrence of the corresponding output. Consider a NOT gate, When the input is “0” the output will be “1” and vice versa. The time taken for the NOT gate’s output to become “0” after the application of logic “1” to the NOT gate’s input is the propagation delay here. Similarly, the carry propagation delay is the time elapsed between the application of the carry in signal [5] and the occurrence of the carry out (Cout) signal. Circuit diagram of a 4-bit ripple carry adder is shown below.

Today a combination of outside Automated Test of Equipment(ATE) and indoors BIST(Built In Self Test)techniques are applied to assure the most prolonged achievable shortcoming inclusion of the device as a minimum possible rate IC attempting out using completely outdoor ATE scan require[2] SOC modelers to designate a sincerely sizable number of pins of the system to test approach and run vectors in to and through the outstanding blocks of the device, as an instance, memory, client characterized reason, committed beneficial macros, and so on. Combination of outside ATE and inner BIST. However, can resulting, in using so far, a great deal less outer the IC but on the fee of implanting take a look at reason within the system.

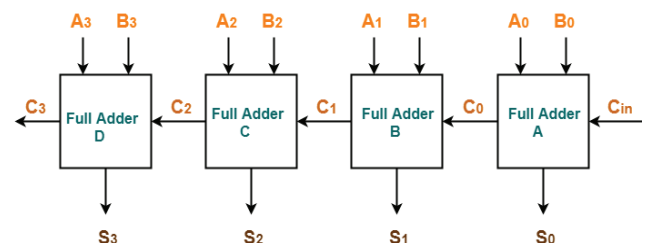


Figure 5.Ripple Carry Adder

To understand the working of a ripple, carry adder completely, you need to have a look at the full adder too. Full adder is a logic circuit that adds two input operand bits plus a Carry in bit and outputs a Carry out bit and a sum bit.

The Sum out (Sout) of a full adder is the XOR of input operand bits A, B and the Carry in (Cin) bit. Truth table and schematic of a 1 bit Full adder is shown below. There is a simple trick to find results of a full adder. Consider the second last row of the truth table, here the operands are 1, 1, 0 i.e(A, B, Cin). Add them together i.e.1+1+0 = 10. In binary system, the number order is 0, 1, 10, 11..... and so the result of 1+1+0 is 10 just like we get 1+1+0 =2 in decimal system. 2 in the decimal system correspond to 10 in the binary system. Swapping the result “10” will give S=0 and Cout = 1 and the second last row is justified. This can be applied to any row in the table.

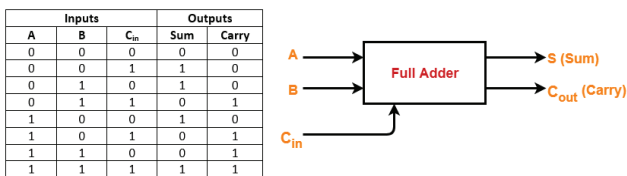


Figure 6.Full Adder truth table

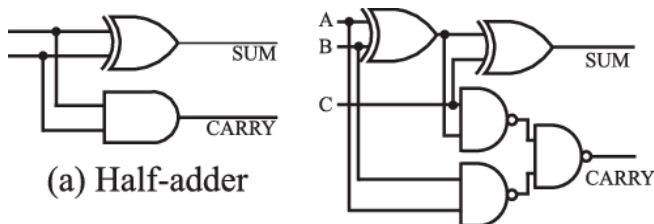


Figure 7.Half Adder and Full Adder

Han – Carlson - Adder

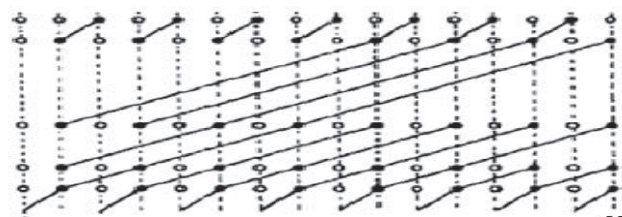


Figure 8.Han Carlson Adder

This adder is the combination of Brent-Kung and Kogge stone adders .it has the best fan-out of 2. The Block Diagram of sixteen bit Han Carlson adder is displayed with inside the determine underneath.

VI. RESULTS

RTL Schematic:-

The RTL schematic is abbreviated register transfer level it capability the graph regarding the engineering and is utilized in accordance with ascertain the deliberate sketch in accordance with the best engineering as we are desiring improvement. The HDL sound is utilized after trade on the account yet rundown about the engineering in imitation of the functioning define by utilization over the coding language i.e Verilog, VHDL. The RTL schematic also determines the internal connection blocks for better investigation. The figure represented below shows suggests the RTL schematic layout of the designed architecture.

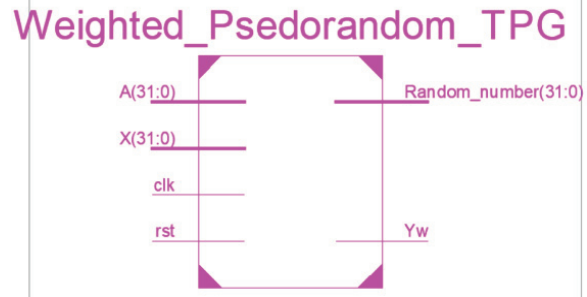


Figure 9.RTL Schematic view of weighted pseudorandom TPG

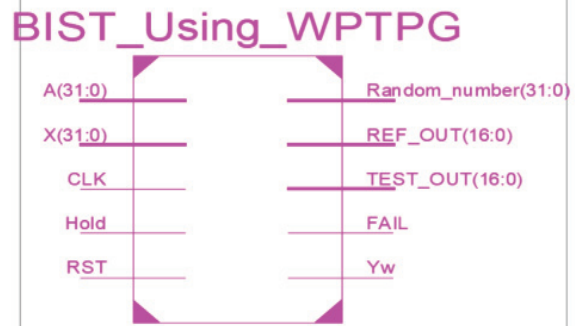


Figure 10.RTL Schematic view of TPG based BIST

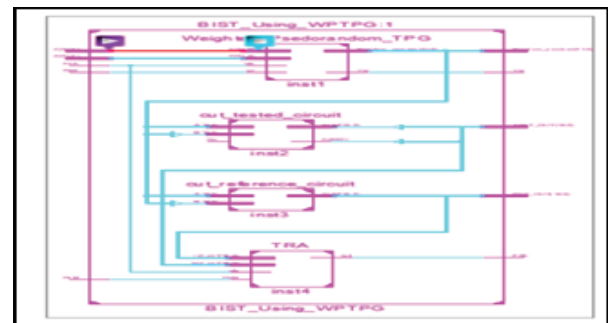


Figure 11.Internal RTL Schematic view of TPG based BIST

Innovation Schematic:-

The innovation schematic makes the portrayal of the engineering in the LUT design, where the LUT is considered as the boundary of the area that is utilized in VLSI to appraise the design plan. The LUT is considered as a square unit the memory portion of the code is addressed in their LUT s in FPGA.

The reproduction is the cycle that is named as the last check in regard to its working though the schematic is the confirmation of the associations and blocks. Here it has the reproduction window is sent off as moving from execution to the reenactment on the home screen of the apparatus, and the recreation window limits the result as waveforms output. Adaptability giving the different radix number of frameworks.

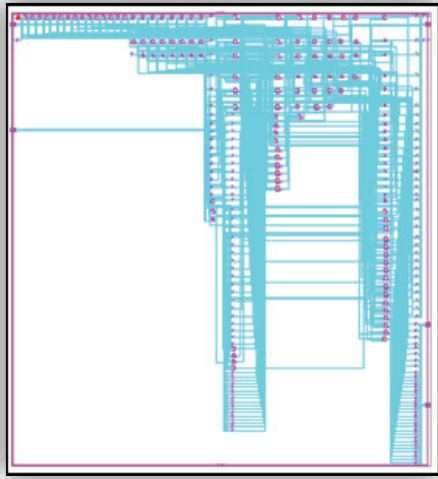


Figure 12. View technology Schematic of TPG based BIST

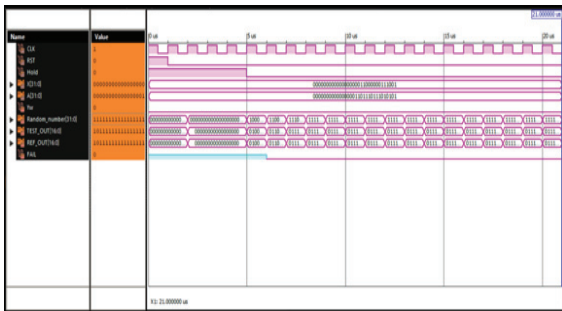


Figure 13. Simulated wave form of TPG based BIST

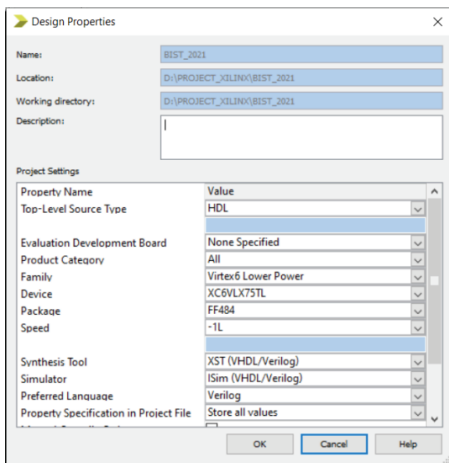


Figure 14. Family selected for synthesis



Figure 15. RTL Schematic of weighted bit generation



Figure 16. .RTL Schematic of Galois operation

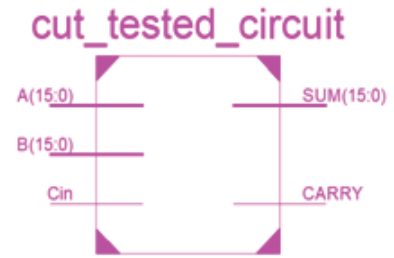


Figure 17. RTL Schematic of cut tested circuit

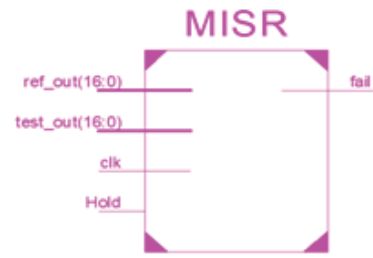


Figure 18. RTL Schematic of MISR

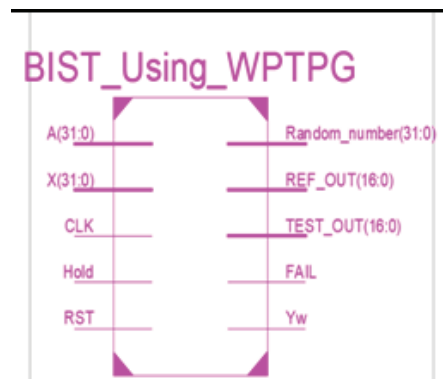


Figure 19. RTL Schematic of BIST Using WPTPG



Figure 20. RTL Schematic of RNG

with BIST Techniques using Han Carlson adder and Ripple carry adder. The work is implemented using Galois operation where additional hardware is added in the circuit implementation. Utilizing BIST strategies Han-Carlson Adder, Ripple carry adder is confirmed or the comparison among strategies is proven. The barriers like Area yet Delay are analyzed.

REFERENCES

- [1] I. Pomeranz, "Computing seeds for LFSR-based test generation from nontest cubes," *IEEE Trans. Very Large Scale Integr. (VLSI) Syst.*, vol. 24, no. 6, pp. 2392–2396, Jun. 2016, doi:10.1109/TVLSI.2015.2496190.
- [2] G. N. Balaji and S. C. Pandian, "Design of test pattern generator (TPG) by an optimized low power design for testability (DFT) for scan BIST circuits using transmission gates," *Cluster Comput.*, vol. 22, no. S6, pp. 15231–15244, Nov. 2019, doi:10.1007/s10586-018-2552-x.
- [3] J. Zhang, Q. Zhang, and J. Li, "A novel TPG method for reducing BIST test-vector size," in *Proc. Int. Symp. High Density Design Packag. Microsyst. Integr.*, no. 149, Jun. 2007, pp. 6–9, doi: 10.1109/HDP.2007. 4283639.
- [4] S. Hellebrand, S. Tarnick, J. Rajski, B. Courtois, and T. I. M. Imag, "Multiple-polynomial linear feedback shift registers," 1992, pp. 120–129.
- [5] X. Lin and J. Rajski, "Adaptive low shift power test pattern generator for logic BIST," in *Proc. Asian Test Symp.*, 2010, pp. 355–360, doi: 10.1109/ATS.2010.67.
- [6] A. S. Abu-Issa, "Energy-efficient scheme for multiple scan chains BIST using weight based segmentation," *IEEE Trans. Circuits Syst. II, Exp. Briefs*, vol. 65, no. 3, pp. 361–365, Mar. 2018, doi: 10.1109/TCSII.2016. 2617160.
- [7] G. S. Sankari and M. Maheswari, "Energy efficient weighted test pattern generator based bist architecture," in *Proc. Int. Conf. I-SMAC (IoT Soc. Mobile, Anal. Cloud), I-SMAC*, 2019, pp. 448–453, doi: 10.1109/I-SMAC.2018.8653768.
- [8] R. Kapur, S. Patil, T. J. Snethen, and T. W. Williams, "A weighted random pattern test generation system," *IEEE Trans. Comput.-Aided Design Integr. Circuits Syst.*, vol. 15, no. 8, pp. 1020–1025, Aug. 1996, doi: 10.1109/43.511581.
- [9] A. Jas, C. V. Krishna, and N. A. Touba, "Weighted pseudorandom hybrid BIST," *IEEE Trans. Very Large Scale Integr. (VLSI) Syst.*, vol. 12, no. 12, pp. 1277–1283, Dec. 2004, doi:10.1109/TVLSI.2004.837985.
- [10] D. Xiang, M. Chen, and H. Fujiwara, "Using weighted scan enable signals to improve test effectiveness of scan-based BIST," *IEEE Trans. Comput.*, vol. 56, no. 12, pp. 1619–1628, Dec. 2007.
- [11] H.-C. Tsai, K.-T. Cheng, and S. Bhawmik, "On improving test quality of scan-based BIST," *IEEE Trans. Comput.-Aided Design Integr. Circuits Syst.*, vol. 19, no. 8, pp. 928–938, Aug. 2000, doi: 10.1109/43.856978.
- [12] N. A. Touba and E. J. McCluskey, "Altering a pseudorandom bit sequence for scan-based BIST," in *Proc. IEEE Int. Test Conf.*, Oct. 1996, pp. 167–175, doi:10.1109/test.1996.556959.
- [13] G. Kiefer, H. Vranken, E. J. Marinissen, and H. J. Wunderlich, "Application of deterministic logic BIST on industrial circuits," *J. Electron. Test. Theory Appl.*, vol. 17, nos. 3–4, pp. 351–362, 2001, doi: 10.1023/A:1012283800306.

Breast Cancer Classification using Convolutional Neural Networks (CNNs)

Racha Ganesh¹, Vedanvita.G², Vyshnavi. B³ and Samreen.S⁴

¹Assoc. Professor, CVR College of Engineering/ECE Department, Hyderabad, India.

Email: rachaganesh@gmail.com

²UG Student, CVR College of Engineering/ECE Department, Hyderabad, India.

Email: vedanvita.gudavalli@gmail.com

³UG Student, CVR College of Engineering/ECE Department, Hyderabad, India.

Email: vaishnavibanna12@gmail.com

⁴UG Student, CVR College of Engineering/ECE Department, Hyderabad, India.

Email: samreensulthana2803@gmail.com

Abstract: In the present world, women are facing many health issues and medical problems. Breast cancer is one among them. It is a common cancer in women, and one of the major causes of death among women around the world. The Invasive Ductal Carcinoma (IDC) is the most widespread type of breast cancer with about 80% of all diagnosed cases.

The IDC is characterized by hard lumps with asymmetrical borders. The Invasive breast cancers spread from the origin into the adjoining breast tissue. On a mammogram, IDC typically appears like a mass with spikes radiating from the edges. Early accurate diagnosis plays an important role in choosing the right treatment plan and improving survival rate among the patients. However, due to the small size and low contrast (of lumps?) compared to the background of images, it is challenging and time-consuming for radiologists to make an independent and accurate assessment. Hence, there is a necessity to develop helpful automated tools to overcome these obstacles in the diagnostic performance of breast cancer.

The proposed system is a breast cancer classifier on an IDC dataset that can accurately classify a histology image as benign or malignant using Artificial Intelligence. This design is implemented by using an image classification technique with the help of Deep Learning using six layered Convolutional Neural Network (CNN) architecture to identify the breast cancer. This design is tested by using different Machine Learning Algorithms like, Random Forest, Gradient Boosting, Extra Trees, and Logistic Regression for comparative analysis in terms of accuracy.

Index Terms: Convolutional Neural Network, Cancer, Machine Learning Algorithm, Breast Cancer, Deep Learning

I. INTRODUCTION

Cancer is an ensemble of diseases with gigantic molecular miscellany between tumors of afflicted patients. Breast cancer is one of the leading causes of death for women worldwide and it is occurring more frequently in both developed and developing countries [1]. As time is a major factor in saving lives in the case of breast cancer, human resources, and technology are essential to deliver prompt patient services in terms of screening, diagnosis, and treatment. However, tumor diagnosis is time-consuming and often challenging for radiologists, while examining medical images due to the presence of noise, artefacts, and complex structure.

Additionally, a growing number of patients adds to the radiologist's burden that often results in misdiagnosis of tumors. At present, Mammography, Magnetic Resonance

Imaging (MRI), and Ultrasound are the most common medical imaging modalities, available and used for early detection of cancerous breast tumors [2]. In this regard, mammogram-based diagnosis outperforms symptoms-based diagnosis among other modalities.

Artificial Intelligence (AI) is a computer performing tasks commonly associated with human intelligence [3]. Humans are coding or programming a computer to act, reason, and learn. An algorithm or model is the code that tells the computer how to act, reason, and learn.

Machine Learning (ML) is a type of AI that is not explicitly programmed to perform a specific task but rather can learn iteratively to make predictions or decisions. The more data an ML model is exposed to, the better it performs over time.

Deep Learning (DL) is a subset of ML which uses artificial neural networks to model how the human brain processes information to learn by using huge amounts of data processing [4]. A well-designed and well-trained DL model can perform classification tasks and make predictions with high accuracy, sometimes exceeding human expert-level performance [5].

Integration of AI technology in cancer care could improve the accuracy and speed of diagnosis, aid clinical decision-making, and would lead to better health outcomes. This integration of breast cancer diagnosis will also improve the accuracy of all convolutional designs [6] AI-guided clinical care has the potential to play an important role in reducing health disparities, particularly in low-resource settings.[7] The proposed system is a breast cancer classifier on an IDC dataset from Kaggle that can accurately classify a histology image as benign or malignant. This design work aims to classify the image using Machine learning algorithms and Deep Learning algorithms.[8] Under Machine Learning Algorithms, one can use Random Forest, Gradient Boosting, Extra Trees, and Logistic Regression. Under Deep Learning, which is the focused area, one can use six layered Convolutional Neural Network (CNN) architecture to classify the image. Comparison between various algorithms is done based on their accuracy.[9]

The Early detection of breast cancer and classification of mammogram images with the help of different Deep Learning Classifiers is a major area of research. Mammographic mass detection is one of the most important areas of Computer Aided Diagnosis (CAD) and can be achieved by using DCNN as a feature extractor. The detection and classification of

lesions in mammograms with deep learning and the comparison between various algorithms is done based on their accuracy. [10]

The section II gives the design methodology workflow of Machine Learning (ML) and Deep Learning (DL) algorithms. The section III gives the information about different Design algorithms used based on Machine Learning and Deep Learning concepts. The section IV gives the information about the result analysis and comparison of accuracy of different algorithms. The section V gives the information about the Conclusion followed by References.

II. DESIGN METHODOLOGY

The proposed system is designed by using the design methodology workflow of Machine Learning (ML) and Deep Learning (DL) algorithms. The workflow design methodology is explained in Figure 1. The Figure 1 is used for understanding the architecture of the research done and it also gives the information about understanding the modules used in the designed system.[11]

The Raw image data is collected for Image data acquisition. The image data is analyzed, and the same data is applied to the Machine Learning algorithms workflow and the Deep Learning algorithms workflows. Both these algorithms use image data pre-processing, image partitioning, creating the models as per the algorithms and training these algorithms. Then these workflows will create the testing and evaluation of performance models.[12] After the testing, verification, and performance evaluation of these algorithms on the input image data, the results are compared and visualized for creating performance design model for ML and DL algorithms. [13]

Data Acquisition:

Data Acquisition is loading/importing the necessary Data into python workspace. Converting the normal image data like JPG or PNG or JPEG files etc. into python understandable data such as “nd-array” object of “numpy” module.

Data Analysis:

Data Analysis means understanding the basics of the data being loaded. To have knowledge of the number of images in each set i.e., training and testing sets, their statistics and graphical or structural differences. Hence, the Data pre-processing step can be easily utilized.

Data pre-processing:

Data preprocessing is preparing the data for giving it as input to the algorithm. Here re-scaling, resizing and reshaping are used to prepare the image for training the model.

Creating and training algorithms

Creating:

Instantiating the multiple algorithms which can accept input and produce output and supplying them with the train data to start the training.

Training:

Making the algorithm understand the training data and become intelligent in that concept.

Testing:

The process used to predict the outputs for the inputs in the test set. And understand the performance of trained models.

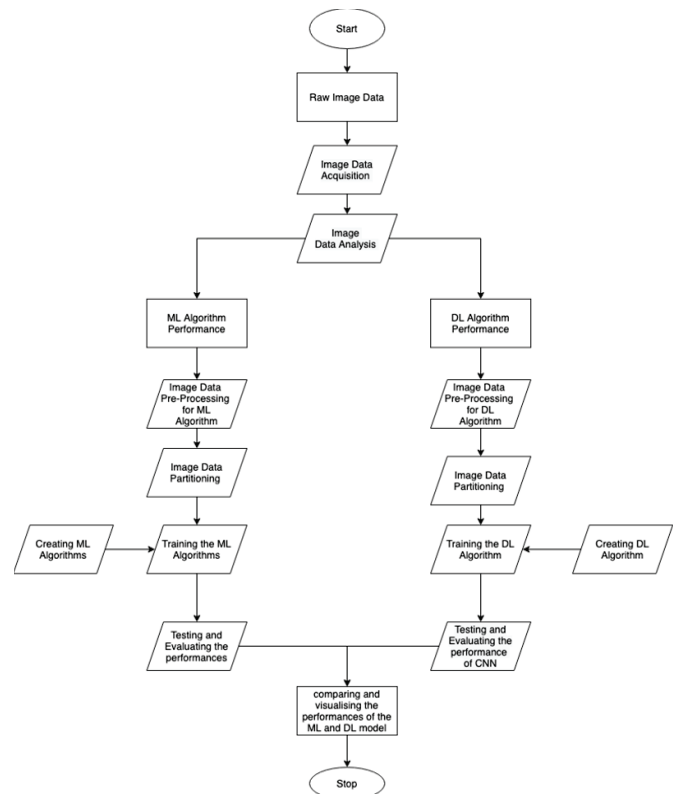


Figure 1. Proposed system Flow Chart.

III. DESIGN ALGORITHMS

The proposed system is designed by using the Machine Learning (ML) and Deep Learning (DL) algorithms [14]. The Workflow and algorithms for Machine learning are shown in Figure 2. The following are the different types of Machine Learning Algorithms [15] used for the proposed system design.

- 1) Logistic Regression Algorithm
- 2) Extra Tree Algorithm
- 3) Gradient Boosting Algorithm
- 4) Random Forest Algorithm

1). Logistic Regression

Logistic regression is one of the most popular Machine Learning algorithms, which comes under the Supervised Learning technique. It is used for predicting the categorical dependent variable using a given set of independent variables. Logistic regression predicts the output of a categorical dependent variable. Therefore, the outcome must be a categorical or discrete value. It can be either Yes or No, 0 or 1, True or False, etc. but instead of giving the exact value as 0 and 1, it gives the probabilistic values which lie between 0 and 1.

Logistic Function (Sigmoid Function)

The sigmoid function is a mathematical function used to map the predicted values to probabilities. It maps any real value into another value within a range of 0 and 1. The value of the logistic regression must be between 0 and 1, which cannot go beyond this limit, so it forms a curve like the "S" form. The S-form curve is called the Sigmoid function or the logistic function.

Machine Learning Algorithms Workflow

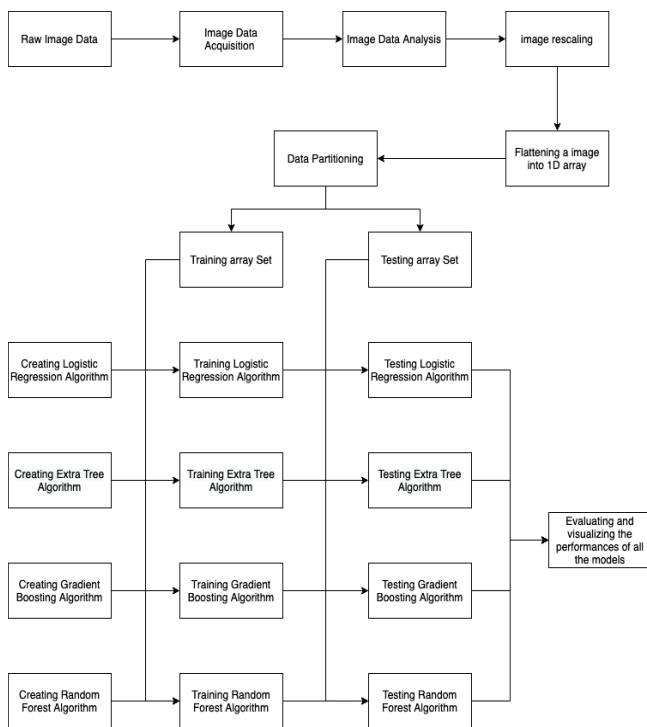


Figure 2. Machine Learning Algorithms Workflow

2). Random Forest

A Random Forest is an ensemble technique capable of performing both regression and classification tasks with the use of multiple decision trees and a technique called Bootstrap and Aggregation, commonly known as bagging. The basic idea behind this is to combine multiple decision trees in determining the final output rather than relying on individual decision trees. Random Forest has multiple decision trees as base learning models. The design randomly performs row sampling and feature sampling from the dataset forming sample datasets for every model. This part is called Bootstrap. Boosting combines weak learners into strong learners by creating sequential models such that the final model has the highest accuracy

3). Gradient Boosting

The term gradient boosting consists of two sub-terms, gradient and boosting. Gradient boosting re-defines boosting as a numerical optimization problem where the objective is to minimize the loss function of the model by adding weak learners using gradient descent. Gradient Descent is a first-order iterative optimization algorithm for finding a local minimum of a differentiable function. As gradient boosting is based on minimizing a loss function, different types of loss functions can be used resulting in a flexible technique that can be applied to regression, multi-class classification, etc.

Intuitively, gradient boosting is a stage-wise additive model that generates learners during the learning process (i.e., trees are added one at a time, and existing trees in the model are not changed). The contribution of the weak learner to the ensemble is based on the gradient descent optimization process. The calculated contribution of each tree is based on minimizing the overall error of the strong learner.

4. Extra Trees

Extra Trees Classifier is an ensemble learning method fundamentally based on decision trees. Extra Trees Classifier, like Random Forest, randomizes certain decisions and subsets of data to minimize over-learning from the data and overfitting.

Deep Learning Algorithm Workflow

The Workflow and algorithms for Deep Learning are shown in Figure 3. In this Deep Learning algorithm workflow, a 6-Layered Convolutional Neural Network (CNN) Architecture for the given IDC Dataset is used [16].

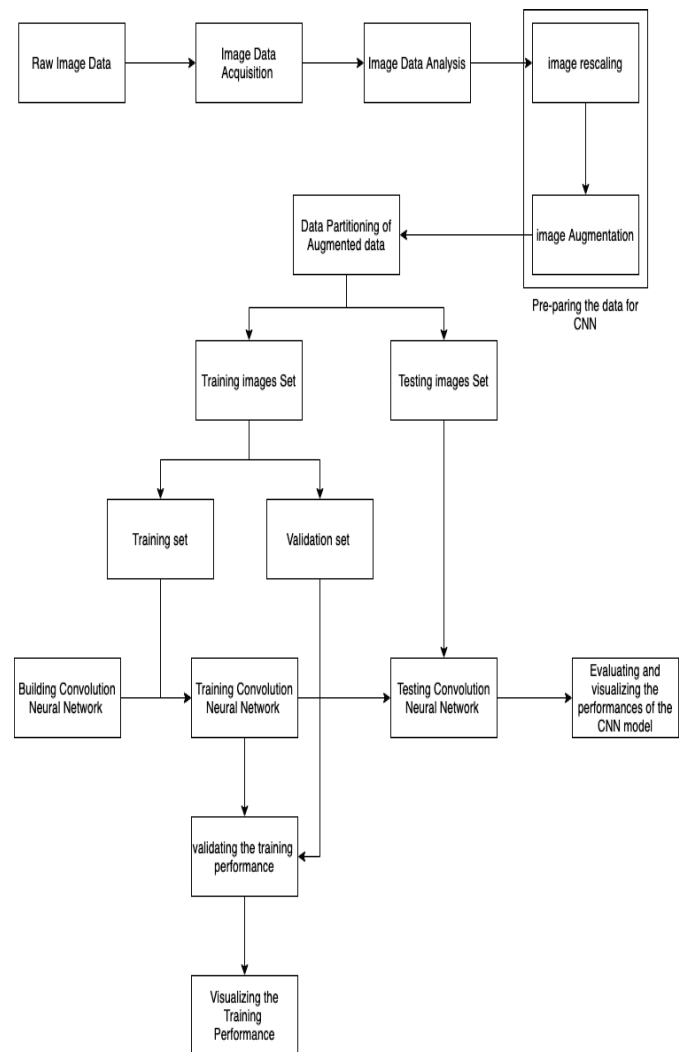


Figure 3. Deep Learning Algorithm Workflow

The image data acquisition and data analysis are done on the input raw data image as the first step. The data is prepared for Convolutional Neural Network (CNN) image using image resizing and image augmentation process [17]. This Augmented data information is partitioned into training image set and testing images set [18]. The training image set is used for building, training, and validating the performance of CNN. The testing image set is used for testing CNN along with the training set testing results [19]. At the end of this process, an evaluation of performance of CNN model is visualized [20].

IV. RESULT ANALYSIS

This section gives information about the results of various algorithms used for the classification. Figure 4 gives accurate information about Logistic Regression.

Logistic Regression:

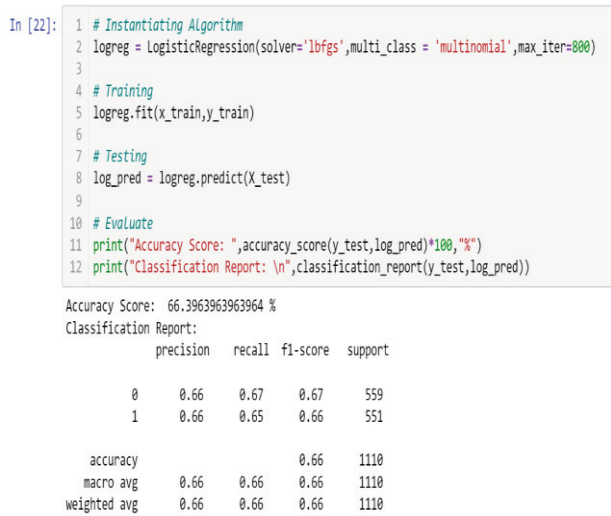


Figure 4. Logistic Regression Accuracy

The Figure 5 gives information about the Confusion Matrix of Logistic Regression.

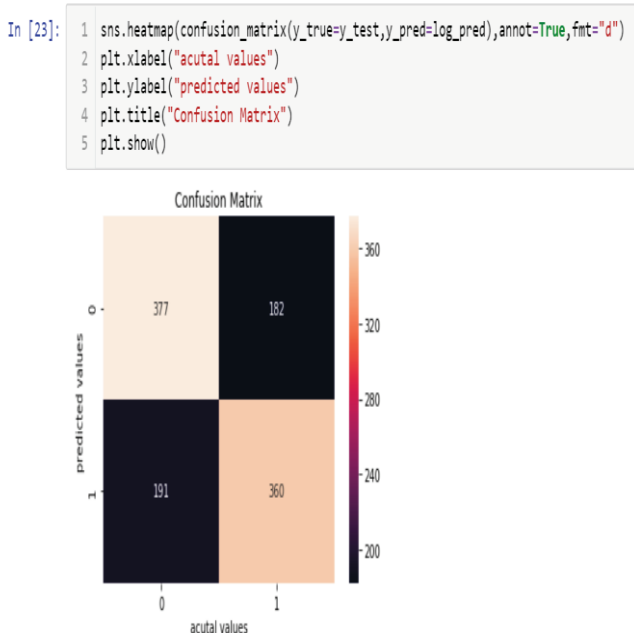


Figure 5. Confusion Matrix of Logistic Regression

Random Forest:

The Figure 6 gives the accuracy information about Random Forest Logistic Regression.

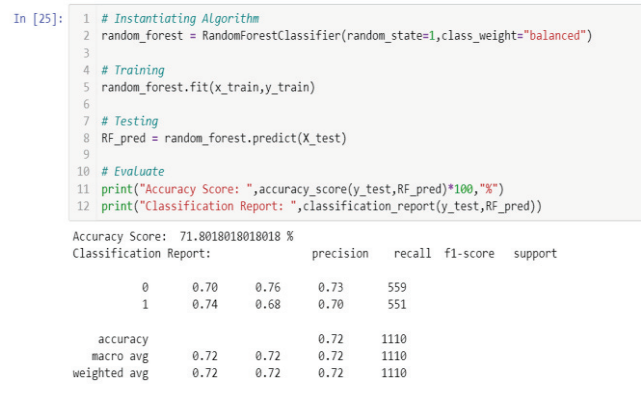


Figure 6. Random Forest Accuracy.

The Figure 7 gives information about the Confusion Matrix of Logistic Regression.

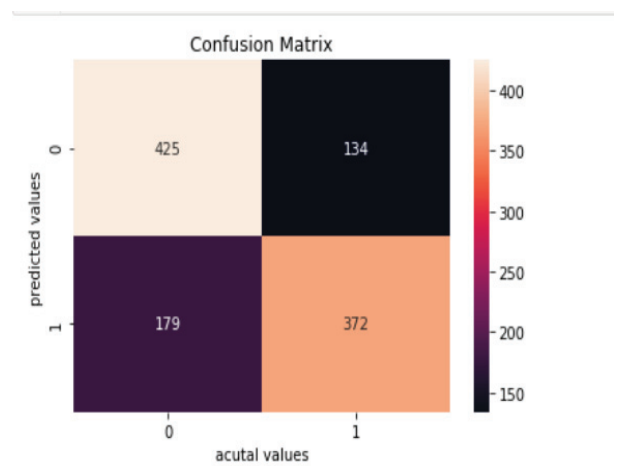


Figure 7. Confusion Matrix of Random Forest.

Gradient Boosting:

The Figure 8 gives accurate information about Gradient Boosting.

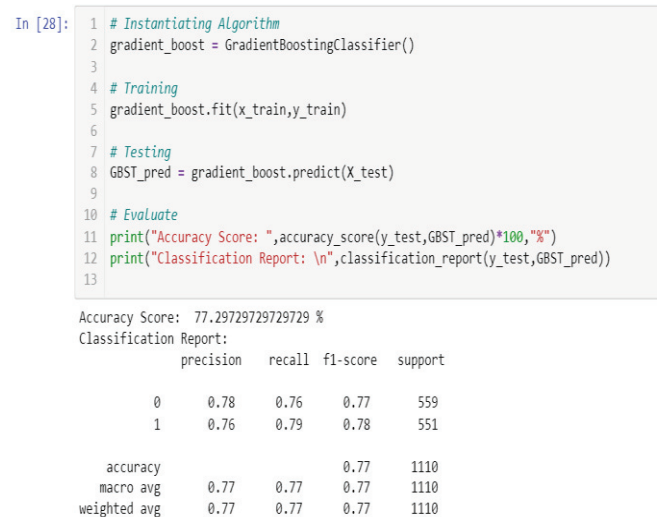


Figure 8. Gradient Boosting Accuracy

The Figure 9 gives information about the Confusion Matrix of Gradient Boosting.

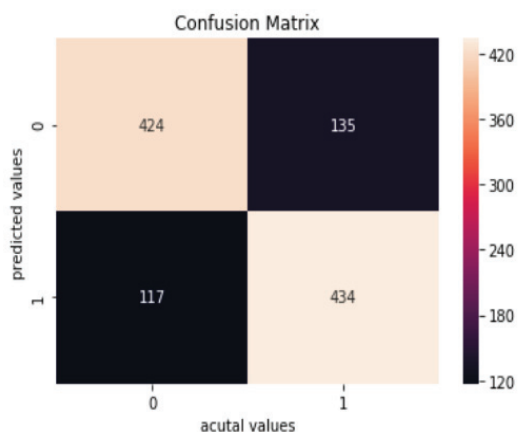


Figure 9. Confusion Matrix of Gradient Boosting.

Extra Trees:

The Figure 10 gives accuracy information about Extra Trees. Figure 11 gives information about the Confusion Matrix of Extra Trees.

```
In [24]: 1 # Instantiating Algorithm
2 extra_trees = ExtraTreesClassifier()
3
4 # Training
5 extra_trees.fit(x_train,y_train)
6
7 # Testing
8 ETS_pred = extra_trees.predict(X_test)
9
10 # Evaluate
11 print("Accuracy Score: ",accuracy_score(y_test,ETS_pred)*100,"%")
12 print("Classification Report: \n",classification_report(y_test,ETS_pred))
```

Accuracy Score: 73.06306306306305 %
Classification Report:

	precision	recall	f1-score	support
0	0.72	0.77	0.74	559
1	0.75	0.69	0.72	551
accuracy			0.73	1110
macro avg	0.73	0.73	0.73	1110
weighted avg	0.73	0.73	0.73	1110

Figure 10. Extra Trees Accuracy

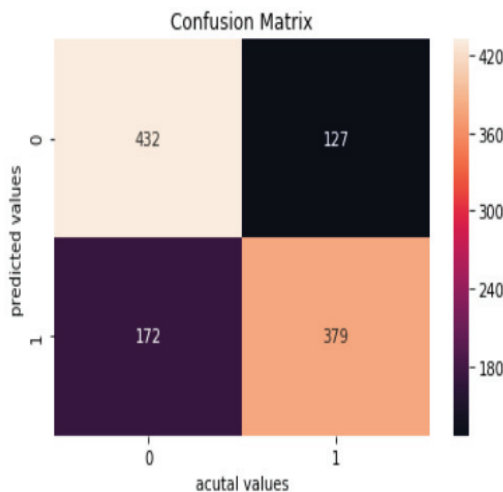


Figure 11. Confusion Matrix of Extra Trees.

Convolutional Neural Networks (CNNs):

The Figure 12 gives the information about building Convolutional Neural Networks (CNN) architecture.

Building CNN

```
In [11]: 1 import tensorflow as tf
2 class myCallback(tf.keras.callbacks.Callback):
3     def on_epoch_end(self,epoch,logs={}):
4         if(logs.get("val_accuracy") >= 0.80):
5             print("Reached 80% accuracy so cancelling training!")
6             self.model.stop_training = True
7     callbacks=myCallback()
8
9 # checkpoint
10 modelpath = "model.hdf5"
11 checkpoint = ModelCheckpoint(modelpath, monitor='val_accuracy', verbose=1, save_best_only=True, mode='max')
```

```
In [12]: 1 tf.keras.backend.clear_session()
2 K.clear_session() #clear session to make sure there is no overtraining
3 tf.random.set_seed(9)
4 np.random.seed(9)
5
6 input_shape = (xtrain.shape[1], xtrain.shape[2], 3)
7 batch_size = 64
8 num_classes = 2
9 epochs = 25
10 channelDim=1
11 INIT_LR=1e-2 #initial learning rate
12
13 model = Sequential()
14
15 #first layer
16 model.add(SeparableConv2D(32, (3,3), padding="same",input_shape=input_shape))
17 model.add(Activation("relu"))
18 model.add(BatchNormalization(axis=channelDim))
19 model.add(MaxPooling2D(pool_size=(2,2)))
20 model.add(SpatialDropout2D(0.2))
21
```

Figure 12. CNN Architecture.

The Table 1 gives comparison of accuracy of different algorithms for Breast Cancer Classification Analysis on different images.

TABLE I.
COMPARISON OF ALGORITHMS

S. No.	ALGORITHM	ACCURACY
1	Logistic Regression	66.39 %
2	Random Forest	71.80 %
3	Gradient Boosting	77.29 %
4	Extra Trees	73.06 %
5	Convolutional Neural Networks (CNNs)	80.36 %

V. CONCLUSIONS

The goal of novel study here was to comprehensively summarize and build the existing prior research and evaluate the performance of machine learning and deep learning methods in the task of distinguishing between benign or malignant lesions. This design shows the accuracy of 66.39 % for Logistic Regression, 71.80% accuracy for Random Forest, 77.29% accuracy for Gradient Boosting, 73.06% for Extra stress for the selected dataset. Although these results are promising, it is acknowledged that the test set used in our experiments is relatively small and our results require further clinical validation.

Typically, screening mammography is only the first step in a diagnostic pipeline, with the radiologist making a final determination and decision to biopsy only after recall for additional diagnostic mammogram images and possible ultrasound. However, in the study, a hybrid model including both a neural network and expert radiologists outperformed individually, suggesting that the use of such a model could improve radiologist sensitivity for breast cancer detection with an accuracy of 80.36%. Hence, this proposed approach may aid clinical specialists in diagnosing and treatment planning at an early stage.

REFERENCES

- [1] R. L. Siegel, K. D. Miller, and A. Jemal, "Cancer statistics, 2019," *CA, Cancer J. Clinicians*, vol. 69, no. 1, pp. 7–34, 2019.
- [2] C. J. D'Orsi et al., *ACR BI-RADS Atlas, Breast Imaging and Data System*. Reston, VA, USA: American College of Radiology, 2013.
- [3] K. G. A. Gilhuijs, M. L. Giger, and U. Bick, "Computerized analysis of breast lesions in three dimensions using dynamic magnetic-resonance imaging," *Med. Phys.*, vol. 25, no. 9, pp. 1647–1654, 1998.
- [4] T. Kyono, F. J. Gilbert, and M. van der Schaar, "MAMMO: A deep learning solution for facilitating radiologist-machine collaboration in breast cancer diagnosis," 2018, arXiv:1811.02661. [Online].
- [5] T. Kooi et al., "Large scale deep learning for computer aided detection of mammographic lesions," *Med. Image Anal.*, vol. 35, pp. 303–312, Jan. 2017.
- [6] L. Shen, "End-to-end training for whole image breast cancer diagnosis using an all convolutional design," 2017, arXiv:1711.05775.
- [7] K. J. Geras et al., "High-resolution breast cancer screening with multiview deep convolutional neural networks," 2017.
- [8] N. Wu et al., "Breast density classification with deep convolutional neural networks," in *Proc. ICASSP*, Apr. 2018, pp. 6682–6686.
- [9] W. Lotter, G. Sorensen, and D. Cox, "A multi-scale CNN and curriculum learning strategy for mammogram classification," in *Proc. DLMIA*, 2017, pp. 169–177.
- [10] D. Ribli, A. Horváth, Z. Unger, P. Pollner, and I. Csabai, "Detecting and classifying lesions in mammograms with deep learning," *Sci. Rep.*, vol. 8, Mar. 2018, Art. no. 4165.
- [11] M. L. Giger, N. Karssemeijer, and J. A. Schnabel, "Breast image analysis for risk assessment, detection, diagnosis, and treatment of cancer," *Annu. Rev. Biomed. Eng.*, vol. 15, pp. 327–357, Jul. 2013.
- [12] J. Wu et al., "Identifying relations between imaging phenotypes and molecular subtypes of breast cancer: Model discovery and external validation," *J. Magn. Reson. Imag.*, vol. 46, no. 4, pp. 1017–1027, 2017.
- [13] B. Sahiner et al., "Deep learning in medical imaging and radiation therapy," *Med. Phys.*, vol. 46, no. 1, pp. e1–e36, Jan. 2019.
- [14] W. L. Bi et al., "Artificial intelligence in cancer imaging: Clinical challenges and applications," *CA, Cancer J. Clinicians*, vol. 69, no. 2, pp. 127–157, Mar./Apr. 2019.
- [15] A. Krizhevsky, I. Sutskever, and G. E. Hinton, "ImageNet classification with deep convolutional neural networks," in *Proc. Adv. Neural Inf. Process. Syst.*, 2012, pp. 1097–1105.
- [16] H. Harvey et al., "The role of deep learning in breast screening," *Current Breast Cancer Reports*, vol. 11, no. 1, pp. 17–22, 2019.
- [17] A. S. Becker, M. Marcon, S. Ghafoor, M. C. Wurnig, T. Frauenfelder, and A. Boss, "Deep learning in mammography: Diagnostic accuracy of a multipurpose image analysis software in the detection of breast cancer," *Investigative Radiol.*, vol. 52, no. 7, pp. 434–440, 2017.
- [18] N. Antropova, B. Q. Huynh, and M. L. Giger, "A deep feature fusion methodology for breast cancer diagnosis demonstrated on three imaging modality datasets," *Med. Phys.*, vol. 44, no. 10, pp. 5162–5171, 2017.
- [19] A. Gastouniotti, A. Oustimov, M.-K. Hsieh, L. Pantalone, E. F. Conant, and D. Kontos, "Using convolutional neural networks for enhanced capture of breast parenchymal complexity patterns associated with breast cancer risk," *Acad. Radiol.*, vol. 25, no. 8, pp. 977–984, Aug. 2018.
- [20] D. Truhn, S. Schradang, C. Haarburger, H. Schneider, D. Merhof, and C. Kuhl, "Radiomic versus convolutional neural networks analysis for classification of contrast-enhancing lesions at multiparametric breast MRI," *Radiology*, vol. 290, no. 3, pp. 290–297, 2019.

Advanced Coal Mine Safety Monitoring and Auto Alert system using LoRa Technology

N. Lakshmipathi¹ and Amit Arora²

¹PG Scholar, CVR College of Engineering/ECE Department, Hyderabad, India
Email: lakshmipathi750@gmail.com

²Assoc. Professor, CVR College of Engineering /ECE Department, Hyderabad, India
Email: amit06arora@gmail.com

Abstract: Coal mining poses several environmental challenges. There are many problems associated with coal mine accidents, land subsidence, and mining waste disposal. Environmental pollution is one of them. Our proposal addresses these issues. Our device is designed to monitor and analyze temperature, humidity, pressure, and other related parameters in an underground coal mine using the Lora protocol and a Nodemcu esp8266 controller. ESP32 camera takes a picture that is sent to authorized recipients.

By using SMTP (simple mail transfer protocol), an individual can send emails to the server. The Nodemcu esp8266 is used in conjunction with a temperature and smoke detector as well as a gas detector to sense the mine's climate parameters and Wi-Fi to send the parameters to Thing Speak, then the OLED display (organic light-emitting diode) will show all sensor values. We must design a cost-effective and reliable device for the solution. To create a device that will ensure the lives of coal miners.

Index Terms: Arduino Nano, ESP32camera, LoRa Technology, Node MCU esp8266 Controller, SMTP Protocol, Thing Speak Server

I. INTRODUCTION

The country relies heavily on coal mining to meet its energy needs. Coal mines are dangerous places where carelessness/unavoidable conditions can cause accidents. As compared to underground coal mines, open cast mines can be considered safer. The workers in open cast mines do not have to worry about humidity, heat, or suffocation. It appears that some miners come out of the underground mine before their shift ends. The mine management does not keep track of early adjournments by such miners, and the number of trapped persons is always unknown. Identifying the victims of accidents may be difficult for mine managers. As mining emits toxic gases such as carbon monoxide and methane, the mining environment is complex [1]. When the concentrations of these gases exceed a certain level, miners' lives could be at risk. The corrosion in enclosed spaces causes different types of damp. In addition to removing oxygen from the atmosphere, they can also lead to explosive environments.

The primary problems in coal mining are accidents caused by a variety of reasons and by improper maintenance or monitoring. Because of the death and resource losses caused by mining, the miners' lives are at risk. The risk of prolonged illnesses may be another cause of death. The semiconductor gas sensor is used for monitoring the concentration level of harmful gases present in coal mines, such as SO₂, NO₂, CO, etc. A wireless sensor network can

address the key issues of communication bandwidth, mobile data transmission, staff orientation, real-time monitoring of the work surface, and synchronization monitoring, among others.

II. RELATED WORK

Hazardous atmospheres increase the risks associated with mining and industrial accidents. The result can be greater environmental damage, as well as property damage and human casualties[2]. There are a variety of moral, legal, and commercial reasons why hazardous sites require greater care and security[3]. As part of various measuring aspects of coal mining, wireless sensor networks are used in the mining environment for process control of the virtual environment. Listed below are a few examples of coal mining monitoring applications.

A. Arduino based smart helmet for coal mine safety

SurajC. Godse, *etal* had proposed an Arduino-based smart helmet for coal mine safety. The system measures temperature, humidity, and oxygen levels. Flammable gases are detected by sensors in the mine[4]. The sensors are activated whenever the sensed parameter exceeds the limit. A comparison is made with the limit of the sensing device to verify the sensed data [5]. Workers in mines will be able to move safely with this alarm system that alerts them when an alarm goes off. With the vibration motor, mineworkers are alerted by vibrating their necks. A report concludes that coal miners are protected and their work methods are altered by the system.

B. Coal mine monitoring and alert system with data acquisition

Kugan raj S, *et al* had proposed a coal mine monitoring and Alert system with Data Acquisition [6]. An ATmega250 board is used to implement a wireless sensor network. The main controller is accompanied by pressure sensors, temperature sensors, heartbeat sensors, oxygen sensors, and an antenna for the wireless transceiver. A design system is composed of data gathering, data processing, and data monitoring components.

The goal of real-time messaging is to communicate different ideas that will enable real-time message delivery within the network. It collects mining-related data in real-time using CAN-based sensors. A transmitter between the mine station and the base station allows data collected within the mine station to be wirelessly communicated to a

transceiver at the base station [7,8]. It monitors underground conditions. Signals transmitted from underground stations are converted into lab view variables by a controller. With this design, an area can be managed using a sensor, automatic detection, and microcomputer technology. Observations and warnings of data in real-time are part of the report. Additionally, IoT systems with advanced functionality can be used.

C. Coal mine safety monitoring and alert system

S.R Deokar, J. S Wakode had proposed a coal mine safety monitoring and alert system [9]. Wireless transmitters and receivers are incorporated into wearable devices. The smart helmet contains several components, including a microcontroller, a sensor, an accelerometer, a flashlight, an alert switch, a headphone, and a memory card. A low amount of power is used in this design. In this experiment, the helmet's sensors detect when the wearer is taking it off. Whenever the system detects a gas level greater than the set level, the helmet flashes [5,10]. All sensor data are amplified by the controller when it transmits it. Through this design, an emergency message is sent to the base station via ZigBee. Information is displayed on the PC.

D. Coal mine safety system using a wireless network(GSM)

VSwarna, *et al* had proposed the development of a coal mine safety system using a wireless network (GSM). The main objective of this system is to receive signals by receiving information from sensors [11]. The system also addresses bandwidth issues. According to the system, conventional approaches are more cost-effective when it comes to data transmission methods used by Arduino microcontrollers, thermometers, gas sensors, IR sensors, and GPS mobile phones. The cost of these systems will be reduced by wireless sensor networks and GPRS. In addition to monitoring any parameters within a coal mine and alerting when they exceed the tolerance limits, it can also assist in implementing coal mining technologies [12].

E. Automatic safety and alarming system for coal mines

NazminA, *et al* had proposed an automatic safety and alarming system for coal mines [13]. This design is aimed at providing underground conditions in mines to reach the stations. In a mining environment, properties such as temperature, humidity, gas sensors, and the water level would be monitored in real-time. When the threshold limits are exceeded, miners would be notified.

There are two parts to the system. The hardware consists of RF transmitters and receivers[14,15]. Sensors in the ground control room continuously monitor underground parameters. Mineworkers wear wristbands attached to sensors in the ground control room.

A variety of sensors are connected to the system, including temperature sensors, humidity sensors, gas sensors, water level indicators, and wireless sensor networks. Based on research, it is necessary to install a real-time safety monitoring system to track underground parameters. The system will alert authorities to take appropriate action.

III. METHODOLOGY

A. Method

This methodology proved to be effective in completing the project and making it usable. In coal mine safety systems, several sensor modules are used, including smoke detectors, temperature, and humidity sensor buzzers, OLED, Arduino Nano, ESP32 cameras, and Lora modules. Monitor and control the system by connecting all of the sensors to the ESP8266NodeMCU. Ultimately, the system is designed for monitoring and controlling[3,16]. When the gas levels exceed the normal range the gas sensor sounds and the esp32 camera takes a picture that is sent to an authorized person via email. The data from the sensors is sent to the cloud regularly for analysis. In coal mines, we carefully monitor the quality of the air, temperature, and humidity levels [17]. The control of the entire system is handled via the IoT thing speak platform. Using the internet of things platform, we have developed widgets that can control the buzzer manually, if there is no internet connection, the Nodemcu, and Arduino Nano exchange data through Lora RF modules.

B. Hardware Description Materials

NODEMCU (ESP8266)

The Nodemcu CP2102 board is a highly integrated Wi-Fi device that can be used for a wide range of applications. Because it is self-contained, it can address a wide range of networking requirements to host or offload various Wi-Fi functions. In addition, ESP8266 has built-in peripherals that make it easy to integrate with a variety of application-specific devices. As a result of the onboard peripherals, the development environment is low-complexity, and external peripherals are minimized. Figure 1 shows the ESP8266 Development board. It is used for a wide range of applications.

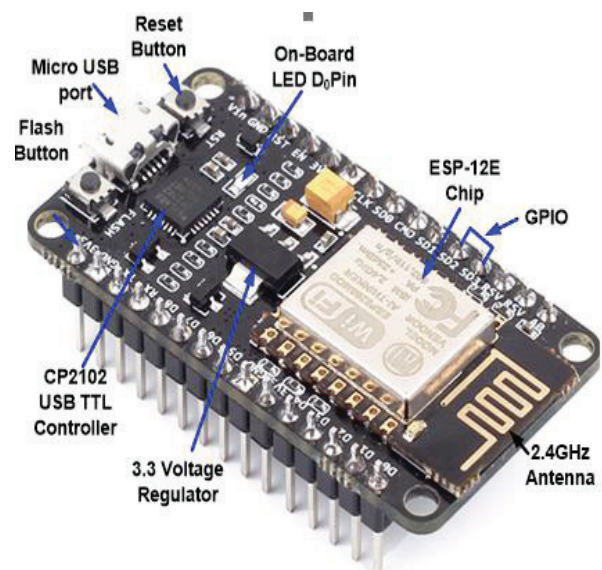


Figure 1. Node MCU ESP8266 Wi-Fi Development Board

ARDUINO NANO

An ATmega328P chip developed in Italy in 2008 is used on the board. It has 30 male DIP30 I/O headers. There are 14 digital pins, 8 analog pins, 2 reset pins, and 6 power pins. The Arduino IDE can be downloaded from the Arduino website. The Arduino Nano has almost all of the same features as the Arduino UNO. The Arduino Nano operates at 5 volts, and input voltage can range from 7 to 12 volts. The maximum current rating of the Arduino Nano is 40mA, so any load connected to its pins shouldn't exceed that. Each digital and analog pin has two main functions: input and output. The Arduino pins connected to sensors must be used as output pins to drive some load. Figure 2 illustrates the Arduino Development board. It is used for an extensive range of applications.

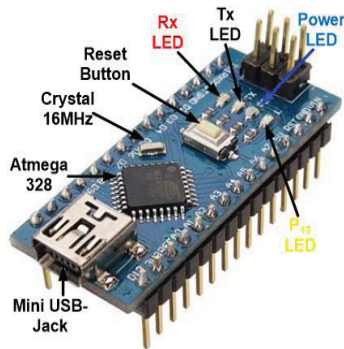


Figure 2. Arduino NANO

ESP32 Camera

The ESP32 has been used to develop a low-power camera module based on the CAM-ESP32. The board has a TF card slot and an OV2640 camera. IoT applications involving Wi-Fi image uploading, QR codes, etc. can be developed using an ESP32-CAM device. With the onboard ESP32-S module WIFI and OV2640 flash camera, data can be stored on a 4G TF card. Images can be uploaded via Wi-Fi. It has multiple sleep modes and a low sleep current of up to 6 mA. Pin headers can be integrated into many products. Wireless LAN connectivity is provided by the ESP-32S module. Devices connected to the internet can use the ESP32-D0WD Processor. Figure 3 demonstrates camera module pin components and how each of them is used for its functioning.

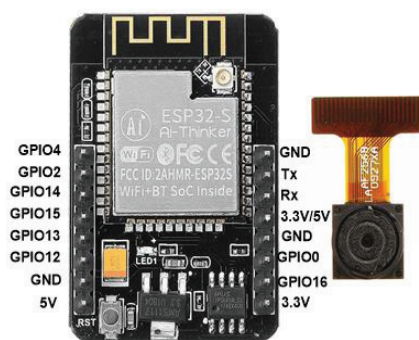


Figure 3. ESP32 Camera

DHT11

Temperature and humidity are measured by an NTC and a microcontroller run on an 8-bit processor. A voltage range of 3.5-5.5 V is used for operation, the device draws 0.3 mA and 60 μA in standby. Serial information is contained in this output. Its temperature range is 0 to 50 degrees Celsius with ± 2 degrees accuracy. The humidity range is from 20% to 80%. There is a 16-bit resolution for temperature and humidity with a precision of 1% and 1°C. Many sensors, such as the DHT11, measure temperature and moisture. An 8-bit microcontroller calculates the humidity and temperature values based on an NTC sensor. Other microcontrollers can easily be connected to it, as well as calibrated. With a sensor that measures 0°C to 50 °C and 20% to 90%, temperature and humidity can be measured within 1°C and 1 percent. When measuring in this range, this might be the best option. Figure 4 explains the DHT11 module pin components and how each of them is used for its working.

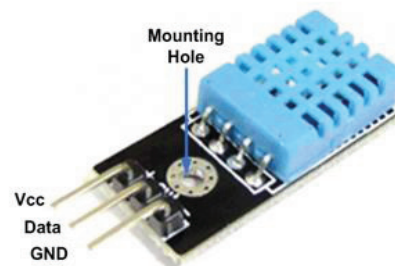


Figure 4. DHT11 Sensor

MQ135

MQ-135 sensors detect poisonous gases in mines and offices, as well as air quality. The sensors use tin dioxide (SnO₂) as their gas sensor. The conductivity of tin dioxide increases pollution. Ammonia, oxides of nitrogen, smoke, CO₂, benzene, and other dangerous gases can be detected by the air quality sensor. On the air quality sensor is a small potentiometer that allows the load strength to be adjusted. For operating 5V power supply is required and it produces digital logic output 0 or 1 or analog output 0-4V. In this project, it is used for measuring the concentration level of benzene gas in free space. Figure 5 elucidates the MQ135 module pin diagram.



Figure 5. MQ135 Sensor

LoRa Module

This LoRa Ra-02 module uses SEMTECH's wireless transceiver SX1278 to transmit data wirelessly. With advanced LoRa spectrum distribution technologies, it is possible to communicate over a distance of 10,000 meters. Air wake-up consumption is highly effective in terms of anti-jamming capability and function. For smart homes, spectrum modulation is used in LoRa technology with sensitivity of -148dBm. It is possible to program approximately 300 kbps FSK, GFSK, MSK, GMSK, LoRa, and OOK modulations are supported by this module. RSSI dynamically adjusted from 127dB to 129dB. The main highlight of LoRa has automatic radio frequency (ARF) sense and CAD with ultra-fast automatic frequency control (AFC) packet engine up to 256 bytes. Figure 6 explains LoRa module pin components.

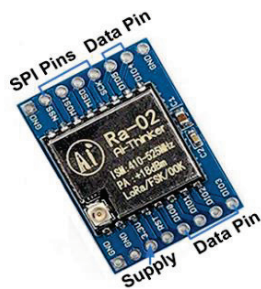


Figure 6. LoRa Module

IV. SYSTEM DESIGN

A. Block Diagram of the proposed models

The input and output devices used to develop the devices are divided into two types: a coal mine unit that fits on the miner's helmet and allows for movement in the mine, and a control room unit that monitors the mining operation. In the mining environment, each sensor is well organized for sensing and transmitting to the cloud for analysis.

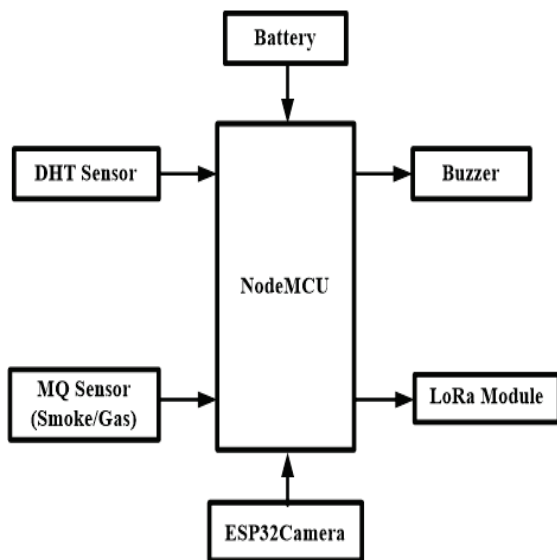


Figure 7. Block diagram of Proposed System at Transmitter

Figure 7 illustrates the proposed model for developing a perfect system, providing a framework for it. In this, all components connect with Node MCU, which control and provides instructions.

B. Control room unit

It is placed at the base station and monitors the coal mine unit. It receives the data from the transmitter unit and analyzes the data and shows it on an OLED display. Figure 8 represents the block diagram of the proposed model at the base station and gives the framework for it.

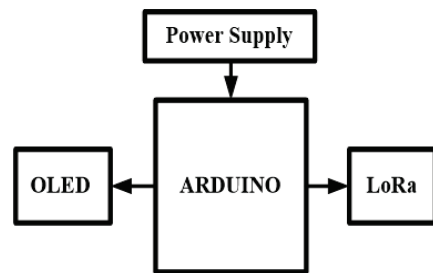


Figure 8. Block diagram of Proposed system at the Receiver

C. Circuit Diagram of Transmitter device

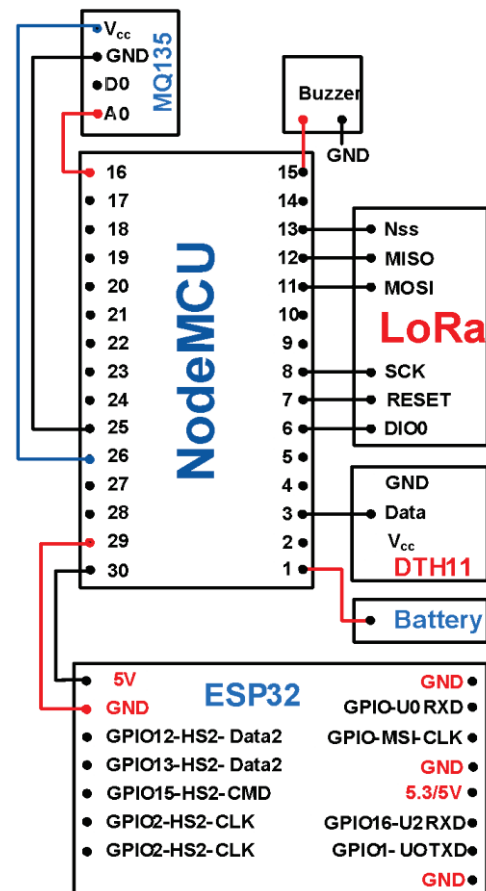


Figure 9. Circuit diagram of a Proposed System at Transmitter

Figure 9 shows the internal connections of the system on the transmitter side.

D. Circuit Diagram of Receiver Device

Figure 10 shows the internal connections of the receiver system. Their pin configuration determines how the receiver system works.

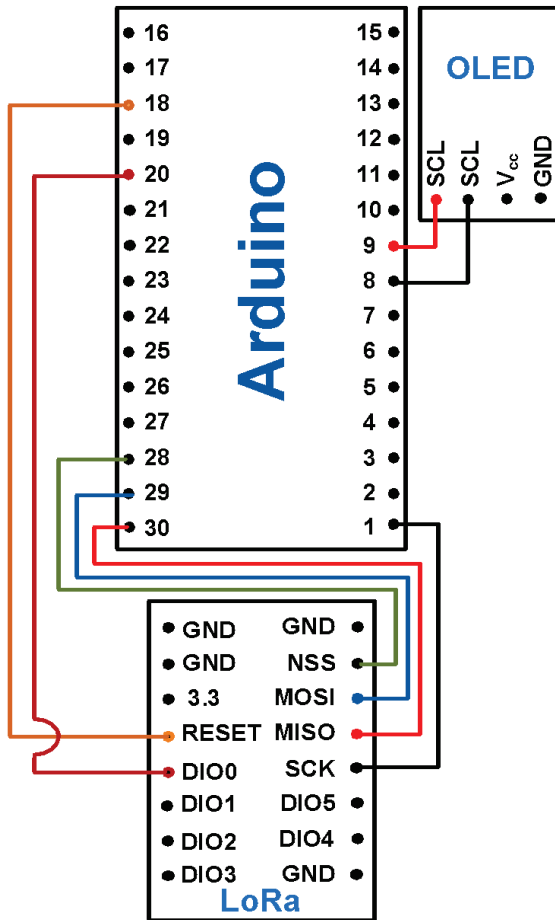


Figure 10. Circuit diagram of Proposed system at Receiver

E. Software Development

Various software techniques are utilized for the working of mine safety systems are

a) Arduino IDE

IDEs integrates code development environments. IDEs provide a wide range of tools for software developers. Computer programmers can create or test software on this device because it has all the tools they need. This environment is composed of a compiler, debugger, editor, etc.

With the Arduino IDE, code can be written quickly and uploaded directly to the board. C++ and C are open-source programming languages that can be used to program your board. All Arduino boards support these languages. USB cables (A or B plugs) are required for Arduino Nano and Node MCU.

b) Things Speak Server

Thing Speak is an IoT analytics platform that aggregates, visualizes, and analyzes real-time data streams. A device posts data to Thing Speak, and Thing Speak provides instant visualizations. Thing Speak allows you to analyze and process data as it is coming in online by executing MATLAB code. The Thing speak is often used to develop prototypes and proofs-of-concept of IoT systems requiring analytics.

An increasing number of embedded devices (things) are connecting to the Internet on the Internet of Things (IoT). These connected devices use cloud storage and computing resources to store and analyze sensor data, which provides valuable insight. Cloud services have become more affordable and widely available, driving this trend.

F. Working on the proposed system

The underground unit is powered by a rechargeable battery, which supplies power to all the components within the unit, and the underground unit is powered by the ground station unit. The system has been fully initialized. Microcontrollers receive data from sensors. Those devices generate data, which is analyzed and displayed by servers in the system. The data are displayed as charts. They are arranged accordingly. Each minute, our camera module captures images of the mining environment and sends them to the respective email address. As the internet cannot be accessed for any reason, LoRa is responsible for controlling the entire system and for transmitting and receiving data.

V. RESULT

Spreading of the spectrum is achieved in LoRa modulation by generating a chirp signal which is continuously varying in frequency. The benefit of the procedure is the time and frequency are counterbalance between transmitter and receiver so that the designing of receiver is simple. The required data are chipped at a higher data rate and modulated onto the chirp signal. The relation between the bit rate, wanted data, chip rate and symbol rate for LoRa modulation is defined as,

$$R_b = SF * \frac{1}{2^{SF}/BW} \text{ bits/sec} \tag{1}$$

$$R_s = \frac{BW}{2^{SF}} \text{ symbols/sec} \tag{2}$$

$$R_c = R_s * 2^{SF} \text{ chips/sec} \tag{3}$$

A variable error correction scheme provides the noiseless transmission by LoRa modulation. The nominal bit rate of the data signals as,

$$R_b = SF * \frac{\left\lceil \frac{4}{4+CR} \right\rceil}{\left\lfloor \frac{2^{SF}}{BW} \right\rfloor} = SF * \frac{\text{RateCode}}{\left\lfloor \frac{2^{SF}}{BW} \right\rfloor} \text{ bits/sec} \tag{4}$$

Another important parameter is the receiver sensitivity is defined as,

$$RS = -174 + 10 \log (BW) + NF + SNR[dBm] \quad (5)$$

Where, SF is spreading factor, BW is bandwidth (Hz), R_b is modulation bit rate, R_s is symbol rate, CR is code rate, NF is the receiver noise figure, SNR is signal-to-noise ratio and R_c is chip rate. ‘-174’ is determined by the thermal noise in 1 Hz of bandwidth

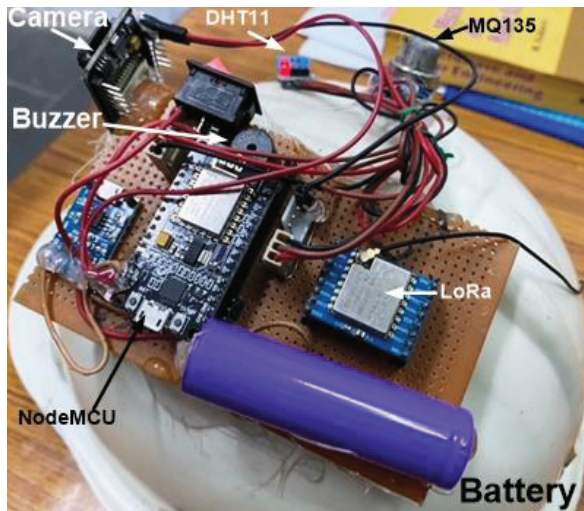


Figure 11. working of a Transmitter Device

Figure 11 illustrates the assembling of the transmitter device and it’s working under the mine conditions. Tests are done to ensure that the sensors mounted on the helmet can be trusted for the specified limits and also specifically for their functions. In addition, alarms are triggered based on data from the sensors. LORA technology is used to build wireless sensor networks that enabled real-time surveillance and early warning of methane, temperature, and humidity in the mining area, thus reducing safety concerns during coal production. By installing this system in mines, can avoid the baneful, deleterious, noxious, and pernicious situation. Apart from that camera send live telecast in the mine.

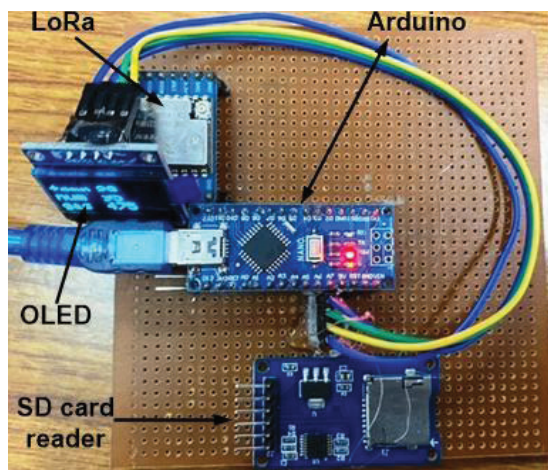


Figure 12. Working of a Receiver Device

Figure 12 illustrates the assembling of the Receiver device and its working. The receiver provides data from the transmitter and displays it. SD card reader is responsible for the collection of the data in the form of bits and stores in a memory card. If any data is lost, it is already stored in the camera module memory card as well as in the mail.

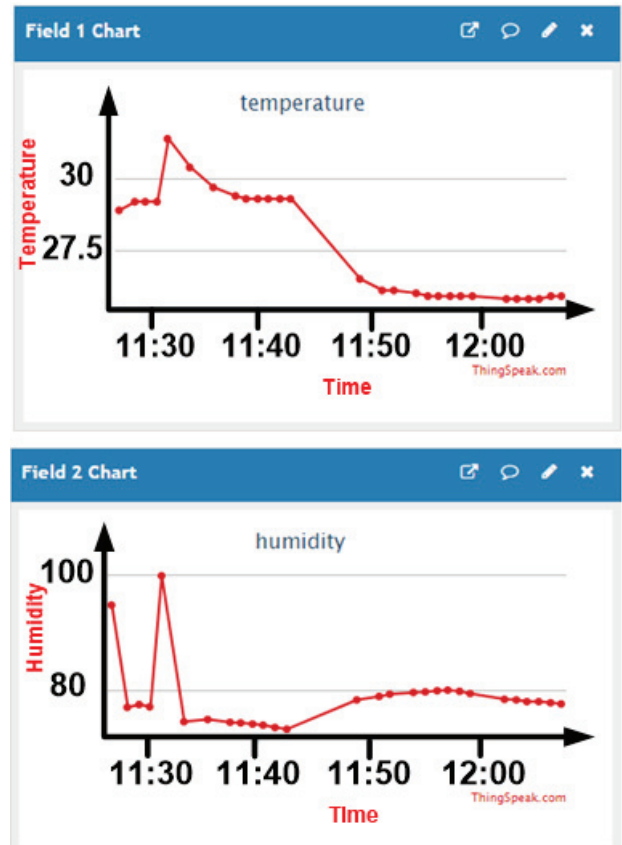


Figure 13. Variation of temperature and humidity with Time

Figure 13 displays the humidity and temperature of the environment. Taking the plot along the time axis and examining how they are related. These plots are stored in a server for analysis.

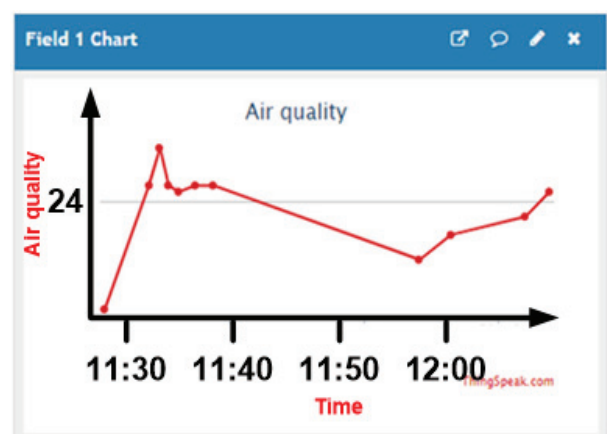


Figure 14. Variation of Air quality with Time

Figure 14 shows the toxic content in the surroundings. It represents the quality of air around the person. A graph is plotted along the time axis and stored in a server for analysis.

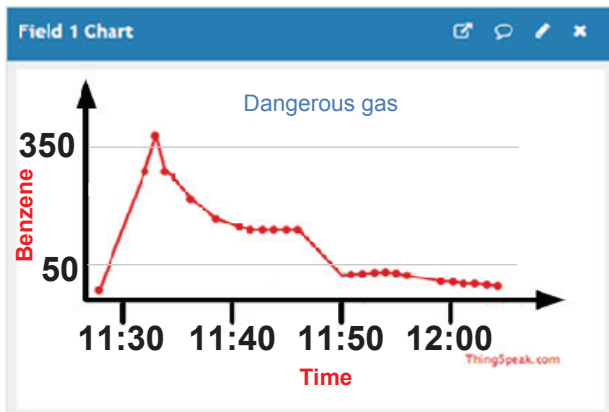


Figure 15. Variation of dangerous gas (Benzene) with Time

Figure 15 shows the sudden variation of benzene. With the analysis of the variation can find the air content in the low-lying area in the mine. By taking pre-precautions in mine can avoid the irritation of the skin, eyes, throat, and nose for the worker.

VI. CONCLUSIONS

Sometimes mine workers are facing very tough conditions like fire, flooding, the collapse of roofs and sides or walls, the emission of poisonous gases and ventilation failures while they are working in mines. Second the wireless internet connectivity is almost zero in the deep mines. For their safety, we assemble an embedded system circuit on the helmet. This system is also useful in the absence of the internet since it creates its network and sends signals from one node to another. In this system sensor and camera is installed, which is controlled by Nodemcu that continuously monitors atmospheric parameter, clips the picture and send to the control room. OLED continuously displays the live atmospheric parameter values in the control room. The control room server is connected to the internet so that any authorized person can monitor the mine conditions from anywhere in the world. If any atmospheric parameter crosses the threshold values, controller alerts the safety team and they take appropriate action to rescue the worker before any accident.

This project made use of components that were reasonably priced, durable and easily accessible. As a result, the project is affordable and easy to maintain.

VII. FUTURE SCOPE

It is possible to prevent sudden flooding by measuring the moisture content of the soil mines with the moisture sensor. We

can use wireless underground networks (WSNs) to improve network infrastructure in underground mines by broadcasting and receiving data through the soil.

REFERENCES

- [1] A. Mishra, S. Malhotra, Ruchira, P. Choudekar, and H. P. Singh, "Real-Time Monitoring & Analyzation Of Hazardous Parameters In Underground Coal Mines Using Intelligent Helmet System," *Int. Conf. "Computational Intell. Commun. Technol. CICT 2018*, no. Cict, pp. 1–5, 2018, doi: 10.1109/CICT.2018.8480177.
- [2] X. Xia, Z. Chen, and W. Wei, "Research on Monitoring and Prewarning System of Accident in the Coal Mine Based on Big Data," *Sci. Program.*, vol. 2018, 2018, doi: 10.1155/2018/9308742.
- [3] S. Kumaresan, P. L. Kumar, R. Manisankar, A. P. Shankar, and R. S. P. D, "Lora Network for Data Transmit in Coal Mine Industry," vol. 9, no. 4, pp. 6–10, 2021.
- [4] P. Sawant, S. Godse, V. Thigale, and K. Kasar, "Arduino Based Smart Helmet for Coal Mine Safety," *SSRN Electron. J.*, 2020, doi: 10.2139/ssrn.3645335.
- [5] W. Chen and X. Wang, "Coal Mine Safety Intelligent Monitoring Based on Wireless Sensor Network," *IEEE Sens. J.*, vol. XX, no. XX, 2020, doi: 10.1109/JSEN.2020.3046287.
- [6] G. K. Kugan, M. Mohan, V. Gowtham, and A. C. Mines, "Coal Mine Monitoring and Alert System With Data Acquisition," vol. 6, no. 03, pp. 186–191, 2019.
- [7] L. Dan and Y. Jun, "Application of IPV6 in coal mine safety production monitoring," *Proc. - 2018 Int. Conf. Sens. Networks Signal Process. SNSP 2018*, pp. 45–48, 2019, doi: 10.1109/SNSP.2018.00018.
- [8] Y. Zhang, G. Fu, Z. Zhao, Z. Huang, H. Li, and J. Yang, "Discussion on the application of IOT technology in coal mine safety supervision," *Procedia Eng.*, vol. 43, pp. 233–237, 2012, doi: 10.1016/j.proeng.2012.08.040.
- [9] [9] A. Nagrale et al., "Coal Mine Safety Monitoring and Alert System," *Int. J. Adv. Res. Sci. Commun. Technol.*, pp. 200–206, 2021, doi: 10.48175/ijarsct-v4-i3-033.
- [10] X. Jia, F. Shi, Y. Guan, S. Tang, and M. Tong, "Zigbee-based wireless gas monitoring sensor alarm system in the coal mine," *IOP Conf. Ser. Earth Environ. Sci.*, vol. 446, no. 2, 2020, doi: 10.1088/1755-1315/446/2/022012.
- [11] V. Swarna, C. Geetha Krishna, Y. U. Mahesh, K. Charan, and Y. Haritha, "Development of Coalmine Safety System using Wireless Sensor Network (GSM)," *Technol. Eng. Manag.*, vol. 6, p. 18, 2020.
- [12] R. Muthaiyan, V. G. Rajaramya, and A. B. Ramya, "Implementation of Wireless Sensor in Coal Mine Safety System," vol. 3, no. 1, pp. 613–620, 2015.
- [13] N. A. Maniyar, P. S. Bodhai, J. K. Tarle, and A. S. Hengade, "Automatic Safety and Alarming System for Coal," vol. 3, no. 3, pp. 2268–2270, 2014.
- [14] X. Liu and L. Liu, "Design of coal mine monitoring system based on internet of things," *Commun. Comput. Inf. Sci.*, vol. 472, pp. 289–294, 2014, doi: 10.1007/978-3-662-45049-9_46.
- [15] U. Shrawankar, "Monitoring and Safety System for," no. April, pp. 0–5, 2018.
- [16] A. Singh, U. K. Singh, and D. Kumar, "IoT in mining for sensing, monitoring, and prediction of underground mines roof support," *Proc. 4th IEEE Int. Conf. Recent Adv. Inf. Technol. RAIT 2018*, pp. 1–5, 2018, doi: 10.1109/RAIT.2018.8389041.
- [17] X. Meng, P. Lu, and B. Wang, "Coal mine safety warning system based on principal component method and neural network," *Proc. 2017 IEEE 6th Data-Driven Control Learn. Syst. Conf. DDCLS 2017*, pp. 226–230, 2017, doi:10.1109/DDCLS.2017.8068073.

IoT Based Smart Power Management in Public Areas along with Public Traffic Monitoring

V. Shilpa¹ and Humaira Nishat²

¹PG Scholar, CVR College of Engineering/ECE Department, Hyderabad, India
Email: vadthyashilpa@gmail.com

² Professor, CVR College of Engineering /ECE Department, Hyderabad, India
Email: dr.humairanishat@gmail.com

Abstract: Electricity consumption is growing rapidly across the globe and has become an essential component in today's life. This allows us to use the various electronic and electrical equipment wherein the electricity is essential for ensuring their proper functionality. These electronic and electrical gadgets are power dependent. People use electricity in their day-to-day life by connecting to power grid without realizing how much it costs to produce it. Energy efficiency is one of the important challenges to minimize the consumption of the resources of the earth. Thus, it is important to find alternatives for power management not only in individual homes but also in public places. This paper aims to design a system that monitors the public traffic in metro trains, stations, and shopping complexes and update the live status of the web application. The system also provides automatic power management by controlling the load automation with the present person count. Based on that, it will turn on/off the fans and control the light intensity using an LDR sensor to save power.

Index Terms: Blynk App, Home Appliances, IoT Application, Relays, Sensors, Wi-Fi

I. INTRODUCTION

With the advancement in automated technology, life is getting easier and simpler. Systems which were handled manually earlier are now being replaced by automated systems. Internet has become a part of life, and this led to rapid increase in internet users. Through networking sharing of information and completing tasks remotely is possible now and thus things like consumer goods, industrial goods, etc., can be networked. Now it is possible to control the basic home functions and features using IoT and this can be done from anywhere in the world. This results in saving the power and electrical energy. The main aim of the proposed work is to monitor public traffic in metro trains, stations, and shopping complexes and to update the live status of the web application. The system will be very useful to public and management to get advance public traffic information in particular areas. Based on the amount of public traffic, people will plan their schedule to visit places, and management will plan to increase train frequency for public comfort. The system also provides automatic power management by controlling the load automation with the present people count. The system monitors the people's entry and exit, and the total count inside the area. Based on that, it will turn on/off the fans and control the light intensity using an LDR sensor. It has been found that IoT plays a

significant role in achieving the said objectives in a more secure way.

Due to the expansion in digital technologies currently, the smart city is becoming smarter than in the past. Many electronic equipments of various kinds such as sensors for various applications are connected and forms a transportation system which also comprises smart cities. Thus, automated power management in public areas using IoT is also a part of smart city. The paper is described in the following way. Section II discusses the related work; the proposed system is discussed in section III followed with results in section IV. Section V concludes the paper.

II. LITERATURE SURVEY

A systematic review of the literature is an assessment of an existing research on one or more specific subject concepts. Here, a Smart Power Management System is considered as a topic of interest in this paper.

In paper [1], the authors Devashish et al., has introduced "Smart Power Monitoring Using IoT". In this system, an automated electric power meter is used in domestic power distribution system. By integrating Wi-Fi, Arduino and GSM a smart power monitoring distribution system is designed. The system provides optimized data and thereby reduces the power consumption. The system is useful for domestic customers wherein the power supply is cut in absence of any human beings.

In [2], Mohammad Hossein Yaghmaee et al., have proposed an IoT based smart energy metering. The system measures the amount of power consumed and the power line parameters and sends this information to a central server through an intermediate gateway on the internet. The system also controls the electric appliances and whenever necessary turns them ON/OFF during the non-peak and peak hours respectively. This reduces the electricity cost for customers and the amount of load is reduced at the electricity grid during peak hours.

Himanshu K Patel et al [3] introduced a system which eliminates the intervention of human in measuring the meter readings and in the generation of bills. This reduces the error caused due to energy related corruption and any other chaos. The system is implemented using Arduino, GSM module, LDR sensor and relay. The system cost is also less, compared to the existing smart meters with the same functionality.

Bibek Kanti Barman et al in [4] proposed a smart energy meter based on IoT. Utilization of energy in an efficient way is very vital in the development of a smart grid in a power system. Thus, it is beneficial to have proper monitoring and controlling of power consumption in a smart grid. Since the communication is only one way, a smart energy meter was required that can provide full duplex communication. The proposed smart meter controls and calculates the consumption of energy using Wi-Fi module ESP 8266 12E and finally updates it to cloud so that the consumers can view the reading. Thus, examination of energy is made easy and is controllable by the consumers. This system also gives the information of energy loss and does the home automation job using IoT.

Fakieh, Khalid [5] proposed a new simple and inexpensive method to regulate the wastage of power by imposing penalties to the individuals or the organizations by the power distribution. The system comprises of thermal sensing and associated hardware and requires less installation cost and maintenance is very cheap. This method allows the government to control the entire power wastage remotely and thus helps in power saving.

III. PROPOSED METHOD

One of the most effective methods for power management is the smart power management system based on IoT. Industrialists and researchers are working towards power management systems and the latest developments in IoT have made it possible to save energy. Saving energy is possible through the usage of IP (Internet Protocol) enabled service.

The main objective of this proposed method is to implement IoT-based smart power management in public areas, along with advanced public traffic monitoring, to create smart technology in cities thus making it a smart city incorporating smart transport, buildings and thus creating a digital society.

The system can be seen in figure 1. The system consists of a micro controller (Arduino) which can communicate with Blynk server via Wi-Fi. The code is written using Arduino IDE editor. Arduino with Wi-Fi module transmits the values i.e., the persons count to Blynk App which is also displayed on LCD screen.

The system uses Blynk Server which is an Open-Source Netty based on Java server. The messages are forwarded between the various microcontroller boards like Raspberry Pi, Arduino etc., and the Blynk mobile application.

The block diagram shows all the hardware components in blocks. It includes blocks of IR sensor 1, IR sensor 2, Light Dependent Resistor (LDR), Relays, Wi-Fi module and Power Supply along with loads. Here the input components are IR sensor modules, LDR sensor. The input components after sensing give input signals to Arduino board. The output devices are 16x2 LCD display, relay module and loads. These take signals from Arduino.

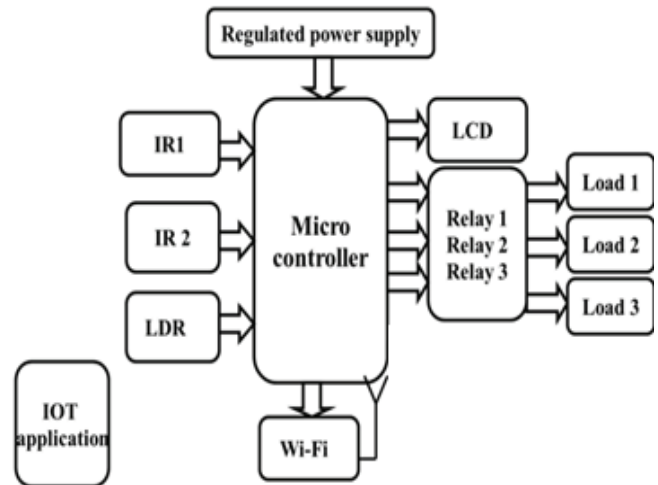


Figure1. Block Diagram of IoT based Smart Power Management System

The following gives the functionality of each block.

A. IR Sensor

These sensors (IR Sensors) are Infrared Sensors made of electronic devices and are used to measure as well as detect infrared radiation from the surrounding environment. The semiconductor chip inside the sensor should be powered to 3-5V for it to function.

It basically consists of two parts i. an LED i.e, a light emitting diode and ii. A receiver. If any human being or an object is close to the sensor, then the infrared LED within the sensor reflects off the object and is detected by the receiver at the sensor. These are the proximity sensors and are mostly used in any obstacle detection system. In the proposed work, two IR sensors are used, one at the entry and the other at exit. These sensors are used to count the number of persons entering and leaving.

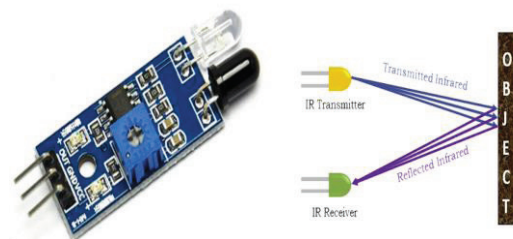


Figure 2. IR Sensor module for Arduino

B. LDR Sensor

LDR sensors are light dependent resistors also called photoresistors. The resistance of these sensors changes with the light intensity falling upon them. The application of LDR sensors is to automatically turn on a light at a certain light level. Thus, the streetlights or the bulbs in rooms will be turned on. In the proposed work one LDR sensor is used and based on the light intensity level i.e., if it is dark then

automatically light(bulb) will be turned on.

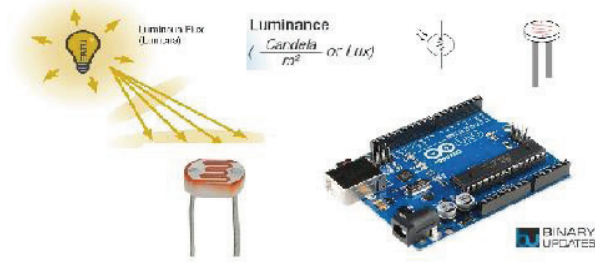


Figure 3. Interface LDR with Arduino

C. Relay

Relay is a switch which can be operated electrically. By using low voltage signals, relays are used to control high voltage circuits. Similarly, with the help of low current signals they are used to control high current circuits. In the proposed work, to protect the load from getting damaged by the high voltage/current a relay is used to connect the light bulbs between Arduino pin and bulb.

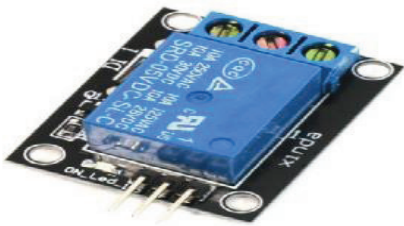


Figure 4. Arduino Relay module

D. LCD Display

In the proposed work, the user can interact with the device through the messages displayed on the LCD display. The liquid crystal display is a kind of display that uses liquid crystals for its operation and helps the user to operate the device. The serial input from the computer is accepted and the sketch is uploaded to the Arduino. The characters will be displayed on the LCD.

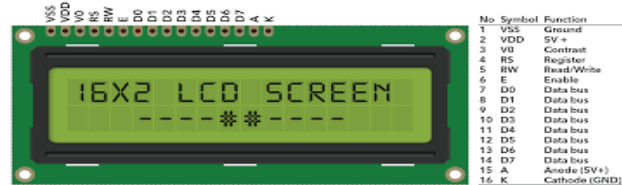


Figure 5. LCD Display

E. Arduino

Arduino is a project for designing and manufacturing single board microcontrollers which is an open-source hardware and software electronics platform and is easy to use.

These Arduino boards uses mostly Atmel 8-bit AVR microcontrollers with different pins and features and varying size of flash memories. The microcontrollers are pre-programmed with a boot loader thus simplifying the uploading of programs to the on-chip flash memory.

Through serial connection the program code is loaded in the boards from other computers. Using sensors and actuators, the electronic devices can interact with the environment through Arduino projects which are low at cost and are very easy for the professionals to work with.

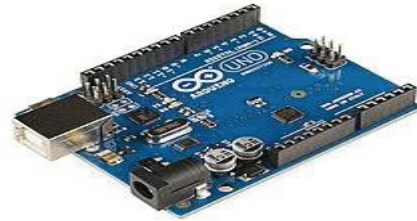


Figure 6. Arduino

F. Wi-Fi Module

Wi-Fi is a local area network of devices and internet access and allows the exchange of data wirelessly among digital devices. The Wi-Fi module can give any microcontroller access to the Wi-Fi network. The module will be capable of either hosting an application or offloading all Wi-Fi networking functions from another application processor.

G. Power Supply

For the components to work, a power supply of +5V is provided. ICLM7805 is used to provide a constant power supply of +5V.

The schematic layout of the proposed model is shown as circuit diagram which is implemented in software.

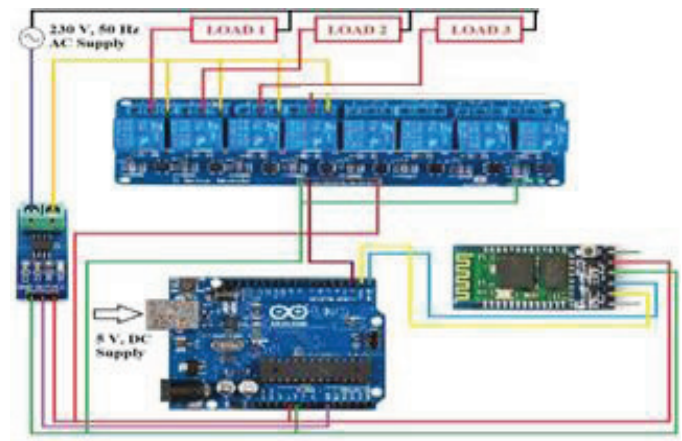


Figure 7. Circuit diagram of the proposed system

Monitoring and controlling of the power i.e., ON/OFF functionality is done by the communication protocol. The environment is sensed and monitored by the sensors which measures and sends the data to the microcontroller which in turn is processed and the sensed data is used to control and to monitor the appliances. Voltage and current sensors are interfaced with the microcontroller to monitor the voltage and current respectively. All the loads are connected to the board through a relay which acts as an electrical switch.

IV. RESULTS

IoT based Smart Power Management with Public Traffic Monitoring System was developed by employing Arduino and Wi-Fi module. It also uses IR sensor module, LDR sensors as inputs to Arduino (microcontroller unit). The system communicates with the Blynk server via Wi-Fi. The system not only controls the appliances but also considers the public traffic in specific areas and the information is sent to the Blynk server through Arduino and Wi-Fi module. In the system an LCD display is also used so that the persons count (public traffic) is available at the Blynk app as well as is displayed on the screen. The results are updated in the server. Figure 8 shows the complete IoT based Smart Power Management with Public Traffic Monitoring System prototype with all the connections, sensors, relays, and load. Results are explained with the help of images.

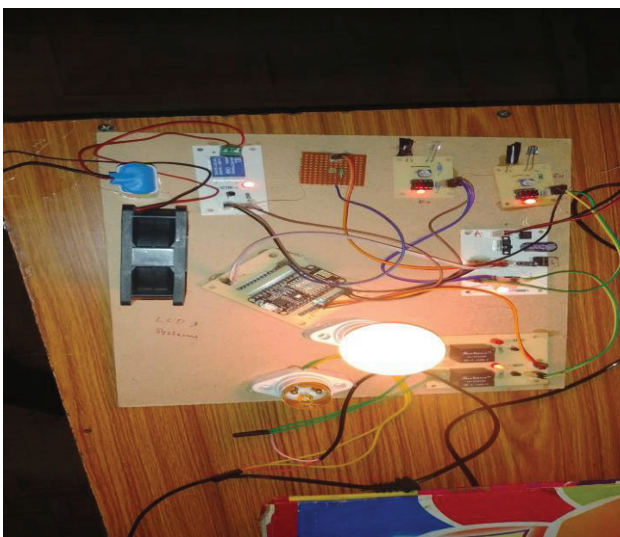


Figure 8. Image with bulb on as per the count

As shown in figure 8, the bulb glows according to the people count. The IR sensor will sense the number of persons entered in the room and leaving the room, if the count is below 5 then it will automatically turn on one bulb and one fan.

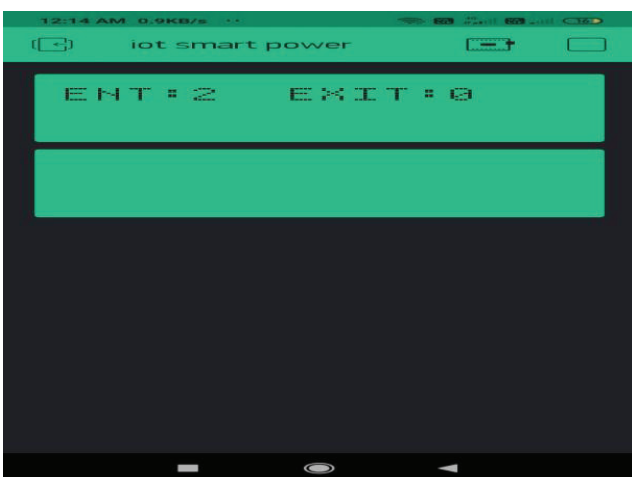


Figure 9. People count on LCD display

Figure 9 displays the number of people entered in the room; the IR sensor will sense the number of counts. The

count will be read by Arduino through IoT application and then the count is displayed on the Blynk app. The count is also displayed on the LCD display.



Figure 10. Image with bulbs and fan on

Figure 10 shows the glowing of bulbs according to the people count. The IR sensor will sense the number of people entered in the room and the number left. If the count is more than 5 it will automatically on two bulbs and one fan.

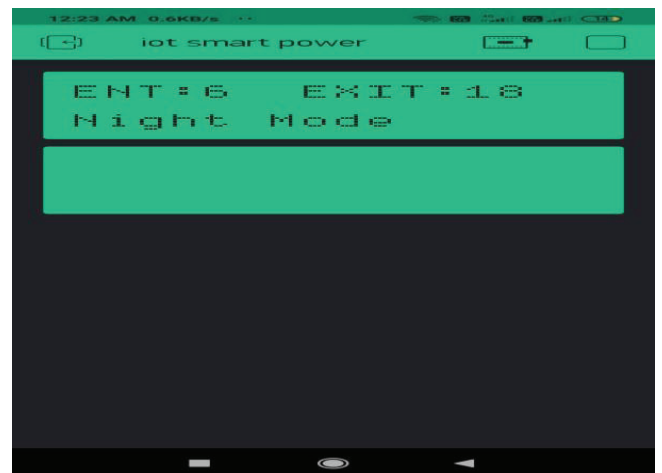


Figure 11. Image displaying number of people

According to figure 11, the count shows 6 persons present in the room and 18 have left. Thus, depending on the number of persons entering and exiting the count is varied and is displayed on the screen. Also, as per the count the appliances are automatically turned ON and OFF. This information regarding the number of persons in a particular area is also uploaded to Blynk server via Wi-Fi network and is useful for both public as well as management to know the crowd at that place such as malls, stations, stadiums, etc.

V. CONCLUSIONS

In this paper, an IOT based smart power management along with advanced public traffic monitoring system has been developed. The system monitors and controls the power consumption of home appliances at home as well as at other places automatically, manually, and remotely by using wireless network. The system is easy to design and consumes less power and is provided at low cost with portable size. The Arduino is programmed accordingly in Arduino IDE software which works without any time lag. The LCD display provides comfortable interaction by displaying essential data without any uncertainties in time. The device is implemented with an idea to provide accessibility at any public place with affordable cost of installation.

FUTURESCOPE

The proposed system will be controlling only two appliances such as bulb and fan and thus is a prototype and is not a completely developed system. In future, it can be extended for controlling other appliances like ovens, washing machines, refrigerator, air conditioners, etc., and that too for real time applications. To control the home appliances human intervention is required. If the usage of appliances is reduced, then power saving will improve and thus whenever the appliances are not needed then they should be turned off automatically to save power. The appliances can also be controlled manually. The system can also be extended to incorporate algorithms that can measure the changes in the weather conditions according to the season. Also to detect, update the changes in season based on the temperature, humidity, and brightness. Thus, IoT based energy management system for numerous applications plays an important role in the scheduling, monitoring, controlling, optimization of enterprise energy, and improving organization/ labor productivity. This can be implemented with low power consumption and can be operated with high speed. In the future advancements of Traffic Monitoring System, a feature of emergency stop can be added, and the components used can be upgraded accordingly.

REFERENCES

- [1] Devadhanishini A Y, Malasri R K, Nandini Priya. N, “Smart Power Monitoring Using IoT”, 5th International Conference on Advanced Computing & Communication Systems (ICACCS) 2019, 813-816.
- [2] Yaghmaee, Mohammah-H & Hejazi, Hossein. (2018). Design and Implementation of an Internet of Things Based Smart Energy Metering. 191-194. 10.1109/SEGE.2018.8499458.
- [3] Himanshu Patel, Tanish Mody, Anshul Goyal, “Arduino based Smart Energy Meter” 4th International Conference on Internet of Things: Smart Innovation and Usages (IoT-SIU), Published 18 April 2019, Computer Science 2019
- [4] Bibek Barman, Shiv Yadav, Shivam Kumar, & Sadhan Gope, “IOT Based Smart Energy Meter for Efficient Energy Utilization in Smart Grid”, 2018 2nd International Conference on Energy, Power and Environment: Towards Smart Technology (ICEPE), 1-5. 10.1109/EPETSG.2018.8658501.
- [5] Fakieh, Khalid. (2016). An IoT based Smart Power Management System for Technical University. International Journal of Computer Applications. 149 2016. 10.5120/ijca2016911344.
- [6] Hao-wei Yao, Xiao-wei Wang, Lu-sen Wu, Dan Jiang, Teng Luo, Dong Liang, “Prediction method for Smart Meter Life Based on Big Data”, Procedia Engineering, vol. 211, pp. 1111–1114, 2018.

A Machine Learning Perspective for Data Analytics in Solar Powered Weather Station using IoT

S. Praveen Chakkravarthy¹, P. Bharath Chandra², D. Anwar Basha³ and G. Sai Kiran⁴

¹Assoc. Professor, CVR College of Engineering/ECE Department, Hyderabad, India

Email: dr.praveen@cvr.ac.in

²UG Scholar, CVR College of Engineering/ECE Department, Hyderabad, India

Email: bharathchandra2002@gmail.com

³UG Scholar, CVR College of Engineering/ECE Department, Hyderabad, India

Email: bashadanwar@gmail.com

⁴UG Scholar, CVR College of Engineering/ECE Department, Hyderabad, India

Email: gsaikiran502@gmail.com

Abstract: In the context of actions for small cities, CVR Solar Powered Weather Station has been developed to monitor changes in Weather. Users can find out the weather changes in the area and can plan their day-to-day activities. In several important productive areas, such as farming, the climate plays a crucial role. These days, there is a lot of climate change, which is why it is bothersome that old weather forecasts are growing closer and less accurate. Therefore, miles are crucial to embellishing and modifying the weather forecast model. To cater the needs of current socio-economic changes, a solar powered IoT Based Weather Monitoring System plays a vital role in predicting changes in weather.

A Machine Learning Model to Predict Weather Conditions in Mangalpalli Area is presented in the article.

Index Terms: LoRaWAN Gateway, Machine Learning Model, Photosynthetically Available Radiation, Total Solar Radiation

I. INTRODUCTION

LoRaWAN weather station enables one to measure atmospheric conditions to provide information for weather forecasts and to study the weather and climate. The Main Process Unit (MPU) Consists of various sensors that include

- Rain Gauge Sensor
- Temperature/Humidity/Pressure sensor,
- Wind Speed/direction sensor,
- Illumination sensor,
- CO2 sensor,
- Rain/Snow sensor,
- PM2.5/10 sensor,
- PAR (Photosynthetically Available Radiation) sensor,
- Total Solar Radiation sensor

Main process device WSC1-L is an outdoor LoRaWAN RS485 end node. It has a built-in lithium-ion backup battery and is fueled by external 12-volt solar power. The LoRaWAN wireless protocol is used by the WSC1-L to read values from a variety of sensors and transfer the sensor data to an IoT server. The WSC1-L can function with a typical LoRaWAN Gateway and is completely compatible with the LoRaWAN Class C protocol. A woody area utilized for weather forecasting is a part of a system of information and statistics analysis techniques. Weather must be considered, including temperature, rain, humidity, pressure and other

protection, as one of the greatest natural barriers in all aspects of our existence, remarkable.

The purpose of the proposed work is to format accurate weather forecasts. Long-term climate change on Earth will occur, and its effects on current and upcoming generations are both unknown. Our ability to forecast end-of-life climates is a fantastic opportunity to provide information so that stadium insurers can make educated wishes for the future of the globe.

The proposed model aims in a way to govern the state of staff inconsistencies and inequalities and performs its function of accurately predicting the weather. There are three basic types of load forecasts: the first is the short-term prediction, which involves estimating demand from a few hours to a few days. Second, there are long-term forecasts, which aim to predict demand from a few years to a few months, and medium forecasts, which aim to predict demand from a few weeks to months. Various potential load forecasting techniques, including the Similar Day Approach, Regression, Time Series Analysis, Artificial Neural Networks, Expert Systems (rule based), Fuzzy Logic, and Support Vector Machine (SVM) are evaluated and presented. In order to exploit these predictions online for efficient energy management, this Work covers the fundamental concept of load forecasting utilizing ML algorithms in an IoT setting.

Internet of Things is a novel paradigm combining telecommunications [1] and any kind of device using sensors. The Internet of Things (IoT) is seen as an innovation and financial wave in the global data sector. The Internet of Things (IoT) is a sophisticated system that connects everything to the Internet in order to exchange data and transmit through devices that can detect it in accordance with established norms. It succeeds in achieving the goal of keenly identifying, tracking, following, overseeing, and observing things. It is an expansion and augmentation of an Internet-based system that increases communication between people or between people and things or between things and things. According to the IoT vision, many objects around us will be connected to systems in some way.

Due to the extraordinary potential of the idea that almost every device may be viewed and controlled remotely through a link to the Internet, the Internet of Things (IoT) concept has recently attracted a great deal of interest from the scientific and industrial sectors. Such widespread

connectivity would make a variety of services possible in many different contexts. Cities might profit from smart lighting control, more effective trash management, and ongoing infrastructure monitoring, for instance.[2]

Connected sensors can be used in industrial settings to continuously monitor the production process, allowing for the quick detection or even prediction of failures, while in the agricultural industry, the extensive collection of environmental data, such as temperature and soil moisture, can increase the quantity and quality of soil production while lowering costs. Various application scenarios could also include health monitoring, home security, and home automation.[3]

The term "smart environment" refers to an environment that is self-protecting and self-monitoring when it is equipped with sensor devices, microcontrollers, and various software applications. When an occurrence takes place in such an environment, the dashboard shows warnings. Intelligent environmental monitoring can help to monitor and manage the consequences of environmental changes on people, plants, and animals.

To gather the information needed to forecast the behavior of a certain area of interest, sensor devices are positioned at various points. The primary goal of the proposed Work is to create and put into place an effective monitoring system that will allow the required parameters to be supervised remotely over internet while the data collected from the sensors is stored in the cloud and the approximated trend is projected on the web browser.

In this work, a wireless embedded computing system is proposed as a method for monitoring the temperature, humidity, and CO levels, or any parameter value crossing its threshold value ranges, for example, CO levels in the air in a particular area exceeding the normal levels, etc., in the environment. Furthermore, the answer provides advanced remote monitoring for data collected.

The last day's weather scenario is entirely dependent on weather prediction difficulties to determine how much the weather might vary in the future correspondingly. The concept of renewable solar systems is presented in this proposed work, along with several factors that have a significant impact on how well weather conditions are appreciated. These factors include the impact of solar radiation because of environmental reactions and reflections, which alter temperature conditions and consequently humidity conditions. Another important component that greatly affects climate conditions, including air velocity, air density, air direction, and air coolness, is wind speed. Thus, the suggested circumstances and variables have a significant impact on how accurately humans can predict the weather each day.

II. LITERATURE SURVEY

A. Conventional Weather Stations

Surface observations are ones that are made close to the surface. Instrument shelters around 2.0 metres above the ground are typically where temperature and humidity instruments are kept. The shelters are designed to provide enough ventilation while also shielding the instruments from direct sunlight, precipitation, and moisture. In the past, these

shelters' designs have differed from nation to nation, and within nations, shelters have changed over time. In certain cases, systematic biases were introduced by the shelters or the tools. A thermometer that routinely reads temperatures that are excessively high or low is an illustration of a systematic mistake. Multiple tools and techniques are used to measure precipitation. The most popular technique is to gauge how deep the water is inside a container.

B. Modern Observing Systems

Meteorological Services will need to update their organisational structure and service model to provide the best service to all users who require meteorological support, continuously provide the users with more reliable data, and put to use the products and innovations created by modern technology in the field of meteorology for both domestic and international users.

On the other hand, AWOSs can offer useful data and goods for a population's general safety and wellbeing as well as the numerous related economic advantages that can be obtained from these systems. In a number of crucial areas, including environmental monitoring for general forecasting and severe weather conditions, transport safety for road, rail, sea, and air vehicles, and educational and research purposes for the present and future understanding of global climatic conditions, the use of a modern automated surface observation system can meet these requirements.

In [4], the author suggested a reliable and cost-effective automatic weather station. The author of this paper explains how the weather prediction system is evolving into a key issue in every weather extreme event that has a negative impact on both lives and property. In order to improve weather, forecast abilities and increase resilience to the effects of unfavourable weather report conditions, the accuracy of weather data is one of the key problems.

Any device running server software is also considered to be a server. Servers are responsible for managing network resources. The Internet-based services and information are connected by LAN and made freely available to consumers via smart phones, internet browsers, or other browser-based devices in order to boost the system's intelligence, adaptability, and efficiency. Through this effort, people can learn about climatic changes. It functions well when it is accurate and efficient. So, the purpose of this work is for the author to develop a weather monitoring system using IoT. This work is straightforward to construct because it uses both hardware and software. The concept's creator uses a different sensor to collect climatic information, which is subsequently stored in the cloud.

III. SYSTEM MODEL FOR PREDICTION USING MACHINE LEARNING

A. Random Forest Algorithm

Popular machine learning algorithm Random Forest is a part of the supervised learning methodology. It can be applied to ML issues involving both classification and regression. It is built on the idea of ensemble learning, which is a method of integrating various classifiers to address difficult issues and enhance model performance.

Multiple models that are combined to solve classification and regression issues are referred to as ensemble algorithms. By examining a training set of data, classification seeks to pinpoint the discrete set of a new observation.

Competitive and cooperative ensemble forecasting are two subcategories of ensemble forecasting. According to a survey done by Soares et al., successful ensemble ML algorithms can be used to solve regression problems. [5] Ren et al. presented state-of-the-art ensemble algorithms in 2015, with a focus on forecasting wind and solar power [6].

As the name suggests, "Random Forest is a classifier that contains a number of decision trees on various subsets of the given dataset and takes the average to improve the predictive accuracy of that dataset." Instead, then depending on a single decision tree, the random forest uses forecasts from each tree and predicts the result based on the votes of the majority of predictions. More trees in the forest result in increased accuracy and mitigate the overfitting issue.

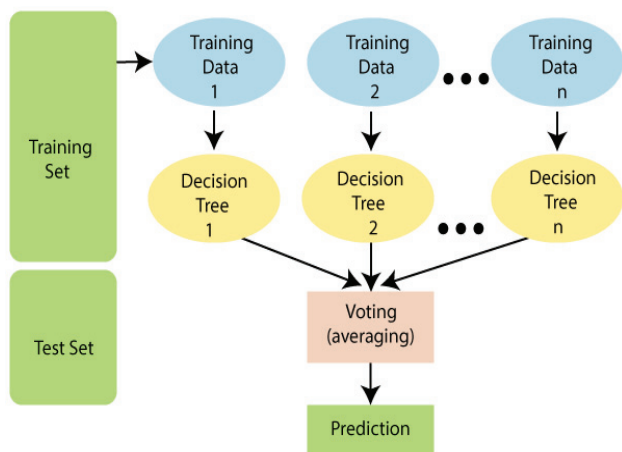


Figure 1. Various Techniques to train dataset

Figure 1 describes the various training techniques of the Random Forest classifier algorithm.

B. How does the Random Forest algorithm work?

First, N decision trees are combined to generate the random forest, and then predictions are made for each tree that was produced in the first phase. The Working process can be explained in the below steps and diagram:

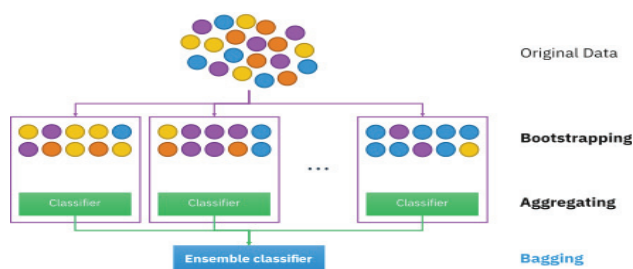


Figure 2. Various methodologies

Figure 2 explains various methodologies involved in training the raw data set to get an accurate prediction.

Step-1: Select random K data points from the training set.

Step-2: Build the decision trees associated with the selected data points (Subsets).

Step-3: Choose the number N for decision trees that you want to build.

Step-4: Repeat Step 1 & 2.

Step-5: For new data points, find the predictions of each decision tree, and assign the new data points to the category that wins the majority votes.

The ensemble method employed by random forest is bagging, sometimes referred to as Bootstrap Aggregation. A random sample is chosen from the data set using bagging. As a result, each model is created using the samples (Bootstrap Samples) that the Original Data gave, with a replacement process known as row sampling. Bootstrap refers to this stage of row sampling with replacement. Each model is currently trained independently, producing results. After merging the outputs of all the models, the final decision is made based on a majority vote. Aggregation is the process of aggregating all the results and producing a result based on a majority vote.

This model was created using a Random Forest classifier, and it has an accuracy of 85.0%. It was trained using 10,000 datasets, while we also tried K-Nearest Neighbours training. However, the accuracy of the Random Forest classifier is higher than that of other models.

IV. RELATED WORK

When compared to traditional weather monitoring systems, the smart weather monitoring system is quite compact and simple to install. The Smart Weather Monitoring System's use of far less expensive sensors makes this work very cost-effective. Data from the sensors may also be sent to a web page that is accessible from any location in the world. Because there are fewer parts, the smart weather monitoring system's maintenance costs are also quite low. The Smart Weather Monitoring System's sensors collect and analyse data that is used to predict the weather. These sensors can easily detect any sudden change in the forecast, because of their high speed. Weather alerts are provided in advance.

The recommended method considers both the practical application of various sensing modalities and their best integration. Additionally, machine learning strategies and deep learning architectures are applied to the various inputs, and the outcome from both strategies is combined to create the final decision, which predicts rainfall and provides an appropriate judgement on how much irrigation should be done. In contrast to current practises, the proposed method has offered a technology-based solution that would be advantageous to the agricultural and scientific communities due to its portability and use of edge analytics, where input is processed, and output is given at the device level only without the use of cloud platforms, the internet, or Wi-Fi.

Wi-Fi, Bluetooth, and Zigbee are a few examples of common wireless network-based protocols that can be used as IoT infrastructure. However, all these protocols have drawbacks, including low range coverage and high-power consumption, and are therefore unsuitable for use in distributed applications with constrained resources. LoRa,

which offers long-distance wireless communication, low power consumption, and a relatively low price, but has a limited data transmission capacity, can be the primary answer to this issue [7].

An outdoor Lora WAN gateway is the DLOS8. Through Wi-Fi, Ethernet, 3G or 4G cellular (the latter two supported by an extra module), you can connect a LoRa wireless network to an IP network.

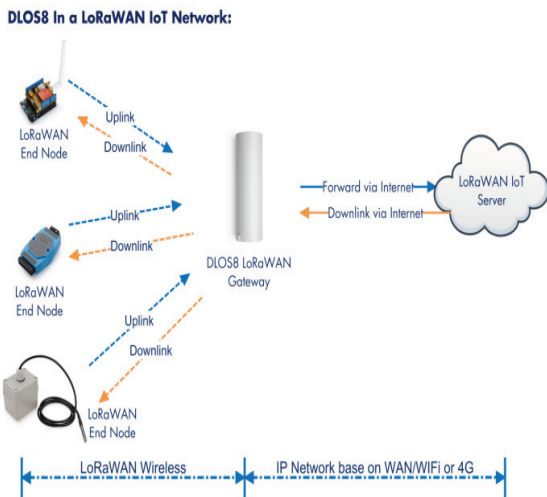


Figure 3. Architecture of LoRaWAN

Figure 3 shows a typical LoRa network. It is designed to allow low-powered devices to communicate with Internet-connected wide area networks [WAN] applications over long-range wireless connections [8]

Many weather monitoring systems are designed by deploying various sensors. Proposed model is Solar Powered IoT Weather Station Using Rain Gauge which senses the values from the LoRaWAN Weather Sensors and sends them to Network Server through LoRaWAN Gateway. LoRaWAN provides unlicensed spectrum so that it's cost free. End Device WSC-1 collects data from various sensors through RS485 Converter board and the data is sent to the gateway from WSC-1 Node. In the Things Mate dashboard, one can see the latest values and the variations of parameters in a plotted graphs and one can know whether it is preferred to stay in the surroundings by Alerts shown in Dashboard indicating Co2, PM2.5, PM10 Levels.



Figure 4. Working Model

Figure 4 delineates the working model of the weather station along with the solar panel and all the sensors as discussed in table 1.

V. RESULTS AND DISCUSSIONS

More consistent and trustworthy meteorological data must be obtained and delivered as soon as possible to those who are affected in order to meet the growing needs of the developing world. There is a great need for meteorological data assistance in many industries today, including aviation, transportation, agriculture, construction, tourism, health, justice, security, national defence, sports, written press, and visual press.

Since the atmosphere is alive, it must be regularly monitored by noting any notable alterations and phenomena. Only AWOS—Automated Weather Observing Systems can be used to do this. Continuous observations cannot be made with non-automated technologies.

Our network and application servers are both hosted on the things mate server. The data on the network server is unstable. Between the gateway and the application server, the network server serves as a medium. The data is erased from the network server as it is saved in the application server.

Cloud management helps one to access the data, and one can monitor the changes happening around them and take preventive measures.

TABLE I.
LIST OF SENSORS DEPLOYED

S.NO	Atmospheric Parameters used	Range
1	Wind speed range	(0-30m/s)
2	Wind direction	(0-360°)
3	CO2	(0-5000ppm)
4	Pm2.5/10	(0-1000µg/m3)
5	Temperature sensor	(-30 ~ 70°C)
6	Humidity	(0 -100%RH)
7	Illuminance	(0-2/20/200Klux)
8	Rain Guage	(0-4mm/minute)
9	Pressure Sensor	(10-1100hPa) (hPa=Hecta pascals)
10	Total Solar Radiation Wavelength	(300nm to 3000nm)
11	Photosynthetically available radiation	(0-2500µmol/m2*s)
12	Rain/snow detect	Yes/No

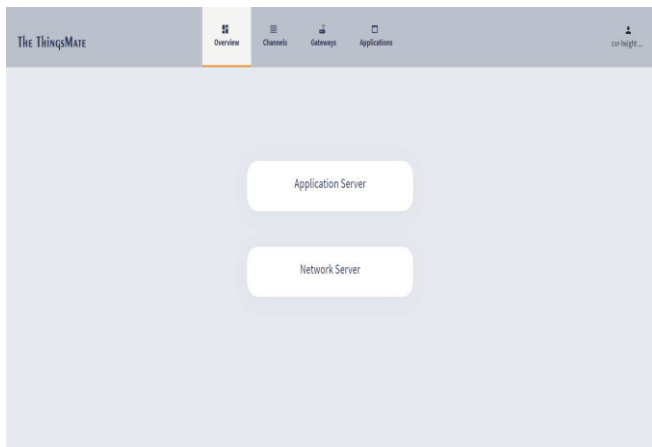


Figure 5. Things mate webpage

Figure 5 shows the application and network server where one can monitor the total number of sensors connected to LoRaWAN gateway. Our network and application servers are both hosted on the things mate server.



Figure 6. LoRaWAN Gateway

Figure 6 depicts a working model of the outdoor gateway which is the backbone of this research work. It enables the communication between the end device and end user. The DLOS8 is an open source outdoor LoRaWAN Gateway. It lets you bridge a LoRa wireless network to an IP network via Wi-Fi, Ethernet, 3G or 4G cellular (3G/4G is supported by optional modules).

TABLE II.
TEMPERATURE READINGS

Days	Sensor Data(°C)	Reference Data(°C)
Day 1	23	25
Day 2	25	26
Day 3	26	27
Day 4	28	29

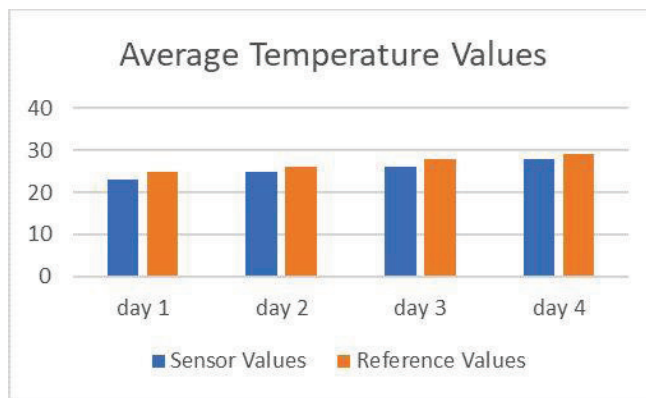


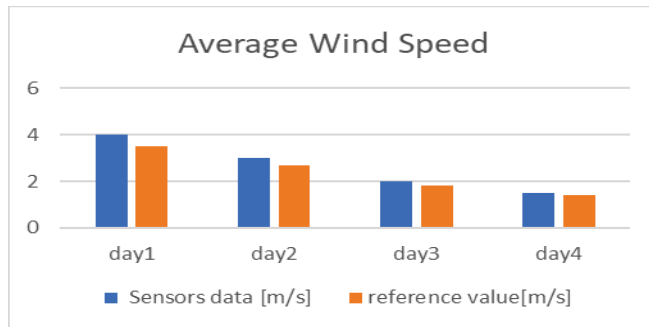
Figure 7. Trends of Temperature Data

From Figure 7 it can be clearly observed that the data received from the Temperature Sensor is relatively equal to that of the Reference Data.

TABLE III.
WIND SPEED READINGS

Days	Sensor Data (m/s)	Reference Data(m/s)
Day 1	4	3.5
Day 2	3	2.7
Day 3	2	1.8
Day 4	1.5	1.4

Figure 8. Trends of Wind Speed



From Figure 8, it can be seen clearly that the wind speed is relatively the same when compared with the reference values.

TABLE IV.
HUMIDITY READINGS

Days	Sensor Data (%)	Reference Data (%)
Day 1	95	93
Day 2	96	97
Day 3	98	97
Day 4	99	98

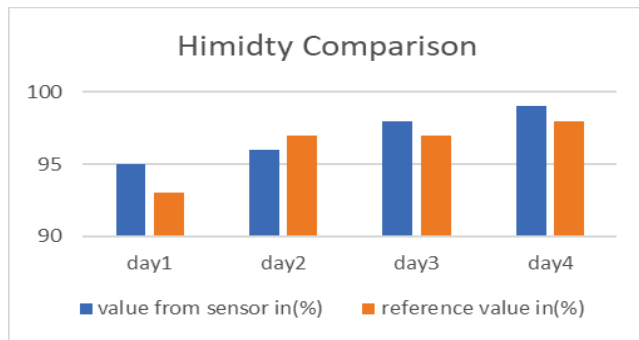


Figure 9. Trends of Humidity

From Figure 9, it can clearly see that humidity levels are relatively the same.

VI. CONCLUSIONS

Weather forecasting is a difficult task but a crucial area of study. because it pertains to our everyday lives. One can forecast the weather using machine learning and deep learning algorithms based on a variety of input features. To achieve better results, IoT approaches can be effectively combined with machine learning and deep learning. The location and timing of the weather station have a significant impact on prediction accuracy. The outcomes demonstrated that deep learning methods and mixed machine learning techniques can both improve accuracy. This concept offers a practical solution for ongoing environmental monitoring through the deployment of weather stations, the development of a smart environment, and the protection of public health from pollution.

REFERENCES

- [1] L. Atzori, A. Iera, and G. Morabito, "The Internet of Things: A survey," *computer. Networks*, vol. 54, no. 15, pp. 2787–2805, 2010.
- [2] A. Zanella, N. Bui, A. Castellani, L. Vangelista, and M. Zorzi, "Internet of things for smart cities," *IEEE Internet of Things Journal*, vol. 1, no. 1, pp. 22–32, 2014
- [3] D. Bandyopadhyay and J. Sen, "Internet of things: Applications and challenges in technology and standardization," *Wireless Personal Communications*, vol. 58, no. 1, pp. 49–69, 2011.
- [4] Mary Nsabagwaa, Maximus Byamukamab, Emmanuel Kondelaa, "Towards a robust and affordable Automatic Weather Station ", *journal homepage: www.elsevier.com/locate/deveng*.
- [5] J. Mendes-Moreira, C. Soares, A. M. Jorge, and J. F. de Sousa, "Ensemble approaches for regression: A survey," *ACM Comput. Surv.*, vol.45, no. 1, pp. 1–10, Nov. 2012.
- [6] Y. Ren, P. N. Suganthan, and N. Srikanth, "Ensemble methods for wind and solar power forecasting: A state-of-the-art review," *Renew Sustain. Energy Rev.*, vol. 50, pp. 82–91, Oct. 2015.
- [7] R. S. Sinha, Y. Wei, and S. H. Hwang, "A survey on LPWA technology: LoRa and NB-IoT," *ICT Express*, vol. 3, issue 1, pp 14-21, March 2017.
- [8] A. Augustin, J. Yi, T. Clausen, and W. M. Townsley, "A study of Lora: Long range & low power networks for the internet of things," *Sensors (Switzerland)*, vol. 16, issue 9, pp 1466,2016.

The project is funded by Department of Science and Technology (DST), under NEWGEN IEDC scheme for the Academic year 2021-2022.

Smart Precision Interface for Conventional Agricultural Methods

S. Praveen Chakkravarthy¹, Gaddam Vivek², Kalakuntla Vishal³, Sahithi Vangala⁴ and Juluri Sai Teja⁵

¹Assoc. Professor, CVR College of Engineering /ECE Department, Hyderabad, India

Email: too.spc@gmail.com

²UG Scholar, CVR College of Engineering/ECE Department, Hyderabad, India

Email: gaddamvivek9@gmail.com

³UG Scholar, CVR College of Engineering/ECE Department, Hyderabad, India

Email: vishalbadri2002@gmail.com

⁴UG Scholar, CVR College of Engineering/ECE Department, Hyderabad, India

Email: svangala56@gmail.com

⁵UG Scholar, CVR College of Engineering/ECE Department, Hyderabad, India

Email: julurisaiteja6789@gmail.com

Abstract: The Indian agricultural industry needs a huge amount of water and fertilizers to produce a significant harvest. Applying precise farming methods can transform the agricultural industry. Utilizing cutting-edge methods like IoT (Internet of Things) and data analytics, the paper seeks to alleviate the gap between farmer and his crop. The goal of the information and technology-based farm management system is to recognize, assess, administer the temporal variability and abstraction among fields for maximum production and profitability, sustainability, and conservation of the land resource by reducing the assembly costs.

Index Terms: Conventional Farming, Internet of Things (IoT), Data Analytics, LoRaWAN Communication Protocol

I. INTRODUCTION

The proposed LoRaWAN based agricultural solution provided improvement in yield of the plant by providing required quantity of water and nutrition, thereby reducing the expenses in terms of less usage of fertilizers compared to conventional agricultural practices. This LoRaWAN based solution can be used to monitor the farm from anywhere in the world and even to the remote areas where public access network is not possible.

A. Conventional Farming

Intensive until age or concentrated monoculture production, genetically modified species, targeted animal feeding operations, substantial irrigation, the use of artificial chemical fertilizers, insecticides, and herbicides are all examples of conventional agricultural practices. As a result, traditional agriculture is not only very energy and resource intensive, but also very productive.

Producers typically use too many inputs in an effort to increase crop output over the entire field. Overusing inputs results in decreased profitability and negative environmental effects on soil, surface water, groundwater, and drainage water resources. This is due to an improper number of fertilizers being added to the soil. However, alternating elements including soil compaction, loss of organic matter, water holding capacity, biological activity, and wind and water erosion of exposed topsoil are the cause of decreased production. It has been discovered that agricultural activities

contribute to non-point source water contaminants, which include salts, fertilizers (particularly nitrate and phosphate), pesticides, and herbicides.

Food now is less nutrient-dense than it was in earlier generations, while having a lot more calories. In addition to polluting food with pesticide residues, conventional agricultural methods can harm the synthesis of vitamins, minerals, proteins, and phytonutrients in fruits and vegetables.

B. Impact of Conventional Farming

Because of the widespread use of synthetic fertilizers and pesticides, conventional farming has come under fire for causing biodiversity loss, soil erosion, and extreme pollution. The soil is affected by geological processes, urbanization, deforestation, erosion, and waterlogging. Traditional farming practices can contaminate food with pesticide residues while adversely affecting the synthesis of important vitamins, minerals, proteins, and phytonutrients in fruits and vegetables. Producers often use a lot of inputs to increase the overall crop output. Excessive input application reduces profitability, degrades soil fertility, and has a negative environmental impact on surface water, ground water, and drainage water.

C. Crop Nutrient Management

A perfect yield is frequently maintained by increasing Nutrient Use Efficiency (NUE). Controlling the usage of fertilizers will significantly improve atmospheric health. Through several on-farm comparative studies, rice and wheat were assessed in both high-input and low-input production systems throughout India's rice-wheat belt. The findings demonstrate that by lowering the chemical element nitrogen input by 15–30%, gains may be scaled up correspondingly by 2–4% and global warming can be decreased. [1]

The rest of the article is organized as follows:

- II. Literature Survey
- III. System Model
- IV. Results and Discussion
- V. Conclusion.

II. LITERATURE SURVEY

For a plant to develop to its full potential and be in a highly healthy state certain conditions must be satisfied i.e., these elements must be present in sufficient quantities in the soil. Ideally, the characteristics will enable caterpillar tracking of the farm's present state. The soil's pH, temperature, moisture content, electrical conductivity (EC), and nutrient content, namely nitrogen (N), phosphorus (P), and potassium, are all critical characteristics (K). [2]

Soil pH: The most significant physical characteristic of soil is pH. It has a significant impact on the concentration and uptake of solutes in soil. For several reasons, including the fact that some plants and soil life prefer either alkaline or acidic conditions, soil pH is a crucial factor for farmers and gardeners. Acidic soil is defined as having a pH of less than 6, normal soil is defined as having a pH of 6 to 8.5, and alkaline soil is defined as having a pH of higher than 8.5. The reality remains that soil response (pH) is not a reliable predictor of a plant's development characteristics; but it does give a decent indication of a number of plant growth parameters, primarily the soil's nutritional condition. The pH of the soil has a strong correlation with the nutrient availability in the soil.

The macronutrients, except for phosphorus, are more readily accessible in the pH range of 6.5-8. These include nitrogen, calcium, potassium, magnesium, and Sulphur. However, the micronutrients are offered in a pH range of 5-7, which is somewhat acidic. These are the ranges where nutrient availability to plants is ideal and beneficial. [3]

Soil Temperature: The soil's temperature has a significant impact on the chemical, physical, and biological processes involved in plant development. Season, time of day, and regional meteorological factors all affect soil temperature variations. The sun and heat produced by the soil's chemical and biological activities are the main sources of warmth. An increase in soil temperature speeds up chemical processes, decreases the solubility of gases, and lowers the pH of the soil. It also contributes significantly to seed germination. Temperature changes in the soil are a result of exchange activities that occurred at the soil surface. Soil temperatures has a profound effect on plant growth by influencing water and nutrient uptake, root and shoot growth. Water uptake decreases with low temperature. Decreased water uptake reduces the rate of photosynthesis. Increased metabolic activities of micro-organisms as a result of increase in soil temperature will stimulate the availability of nutrients for plants. Soil temperature influences soil moisture, aeration, and availability of plant nutrients which are necessary for plant growth. [4]

Soil Moisture: The most important physical characteristic of soil is moisture. As a nutrient and a solvent for other nutrients including salt, potassium, carbon, and nitrogen, soil moisture content is crucial to crop productivity. The soil's moisture affects how well nutrients are absorbed. Furthermore, the texture and structure of soil are related to its water content. The quantity of voids, particle size, clay minerals, organic content, and the state of the ground water, these all affect how wet the soil is. Since soil consistency

mostly determines how wet anything is, clayey soil, which has a high porosity, often contains more water in it than do sandy soils. Intelligent water retention capacity reveals the excellent form of the soil. It is an important parameter for many hydrological, horticultural, agricultural, and meteorological applications. [5]

Soil Electrical Conductivity (EC): One of the simplest and most affordable soil measures now accessible to precision farmers is soil EC. It measures the number of ions in a solution. A soil solution's electrical physical phenomena get stronger as its ion concentration rises. Electrical conductivity changes with depth, although its range of variation was reduced in upland profiles. This was likely caused by the slope of the land's surface, as well as by its high permeability and high downfall, which caused alkali and alkaline bases to be leached away. Electrical conductivity is used to calculate the amount of soluble salt present in soil and is often used as a salinity indicator. It can serve as a measure of soluble nutrients but has often been used to determine soil salinity. One of the soil qualities that has a good association with the other soil characteristics is soil electrical conductivity (EC). It is possible to utilize measuring soil electrical conductivity as a suitable method for acquiring meaningful information about soil since it is simpler, less costly, and faster than other soil property tests.[6]

Nitrogen Content: The most vital component of plant nourishment is nitrogen. When salts of chemical elements are applied to plants, they react swiftly. This component promotes the development of above-ground plants and gives the leaves a rich shade of indigo, green. Biological processes have an impact on the organic cycle, which is crucial to the soil system. It is essential for plant growth and may be a component of nucleic acid, chlorophyll, and plant proteins. In addition, the relationship between soil organic carbon and nitrogen is direct. Nitrogen affects the quality of plants and fruit and raises the protein level of the latter.

Phosphorus Content: Every live cell in a plant, even the most advanced ones, may contain phosphorus. It is one of the most important micronutrients required for plant development. Most typically, phosphorus acts as an energy storage substance and restricts the amount of nutrients that may be found in plant nuclei. It facilitates the movement of energy. Since phosphorus is necessary in significant quantities for plant development, it is a crucial element. It also plays a vital role in the process of photosynthesis and is involved in the production of all fats, sugars, and carbohydrates. The amount of phosphorus in the soil in which a plant is growing is a major factor in determining how active the plant is, including its ability to grow, breathe, and reproduce.

Potassium Content: Although metallic content is not a fundamental element of any significant plant component, it is crucial to a wide range of physiological activities necessary for plant growth, from protein synthesis to maintaining the water balance in the plant. It is engaged in number of plant metabolism events, from the generation of cellulose and lignin for cellular structural components to the

control of photosynthesis and the production of plant sugars for diverse metabolic requirements. In its mineral form, potassium is present and has an impact on plant growth, the production of carbohydrates, the movement of sugar, the activity of different enzymes, and disease resistance. [7]

III. SYSTEM MODEL

A. IoT Based Plant Growth System

The Internet of Things (IoT) is one of the most obvious essential technology advancements in modern farming. IoT refers to networks of digitalized physical objects, each of which has a special identification number. A network of seamlessly linked sensors is utilized to supply data targeted at delivering healthier plant development and a much better environment, making the usage of Internet of Things (IoT) for plant growth and environmental management a potential strategy. Modern farming requires high levels of output without requiring more land. One way to increase productivity is to repurpose existing land, however owing to a variety of environmental factors, this approach may not always succeed. Contemplating the current international scenario of farmlands, an IoT based smart farming device will impact the eco-friendly country. So as to monitor several factors differently related to the conditions of crops, soil, and environment. Potency in terms of plant growth and agriculture could also be achieved in various ways, one among those is healthier management of the basic farming environment. Through IoT it is attainable for farmers to study their land far better and observe changes in it. IoT will give humans free aid to the agriculture sector. The field can be machine-controlled exploitation technology and therefore the method of watering the field can be done without delay and only at required intervals. [8]

B. Data Analytics in Agriculture.

We may get information about which crop can be cultivated for specific pH and other parameter levels by analyzing the data. By estimating the quantity of drainage capacity in the particular soil, it also aids in our investigation into whether agriculture is practical or not. The act of acquiring, organizing, and analyzing huge collections of data in order to identify patterns and other important information is known as big data analytics. Organizations may benefit from using big data analytics to better comprehend the data that is present in their information. These analytics will also help them discover the data that is more important to their operations and upcoming business choices. Fundamentally, analysts working with vast amounts of data need the information gleaned through the analysis of the data. Big data analytics often makes use of sophisticated computer-coded software tools and applications for text mining, forecasting, and data optimization as well as predictive analytics and data mining to evaluate such a massive amount of data. These procedures work together as distinct but highly interconnected components of outstanding performance analytics. The ability to process enormous amounts of data that a company has gathered and identify the data that is useful and can be studied to inform

future business choices is made possible by using big data tools and technologies. [9]

C. Smart Precision Interface

The current standard technique for practical farming is based mostly on GSM. It frequently requires a monthly expenditure, requires electricity to operate, and, in many cases, is located in a remote place where it is difficult to encourage sufficient network coverage for using GSM. As a result, it is nearly impossible to implement automation in such situations. In contrast to the current strategy, including IoT and Data Analytics can have a significant influence on agriculture production, improving accuracy and moving the industry toward more logical and improved farming practices. The farm may be linked with the IoT nodes to monitor the field's trend and make the required adjustments regarding the resources. Resources might be made available in sufficient quantities, and investments for buying different fertilizers could be managed. The LoRaWAN (Long Range Wide Area Network) communication protocol may be utilized successfully to improve the farm's technical capabilities. The full prototype is made up of LoRaWAN based sensors that measure the parameters in part II, evaluate the gleaned information, and alert the farmer to supply the field with enough resources.

D. LoRaWAN Communication Protocol

To establish communication between the farm and the end user, the Long Range Wide Area Network (LoRaWAN) communication protocol is used. LoRaWAN offers unlicensed spectrum with low latency of 1–10ms and coverage of roughly 10 km, which is our desired Indian frequency of 865-867 MHz. It has an SX1301 LoRaWAN concentrator, which offers 10 demodulation methods that may be processed concurrently. The frequency bands can be changed by end users for usage in their specific LoRaWAN networks. Along with the Dragino Outdoor gateway, soil moisture, EC, NPK, pH, and temperature sensors are utilized to create a link between the farm and the farmer. Sensors are used to measure the parameters, and the data is analyzed by comparing it to the optimal values needed for the crop in question. This is accomplished by using data analytics to transform the measured raw data into information that farmers can easily understand and by prompting the farmer with the current status of his field.

NPK Sensor: A LoRaWAN Soil NPK Sensor for IoT in Agriculture is the Dragino LSNPK01. It is intended to measure the Soil Fertility Nutrient, Nitrogen (N), Potassium (K), and Phosphorus (P) in the soil and serve as a reference for plant growth. The probe may be submerged into soil for long-term use and is waterproof to IP68 standards.

Outdoor Gateway: An open source outdoor LoRaWAN gateway is DLOS8. It enables you to connect a LoRa wireless network to an IP network using Wi-Fi, Ethernet, 3G, or 4G cellular (optional module supports 3G/4G). Users can send data and cover incredibly vast distances at little cost with LoRa wireless data-rates. Figure 1 represents the complete architecture of the prototype beginning from the

sensors on the field followed by the gateway, server, cloud storage and lastly the end user.

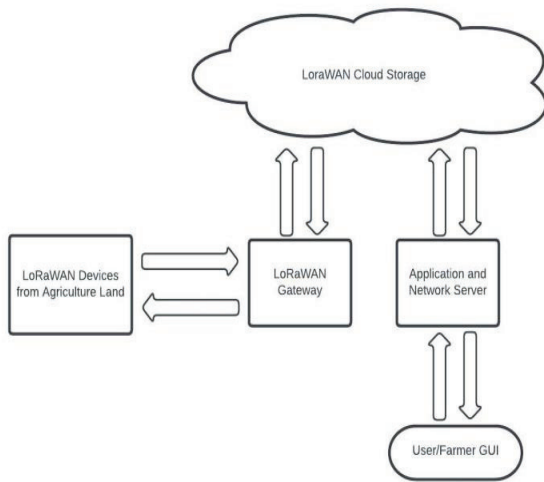


Figure 1. Block Diagram of the Proposed Work

The LoRaWAN gateway, which serves as a communication route between the users, has embedded sensors. Utilizing the TTN, the obtained data is kept on the cloud server (The Things Mate Network). Data is retrieved from the gateway via the Things Mate network server so that it may be saved, examined, and seen by the end user. Both the network server and the application are present in the TTN server. While the network server is utilized by the service provider and keeps measured data in hexadecimal form, the application server stores values that may be comprehended by the end user. The Outdoor Gateway must always have a reliable internet connection and a DC power source. Both wireless and cellular networks can be used to deliver internet service. The sensors and gateway are first set up using the TTN network server's Application EUI and Device EUI (Extended Unique Identifiers) and OTAA (Over the Air Activation) keys. For the needed period of data retrieval, a payload must be provided. Direct access to the findings is available via the TTN network dashboard. The end user may see both tabular data and graphical depiction on the application server. However, the information can be shown to the public or depicted on any digital device, such as a smartphone or television. "The Things Mate" has a versatile usage since it may be used from any location and with any device. Figure 2 illustrates the three sensors deployed in the field.



Figure 2. Sensors deployed on field



Figure 3. Outdoor Gateway

Figure 3 depicts the installation of the LoRaWAN outdoor gateway. Smart precision farming, by facilitating remote crop monitoring, reduces hazards for farmers. To avoid poor output, crop delays, and crop current conditions that would make more accurate maintenance possible. One advantage of linking agricultural solutions to crop yields is that information can be shared more easily between farmworkers and external stakeholders. Additionally, by examining and comparing the present crop values to the assessed ideal values, data analytics enables the farmer to determine how best to use his resources to save time, effort, and energy. Farmers may check on their fields at any time because the data is accessible from anywhere in the globe and can be seen using an application. Additionally, the water motor may be remotely operated to water the field automatically based on the moisture level. Additionally, the application that is offered for the smart farming visualization may be used to run the motor.

IV. RESULT AND DISCUSSION

Sensor specifications:

1. LoRaWAN soil NPK sensor:



Figure 4. LSNPK01 sensor

- LoRaWAN 1.0.3 class A
- Ultra low power consumption
- Default band: IN865
- IP66 & IP68 water proof enclosure

Figure 4 shows the soil NPK sensor with probe along with transmitter and antenna.

2. Outdoor Gateway:

Outdoor gateway is displayed in figure 3.

- 1xSx1301 + 2X1257 LoRa Transceiver
- 1x2.4G Wi-Fi
- Default band: IN865
- 802.3 of PoE
- IP65

3. LT3322RL I/O Controller:



Figure 5. LT3322RL I/O Controller

- STM32L072CZT6 MCU
- SX1276/78 LoRa Wireless Chip
- LoRaWAN Class A & Class C protocol
- Power input (0-24V)

Figure 5 shows the I/O controller that connects input and output devices.

The nitrogen, phosphorus, and potassium of a paddy field are periodically monitored using the NPK Sensor, and the acquired data is displayed using the TTN application server, as fertilizers play a significant role in the growth of a crop. The clay, slit clay, and slit clay loamy soils are the most optimal for an optimum paddy crop. For a higher yield with less resources, the optimal NPK ratio for paddy crop is 55:80:160.

TABLE I.
NPK TREND IN PADDY FARM

TIME	NITROGEN	PHOSPHORUS	POTASSIUM
12:00	5632	8192	16384
12:10	5888	8182	16389
12:30	5888	8192	16384
1:00	5878	8194	16640
1:10	5888	8196	16648
1:30	5845	8456	16658

The paddy field was monitored for the nutrient contents at particular interval of time. Figure 6 illustrates the variation in the soil NPK content in the paddy field, phosphorus content was the maximum compared to the other nutrients.

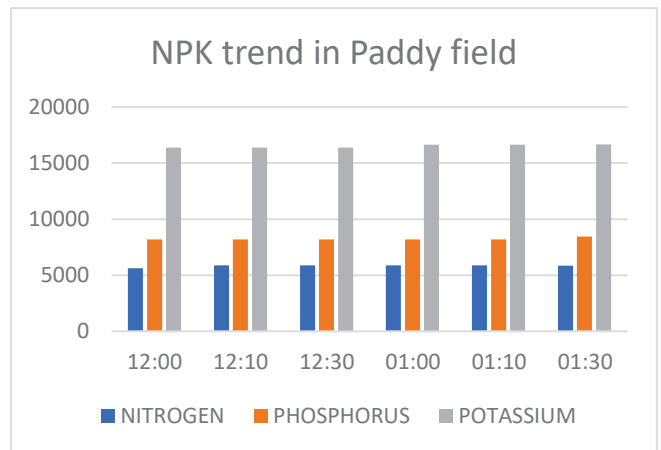


Figure 6. NPK values versus time.

TABLE II.
NPK CONTENT MEASURED ON PADDY FIELD

TIME	NITROGEN	PHOSPHORUS	POTASSIUM
12:25	7168	10240	20736
13:10	7158	10256	20738
13:45	7169	10240	20480
14:15	7166	10235	20690
14:45	7168	10245	20736

The paddy field is monitored for NPK content on a different day with respect to time. Figure 7 depicts the trend of the NPK content of the paddy field, when compared to the previous tendency, the nutrient contents raised.

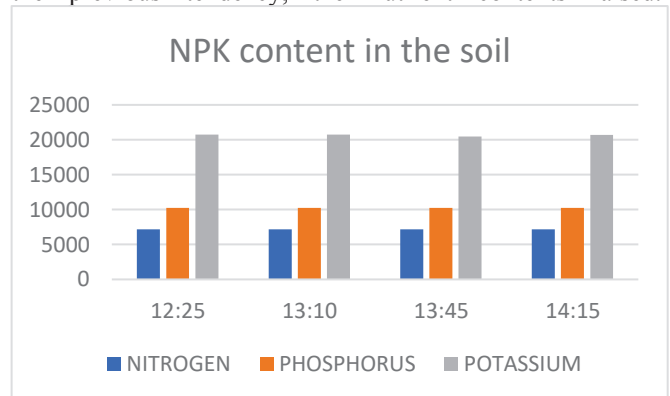


Figure 7. NPK content in the paddy field on another day at time intervals.

TABLE III.
NPK TREND IN BOTTLE GUARD FARM

TIME	NITROGEN	PHOSPHORUS	POTASSIUM
12:06	9472	13312	26880
13:06	9728	13824	27648
13:26	9726	13824	27649
14:06	9725	13725	27705
14:26	9735	13728	27650

The nutrient content in the bottle guard field was measured for particular time interval.

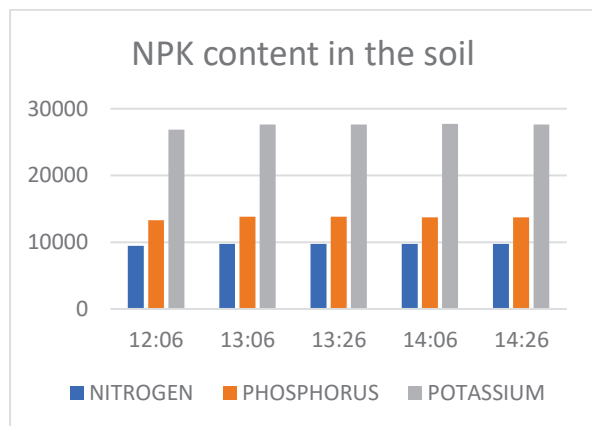


Figure 8. NPK trend on the bottle guard field versus time.

The bar chart in Figure 8 illustrates the nutrient contents in the bottle guard field, nitrogen content is the least when compared to other nutrients. Overall, the fore mentioned result shows that, during a period of half an hour, the paddy field is rich in potassium relative to nitrogen and phosphorus. As a result, the farmer is advised to provide the crop with only the nutrients needed based on the analysis by contrasting with the predetermined results. For instance, if the soil's nitrogen concentration is significantly higher than the desired level, the farmer will be advised to lower the nitrogen content and only add phosphorus and potassium as needed after the study. After comparing the present parameter values in the soil at that moment to the real values that are required by the crop, the conclusion on the composition of the soil is given. If certain values deviate from the ideal value, the inputs are changed. Investment may be regulated and managed in this way.

V. CONCLUSIONS

Smart precision farming is a promising technology that has the potential to replace outdated and erroneous farming practices with one that is reliable and accurate. From anywhere around the world, one may keep an eye on their

field's condition. The necessary adjustments may be made with ease. It is affordable because the farmers in each hamlet may band together to buy one gateway. The farmer has the option to buy the sensors for their land. The sensors are dependable and require little upkeep. The gateway, on the other hand, is water-resistant and can be positioned at a reasonable level to cover as many nodes as possible within a 10-kilometer radius. Additionally, data analytics may be quite helpful in comparing and delivering precise findings. When put at close ranges, the different soil properties cannot exhibit significant variations. As a result, the sensors may be strategically arranged to cover the largest possible area with the fewest number of nodes.

REFERENCES

- [1] Tek B. Sapkota 1, Mangi L. Jat, Dharamvir S.Rana, Arun Khatri-Chhetri, Hanuman S.Jat, Deepak Bijarniya, Jhabar M.Sutaliya, Manish Kumar, Love K. Singh, Raj K.Jat, Kailash Kalvaniya “ Crop nutrient management using Nutrient Expert improves yield, increases farmers income and reduces greenhouse gas emissions” Scientific report, vol. 11, Number 1564, January 2021.
- [2] Ku. Sumita Tale and Dr. Sangitha Ingole “A Review on Role of Physico-Chemical Properties in Soil Quality” ISSN 2278-6783 vol. 4, Number 13, pp. 57-66, February 2015.
- [3] Khaidem Jackson, Thounaojam Thomas Meetei “Influence of soil pH on nutrient availability” JETIR, vol. 5, Issue 12, pp. 707-713, December 2018.
- [4] Onwuka, B.M “Effects of soil temperature on Some Soil properties and plant growth” Michael Okpara University of Agriculture, Umudike, Abia State, pp. 89-93, July 2016.
- [5] Saima Ansari and Ratnadeep R. Deshmukh “Estimation of Soil Moisture Content” ISSN:0973-6085, vol. 12, pp. 571-577, November 2017.
- [6] Pravin R. Chaudhari, Dodha V. Ahire , Manab Chkravarty and Saroj Maity “Electrical Conductivity as a Tool for Determining the Physical Properties of Indian Soils” ISSN: 2250-3153 vol. 4, Issue 4, pp. 1-4, April 2014.
- [7] C.V. Swarna Under Shade Net Condition “Effect of NPK on Plant Growth, Yield and Quality of Capsicum (Capsicum annum L.)” ISSN: 2319-7706 vol. 6, Number 3, pp. 1085-1091 March 2017.
- [8] Syed Mohammad Kamruzzaman, Saifur Rahman Sabuj, Monirul Islam Pavel “Promoting Greenness with IoT-Based Plant Growth System: Intelligence and Sustainable Computing”research gate publications, chapter 12, September 2020.
- [9] Priyanka Gnanalingam “Data Analytics in Agriculture” IISN: 2394-6598, vol. 4, Issue 5, pp.91-94, August 2018.

Trust-based Model to Alleviate Selfish Node Attacks in MANETs

M. Deva Priya

Assoc. Professor, Sri Eshwar College of Engineering/CSE Department, Coimbatore, Tamilnadu, India
Email: devapriya.m@sece.ac.in

Abstract: MANETs are dynamic in nature. So, they are subject to several attacks. It is always essential to ensure confidentiality, availability, authenticity and reliability of the network. Conserving energy in MANETs is an uphill task. Hence, it is mandatory to design an energy-aware inter-clustering scheme that involves Residual Energy (RE) and resources. Confirming security in MANET is another challenge. In this Paper, selfish nodes are determined based on a Trust Value (TV) that involves packet forwarding behavior, resource utilization, reliability and RE. In this paper, Reliable History dependent Resource Conscious Clustered-OLSR (RHRCC-OLSR) protocol is proposed to overcome degradation of network performance owing to selfish node attacks. It is evident that the propounded protocol offers improved PDR and throughput with reduced delay, PLR, energy and routing overhead.

Index Terms: Selfish node attack, MANET, Trust, Reputation, History, OLSR

I. INTRODUCTION

As MANETS are self-organizing wireless networks and do not demand any static infrastructure for configuration, it is more appropriate to be applied in surroundings that need immediate setup. Security in MANETs is an issue which has to be addressed. The presence of selfish nodes greatly worsens the performance of the network [1, 2].

A. Ensuring Trust in the Network

A trust factor is defined to depict the security level. Researchers have focused only on subjective trust. Trust is categorized into direct as well as indirect trusts [3, 4].

- **Direct Trust:** Each node retains direct relationship with neighboring nodes. The behaviors of neighbors are observed during routing. The experience with neighboring nodes is also taken into consideration.
- **Indirect Trust:** It is determined based on nodes located outside the range of communication. Requests as well as responses may flood the network.

Trust computation consumes more time, bandwidth as well as energy. This leads to delay in discovering routes with an increase in computational overhead [5, 6].

The dynamic nature of network topology makes trust management difficult. Hence, to deal with this issue, a trust factor is added to the proposed scheme for mitigating routing attacks. TVs are computed for every node making it suitable for sending data to destination [7].

B. Selfish Node Attack

Selfish nodes focus on getting services from the network while preserving resources like battery or bandwidth. These nodes attempt to preserve communication amid nodes. But

they do not collaborate to transmit packets. These nodes are involved in any one of the ensuing actions.

- Turn off power when active communication is not present
- Do not forward Route REQuests (RREQs) on receiving one
- Forward RREQ on the inverse path but not Route REPLY (RREP). The source is not capable of identifying a path to destination and hence RREQ is sent again
- Do not unicast or broadcast Route ERRor (RERR) packets in case paths are not available.
- Selectively drop packets

The delivery rate is lessened by dropping packets.

C. Dynamic Reputation Management

The reputation of a node is determined based on type of packets namely, data and control packets [8]. As nodes join a network, they are ignorant of reputations of adjoining nodes. This demands assigning a default reputation to every node in the network [9]. The node reputation takes values in the range [0-2]. The corrective module includes a punishment scheme and a path administrator [10].

A node table is maintained to store the reputation of nodes. As packets are transmitted, there should be an increase in the total reputation of nodes. The status of nodes is found based on total reputation associated with a grading criterion. The path administrator takes the responsibility of removing nodes with reduced reputation from the route cache based on information obtained from the punishment mechanism [11, 12]. It ensures that packets are not forwarded through a path involving black-listed nodes.

In the proposed system, the node's trust is computed based on Residual Energy (RE), resource utilization and packet forwarding behavior along with reliability rate. The propounded Reliable History dependent Resource Conscious Clustered-OLSR (RHRCC-OLSR) protocol includes modules for detecting RE and computing trust.

In case of RE detection module, along with RE and reliability, rates of drain, packet drop and failure are determined. The rate of drain of a node is determined using an exponential weighted mechanism. The rate of packet drop is the difference amid the number of packets received as well as relayed to next hop nodes. Likewise, the failure rate is given by the sum of product of packet drop rate as well as weighted average of every session. Node reliability is determined from the failure rate of a node. TV is defined in terms of quantity of forwarded packets, RE, used bandwidth and node reliability.

II. RELATED WORK

Arboit et al (2008) [13] have propounded localized certificate revocation for MANETs. The main issue related to certificate revocation is that there is no on-line acquisition to trustworthy authorities. In case of wired networks, if certificates are to be withdrawn, Certificate Authorities (CAs) add information associated with certificates to Certificate Revocation Lists (CRLs) and submit them to repositories or dispense them to suitable entities. In case of simple networks, there is no acquisition of centralized repositories or trusted authorities. Hence, the traditional method of certificate revocation is not applicable. The proposed decentralized scheme for certificate revocation allows nodes to handle challenging entities. The method is not based on input from central or external entities.

Li et al (2012) [14] have offered a framework for offering context-based security as well as trust based on some policies. The proposed scheme incorporates contextual information in terms of status of battery and communication channel including weather conditions. It is used in determining whether misbehavior is the result of malevolent action or not. It identifies malicious and malfunctioning nodes.

Eissa et al (2013) [15] have designed a trust-dependent routing scheme. The challenging problems related to routing and security are discussed. Friend Ad hoc On-Demand Distance Vector (FrAODV), a trust-based scheme, is proposed for securing AODV protocol. The routing paths are identified depending on node reputation and identity before routing data. This scheme offers a robust environment where nodes rely on one another in a secure community.

Wei et al (2013) [16] have offered cluster-based certificate revocation along with a vindication feature. Though networks offer mobility with effective positioning, they are susceptible to numerous classes of security attacks in contrast to wired networks. Secured services are to be assured. To handle this confrontation, revocation of certificates is taken as an essential integral element for securing communication. It focuses on segregating attackers from added participation in network functions. Cluster-based Certificate Revocation with Vindication Capability (CCRVC) scheme offers quick as well as precise revocation. The mechanism improves reliability and accuracy. The threshold-based scheme helps in deciding whether vindictive alerted nodes are candid nodes or not before convalescing them.

Adnane et al (2013) [17] have proposed a trust dependent security for OLSR routing protocol. Trust is implicitly included in the protocols based on co-operation, particularly, amid the entities included in routing. Certainly, as the range of nodes is restricted, they jointly collaborate with their neighbors so that they extend to distant nodes and then the whole network. Moreover, trust administration allows objects to deal with trust and get decisions concerning other entities. Trust-based OLSR protocol is designed to permit every node to evaluate behavior of nodes. Once malevolent nodes are determined, preventive measures along with countermeasures to deal with irregularity are also presented.

Shurman et al (2014) [18] have proposed a co-operative reputation scheme to circumvent malevolent nodes. Routing as well as forwarding takes place through existing nodes. The BSs are concerned with route detection and maintenance,

stimulating traffic along with network management. More amount of energy is spent for forwarding packets without any direct gain. A misbehaving as well as greedy node has short-term efficacy and may not contribute to routing. The proposed Reputation Approach (RAP) involves a reputation model that identifies and segregates misbehaving nodes which are not involved in collaboration for sending packets of added nodes.

Chatterjee et al (2014) [19] have designed a trust-based secure clustering framework. Secure clustering is highly essential. Conventional cryptographic solutions cannot be applied to threats from attacked nodes. Nodes' trust is computed using self as well as recommendation support of 1-hop neighbors. Based on communication as well as computational demands, the scheme is lightweight but dominant depending on flexibility in dealing with trust. Furthermore, this clustering protocol splits the network into 1-hop separate clusters and chooses nodes that are highly fit and reliable as CHs. An authentic voting scheme using parallel signatures is used for selection.

Abdel-Halim et al (2015) [20] have propounded a trusted on-demand routing protocol based on an agent. The overall routing ability is dependent on support of nodes which form the network. This behavior is handled by considering node reliability for choosing routes in addition to hop count. Trustworthiness is obtained by finding the TV of every node. This agent-based protocol is based on Dynamic Source Routing (DSR). This handles trust-dependent information with insignificant load depending on added messages as well as delay. Multi-Agent System (MAS) is used in every node. It includes monitoring as well as routing agents. A mathematical model is used for finding the TV. This method is based on the amount and size of packets which reveal selective forwarding features of a node.

Ullah et al (2016) [21] have proposed a fuzzy-based trusted model for finding selfish nodes involved in routing data. A node may not be ready to offer resources for helping others in case there is no profit for its service. Such nodes are said to be non-cooperative or selfish. This may cause partitioning of the network. Fuzzy-based analyzer is used for splitting nodes into non-cooperative and trustworthy ones. TVs are forwarded to fuzzy functions mapped to varied classes. The resulting class shows trust levels of observed nodes. Depending on computed TV, the malevolent nodes are determined and removed from active routes.

Sengathir&Manoharan (2017) [22] have focused on identifying and highlighting diverse reputation-dependent mitigation schemes for selfish node attacks along with their merits and demerits. They have presented a context-and reputation-dependent mitigation scheme categorized based on history, condition probability and futuristic probability. They have presented a review on several selfish node mitigation architectures and also aim to highlight statistical trustworthiness co-efficient which aids in efficient alleviation of selfish nodes.

Kumar & Dutta (2018) [23] have proposed an intrusion identification scheme based on dynamic trust to find and segregate selfish nodes from the network. The direct trust depending on direct communications and indirect trust depending on neighbors' endorsements are taken into

consideration to precisely find selfishness of nodes. The proposed scheme offers better results.

Nodes that are idle are considered to be selfish and are circumvented from routing. To deal with this issue, Rama Abirami&Sumithra (2019) [24] have proposed neighbor and improved neighbor credit values-based AODV routing schemes. These protocols are assessed against AODV for identification of selfish nodes. Neighbor Credit Value based AODV (NCV-AODV) protocol avoids false detection. Improved Neighbor credit value based AODV (iNCV-AODV) protocol is also proposed. In both the protocols, it is assumed that only some nodes exhibit malicious behavior.

Abdelhaq et al (2020) [25] have studied the influence of selfish node attack on AODV and DSDV to determine resilient protocol. Selfishness Attack Model (SAM) is proposed to deal with selfish node attack on routing protocols. AODV offers better performance in contrast to DSDV.

Deva Priya et al (2021) [26] have proposed Skellam Distribution Inspired Trust Factor-based Selfish Node Detection Technique (SDITF-SNDT) for ensuring efficient detection and segregation of selfish nodes from the network. The proposed scheme induces selfish node detection by finding the average packet deviance using which Standard Deviation (SD) and Variance are determined for finding Skellam Distribution Inspired Trust Factor (SDITF). This computation helps in estimating the reliability to classify them into selfish as well as co-operative nodes. From the examinations performed for the proposed scheme, an outstanding enhancement in Packet Delivery Ratio (PDR) and remarkable reduction in the amount of energy consumed are confirmed for varying amounts of nodes.

Jim et al (2022) [27] have presented a bio-inspired algorithm called Artificial Immune System Based Algorithm (AISBA) to identify selfish nodes. It is based on the principle of Artificial Immune Systems (AIS). Unlike Combined Immune Theories Algorithm (CITA), AISBA does not involve a learning stage. Two dissimilar trust models are designed to distinguish genuine and selfish nodes. The proposed scheme offers better results in terms of mean detection rate, PDR and False Positive Probability (FPP) based on weight as well as trust on threshold.

III. PROPOSED RELIABLE HRCC-OLSR (RHRCC-OLSR) PROTOCOL

Selfish nodes are involved in discovering routes and maintaining functionalities of routing protocol. They remain idle by not forwarding packets but get benefited from other nodes. The proposed Reliable HRCC-OLSR (RHRCC-OLSR) protocol assesses the reliability of node based on RE, bandwidth utilized, quantity of sent and received packets along with reliability rate.

The proposed mechanism includes modules for RE based detection as well as computation of trust.

A node that seems to be selfish drops packets owing to limited energy and data rate, along with poor channel conditions. They can be identified by analyzing the routing table of adjacent nodes of a malevolent one. In case information related to neighbors does not get modified, the node is considered as a selfish node.

The presence of these nodes degrades network performance. These nodes do not forward packets even when they are active. Routing tables of adjoining nodes of malevolent node are not updated. Acknowledgements are not received in specified time. They drop packets which affect the dropping rate of packets. These nodes may be isolated in 3 varying ways. Firstly, TV is computed based on behavior of adjacent nodes in addition to RE. The RE of nodes is analyzed. There are chances for a co-operative node to become a selfish node. A nodes' selfish behavior is dependent on the exponential reliability factor. These nodes should be removed from the routing path.

A. Residual Energy (RE) based Detection

RE-based model for isolating selfish nodes is proposed to determine the available energy (E_A) of nodes along the path from source to destination by taking into consideration the node energy after data transmission. Energy Drain Rate (E_{DR}) shows the amount of energy drained in a participating node.

The energy of a node at any instance of time 't' is given by,

$$E_A = \frac{RE}{E_{DR}} \quad (1)$$

The drain rate of a node is computed using an exponential weight-based scheme.

$$E_{DR} = \rho \times E_{DR}^K + (1 - \rho)E_{DR}^{K-1} \quad (2)$$

$$\rho = \frac{E_{TR}}{\text{Number of Hops}} \quad (3)$$

Where

ρ - Weighted average

E_{DR}^K - Rate of drain of a node at session 'k'

E_{DR}^{K-1} - Rate of drain of a node at session 'k-1'

E_{TR} - Energy required for transmission

A node is said to be selfish, if ' E_A ' is less than the threshold (E_{TH}).

E_{TH} - Energy level essential for a participating node (50 Joules)

Packet Drop (PD_i) is the variance quantity of packets received (P_{RC_i}) and relayed (P_{RL_i}) by a node (i) as shown in Equation (4).

$$PD_i = P_{RC_i} - P_{RL_i} \quad (4)$$

' PDR_i ' of a node for session 'k' is given in Equation (5).

$$PDR_i^k = \frac{PD_i^k}{P_{RC_i}^k} \quad (5)$$

Rate of Failure (RF_i) is the weighted average of ' PDR_i ' for each session.

$$RF_i = \frac{\sum_{i=1}^k PDR_i}{k} \quad (6)$$

' RF_i ' is computed using PDR of node. The reputation of a node is manipulated depending on the Predicted Reliability Factor (PRF_i).

$$PRF_i = e^{-FR_i} \quad (7)$$

In case a node’s reliability goes below 0.4, then it is said to be selfish and is removed from the routing path. Once they are identified, the network should be restored to increase performance.

B. Trust Computation

TV (Abdel-Halim et al 2015) is based on neighbors’ REQ status. In the proposed work, reliability is measured by considering the RE, bandwidth utilized and PRF. At very node, ‘RE_i’ is determined. It is the difference between presently available and expended energy at a node.

$$RE_i = E_{Cur_i} - E_{Con_i} \tag{8}$$

Where,

E_{Cur_i} - Energy currently available

E_{Con_i} - Energy that is consumed

TV is given by the following formula.

$$TV = \frac{HF_i^j}{RF_i^j} \times \frac{RE_i}{BW_U} \times PRF_N \tag{9}$$

Where,

BW_U - Bandwidth utilized

RF_i^j - Quantity of packets requested by node ‘j’ to be forwarded by ‘i’

HF_i^j - Quantity of packets forwarded by node ‘i’ and received by ‘j’

Counter ‘*RF_i^j*’ is increased when ‘j’ sends a packet to ‘i’. It is essential to make sure that node ‘i’ sends packets. If ‘j’ identifies that ‘i’ sends packets before a pre-determined period, then counter ‘*HF_i^j*’ is incremented.

In case the RE of nodes go below 50%, then those nodes will not be involved in routing. Increased energy reserve (RE) with better TV confirms trustworthiness of a route.

Nodes with TV<TH are identified as malicious. TH is set as 0.3 and those nodes with TV< 0.3 will not be involved in the process of routing. This overcomes packet losses as well as delays involved in data transmission.

IV. RESULTS AND DISCUSSION

The system is implemented using ns2. It is seen that the proposed RHRCC-OLSR protocol outdoes OLSR, E-OLSR and HRAC-OLSR protocols based on diverse parameters including PDR, total energy consumption, average delay, PLR, throughput, RE and routing overhead.

The performance of the proposed scheme is compared with the above-mentioned standard protocols for varying number of nodes.

Performance depending on Varying Number of Nodes

The performance of the proposed RHRCC-OLSR is investigated by varying the quantity of nodes. It is evident from the results that the proposed scheme offers improved results in contrast to existing OLSR, E-OLSR and HRAC-OLSR protocols. The number of nodes is varied from 100 to 1000.

From Figure 1, it is evident that the proposed protocol offers better PDR for varying number of nodes in contrast to the standard protocols taken for study. With increase in the number of nodes, the schemes show a decrease in PDR. The proposed scheme is efficient in predicting the malevolent activity of nodes by considering RE and TV, thus making the system less susceptible to attacks. This facilitates the proposed system to offer greater enhancement in delivering packets when compared to benchmarked protocols. RHRCC-OLSR offers 31%, 21% and 6% better PDR when compared to OLSR, E-OLSR and HRAC-OLSR schemes respectively.

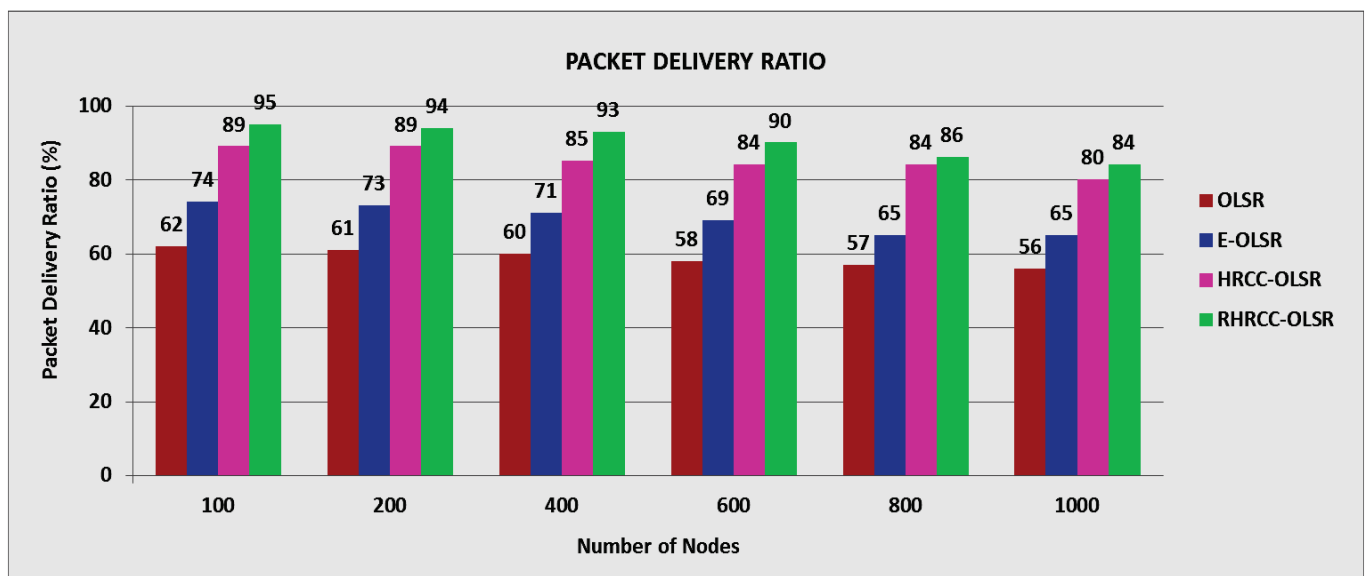


Figure 1. Packet Delivery Ratio of RHRCC-OLSR based on Number of Nodes

On the other hand, the existing OLSR, E-OLSR and HRAC-OLSR protocols offer 66%, 52% and 16% reduced

throughput when compared to the proposed protocol (Figure 2). As selfish nodes are isolated from the network, they do not

participate in the routing process. The reliable nodes along the path guarantees well-timed delivery of packets, thus offering increased throughput.

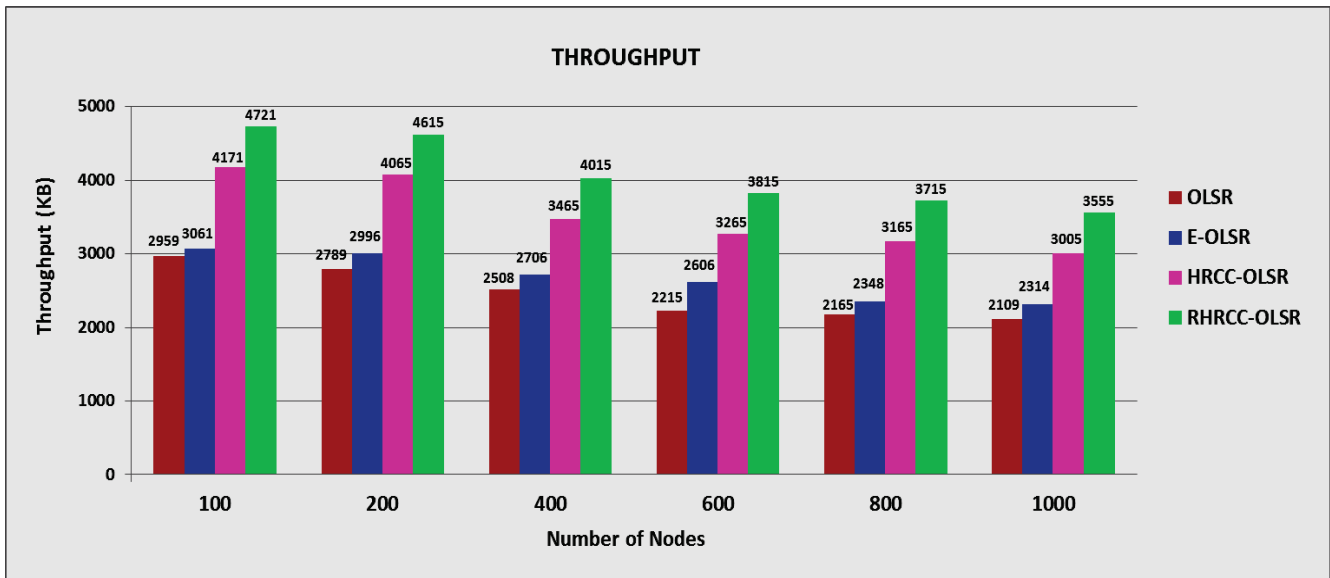


Figure 2. Throughput of RHRCC-OLSR based on Number of Nodes

From Figure 3, it is evident that performance of the proposed protocol is examined depending on RE and performance is compared with standard protocols for varying quantities of nodes. Energy consumption of existing protocols is more when compared to the proposed protocol.

The RE decreases with increase in the quantity of nodes. Proposed protocol conserves energy to a greater extent and hence has increased RE in contrast to standard protocols. It has 42%, 23% and 6% more RE when compared to OLSR, E-OLSR and HRAC-OLSR protocols correspondingly.

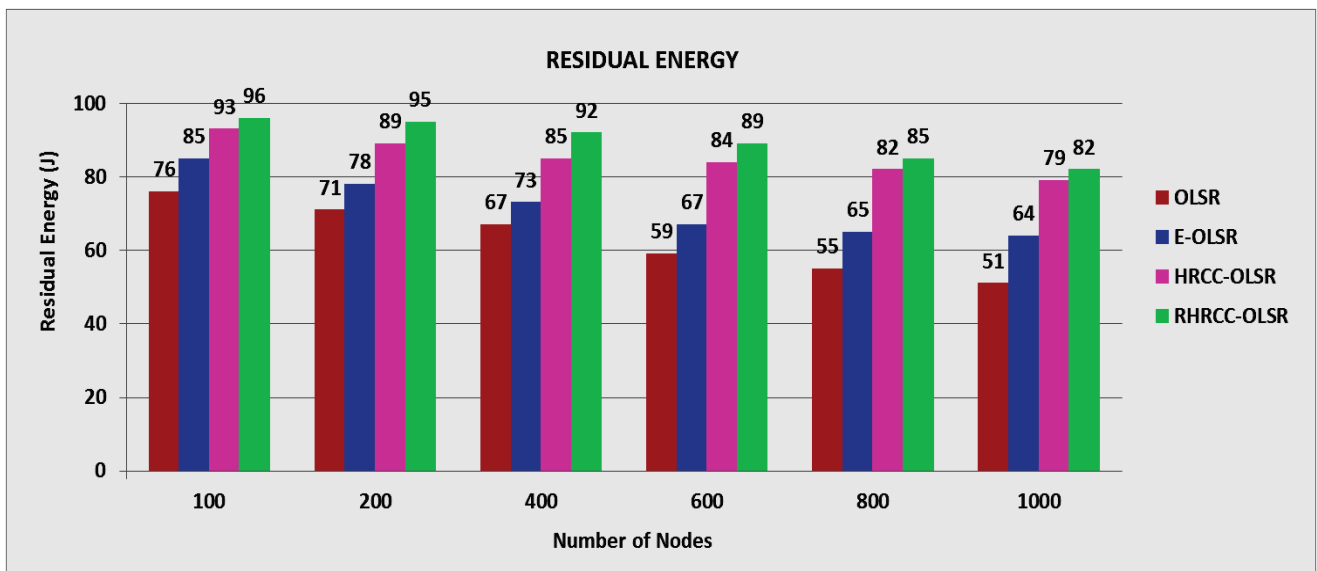


Figure 3. Residual Energy of RHRCC-OLSR based on Number of Nodes

From Figure 4, it is obvious that the proposed protocol involves lesser average delay. The existing protocols show an increase in delay in contrast to proposed RHRCC-OLSR. The malevolent nodes are isolated by determining the TV of

participating nodes, which ensures route reliability. The average delays of existing OLSR, E-OLSR and HRAC-OLSR protocols are 32%, 20% and 11% more when compared to the proposed protocol.

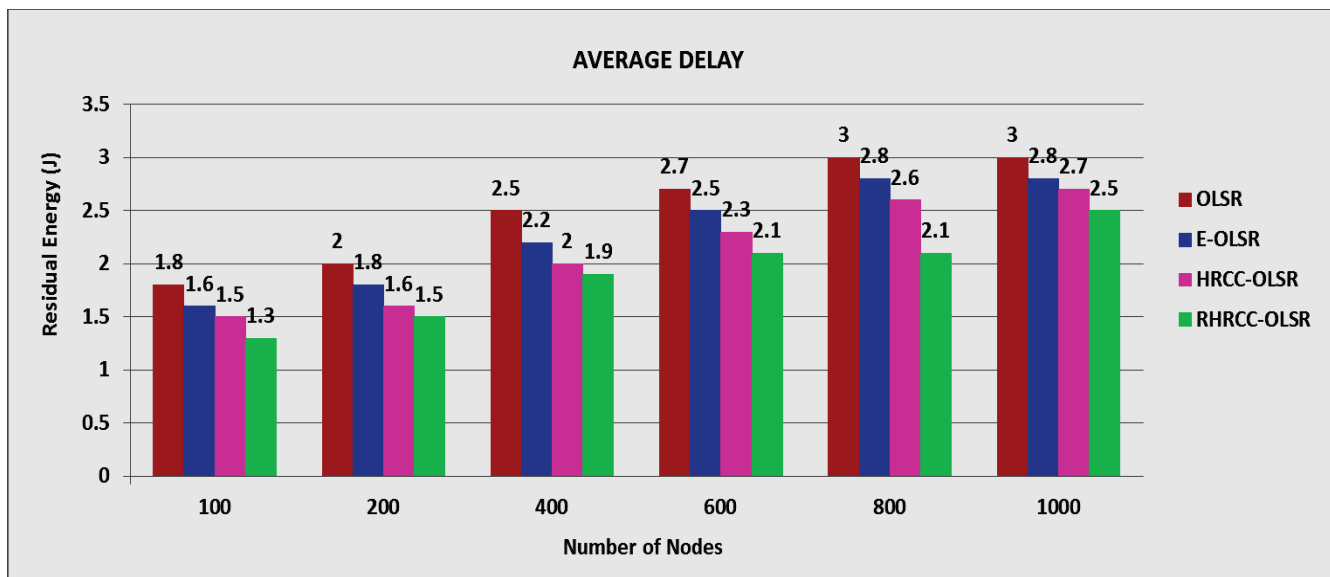


Figure 4. Average Delay of RHRCC-OLSR based on Number of Nodes

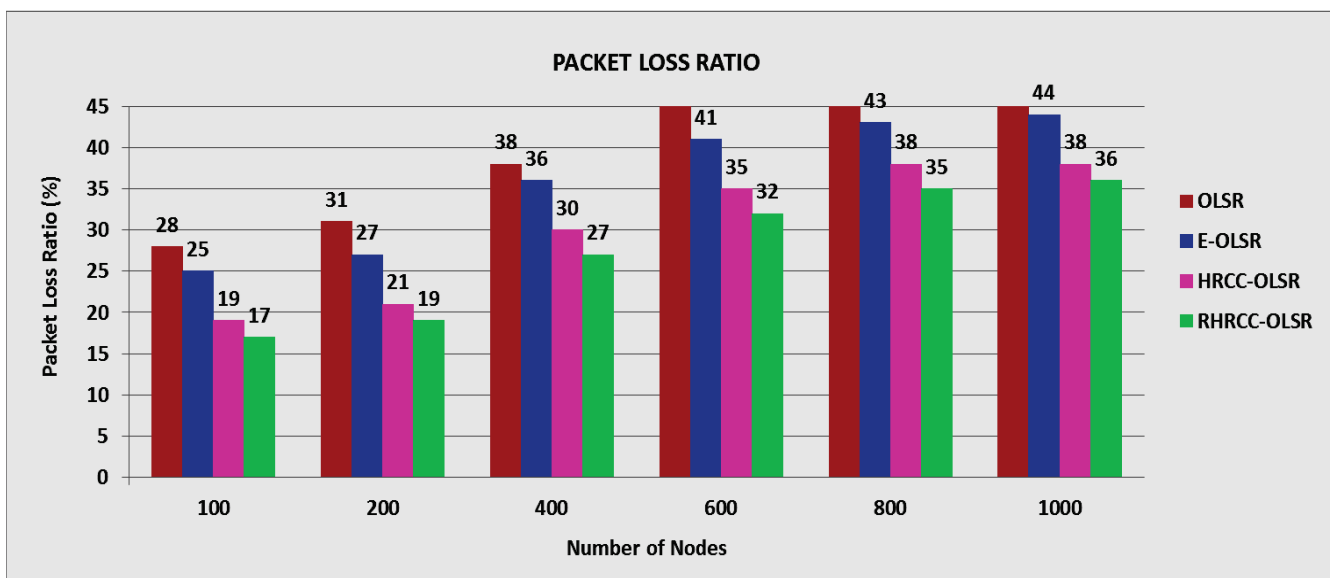


Figure 5. Packet Loss Ratio of RHRCC-OLSR based on Number of Nodes

Similarly, the proposed protocol involves reduced PLR when compared to the standard protocols. It involves 45%, 30% and 10% less PLR when compared to OLSR, E-OLSR and HRAC-OLSR protocols respectively (Figure 5).

The performance of the proposed protocol is also analyzed in terms of routing overhead and compared with standard

protocols. RHRCC-OLSR involves reduced routing overhead as it permits only trusted nodes to be involved in routing, thus dropping the likelihood of performing malevolent activity. OLSR, E-OLSR and HRAC-OLSR protocols involve 32%, 23% and 7% more routing overhead when compared to the proposed protocol (Figure 6).

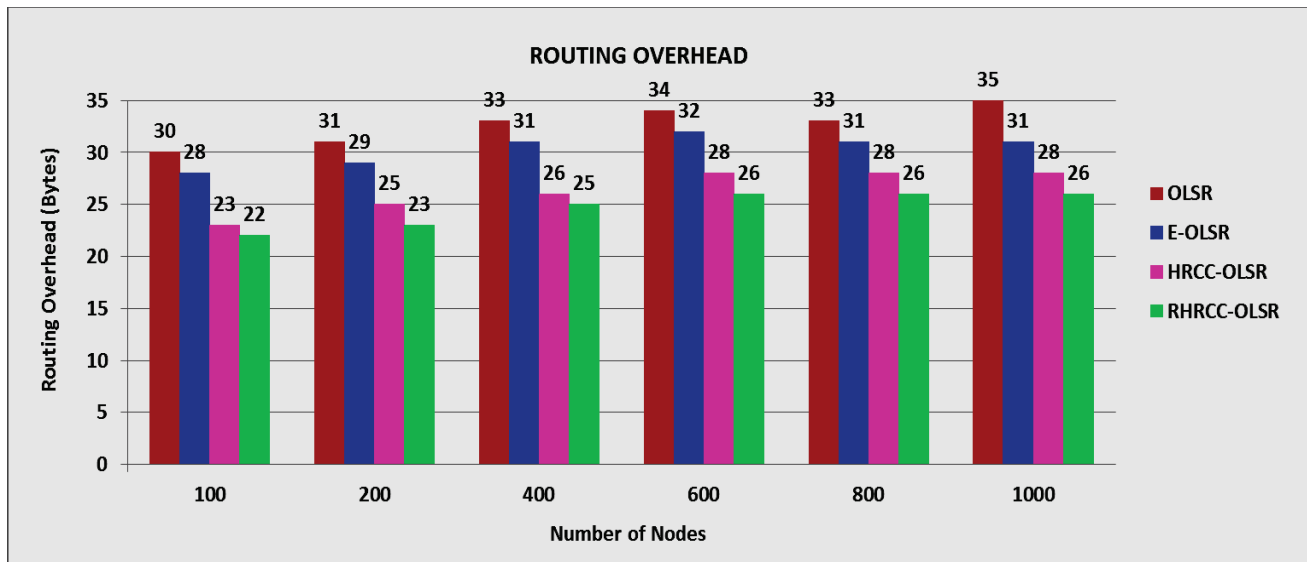


Figure 6. Routing Overhead of RHRCC-OLSR based on Number of Nodes

V. CONCLUSIONS

The Reliable HRCC-OLSR (RHRCC-OLSR) protocol propounded in this paper aids in determining the trustworthiness of mobile nodes in MANET depending on RE, bandwidth and reliability along with the quantity of packets received as well as forwarded. The selfish behavior of nodes is analyzed and TV is computed based on which nodes exhibiting such behavior are removed from the network. Residual Energy (RE)-based detection aids in determining the available energy of nodes. RHRCC-OLSR determines TV based on RE. The nodes with RE and TV below threshold limit are marked as malevolent and are not allowed to take part in routing. Computations based on energy and trust makes the system less susceptible to security attacks. The proposed scheme offers improved PDR and throughput involving reduced average delay, PLR, energy and routing overhead.

REFERENCES

- [1] Sheikh, R., Chande, M. S., & Mishra, D. K. (2010, September). Security issues in MANET: A review. In 7th IEEE International Conference on Wireless and Optical Communications Networks-(WOCN), pp. 1-4.
- [2] Ishrat, Z. (2011). Security issues, challenges & solution in MANET. IJCST, 2(4), 108-112.
- [3] Alani, M. M. (2014, November). MANET security: A survey. In IEEE International Conference on Control System, Computing and Engineering (ICCSCE 2014), pp. 559-564.
- [4] Sharma, S. B., & Chauhan, N. (2015, February). Security issues and their solutions in MANET. In international conference on futuristic trends on computational analysis and knowledge management (ABLAZE), pp. 289-294.
- [5] Gupta, K., & Mittal, P. K. (2017). An overview of security in MANET. International Journals of Advanced Research in Computer Science and Software Engineering ISSN, 7, 2277-3128.
- [6] Roy, D. B., & Chaki, R. (2011). MADSN: mobile agent based detection of selfish node in MANET. International Journal of Wireless & Mobile Networks (IJWMN) Vol, 3, 225-235.
- [7] Padiya, S. A. G. A. R., Pandit, R., & Patel, S. (2013). Survey of innovated techniques to detect selfish nodes in MANET. IJCNWMC, 3(1), 221-230.
- [8] Mittal, S., & Dahiya, S. (2015). Identification technique for all passive selfish node attacks in a mobile network. International Journal, 3(4).
- [9] Ramya, N., & Rathi, S. (2016, January). Detection of selfish Nodes in MANET-a survey. In 3rd International Conference on Advanced Computing and Communication Systems (ICACCS), Vol. 1, pp. 1-6.
- [10] Janakiraman, S., Priya, M., & Jebamalar, A. C. (2021). Integrated context-based mitigation framework for enforcing security against rendezvous point attack in MANETs. Wireless Personal Communications, 119(3), 2147-2163.
- [11] Ghonge, M. M., Jawandhiya, P. M., & Thakare, V. M. (2017, March). Selfish attack detection in mobile Ad hoc networks. In IEEE International Conference on Innovations in Information, Embedded and Communication Systems (ICIIECS), pp. 1-4.
- [12] Janakiraman, S., Deva Priya, M., Aishwaryalakshmi, G., Suganya, T., Sam Peter, S., Karthick, S., & Christy Jeba Malar, A. (2022). Improved Rider Optimization Algorithm-Based Link Aware Fault Detection (IROA-LAFD) Scheme for Securing Mobile Ad Hoc Networks (MANETs). In 3rd EAI International Conference on Big Data Innovation for Sustainable Cognitive Computing, pp. 155-169, Springer, Cham.
- [13] Arboit, G., Crépeau, C., Davis, C. R., & Maheswaran, M. (2008). A localized certificate revocation scheme for mobile ad hoc networks. Ad hoc networks, 6(1), 17-31.
- [14] Li, W., Parker, J., & Joshi, A. (2012). Security through collaboration and trust in MANETs. Mobile Networks and Applications, 17(3), 342-352.
- [15] Eissa, T., Abdul Razak, S., Khokhar, R. H., & Samian, N. (2013). Trust-based routing mechanism in MANET: Design and implementation. Mobile Networks and Applications, 18(5), 666-677.
- [16] Wei, L., Nishiyama, H., Ansari, N., Jie, Y., & Kato, N. (2013). Cluster-based certificate revocation with vindication capability for mobile ad hoc networks. IEEE Transactions on Parallel and Distributed Systems, 24, 239-249.
- [17] Adnane, A., Bidan, C., & de Sousa Júnior, R. T. (2013). Trust-based security for the OLSR routing protocol. Computer Communications, 36(10-11), 1159-1171.

- [18] Shurman, M., Alfawares, M., Al-Mistarihi, M. F., & Darabkh, K. A. (2014, February). A collaborative reputation approach to avoid misbehaving nodes in MANETs. In 11th IEEE International Multi-Conference on Systems, Signals & Devices (SSD14), pp. 1-4.
- [19] Chatterjee, P., Ghosh, U., Sengupta, I., & Ghosh, S. K. (2014). A trust enhanced secure clustering framework for wireless ad hoc networks. *Wireless networks*, 20(7), 1669-1684.
- [20] Abdel-Halim, I. T., Fahmy, H. M. A., & Bahaa-Eldin, A. M. (2015). Agent-based trusted on-demand routing protocol for mobile ad-hoc networks. *Wireless Networks*, 21(2), 467-483.
- [21] Ullah, Z., Khan, M. S., Ahmed, I., Javaid, N., & Khan, M. I. (2016, March). Fuzzy-based trust model for detection of selfish nodes in MANETs. In 30th IEEE international conference on advanced information networking and applications (AINA), pp. 965-972.
- [22] Sengathir, J., & Manoharan, R. (2017). Co-operation enforcing reputation-based detection techniques and frameworks for handling selfish node behaviour in MANETs: A review. *Wireless Personal Communications*, 97(3), 3427-3447.
- [23] Kumar, S., & Dutta, K. (2018). Trust based intrusion detection technique to detect selfish nodes in mobile ad hoc networks. *Wireless Personal Communications*, 101(4), 2029-2052.
- [24] Rama Abirami, K., & Sumithra, M. G. (2019). Evaluation of neighbor credit value based AODV routing algorithms for selfish node behavior detection. *Cluster Computing*, 22(6), 13307-13316.
- [25] Abdelhaq, M., Alsaqour, R., Albrahim, N., Alshehri, M., Alshehri, M., Alserayee, S., ...& Alnajjar, F. (2020). The impact of selfishness attack on mobile ad hoc network. *International Journal of Communication Networks and Information Security*, 12(1), 42-46.
- [26] Deva Priya, M., Christy Jeba Malar, A., Sengathir, J., & Akash, T. (2021). A Skellam Distribution Inspired Trust Factor-Based Selfish Node Detection Technique in MANETs. In *Proceedings of 6th International Conference on Recent Trends in Computing*, pp. 357-368, Springer, Singapore.
- [27] Jim, L. E., Islam, N., & Gregory, M. A. (2022). Enhanced MANET security using artificial immune system based danger theory to detect selfish nodes. *Computers & Security*, 113, 102538.

Augmented Corvus Search Optimization for Image Retrieval in Content Based Images

A. Srinivasa Reddy

Assoc. Professor, CVR College of Engineering/CSIT Department, Hyderabad, India

Email: srinivas.asr@gmail.com

Abstract: One of the most distinctive study areas in the field of Computer applications has been Content-Based Image Retrieval (CBIR). The goal of this research is to increase the recovery presentation of the CBIR framework by combining advanced approaches to predict appropriate centroid in Fuzzy C-Means (FCM). The use of a consolidated approach to predict FCM centroid should reduce complexity and computing time. When compared to existing procedures such as PWO, SSO, and CSO, the results show that combining ACSO with FCM yields better results when compared to challenge procedures.

Index Terms: Corvus Search Optimization, FCM, CSO, SSO, Augmentation.

I. INTRODUCTION

Content-Based Image Retrieval (CBIR) frameworks focus on features from raw images and calculate a secondary measure (comparability or disparity) between an inquiry image and database images using these features [1]. CBIR is a system in which a structure organizes a customer's desire by selecting several images from a potentially huge collection and communicating it either verbally or graphically [2]. There are two types of image recovery processes: those that rely on global highlights (global features) and those that rely on nearby highlights (local features). One of the most difficult aspects of picture recovery, regardless of whether global or local highlights are recovered, is the extraction of the fundamental visual highlights [3]. Component extraction is a crucial operation in CBIR, and the method for isolating highlights from given images determines its effectiveness [4]. Picture properties like as coloring, surface, and shape are represented by element vectors. The similarity of two photographs is determined as a percentage of their element vector differences [5]. CBIR [6] was designed to recover photographs with similar visual components from a query image, which has proven to be a difficult challenge in the field of computer vision and artificial intelligence. In a similar way that the content-based recovery is enlarged, the standard CBIR can be extended by the inventive method. There is no access to content information here, and just visual highlights are used. As content-based recovery performs in multimodal ways, the CBIR finds the important articles. The comment recognizer may arrange explanations and ROIs in the recovered images and using them re-audits the results [1,3]. The recovery of annotated images is dependent on the image metadata or watchwords that link to the visual content or attributes of the image document. Fuzzy C-Means (FCM) is a well-known clustering algorithm that is a standalone learning system that is simple to use and

may retain more data from a dataset than other techniques [4,6]. The enhancement of the centroid in FCM is performed utilizing specific improvement computations and centroid esteems. To overcome the problems caused by employing a single element and improve recovery precision, an image recovery technique is proposed that connects shading, surface, and shape, these three key features.

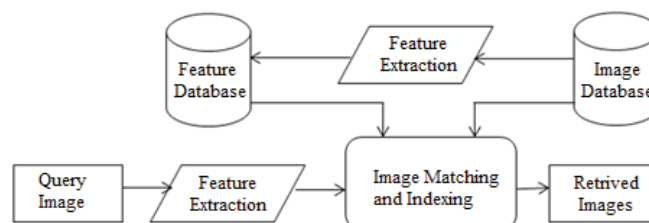


Figure 1. Model of CBIR

II. CONTENT BASED IMAGE RETRIEVAL

The use of computer vision algorithms to the picture recovery problem, i.e., the difficulty of searching enormous databases for digital photographs is known as content-based image recovery (CBIR) [2,3] or query by image content (QBIC). Traditional idea-based methodologies are incompatible with content-based image recovery. The term "content-based" denotes that the investigation focuses on the picture's content rather than its metadata, such as watchwords, labels, or portrayals. Traditional concept-based approaches are in opposition to content-based image retrieval. The problem of searching for digital photographs in huge databases is known as CBIR. Colors, forms, surfaces, and any other information that may be derived from the image are all examples of "content" in this context. Because searches based only on metadata are reliant on the quality and completeness of the explanation, CBIR is intriguing. The term "content-based" refers to a search that looks at a picture's content rather than metadata like keywords, tags, or descriptions. Because searches based entirely on metadata rely on the quality and completeness of annotations, CBIR is excellent.

T. Kato used the term "content-based picture recovery" in 1992 to characterize his experiments with automatic image retrieval from a database. Images are retrieved based on color and shape in the CBIR [2]. Since then, the term CBIR has been used to characterize the technique of leveraging linguistic image attributes to retrieve desired photos from a vast collection. Insights, design recognition, signal preparation, and computer vision are some of the disciplines where techniques, gadgets, and calculations are used.

Because of the limitations of metadata-based systems and the large range of potential applications for effective picture retrieval, interest in CBIR has developed. Existing technology can quickly search textual information about photos; however, this necessitates people manually describing each image in the database. For exceptionally large databases or automatically generated photos, such as those from surveillance cameras, this may be impracticable. It's also possible that photographs with various synonyms in their descriptions will go unnoticed.

Particle swarm optimization (PSO) is one of the bio-inspired algorithms and it is a simple one to search for an optimal solution in the solution space. It is different from other optimization algorithms in such a way that only the objective function is needed and it is not dependent on the gradient or any differential form of the objective. It also has very few hyperparameters.

The Social Spider Optimization (SSO) is a novel swarm algorithm that is based on the cooperative characteristics of the social spider. In SSO, search agents represent a set of spiders which collectively move according to the biological behavior of the colony. In most of SI algorithms, all individuals are modeled considering the same properties and behavior. In contrast, SSO defines two different search agents: male and female. Therefore, according to the gender, everyone is conducted by using a different evolutionary operation which emulates its biological role in the colony. This individual categorization allows reducing critical flaws present in several SI approaches such as incorrect exploration-exploitation balance and premature convergence.

image, which are then separated into different sets. These are the sets describe the surface as well as the location of the surface in the image.

B. Color

Creating a shading histogram for each image that recognizes the number of pixels within the image containing specific values is the first step in registering separation estimates based on shading similitude. One of the most common approaches is to examine images based on the colours they contain, as this can be done independent of the size or orientation of the image. In contrast, Search has sought to split shading extent by area and by the spatial link between a few shade zones.

C. Shape

The term "shape" does not refer to the state of a painting, but rather to the state of a sought-after location. Shapes are usually resolved by first dividing or identifying edges in a picture. Shape channels are used by several ways to recognise different states of a picture. Shape descriptors could also be invariant to interpretation, turn, and scale.

D. Image Retrieval

The terms recall and precision are discussed in image retrieval contexts in terms of a set of retrieved images, a collection of relevant images, which is a list of all photographs on the internet that are relevant for a specific image, and a set of photos gathered by a web search engine for a query.

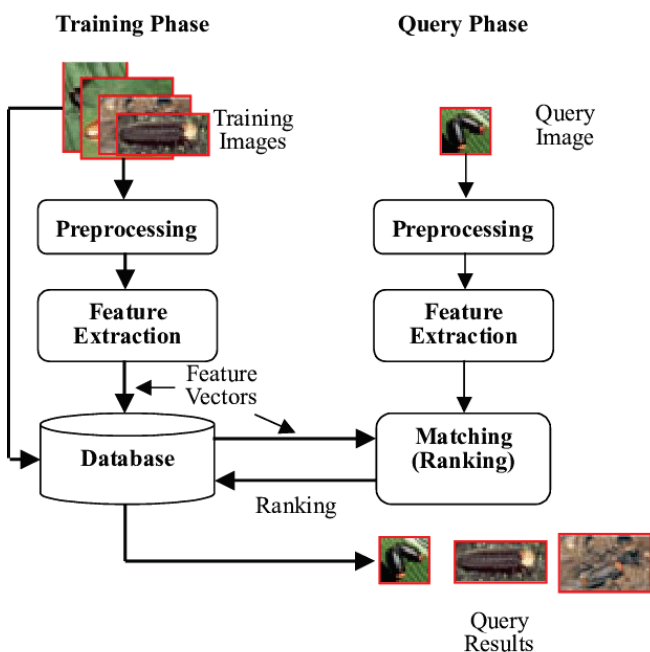


Figure 2. CBIR architecture

A. Texture

Surface estimations look for visual examples in photos and how they are classified geographically. Texel's speak to surfaces, based on how many surfaces are visible in the

Recall

Recall is the percentage of relevant photographs that are successfully recovered.

$$Recall = \frac{|{\{relevant\ images\}} \cap {\{retrieved\ images\}}|}{|{\{relevant\ images\}}|} \quad (1)$$

$$Recall = \frac{TP}{TP + FN} \quad (2)$$

Precision

Precision is the percentage of retrieved photographs that are related to the query.

$$Precision = \frac{|{\{relevant\ images\}} \cap {\{retrieved\ images\}}|}{|{\{retrieved\ images\}}|} \quad (3)$$

$$Precision = \frac{TP}{TP + FP} \quad (4)$$

III. PROPOSED METHODOLOGY

For image recovery, this evaluation includes both text and image attributes (shape, shading, and surface). To achieve the best centroid esteem, the isolated highlights group used Fuzzy C-Means (FCM) in conjunction with advancement

techniques. The CSO, SSO, and PSO streamlining systems are used to predict fitting centroid values. Predicting optimum centroid values for each group using Computation time and complexity are greatly reduced when FCM is used in conjunction with improvement strategies. The highlights of a specific query image contrast with the centroid esteems in testing with the smallest separating groups. For picture recovery, this evaluation includes both text and image attributes (shape, shading, and surface). To achieve the best centroid esteem, the isolated highlights group used Fuzzy C-Means (FCM) in conjunction with advancement techniques. CSO, SSO, and PSO are three streamlining systems that aim to predict appropriate centroid values.

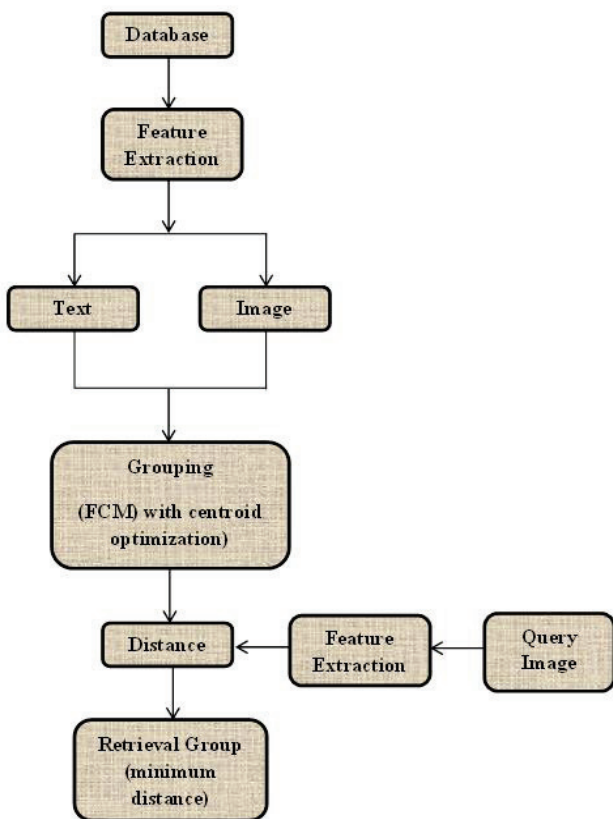


Figure 3. Proposed Methodology

A. Feature Extraction

To recover photographs for a specific database, this function combines text elements such as filename and catchphrases with picture highlights like as surface, shading, and shape if the filename contains a string or other strange characters, it is converted to ASCII code in text highlights and the numbering is preserved. Watchword, on the other hand, denotes the envelope name of related photographs. If a shape is used as a highlight in a photograph, it's possible that identifying the edge is the first step in removing that element. The watchful edge indicator is used to determine the edge of an item in the scene.

After the scene, follow the bunch of the piece edge that has been recognized is a huge advance. The shading histogram can be applied to any shading space, while it is most associated with three-dimensional spaces such as RGB

or HSV. The phrase power histogram can be used to describe monochrome images. The shading histogram is N-dimensional for multi-ghostly images, where each pixel is spoken to by a discretionary number of assessments. Every estimate has its own wavelength range of light, some of which may be visible and others of which may be invisible. GLCM is the best method for extracting the required features from photographs.

B. GLCM

GLCM (Gray Level Co-occurrence Matrix) is a factual surface exploration approach that considers the spatial relationship between pixels in images. GLCM is mostly used in example recognition and determines the power variation at the pixel of interest. The GLCM surface considers the relationship between two pixels at some random minute, referred to as the pixels that serve as a reference and those that are close by. The GLCM set of characteristics can be used to express a general average for the degree of linkage between pixels in distinct edges. such as homogeneity, consistency, and so on.

The partition evacuate between pixels is one of the guiding parameters that influences the isolation capacities of GLCM. When you select detachment 1, you'll be asked to think about the degree of connection between consecutive pixels. In this case, increasing the division causes the level of connection between removed pixels to be reflected. Contrast, correlation, and energy are all terms that can be used to describe something. Homogeneity and entropy are among the GLCM's features.

$$Contrast = \sum_v \sum_u (u - v)^2 * p(u, v) \quad (5)$$

$$Correlation = \sum_v \sum_u \frac{(u - m_u)(v - m_v) * p(u, v)}{\delta_u \delta_v} \quad (6)$$

$$Energy = \sum_v \sum_u (u - v)^2 \quad (7)$$

$$Entropy = - \sum_{u,v} p(u, v) * \log(p(u, v)) \quad (8)$$

$$Homogeneity = \sum_v \sum_u \frac{p(u, v)}{1 + |u - v|} \quad (9)$$

C. Fuzzy C-Means Clustering (FCM)

FCM is an unsupervised clustering-based information bunching process that collects the informative index into n groups, with those untruths near a group's focal point having an abnormal state of having a place and vice versa. It is based on minimizing the desired work.

$$FCM = \sum_{i=1}^n \sum_{j=1}^c (\mu_{ij})^m \|x_i - v_j\|^2 \quad (10)$$

Here $1 \leq m \leq \infty$ and μ_{ij} is the relationship of x_i in the cluster j and $\|x_i - v_j\|$ is Euclidean distance.

D. Corvus Search Optimization

Particle Swarm Optimization, Social Spider Optimization, Harmony Search, Bat Algorithm, and Genetic Algorithms other nature-inspired approaches are among the most recent optimizations. We employ the Corvus or Crow Search Algorithm for optimization when retrieving photos based on content in our proposed methodology.

Crows are a widely distributed class of winged birds that are now considered to be among the most intelligent creatures on the planet. Crows, as a group, display incredible understanding and consistently pass knowledge tests with flying colours. They can keep their faces, use instruments, communicate in complex ways, and hide and retrieve food at all times of the year.

In a crow mob, there will be a behavior that has many similarities to a streamlining operation. According to this behaviour, crows hide their excess food in specified natural locations (hiding sites) and retrieve it when it is needed. Crows are ruthless winged creatures who pursue each other in search of better food supplies. Finding a food supply hidden by a crow isn't easy because if a crow notices another crow following it, the crow will try to fool the other crow by fleeing to a different part of the earth. The nature of sustenance source is objective (health) labour, and the best nutrition wellspring of the earth is the global solution to the issue.

CSO tries to emulate the crows' sophisticated behavior by considering these resemblances to find solutions to challenges.

The CSO Principles are:

- i. Crows live in groups.
- ii. Crows maintain the location of their hiding places.
- iii. A gang of crows is pursuing each other for a break-in.
- iv. By default, crows protect their supplies from theft.

Assume that crow A wants to get to its hiding spot for food, and that crow B wants to follow crow A to find that hiding place at some point in the future. In this scenario, there could be two possibilities.

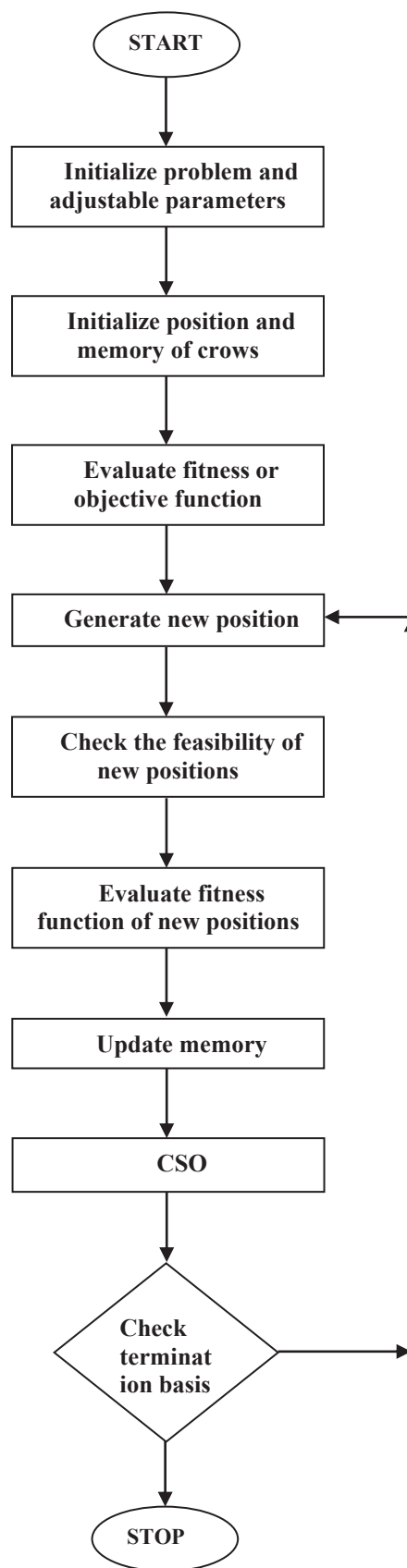


Figure 4: CSO flow chart

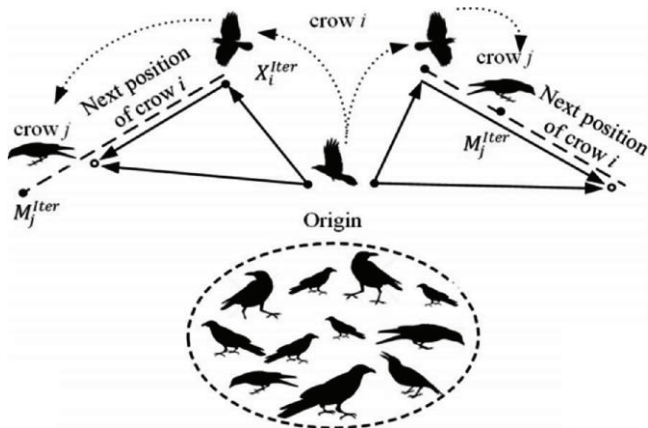


Figure 5. Corvus Optimization Overview


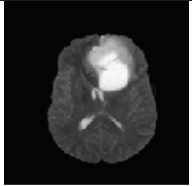
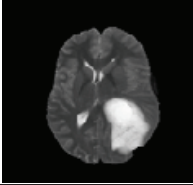
Case-1: Crow A is unaware that crow B is following him. As a result, crow B will approach crow A's hiding spot.

Case-2: Crow A is aware that crow B is pursuing it. As a result, to prevent its cache from being stolen, crow A will deceive crow B by moving to a different part of the search arena.

IV. RESULTS AND DISCUSSION

The purpose of retrieving images for a given question is to compare the results of subsequent tests. The test includes many inquiry images, each with five different photos for approval (table-1), and the display of each question picture is evaluated using three standard estimates Accuracy, Recall, and F-measures for PSO, SSO, and CSO (table-2). The examinations contain the usual execution results of each inquiry picture in the set for various streamlining strategies that function with FCM in predicting ideal centroid. Finally, the below table clearly shows the performance of existing and proposed methods.

TABLE I.
QUERY IMAGES

S. No	Brain & Lung Images
Br1	
Br2	
Br3	

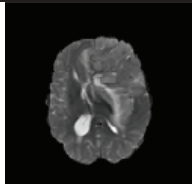
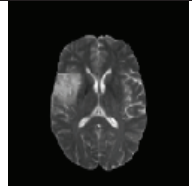

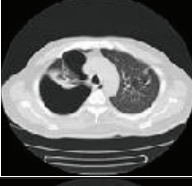



Br4	
Br5	
Ln1	
Ln2	
Ln3	
Ln4	
Ln5	

TABLE II.
PERFORMANCE EVALUATION

Output	Corvus Search Optimization			Social Spider Optimization			Particle Swarm Optimization		
	A	R	F	A	R	F	A	R	F
Ln1	92	88	90	89	90	87	87	87	87
Ln2	90	89	89	88	83	85	85	85	85
Ln3	92	91	91	90	85	87	87	87	87
Ln4	90	89	90	88	83	85	85	85	85
Ln5	92	91	91	89	85	87	87	87	87
Br1	94	93	93	88	86	87	89	87	88
Br2	96	95	94	90	88	87	91	89	90
Br3	94	93	93	88	86	87	89	87	88
Br4	96	95	95	90	88	89	91	89	90
Br5	94	93	93	88	86	87	89	87	88

V. CONCLUSIONS

The preceding data demonstrate that Augmented Corvus Search Optimization outperforms traditional SSO and PSO approaches. We used Brain and Lung photos as input Query images and ran our suggested algorithm on them, comparing Precision, Recall, and F-measures with current mythologies, and then presenting the findings. We can easily see from the results that our recommended method produces superior results. Color photos can be used to test the same procedures.

REFERENCES

- [1] A. Srinivasa Reddy, "Prediction of Brain Tumor Image Segmentation using MRG and GLCM Algorithms", International Journal of Engineering and Advanced Technology, Volume-8 Issue-4, pages:1159-1165, April 2019.
- [2] Guang-Hai Liu, Jing-Yu Yang and ZuoYong Li," Content-based image retrieval using computational visual attention model", Pattern Recognition, pp.1-42, 2013.
- [3] Ferreira, Santos, Torres, Goncalves, Rezende and Weiguo Fan, "Relevance feedback based on genetic programming for image retrieval", Pattern Recognition Letters, Vol.32, No.1, pp.27–37, 2011.
- [4] Srinivasa Reddy A, Chenna Reddy P (2019) A hybrid K-means algorithm improving low-density map based medical image segmentation with density modification. Int J Biomed Eng Technol 31(2):176–192.
- [5] Alireza Askarzadeh, "A novel metaheuristic method for solving constrained engineering optimization problems: Crow search algorithm", Computers and Structures - Elsevier, 169 (2016) 1–12.
- [6] A. S. Reddy and P. C. Reddy, "Novel Algorithm based on Region Growing Method for Better Image Segmentation," IEEE. 2018 3rd International Conference on Communication and Electronics Systems (ICCES), 2018.

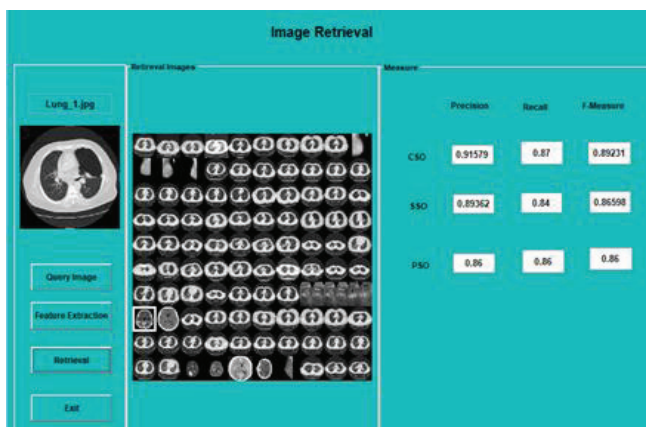


Figure 6: Sample Output

Automatic Aspect-Based Sentiment Analysis for Motor Vehicle Sales Forecasting

C. Raghavendra

Assoc. Professor, CVR College of Engineering/ CSIT Department, Hyderabad, India
Email: drraghavendra@cvr.ac.in

Abstract: For evaluating the vehicle's services and sales, the online review offers a bunch of information. The study looks at how a customer feels about the vehicle, which affects how many cars are sold. The brand image is damaged, and sales are affected when a review is wrong about a car, while positive reviews contribute to increased sales. The sales forecast process considers the online review data and previous sales data as potential sources for more precise sales predictions. Machine learning might speed up the time-consuming process of forecasting sales and understanding market trends. This method makes it easier to find the relevant words in postal correspondence relating to finance, automobile rules, environmental regulations, and customer service. In this study, we used a BERT (Bidirectional Encoder Representation Transformer) to collect consumer reviews of automobiles. The technique is made more visible and understandable by the ML algorithm, which also facilitates the creation and management of such assessments. So, the sales staff will have access to accurate information about the automotive industry, which will help them predict sales.

Index Terms: BERT; Sentiment Analysis; Machine Learning

I. INTRODUCTION

Long-term viability in any manufacturing business is ensured by understanding past performance, current events, and most crucially, anticipating future performance. Forecasting the company's future performance will calculate fortune and demand. Primary sales data must be compiled and reviewed to estimate future sales, fulfill the need, or reduce risk. The discipline of foreseeing the future is called predictive analytics, a subfield of data science. Predictive analysis requires a statistical technique, mathematical procedures, and visualization. We propose a fully automated sentiment analysis model (AABSA) based on these aspects. The model can generate aspect-based sentiment scores from online reviews without human intervention or domain knowledge. We used K-means clustering to group sentence embedding in the AABSA model, then selected the center words from each cluster as aspects.

The choice of a vehicle for a consumer is heavily influenced by its performance, appearance, efficiency, and safety [8]. To expand the brand's client base, the manufacturer must consider the feedback. The sentiment analysis of the brand and product released might help the firm enhance its sales predictions even further [9].

Products, territories, clientele groups, and other relevant information is used to examine prior sales experience. Managers must also look back over a long period to find trends and patterns in the growth and decrease of sales volume [10].

The capability of a company's manufacturing, marketing, funding, leadership, and ability to react to optimize profit potential all affect how well it can respond to sales forecast outcomes. The position of sales in the market is considered

The intention is to apply aspect-based sentiment analysis to comprehend market trends, the state of the country, and brand perception. But first, maintaining the course and manually identifying components for each newly established category and new customer requirements [1].

Businesses find it difficult to derive insights from the vast volumes of unstructured review information regarding their own and rivals' products. A one-dimensional number cannot adequately represent the many facets of a product [2].

To identify word similarities, some subsequent studies used word embedding methods such as word2vec and wordnet clustering [3]. These efforts, however, fall short in capturing the intricate semantic linkages of aspect keywords.

Based on the features of the cars, the review system assigns a rating. The evaluation of the product's effectiveness, the success of the previous vehicle models, safety, performance, and the vehicle's appearance and feel is calculated. For sales forecasting, the exact numbers are employed [4]. Every client considers these essential aspects before purchasing a car; therefore, considering them when predicting sales would result in more accurate predictions.

This work makes several significant and methodological contributions. This paper proposes a hierarchical framework, which makes several substantive and methodological advances. We offer a novel approach to determine product qualities by submitting a hierarchical framework. We demonstrate three comparative benefits of the proposed method over benchmark techniques: 1) greater precision, 2) more accurate sales forecasting and 3) full automation without laborious hand-coding to increase prediction accuracy; this review rating is used to the other sales forecasting characteristics.

II. STATISTICAL APPROACH

Data analysis using statistical approach can provide insight into future business performance. For instance, in work [13], weather-based Machine Learning Technique for Day-Ahead wind power forecasting, wind power is forecasted statistically using historical data. Similarly, the article Intelligent Sales Prediction the Gradient Boost Algorithm, a machine learning technique, anticipates predicting sales turnover [14].

The study [12] demonstrates how businesses generate competitive information using data analytics. The business organization can select the Analytics type based on its requirements and available resources [11].

TABLE I.
CUSTOMER REVIEW DATA ON THEIR VEHICLE

Sl. No.	Review Date	Name	Vehicle Name	Review Title	Review	Rating
1	04/14/08 10:47 PM (PDT)	Thomas	1997 Maruthi Passenger vehicle Minivan All- Trac 3drMin...	Best Minivan ever	My 1997 Passenger vehicle is the third one that I	5
2	11/12/08 05:31 PM (PST)	Susruta	1997 Maruthi Passenger vehicle Minivan All- Trac 3drMin...	My Favorite car Ever	I have owned lots of vans, and the Passenger vehicle is ...	4.8
3	04/14/10 07:43AM (PDT)	Andra	1997 Maruthi Passenger vehicle Minivan 3dr	Mom's Taxi Babies Ride	Sold 86 Maruthi Van 285K miles to be replaced ...	5
4	12/17/16 04:40 PM (PST)	Nitish	1997 Maruthi Passenger vehicle Minivan All- Trac 3drMin...	My 4th Passenger vehicle, the best van ever made!	1st 95 went over 300k before being totaled	5
5	02/02/17 07:53 PM (PST)	Deven	1997 Maruthi Passenger vehicle Minivan	Great Vehicle, Maruthi's best design ever. Thankyou	There is no way back. Enjoy what you have.	5

The Automatic Aspect-Based Sentiment Analysis (AABSA) method was designed to extract hierarchical product attributes from online consumer reviews [5]. Table I. Based on these factors, we provide a completely automated sentiment analysis technique (AABSA). The algorithm can produce aspect-based sentiment scores from web reviews without assistance from a person or specialized knowledge. In the AABSA model, we grouped phrase embeddings using k-means clustering and selected the center words from clusters as attributes [6], [7]. A significant benefit is that since k-means clustering is an unsupervised learning model, we don't need to select the characteristics beforehand manually. Instead, AABSA may automatically identify several elements as well as aspect structures [16].

Furthermore, labels are not required throughout the learning process. As a result, it may independently determine the format of its information. The concept eliminates labeling and automatically allows us to identify aspects.

III. BIDIRECTIONAL ENCODER REPRESENTATION TRANSFORMER (BERT)

BERT is a pretraining approach for language representation to create open-source NLP models that can be downloaded and utilized [15]. These algorithms may be adjusted to deliver state-of-the-art predictions for a

particular profession using your data or to extract top-notch linguistic traits from text data.

The aspect-based sentiment analysis uses the processes listed below to get the sentiment score.

1. Preprocess reviews.
2. Train word embeddings.
3. Train sentence embeddings.
4. Select hypernym candidates.
5. Hyponyms to assist in the subsequent
6. Sentiment analysis.
7. Merge hypernyms and hyponym candidates.
8. Match hypernyms to reviews
9. We use the Maximum Entropy (MaxEnt)

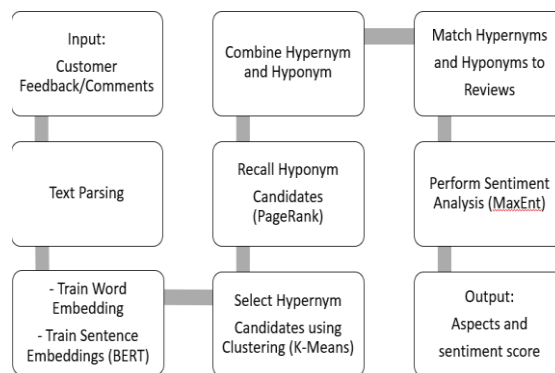


Figure 1. AABSA Framework

A multi-layer bidirectional Transformer encoder is called a BERT. BERT was developed by Google researchers in 2018 and has been shown to be cutting-edge for various natural language processing tasks such as text categorization, text summarization, and text production. Furthermore, a new disclosure claims that BERT plays a substantial role in Google's search algorithm, which helps it better evaluate queries. The study introduces two models, as seen in Figure 2.

BERT base – 12 layers (transformer blocks), 12 attention heads, and 110 million parameters.

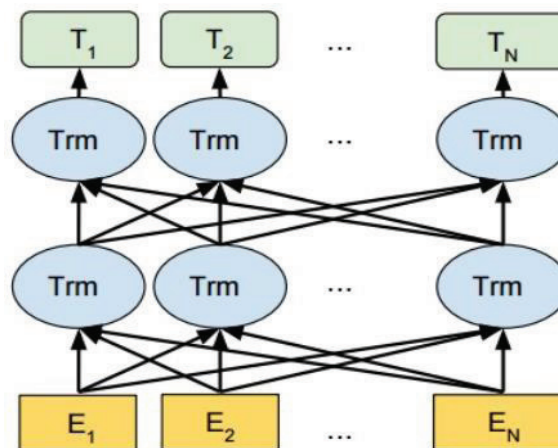


Figure 2. BERT Layers

BERT Large – 24 layers, 16 attention heads, and 340 million parameters.

Position Embeddings: To represent the placement of words in a sentence, BERT learns and uses positional embeddings. These are intended to make up for the fact that, Transformer cannot record "sequence" or "order" information Figure 3.

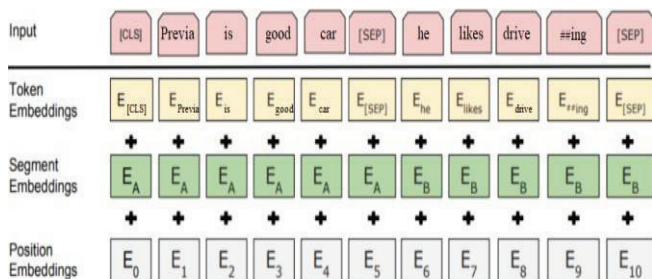


Figure 3. BERT sentiment analysis

Segment Embeddings: BERT can now accept sentence pairs as task inputs (Question-Answering). It learns a unique embedding for each to help the model distinguish between the first and second sentences. All the tokens marked as EA in the above example belong to sentence A.

TABLE II.
DATASET WITH A SENTIMENT SCORE

Month	Year	Brand	Sales	Inflation	Vehicle Sentiment
1	2021	Maruthi	1,36,591	1.10	1
2	2021	Maruthi	1,51,625	1.51	1
3	2021	Maruthi	2,00,801	2.22	1
4	2021	Maruthi	2,01,491	4.43	1
5	2021	Maruthi	2,03,009	5.21	1
6	2021	Maruthi	1,73,609	5.52	1
7	2021	Maruthi	1,54,731	5.61	1
8	2021	Maruthi	1,56,073	5.13	1
9	2021	Maruthi	1,28,495	5.34	1
10	2021	Maruthi	1,19,400	6.13	1
11	2021	Maruthi	1,24,506	6.52	1
12	2021	Maruthi	1,42,591	7.14	1

These are the embeddings for a particular token from the Word Piece token vocabulary that has been learned.

There are a lot of transformer encoders available from BERT. BERT assists with self-attention in both directions and is bidirectional.

The many preprocessing techniques are the source of BERT's adaptability. Thus, we can train the model on various NLP tasks without substantially altering its design Figure 1.

BERT uses WordPress tokenization. The vocabulary first starts with all of the constituent characters of the language, and then the most frequent/likely word combinations are repeatedly added.

TABLE III.
CORRELATION OF INPUT COLUMNS

	Month	Year	Total sales	Inflation	semiconductor Ship shortage	Vehicle Sentiment
Month	1.0	0.0	0.2	0.2	0.0	0.1
Year	0.0	1.0	0.3	0.5	0.6	0.8
Total Sales	0.2	-0.3	1.0	0.2	0.3	0.5
Inflation	0.1	0.5	0.2	1.0	0.8	0.4
Semiconductor Ship shortage	0.0	0.6	0.3	0.8	1.0	0.7
Vehicle Sentiment	0.1	0.7	0.5	0.4	0.7	1.0

Table 3 shows that the cell values with minus signs represent the positive and negative correlation. We can observe that the epidemic has a stronger association with decreased sales. By determining the external factors correlated with the overall sales, we might arrive at a reasonable sales projection.

IV. METHODOLOGY

The prediction model must include the following stages to create a realistic machine learning model to anticipate automobile sales.

1. Find the highly connected variables that affect the vehicle's sales.
2. Three methods are used to build the model: Random Forest, Support Vector Regression, and Multiple Linear Regression.
3. All three models' accuracy and sales are calculated using the Mean squared error approach while building the models.
4. With the sales and affecting factor, the identical procedure was performed, and the accuracy for the three models was determined using the Mean squared error technique.
5. The effectiveness of both approaches is determined by comparing the results.

Along with sentiment analysis, the dataset includes the values of previous sales and elements that may influence future sales—table 2.

$$MSE = \frac{1}{n} \sum_{i=1}^n (Y_i - \hat{Y}_i)^2$$

MSE = Mean Squared Error

n = number of data points

Y_i = Observed values

Ŷ_i = Predicted values

A standard error metric for regression problems is the Mean Squared Error MSE. It is a loss function for algorithms that optimize or fit regression scenarios using the least-squares framework. Reducing the mean squared error between the anticipated and expected values is referred to as "least squares."

The squaring also inflates or amplifies significant errors; the more positive squared errors there are, the more significant the difference between the expected and predicted figures. Models receive a greater "punishment" for more severe mistakes when MSE is used as a loss function. Increasing the average error score when employed as a statistic also has the effect of "punishing" models.

The loss function is computed using the actual and expected values in Table 4. The outcomes of the three algorithms are then contrasted.

TABLE IV.
ACCURACY OF ML MODELS

Algorithm	Accuracy Without Review Factors	Accuracy With the Review Factors
Linear Regression	2500	1800
SVM.SVR	1900	1500
Random Forest Regressor	1600	1200

Table 4 shows that the Model's Accuracy is increased for all three models with the review score. By comparing without review factors and review factors, the loss can be reduced by 72% of Linear Regression, 78.94% of SVM, and 75% of Random Forest Regression.

V. CONCLUSIONS

Using sentiment analysis to make predictions has increased prediction accuracy. The AABSA model improves sales forecasting's thoroughness and accuracy. As aspect identification is automated, it does not require labor-intensive manual coding. To anticipate sales, robust machine learning algorithms are also used.

REFERENCES

- [1] Johnson, R., Zhang, T.: Supervised and semi-supervised text categorization using lstm for region embeddings. arXiv preprint arXiv:1602.02373(2016)
- [2] Nguyen, T.H., Shirai, K.: Phrasernn: Phrase recursive neural network for aspect-based sentiment analysis. In: Proceedings of the 2015 Conference on empirical methods in Natural Language Processing. pp. 2509{2514 (2015)
- [3] Contiki, M., Galanis, D., Papageorgiou, H., Androutsopoulos, I., Manandhar, S., Mohammad, A.S., Al-Ayyoub, M., Zhao, Y., Qin, B., De Clercq, O., et al.: Semeval-2016 task 5: Aspect based sentiment analysis. In: Proceedings of the 10th international workshop on semantic evaluation (SemEval-2016). pp. 19{30 (2016)
- [4] Radford, A., Jozefowicz, R., Sutskever, I.: Learning to generate reviews and discovering sentiment. arXiv preprint arXiv:1704.01444 (2017)
- [5] Timoshenko, A., Hauser, J.R.: Identifying customer needs from user-generated content. Marketing Science 38(1), 1{20 (2019)
- [6] Yang, Z., Dai, Z., Yang, Y., Carbonell, J., Salakhutdinov, R., e, Q.V.: Xlnet: Generalized autoregressive pretraining for language understanding. arXiv preprint arXiv:1906.08237 (2019)
- [7] Cheriyan, S., Ibrahim, S., Mohanan, S., & Treesa, S. (2018, August). Intelligent Sales Prediction Using Machine Learning Techniques. In 2018 International Conference on Computing, Electronics & Communications Engineering (iCCECE) (pp. 53-58).IEEE.
- [8] CyrilForopon, JayanthiRanjan Big Data Analytics in Building the Competitive Intelligence of Organizations, 2020, Elsevier
- [9] Makridakis, S., Spiliotis, E., & Assimakopoulos, V. (2018). Statistical and Machine Learning forecasting methods: Concerns and ways forward. PloS one, 13(3).
- [10] Gurnani, M., Korke, Y., Shah, P., Udmale, S., Sambhe, V., & Bhirud, S. (2017, February). Forecasting of sales by using a fusion of machine learning techniques. In 2017 International Conference on Data Management, Analytics and Innovation (ICDMAI) (pp. 93-101). IEEE.
- [11] Kilimci, Z. H., Akyuz, A. O., Uysal, M., Akyokus, S., Uysal, M. O., Atak Bulbul, B., & Ekemis, M. A. (2019). An improved demand forecasting model using a deep learning approach and proposed decision integration strategy for the supply chain: *complexity*, 2019.
- [12] Zhi-Ping Fan, Yu-Jie Che, Zhen-Yu Chen Product sales forecasting using online reviews and historical sales data: A method combining the Bass model and sentiment analysis.2017 - Elsevier
- [13] Dolara, A., Gandelli, A., Grimaccia, F., Leva, S., & Mussetta, M. (2017, November). Weather-based machine learning technique for Day-Ahead windpower forecasting. In 2017 IEEE 6th international conference on renewable energy research and applications (ICRERA) (pp. 206-209). IEEE.
- [14] Sai, B. K., & Sasikala, T. (2019, April). Predictive Analysis and Modeling of Customer Churn in Telecom using Machine Learning Technique. In 2019 3rd International Conference on Trends in Electronics and Informatics (ICOEI) (pp. 6-11). IEEE.
- [15] Hoang M, Bihorac OA, Routes J. Aspect-based sentiment analysis using best. In Proceedings of the 22nd Nordic Conference on Computational Linguistics 2019 (pp. 187-196).
- [16] Baboota, Rahul, and Harleen Kaur. "Predictive analysis and modeling football results using machine learning approach for English Premier League." International Journal of Forecasting 35.2(2019): 741-755.

Deep Learning Model to Predict the Risk of Developing Diabetic Retinopathy

P. Prathyusha¹ A. Mallareddy² and S.V. Suryanarayana³

¹PG Scholar, CVR College of Engineering/IT Department, Hyderabad, India
Email: prathyu54parakala@gmail.com

²Assoc. Professor, CVR College of Engineering/IT Department, Hyderabad, India
Email: dramallareddy@gmail.com

³Professor, CVR College of Engineering/IT Department, Hyderabad, India
Email: suryahcu@gmail.com

Abstract: Diabetic retinopathy (DR) is a frequent eye disease that causes diabetic patients to go blind due to the damage of retinal blood vessels. Initially it is asymptomatic, but it affects both the eyes and eventually causes partial or complete vision loss if it becomes severe. The most effective strategy to manage the condition is to have regular fundus photography screenings and timely management. The increased number of diabetic patients and their extensive screening needs have sparked interest in a computer-assisted, totally automatic diagnosis of DR. The early detection of DR can save the diabetic people from permanent blindness. The goal is to design a deep-learning system, specifically an Inception-v3 model, that could predict the probability of diabetic retinopathy developing within two years in patients with diabetes. The present work is developed and tested on two versions of a deep-learning system to predict the progression of diabetic retinopathy in diabetic patients who have undergone tele-retinal diabetic retinopathy screening in a primary care environment. A risk categorization technique like this could help to improve screening intervals while lowering costs and increasing vision-related outcomes.

Keywords: Diabetic Retinopathy, Inception-v3, deep learning, Gabor filter, fundus images.

I. INTRODUCTION

The most prevalent cause of blindness in diabetic people is diabetic retinopathy (DR) [1]. According to the World Health Organization (WHO), there were 422 million people with diabetes in 2014, with 35 percent of them developing retinopathy because of damage to the retina's tiny blood vessels [2]. The prevalence of DR is substantially higher in some patient categories. Personalizing screening frequencies based on the possibility of diabetic retinopathy development or progression could improve the efficiency of diabetic retinopathy screening programs. We have developed a deep-learning system that can predict the risk of diabetic retinopathy using colour fundus pictures. Here, mainly our focus is on developing a deep learning machine in order to forecast the upcoming disease in the subsequent years.

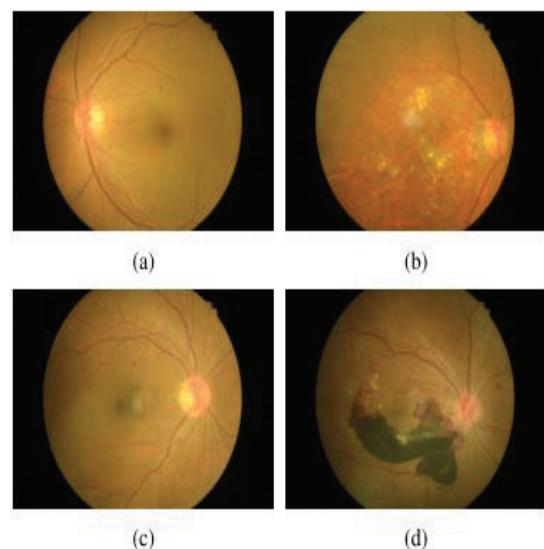


Figure 1. Sample fundus images

Fundus images which can be obtained by capturing the eyes directly are frequently used in clinical practice to diagnose DR. Exudates, microaneurysms, and hemorrhages are some of the most prevalent lesions that indicate DR. Fundus imaging can be used to identify all these lesions [3]. A variety of fundus pictures with distinct types of lesions are shown in figure 1. Fluorescein angiography [4] can be utilized to provide a more accurate diagnosis because it can highlight small vascular structures in the retina. Fluorescein dyes, on the other hand, can provoke an allergic reaction and require working kidneys to expel, thus they are rarely available in small facilities. Currently fundus pictures are the most extensively used method for routine DR screening, due to the ease with which they may give more information and clarity of various lesions. Sample retinal images without diabetic retinopathy and with retinopathy are shown in figure 2(a) and 2(b).

NORMAL RETINA

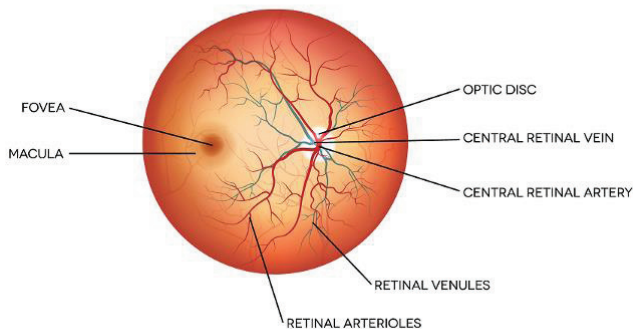


Figure 2(a). Normal Retina without Retinopathy



Figure 3(b). Eye vision with retinopathy

DIABETIC RETINOPATHY

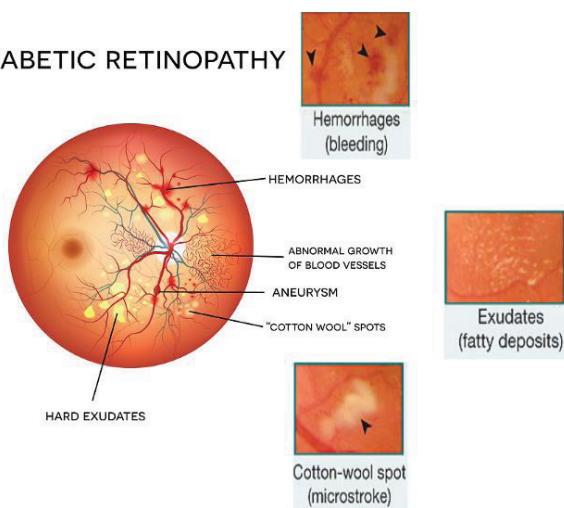


Figure 2(b). Retina with Diabetic Retinopathy

We need to change our lifestyle as it has no correct medication to prevent it. The eye vision images of a person without diabetic retinopathy and with retinopathy are shown in Figure 3(a) and 3(b).



Figure 3(a). Eye vision without retinopathy

II. LITERATURE REVIEW

Deep Learning (DL) is a new advent of Machine Learning (ML) and inherits the appropriate and advantageous attributes of ML such as performing complex tasks, smart and automated, better generalization, domain knowledge, decision making etc. and efficiently applies them upon image data, thereby outperforming shallow ML algorithms. DL models have the capability to learn and to generate new features from extracted and existing features such as points, lines, edges, gradients, vessel structure, corners, boundaries etc. using representation learning.

Colin D. Jones et al. [5] stated in 2012 that they were able to estimate the incidence of diabetic retinopathy in relation to retinopathy grade at first examination and other prognostic factors. Between 1990 and 2006, a dynamic cohort study of 20,686 adults with type 2 diabetes had annual retinal photography up to 14 times. Life tables were used to estimate cumulative and annual incidence rates, and Cox regression analysis was used to identify risk factors for progression.

Convolutional networks [6] are at the heart of most cutting-edge computer vision solutions for a wide range of jobs in 2016. Since 2014, very deep convolutional networks [7] have become popular, resulting in significant improvements in a variety of benchmarks. They are looking into ways to scale up networks that use appropriately factorized convolutions and aggressive regularization to make the extra processing as efficient as possible. They demonstrate significant increases above the state of the art by benchmarking their algorithms against the ILSVRC 2012 classification challenge [8] validation set: For single frame evaluation utilizing a network with a computational cost of 5 billion multiply-adds per inference and less than 25 million parameters, the top-1 error was 21.2 percent and the top-5 error was 5.6 percent.

Gargeya et al. [8] have proposed a data-driven DL algorithm for deep feature extraction and image classification, using Deep Residual Learning (DRL) to develop a CNN for automated DR detection. The model is trained using 75,137 fundus images from EyePACS dataset

and tested using an augmented MESSIDOR-2 dataset and E-Ophtha dataset, containing 1748 and 463 images, respectively. The proposed model has performed preprocessing, dataset augmentation, batch normalization, ReLU activation, and categorical cross entropy loss function for class discrimination using gradient boosting classifiers. The model has extracted 1024 deep features using the convolutional method. The model has detected retinal HEs, hard EXs and NV, through visualization of heatmaps. The proposed model has achieved an AUC of 0.97 with an average sensitivity of 94% and specificity of 98% on EyePACS dataset, whereas it has achieved and AUC of 0.94, with an average sensitivity of 93% and specificity of 87% on MESSIDOR-2 dataset, and an AUC of 0.95 with an average sensitivity of 90% and specificity of 94% on E-Ophtha dataset.

Eftekhari et al. [9] have proposed a Deep Learning Neural Network (DLNN), which is a two-stage training architecture consisting of two completely different structures of CNN namely a basic CNN and a final CNN, for detection of MAs, for the diagnosis of DR. The proposed model has used images acquired from datasets such as Retinopathy Online Challenge (ROC) containing 100 images and E-Ophtha-MA containing 381 images, to train and test the model. This model performs pre-processing and generates a probability map in the basic CNN to detect MAs and non-MAs, which led to a balanced dataset. This model has performed backpropagation for optimization of parameters, post processing upon the output of final CNN, and has used Stochastic Gradient Descent (SGD), Multimedia Tools and Applications dropout and binary cross-entropy loss function for training. The proposed method is assessed on ROC and E-Ophtha-MA datasets, and has achieved a sensitivity of 0.8.

Al-Bander et al. [10] have proposed a multi-sequential DL technique for detecting the centers of OD and fovea, for the detection of DR, using CNNs. The model has used the MESSIDOR database of 1200 images and 10,000 images from the Kaggle dataset, for training and testing respectively. The proposed model has enhanced the contrast of the resized image using CLAHE and has obtained the ROIs using the first CNN and performed classification using the second CNN. The proposed model is trained on augmented data using Stochastic Gradient Descent (SGD).

Mansour et al. [11] have proposed Alex Net-based DR model, which performs a comparative study on DL based feature extraction techniques against ML based feature extraction methods, and classifies the fundus images for the recognition of DR. The proposed methodology has applied a multi-level optimization measure that incorporates data collection from Kaggle dataset, preprocessing, adaptive learning Gaussian Mixture Model (GMM)-based region segmentation, Connected Component Analysis (CCA) based localization and DNN feature extraction. The model has segmented hard EXs, blot intraretinal HEs and MAs.

Deep learning algorithms were utilized in 2019 to identify diabetic retinopathy (DR) with expert-level precision. The goal of this research is to validate one of these algorithms on a large-scale clinical population and compare its performance to that of human graders [12]. A total of 25,326

gradable retinal pictures of diabetic patients were examined for DR severity and referable diabetic macular edoema in Thailand's community-based, countrywide diabetic macular edoema (DME).

The RETINARISK algorithm [13,14] was deployed at a Norwegian ophthalmology clinic in 2020. On a voluntary basis, the diabetes cohort was divided into two groups: one with variable screening intervals based on their specific risk profile, and the other with traditional fixed interval diabetic eye screening. Compliance, clinical results, safety, and cost-effectiveness were assessed between 2014 and 2019, 843 diabetic patients took part in the programme.

III. METHODOLOGY

The main objective of this work is to build a stable and noise compatible system for detection of diabetic retinopathy. This work employs the deep learning methodology for detecting the diabetic retinopathy based on severity level (No DR, Mild, Moderate, Severe and Proliferative DR). Figure 4 shows the proposed methodology. We have used the Inception V3 model to detect the Diabetic Retinopathy.

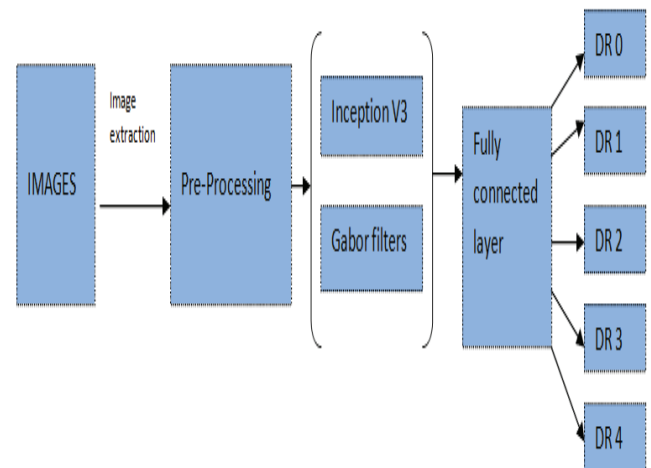


Figure 4. Proposed Methodology

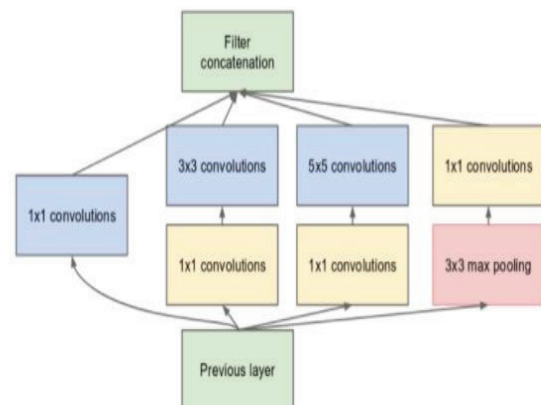


Figure 5. Inception Module with dimension reductions

THE INCEPTION-V3 MODEL:

The initial Inception-V3 model was created for images with a resolution of 299 by 299 pixels. If the input image is blown up too much, the feature maps inside the model will be blown up as well, by reducing the depth of the model. Inception module with dimension reductions is shown in figure 5. The Inception-V3 model can be represented with two parts like feature extraction and classification. In feature extraction it performs the convolutional neural network functions and in classification it works like fully connected activation layer. As it is a pre-trained model, it can classify thousands of images. The Inception-V3 model is sophisticated, so that it gives optimized and highly effective results. The Network structure of Inception-V3 Model is shown in figure 6. The number of deeper layers in Inception-V3 are more the compared with Inception-V1 and Inception-V2. The cost incurred to Inception-V3 is also less.

Inception-V3 architecture can be explained in a sequential manner as follows:

- a) Factorized convolutions
- b) Smaller convolutions
- c) Asymmetric convolutions
- d) Auxiliary classifier
- e) Grid size reduction

Layer Index	Layer Type	Layer Configuration	Data Shape
0	Data	-	(3,299,299)
1	Convolution	(3x3,2x2,32)	(32,149,149)
2	Convolution	(3x3,1x1,32)	(32,147,147)
3	Convolution	(3x3,1x1,64)	(64,147,147)
4	Pooling	(max,3x3,2x2)	(64,73,73)
5	Convolution	(1x1,1x1,80)	(80,73,73)
6	Convolution	(3x3/1x1,192)	(192,71,71)
7	Pooling	(max,3x3,2x2)	(192,35,35)
8	Inception A	-	(256,35,35)
9	Inception A	-	(288,35,35)
10	Inception A	-	(288,35,35)
11	Inception B	-	(768,17,17)
12	Inception C	-	(768,17,17)
13	Inception C	-	(768,17,17)
14	Inception C	-	(768,17,17)
15	Inception C	-	(768,17,17)
16	Inception D	-	(1280,8,8)
17	Inception E	-	(2048,8,8)
18	Inception E	-	(2048,8,8)
19	Pooling	(avg,8x8,1x1)	(2048,1,1)
20	Softmax Output	-	4

Figure 6. Network structure of Inception-V3 Model

MODULES:

- 1) *Upload Diabetes Retinopathy Dataset:* Using this module we will upload dataset training images
- 2) *Preprocess Images:* Using this module we will read all images and then normalize images by converting all pixels values between 0 and 1. Divide each pixel values by 255 will convert image pixel between 0 and 1
- 3) *Train Diabetes Images Using Deep Learning:* Using this module we will train above processed images with Inception-V3 algorithm and the below code shows training image with INCEPTION
- 4) *Upload Test Image & Predict Disease:* After training the model we will upload new test images and then inception model will predict upcoming disease
- 5) *Accuracy & Loss Graph:* Using this module we will plot accuracy graph of deep learning
- 6) *Confusion Matrix:* It is mainly used for the classification of the classes. Confusion Matrix gives the count of correctly predicted classes and the classes which are not correctly predicted in a count format.

IV. DATASET INFORMATION

The Inception-V3 algorithm is trained on the EYEPACS [15] dataset available from the Kaggle repository. The diabetic retinopathy associated with each image has been rated on the scale of 0-4 as follows and fundus images corresponding to all stages are shown in Figure 7.

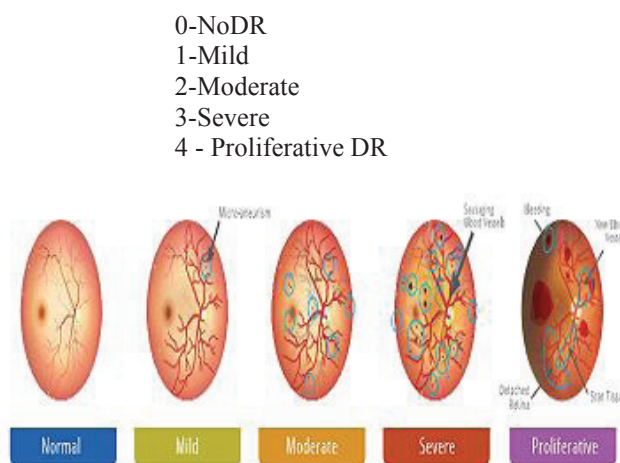


Figure 7. Fundus images at different stages of Diabetic Retinopathy

The Inception-V3 network will be used to develop a deep learning model, which may subsequently be used to new patient retinas to forecast imminent disease or the presence of the worst disease. The presence of red color cells in the photograph will indicate the presence of an upcoming disease.

V. EXPERIMENTAL RESULTS

In the initial stages of retinopathy, there will be no indications of vision related problems. As years pass, they will cause blindness to the patients. It is a symptom in both type 1 and type 2 diabetes. As the blood sugar level increases the level of complications will also increase accordingly. The fundus images that are captured on each eye (one or two images per eye) are handled as a single sample, and we have divided our data into a training set and a test set randomly. The screenshot of the main page of our project is shown in figure 8.

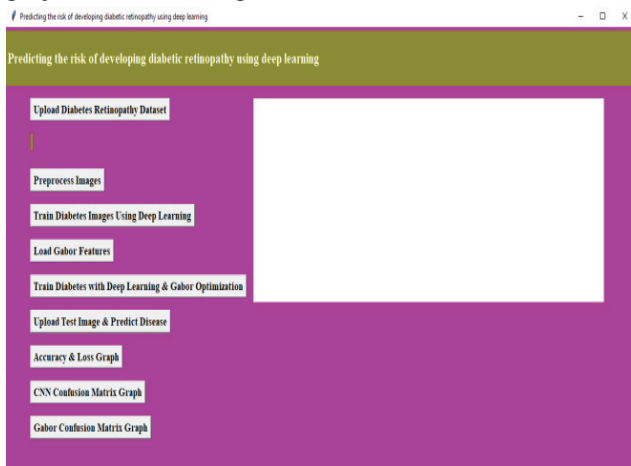


Figure 8. Screenshot of main page of the project

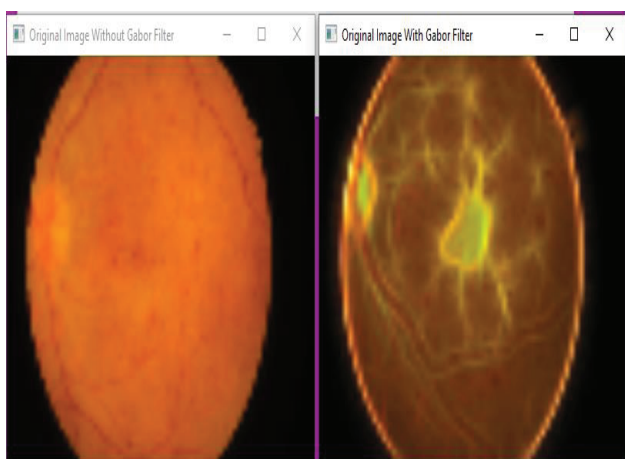


Figure 9. Preprocess images

The Gabor filter is used for finding different textures, edges, and feature extractions and it is found by using a Gaussian kernel function that is modulated by a sinusoidal wave. The filter is able to modulate over an image to extract features on different angles. The Gabor filter is a good candidate filter to be used before or during training. The preprocessed image is shown in Figure 9.

Performance evaluation consists of several standard measurements including accuracy, sensitivity, specificity, and the area under the receiver-operating characteristic curve (AUC of the ROC curve) of the automatic screening for the presence of referable DR.

TABLE I.

COMPARISON OF DIFFERENT DEEP LEARNING MODELS USED FOR DR

Deep Learning Model	Training Accuracy %	Validation Accuracy %
VGG16	77.52	75.67
Inception V3	99.29	76.82
Inception V3 with Gabor filter	99.57	82.94
Mobile Net V1	98.90	76.55
Exception	99.46	75.22

Diabetes Retinopathy using Inception V3 & gabor Inception V3 Accuracy & Loss Comparison Graph

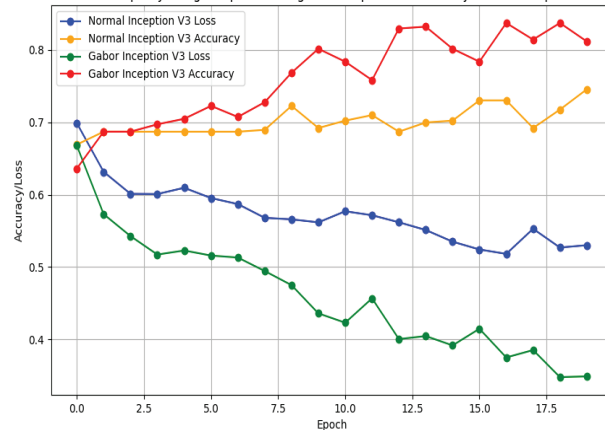


Figure 10. Accuracy & Loss comparison graph

In Table.1 we have represented the performance of different deep learning models used for the prediction of Diabetic Retinopathy. Similarly, in figure10, we have shown the comparison graph between the accuracy and loss of normal Inception v3 model and Inception v3 model with Gabor filter.

VI. CONCLUSIONS

Because of the large number of diabetes patients and the high prevalence of DR among them, there is a high demand for automatic DR diagnosis methods. Numerous accomplishments have been made thus far, with satisfying results in many subproblems such as vessel segmentation and lesion identification. In this work, the extensive experiments show that the Inception v3 model with the Gabor filter significantly improved the accuracy of the model.

However, these findings are based on limited datasets. For the real-world applications, we need to work on a high-dimensional balanced dataset. Finally, in retrospective scenarios, we have evaluated a single randomly selected eye per patient. A patient-level investigation, categorization, preferably in prospective settings, will aid in determining clinical relevance. Our findings shows that a deep-learning system could be built to improve risk stratification for developing diabetic retinopathy.

REFERENCES

- [1] The Royal College of Ophthalmologists. The Royal College of Ophthalmologists diabetic retinopathy guidelines, 2013.
- [2] S. Wang, et al, “hierarchical retinal blood vessel segmentation based on feature and ensemble learning”, *Neurocomputing* (2014), <http://dx.doi.org/10.1016/j.neucom.2014.07.059>.
- [3] Agardh E, Tababat-Khani P. Adopting 3-year screening intervals for sight-threatening retinal vascular lesions in type 2 diabetic subjects without retinopathy. *Diabetes Care*. 2011;34(6):1318–9. <https://doi.org/10.2337/dc10-2308>.
- [4] Ting DSW, Cheung CY-L, Lim G, Tan GSW, Quang ND, Gan A, et al. Development and Validation of a Deep Learning System for Diabetic Retinopathy and Related Eye Diseases Using Retinal Images from Multiethnic Populations with Diabetes. *JAMA*. 2017 Dec 12;318(22):2211–23.
- [5] Colin D. Jones, Richard H. Greenwood, Aseema Misra, Max O. Bachmann, Incidence and Progression of Diabetic Retinopathy During 17 Years of a Population-Based Screening Program in England, *Diabetes Care*, Volume 35, March 2012.
- [6] Szegedy C, Vanhoucke V, Ioffe S, Shlens J, Wojna Z. Rethinking the inception architecture for computer vision. In: *IEEE Conference on computer Vision and pattern recognition*; 2016. p. 2818–26.
- [7] Simonyan K, Zisserman A. Very deep convolutional networks for large-scale image recognition. In: *International Conference on learning representations*; 2015.
- [8] Gargeya R, Leng T (2017) Automated identification of diabetic retinopathy using DL. *Ophthalmology*. 124(7):962–969. <https://doi.org/10.1016/j.ophtha.2017.02.008>
- [9] Eftekhari N, Pourreza HR, Masoudi M, Ghiasi-Shirazi K, Saeedi E (2019) Microaneurysm detection in fundus images using a two-step convolutional neural network. *Biomed Eng Online* 18(1):1–16. <https://doi.org/10.1186/s12938-019-0675-9>
- [10] Al-Bander B., Williams B.M., Al-Nuaimy W., Al-Tae M.A., Pratt H., Zheng Y. Dense fully convolutional segmentation of the optic disc and cup in colour fundus for glaucoma diagnosis. *Symmetry*. 2018;10:87. [oi: 10.3390/sym10040087](https://doi.org/10.3390/sym10040087).
- [11] Mansour RF (2017) Evolutionary computing enriched computer aided diagnosis system for diabetic retinopathy: a survey. *IEEE Rev Biomed Eng* 10:334–349. <https://doi.org/10.1109/RBME.2017.2705064>
- [12] Ruamviboonsuk P, Krause J, Chotcomwongse P, et al. Deep learning versus human graders for classifying diabetic retinopathy severity in a nationwide screening program. *NJP Digital Med* 2019; 2: 25.
- [13] Estil S, Steinarsson AB, Einarsson S, Aspelund T, Stefánsson E. Diabetic eye screening with variable screening intervals based on individual risk factors is safe and effective in ophthalmic practice. *Acta Ophthalmol* 2020; 98: 343–46.
- [14] Scanlon PH, Aldington SJ, Leal J, Luengo-Fernandez R, Oke J, Sivaprasad S, et al. Development of a cost-effectiveness model for optimisation of the screening interval in diabetic retinopathy screening. *Health Technol Assess*. 2015;19(74): 1–116. <https://doi.org/10.3310/hta19740>.
- [15] <https://www.kaggle.com/competitions/diabetic-retinopathy-detection/data>

Limitations of CNN-Model and Enhanced AI-Model for Driver Drowsiness Detection

S. Nikhila¹ and V. Sidda Reddy²

¹PG Scholar, CVR College of Engineering/ IT Department, Hyderabad, India

Email: sistla.nikhila@gmail.com

²Assoc. professor, CVR College of Engineering/ IT Department, Hyderabad, India

Email: siddareddy.v@gmail.com

Abstract: Contemporarily driver drowsiness is one of the major universal facts of road accidents across the globe. Integrating enhanced Information Technology (IT) for instance Neural Network (NN), Computer Vision (CV), and Image Processing (IP), enormously reduce road accidents from drivers' drowsiness while driving. Advanced computer vision technology, artificial neural network, and intelligent cameras dynamically predicate as well as alert the drivers when they are in drowsiness. Drowsiness Detection (DD) has been an important research domain in real-time biomedical and traffic signal applications. Recently various Deep Learning (DL) algorithms implemented to study and diagnose fatigue situations in Electroencephalograms Signals (EEGs). The primary objective proposed in the present article is to study a survey of literature on drivers' drowsiness detection based on driver behavioral measures by using computer vision and artificial neural network algorithms. Furthermore, in this article, traditional drivers' drowsiness architecture models, limitations, challenges, and conventional neural network algorithms have been addressed. As regards to study also addressed the role of enhanced convolution neural networks and limitations in the present and future scenario to detect and alert drivers' drowsiness during driving which leads to reduced road accidents in the future globally.

Keywords: Computer vision, convolutional neural network, drowsiness detection, deep learning, and information technology

I. INTRODUCTION

Due to the extensive efforts of research studies and government organizations over the last three decades, changes in driving conditions and driver safety have been observed. The present study: addressed various major driver drowsiness behavioral measures that cause around 1.3 million population die every year in traffic accidents, as well as another 20 to 50 million, who are being suffered from non-fatal injuries [1]. Fig 1 illustrated various levels of driver drowsiness based on behavioral measures during driving.

Face Symptoms	Output
Eyes Open and no Yawning	Not Drowsy
Eyes Blinking and Yawning	Less Drowsy
Eyes closed over 1.5 seconds	Drowsiness

Figure 1. Levels of Drowsiness

Drowsiness and exhaustion, which occur shortly after high speed and alcoholism, are the contributing factors of traffic injuries in a number of industries, including aviation, the army, and transportation [2]. However, in recent years, Drowsiness Detection (DD) research has piqued people's curiosity [6, 7]. In the present Covid-19 pandemic, when medical equipment is ubiquitous, this is a major problem [8].

Drunken driving is a major cause of road accidents all over the globe, but especially in the USA. According to statistical analysis from the National Highway Traffic Safety Administration (NHTSA), about 90,000 crashes were caused by drowsy driving between 2015 and 2017, with around 4000 persons killed [1]. There are various factors that cause people to fall asleep while driving; one study found that driving for a lengthy period of time produces a loss of self-control as well as a focus [1]. Drowsiness will impair a driver's ability to notice the environment and drive safely. Drivers, on the other hand, will not stop driving even if they fall asleep, according to the majority of them "I will be fine, I can continue driving". According to the National Sleep Foundation (NSF), several earlier indicators of drowsiness, such as frequent blinking, yawning repeatedly, eye closing continually, mouth opening, and/or keeping his/her head up, can alert a motorist to stop and rest [2].

II. RELATED WORKS

Two pruning techniques for artificial neural network structure optimization are discussed in this study [3]. Nonlinear dynamic systems will be modeled using these networks. The accuracy of these algorithms will be tested and compared using real steam turbine data from a thermal power plant. To capture the behavior of a selected real system, four distinct models will be created: a neural network model, an adaptive neuro-fuzzy model, and two optimized neural network models utilizing the Optimal Brain Damage and Optimal Brain Surgeon algorithms.

The prevalence of diabetes in adults aged 20–79 years was estimated at 8.8% in 2015 and is expected to increase to 10.4% by 2040 [4]. Diabetes' high incidence in adults has significant social, economic, and developmental ramifications. Governments are under increasing pressure to establish policies that reduce the risk factors for type II diabetes and gestational diabetes, as well as gestational diabetes, and also to ensure that certain diabetics have adequate access to care. Taking on the global impact of diabetes is a huge undertaking, and the IDF continues to be

a voice for diabetics, by informing individuals and governments about the activities that can be taken to prevent and manage the disease.



Figure 2. Example of Training Data

The topic of the comparison of optimization strategies employing gradient descent, gradient descent with momentum, Adam, and learning rate investigate decay in conjunction with previous optimization techniques for feature extraction utilizing deep neural networks in this article [5]. To correctly recognize the sex of a person caught, this study analyses many settings of these strategies as well as techniques over themselves using a mixture of regularization approaches that vary in their use from no regularization, L2 regularization, and dropouts.

Convolutional networks can be significantly deeper, more accurate, and efficient to train if they feature fewer links between layers near the input as well as those near the output [6]. In this research, the authors embrace this discovery and introduce the Dense Convolutional Network (Dense Net), feed-forward networking in which every layer is connected to any other layer. Our network contains L $(L+1)/2$ direct connections, whereas standard convolutional networks with L layers have L connections—one between each layer and its succeeding layer. All previous layers' feature maps are utilized as inputs into each layer, and their own feature maps are used as inputs into all subsequent layers.

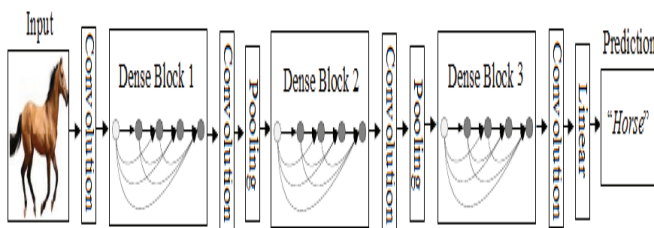


Figure 3. Deep dense-net three Dense Blocks

It's more difficult to train deeper neural networks for image identification using deep residual learning. They propose a residual learning strategy for training significantly deeper networks than previously used networks [7]. They explicitly reformulate the layers as learning residual functions with reference to the layer inputs, rather than learning unreferenced functions. They show extensive empirical evidence that residual networks are easier to tune and can achieve accuracy from greater depth. They look at residual nets on the Image-Net database with a depth of up

to 152 layers, which is 8 layers deeper than VGG nets but still has less complexity. An ensemble of these residual nets scores 3.57 percent error on the Image-Net test set. The ILSVRC 2015 classification task awarded this effort first place. There's also a CIFAR-10 analysis with 100 and 1000 layers. Many visual recognition tasks require a high level of representation depth. They can only achieve a 28 percent relative improvement on the COCO object identification dataset because of their extraordinarily deep representations. Our contributions to the ILSVRC and COCO 2015 contests used deep residual nets as the foundation, and they won first place in the Image-Net detection, Image-Net localization, COCO detection, and COCO segmentation tasks. Rethinking the inception architecture for computer vision, most state-of-the-art computer vision solutions for a wide range of tasks used convolutional networks as their foundation [8]. Since 2014, very deep convolutional networks have become popular, resulting in significant improvements in a variety of benchmarks. Although the increased model size and computational cost typically result in immediate quality gains for most tasks (as long as enough labeled data is provided for the training), computational efficiency and low parameter count are still enabling factors for various use of the cases such as mobile vision and big-data scenarios. They are looking into ways to scale up networks in a way that makes the most of the extra computing by using appropriately factorized convolutions and aggressive regularization.

Deep Face Recognition, Face recognition is done from a single snapshot, or a group of faces tracked in a video is the purpose of this paper [9]. The use of a Convolutional Neural Network (CNN) for end-to-end task learning, as well as the availability of very large-scale training datasets, have both led to recent success in this area. They make two contributions: first, they show how a large dataset (2.6 million photos, over 2.6 thousand people) can be built using a combination of automation and human in the loop, and they analyze the trade-off between data purity and time; second, we walk you through the complexities of deep network training and face recognition to show you how to get equivalent state-of-the-art results on the common LFW and YTF face benchmarks. Deep Face Recognition with Keras, Face recognition has always been a difficult problem for science fiction and science [10]. To hide her identity, a woman colored her hair or wore a hat. To learn, deep learning tasks often expect to be fed several instances of a custom class (e.g. lots of pictures of someone). This is satisfactory for the face recognition problem because training should be done with a limited number of examples — usually, just one shot of a person exists. In addition, introducing new classes should not necessitate re-creating the model.

Driver fatigue detection survey from internal sources [11], the number of traffic accidents occurred every year owing to driver weariness based on Eye Tracking. As a result, a system to identify early driver drowsiness and issue a warning signal may be required to avert many road accidents, as well as to reduce personal suffering and save money. As a result, the authors created a method in which the camera may be mounted in front of the driver's seat for

quick fatigue detection. As a result, if driver fatigue is detected while driving, this system will alert the driver immediately. They used video files collected from cameras in this system, then frames were taken from these video files and the eyes region was tracked to determine the distances between open and closed eyes. When the drivers' closed eyes are detected back-to-back for a few frames, the system determines that the driver is falling asleep and alerts the driver to save their life. According to the system design, the driver images or frames will be extracted from the video file and used to detect facial descriptors using the complexion-based technique on the frames.

Generally, the eyes are placed on the upper half of the face location, so the remaining lower half of the face portion will be removed for easy searching of eyes locations. Later from the top of the face, this system can calculate horizontal averages. The heavy changes in horizontal averages then can detect the eyes in closed or open states. If the eyes are closed for some consecutive frames, this system detects the driver's fatigue then it can generate the warning alarm to alert the driver.

Detecting drowsiness for drivers using a condition-adaptive representations learning approach, we develop a condition-adaptive representations teaching model based on a 3D-deep convolutional neural network for detecting driver sleepiness [12]. The suggested approach is built upon four different models: spatiotemporal representations training, scene state understanding, feature fusion, as well as drowsiness detection. Around the same time, the Spatio-temporal representation modeling collects characteristics that may define motions as well as appearances via video. The scene condition awareness identifies the scene conditions linked to different circumstances regarding the drivers and driving scenario, such as the status of wearing glasses, the lighting condition of driving, and the movements of facial features such as the head, eye, and nose as well as mouth.

Using two features taken from the previous models, feature fusion creates a condition-adaptive representation. Using the condition-adaptive representation, the detection model detects the driver's sleepiness [13]. The condition-adaptive representation educational approach will retrieve extra discriminative characteristics more unique to every scene situation than that of the generic representation, enabling the drowsiness detection approach to provide more accurate results in a variety of driving conditions. The suggested approach is tested using the video dataset NTHU Drowsy Driver Detection.

Various classification EEG signal models have been proposed [14] which are based on the Support Vector Machine (SVM) approach even performance challenges due to background noise. SVM benchmark SVM models predicated fatigues and drowsiness are the primary causes most of traffic accidents. Fatigue detection mainly focuses on the driver's facial behaviors for instance facial expression, eye blinking, and mouth yawning. Open CV and Dlib libraries were utilized to detect the expressions of drivers' faces. Benchmark SVM approaches predicated on five fatigue features such as count of a yawn, internal zone of the mouth opening, count of eye blinking, PERCLOS,

and head are used to detect drowsiness from real-time video. At the same time, facial expressions were trained with SVM. In this study, SVM-based driver fatigue detection is recommended.

Article [15] addressed the hypo-vigilance prediction approach for Unmanned Combat Aerial Vehicle (UCAV) based on EEG signals to reduce the occurrence of hypo-vigilance. Drowsiness Detection and Warning System for Automobile Drivers Using Smartphones. This study describes a smartphone-based method for detecting sleepiness in car drivers. The suggested system detects sleepiness in three stages. The first step employs a modified eye state classification algorithm to calculate the percentage of eyelid closure (PERCLOS) from pictures acquired by the front camera. During nighttime driving, the technology illuminates the driver's face with near-infrared lights. In the case that PERCLOS exceeds the threshold, the second step uses the voiced to unvoiced ratio derived from the microphone's speech data.

A final verification stage uses a touch response within a predetermined time frame to declare the driver sleepy and raise an alert. The gadget keeps a log file of the metric's periodic occurrences, together with the accompanying GPS locations. The technology outperforms previous sleepiness detection methods in three ways. For starters, the three-stage verification procedure increases the system's reliability. The second benefit is that it is implemented on an Android smartphone, which is more easily available to most drivers or taxi owners than other general-purpose embedded platforms. The third benefit is the usage of SMS service to notify both the control room and the passengers.

III. DROWSINESS DETECTION SYSTEM

The general architecture of driver drowsiness detection is shown in Figure 4. Various EEG and ECG face detection techniques were employed in the Facial Detection phase to identify the face regions from the input photos. The research study [16] proposed an EEG-based approach that explored Hypo-vigilance real-time approach to predicate drowsiness, fatigued state, and alertness in biomedical applications. The ECG-based model [17] addressed non-invasive signals that analyze Heart Rate Variability (HRV) and applied filters to the ECG data to extract 13 statistical features. Extracted features trained by classification models SVM, KNN, and Ensemble to predicate driver fatigues state.

Face detection algorithms are divided into two categories: feature-based and image-based. Image-based algorithms for face detection have used statistical, neural network, and linear subspace methods. Different eye area detection techniques were employed in the second stage to detect and extract the eye region from facial photographs. After finding face regions, normalization is performed in the preprocessing stage to reduce the impacts of illumination.

Histogram equalization can be used to adjust the contrast discrepancies between face photographs. Feature extraction was applied to the input ocular region images in the third stage. The fourth phase in detecting driver's drowsiness is a classification, which employs a classifier to divide, using the characteristics obtained in the preceding two steps, divide pictures into asleep and non-sleeping groups.

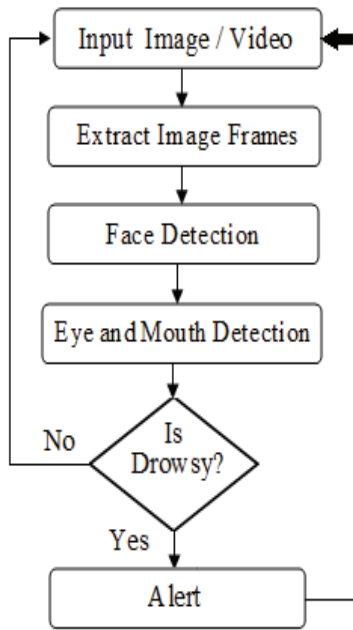


Figure 4. General Architecture of Drowsiness Detection.

IV. DATASET SELECTION

Many datasets have been used in various articles, although the majority of them are not public or realistic. As a result, each study used a distinct dataset to tackle the drowsiness detection problem. Unfortunately, the lack of a uniform dataset makes comparing different algorithms impossible. Several techniques, such as the ULG Multimodality Drowsiness (DROZY) database, achieve high validation accuracy of 91.6 percent and 95.8% by utilizing private datasets; others use public datasets, although they are unrealistic and lack sufficient training samples addressed in [18],[19].

V. CNN MODEL

Driver’s drowsiness also cited sleepiness and fatigue which cause physical and mental tiredness [20]. The CNN model explores eye state categorization and drowsiness level detection in real-time video based on eye and mouth symptoms. Figure 5 depicts the system workflow and the drowsiness detection mechanism. The overview of the offline learning process is the initial stage in the system workflow. This stage summarizes the processes involved in the CNN training process for classifying open and closed eyes. Following the offline training, the online operation process can recognize the eye and mouth states in real-time video. As a result, symptoms from these states are used to predict the level of drowsiness.

From the input image, the convolutional layer will extract valuable characteristics. To increase the non-linear characteristics in each image, each convolutional layer is coupled to RELU activation. Then, it’s not only to maintain the primary features but also to reduce the size of the photos, a max-pooling layer is applied. This aids the CNN model in reducing the quantity of irrelevant data while identifying the eye states.

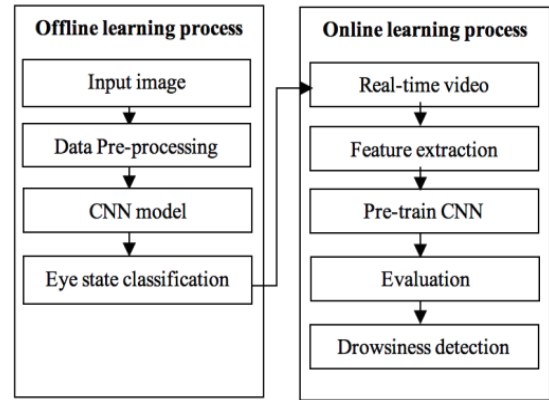


Figure 5. CNN Workflow.

VI. THE CNN BASED DROWSINESS DETECTION SYSTEM

ALGORITHM STEPS:

- (1) The Viola-jones face detection algorithm is utilized to recognize the faces in the photos, which is then passed on to the Viola-jones eye detection algorithm as input
- (2) Once the face has been recognized, the Viola-jones iris recognition approach is utilized to extract the eye area from the face pictures, which is subsequently supplied as input to CNN.
- (3) Deep features are extracted using a CNN with four convolutional layers, which are then sent to a fully connected layer.
- (4) In CNN, the SoftMax layer classifies the pictures as sleepy or non-sleepy.

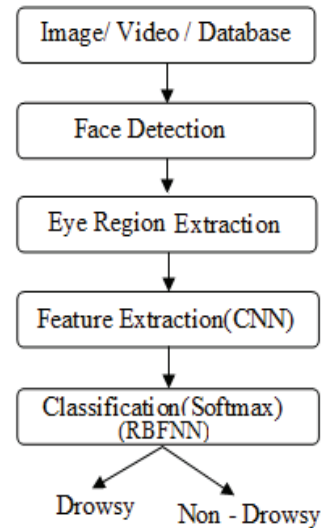


Figure 6. Drowsiness Architecture

VII. DISCUSSION

Despite strong results, when a neural network is tested on a completely new person who was not included in the dataset, it struggles to detect drowsiness in a person's facial expression, implying that the person is awake the majority of the time. A useful gesture that is recognized by others is a small head droop. On the other hand, all films of captured subjects, including those produced afterward were effectively recognized.

VIII. CONCLUSIONS

This study indicates that in order to develop an application that could assist drivers in identifying, they were able to create a design that fits virtually flawlessly for varied frames despite their mental state of sleepiness. A network must be retrained for each new person in order to achieve acceptable outcomes for the subject. This article identified the limitations of CNN models and suggested an enhanced AI model for driver drowsiness detection. In the future, it must be necessary to enhance robust AI models to predicate and alert driver fatigues to reduce road accidents.

REFERENCES

- [1] Sahayadhas, A.; Sundaraj, K.; Murugappan, M.; Palaniappan, R. Physiological Signal based Detection of Driver Hypovigilance using Higher-Order Spectra. *Expert Syst. Appl.* 2015, 42, 8669–8677. [CrossRef]
- [2] Ghandour, A.; Hammoud, H.; Al-Hajj, S. Analyzing Factors Associated with Fatal Road Crashes: A Machine Learning Approach. *Int. J. Environ. Res. Public Health* 2020, 17, 4111. [CrossRef] [PubMed]
- [3] J. Cigánek and J. Osuský, "Structure optimization of artificial neural networks using pruning methods," 2018 *Cybernetics & Informatics (K&I)*, 2018, pp. 1-6, doi: 10.1109/CYBERI.2018.8337554.
- [4] Krizhevsky Alex, Sutskever Ilya, and Geoffrey E. Hinton, "ImageNet Classification with Deep Convolutional Neural Network", *Advances in Neural Information Processing System* 25, 2012.
- [5] Kepesiova, Z., Cigánek, J., Kozak, S.: Driver drowsiness detection using convolutional neural networks. In: 2020 *Cybernetics & Informatics (K&I)* (2020).
- [6] Gao Huang, Zhuang Liu, Laurens van der Maaten, Kilian Q. Weinberger; *Proceedings of the IEEE Conference on Computer Vision and Pattern Recognition (CVPR)*, 2017, pp. 4700-4708
- [7] Murugan, S.; Selvaraj, J.; Sahayadhas, A. Driver Hypovigilance Detection for Safe Driving using Infrared Camera. In *Proceedings of the Fifth International Conference on Inventive Computation Technologies (ICICT)*, Tamilnadu, India, 26–28 February 2020; pp. 413–418.
- [8] Chaari, L.; Golubnitschaja, O. Covid-19 pandemic by the "real-time" monitoring: The Tunisian case and lessons for global epidemics in the context of 3 PM strategies. *EPMA J.* 2020, 11, 133–138. [CrossRef]
- [9] Gwak, J.; Hirao, A.; Shino, M. An Investigation of Early Detection of Driver Drowsiness Using Ensemble Machine Learning Based on Hybrid Sensing. *Appl. Sci.* 2020, 10, 2890. [CrossRef]
- [10] Houssaini, A.; Sabri, A.; Qjidaa, H.; Aarab, A. Real-Time Driver's Hypovigilance Detection using Facial Landmarks. In *Proceedings of the International Conference on Wireless Technologies, Embedded and Intelligent Systems (WITS)*, Fez, Morocco, 30 May 2019; pp. 1–4.
- [11] M. S. Devi and P. R. Bajaj, "Driver Fatigue Detection Based on Eye Tracking," 2008 *First International Conference on Emerging Trends in Engineering and Technology*, 2008, pp. 649-652, doi: 10.1109/ICETET.2008.17.
- [12] Thomas, L.; Gast, C.; Grube, R.; Craig, K. Fatigue Detection in Commercial Flight Operations: Results Using Physiological Measures. *Procedia Manuf.* 2015, 3, 2357–2364. [CrossRef]
- [13] Neri, D.; Shappell, S.; DeJohn, C. Simulated Sustained Flight Operations and Performance, Part 1: Effects of Fatigue. *Mil. Psychol.* 1992, 4, 137–155. [CrossRef]
- [14] Hu, J.; Wang, P. Noise Robustness Analysis of Performance for EEG-Based Driver Fatigue Detection Using Different Entropy Feature Sets. *Entropy* 2017, 19, 385.
- [15] Choi, Y.; Kwon, N.; Lee, S.; Shin, Y.; Ryo, C.; Park, J.; Shin, D. Hypovigilance Detection for UCAV Operators Based on a Hidden Markov Model. *Comput. Math. Methods Med.* 2014, 2014, 567–645. [CrossRef]
- [16] Boudaya, A.; Bouaziz, B.; Chaabene, S.; Chaari, L.; Ammar, A.; Hökelmann, A. EEG-Based Hypo-vigilance Detection Using Convolutional Neural Network. In *Proceedings of the International Conference on Smart Living and Public Health (ICOST)*, Hammamet, Tunisia, 24–26 June 2020; pp. 69–78.
- [17] Stanley, P.; Prahash, T.; Lal, S.; Daniel, P. Embedded based drowsiness detection using EEG signals. In *Proceedings of the IEEE International Conference on Power, Control, Signals and Instrumentation Engineering (ICPCSI)*, Chennai, India, 21–22 September 2017; pp. 2596–2600.
- [18] Murugan, S.; Selvaraj, J.; Sahayadhas, A. Detection and analysis: Driver state with electrocardiogram (ECG). *Phys. Eng. Sci. Med.* 2020, 43. [CrossRef]
- [19] Zhang, L.; Liu, F.; Tang, J. Real-Time System for Driver Fatigue Detection by RGB-D Camera. *Assoc. Comput. Mach.* 2015, 6. [CrossRef]
- [20] Dinges, D. An overview of drowsiness and accidents. *J. Sleep Res.* 1995, 4, 4–14. [CrossRef]

Classification of COVID-19 and Pneumonia from Chest X-ray Images using Deep Learning Techniques

Talapaneni Jyothi¹ and Bipin Bihari Jayasingh²

¹ PG Scholar, CVR College of Engineering/IT Department, Hyderabad, India
Email: 20b81db007@cvr.ac.in

² Professor, CVR College of Engineering/IT Department, Hyderabad, India
Email: bipinbjayasingh@cvr.ac.in

Abstract: A Covid-19 diagnosis utilizing nasopharyngeal swabs and RT-PCR has a low positive rate. Chest X-rays are crucial for early diagnosis of COVID-19, normal and pneumonia. Its symptoms differed from the common cold, influenza, and healthy people. COVID-19 is a major hazard to global health. The diseases are detected through the chest x-ray image dataset by using image classification for deep learning techniques. The image classification for deep learning techniques recognizes the image data and generates the categorized output. As deep neural networks perform the most essential aspect of medical image recognition, pre-processing of the raw image, which are converted into an understandable format by models are required. The models trained for this research include pre-trained CNN models such as VGG, Xception and Dense Net versions. The proposed model's performance validation is summarised in terms of accuracy, precision, recall, F1 score and AUC values that can aid in early diagnosis and differentiate COVID-19 from other kinds of pneumonia when all the deep learning classifiers and performance parameters were considered, the DenseNet121 achieved the highest model classification of accuracy for COVID-19 at 100%, the Xception of the normal class achieved 95.49% and the DenseNet201 achieved the highest for the viral pneumonia class at 97.14%. Additionally, the suggested method is useful and aids medical professionals in recognizing disorders from chest X-ray images. Even though our architectures are easier to use, the performance of the classifiers is used to prove that the therapies are effective and efficient.

Index Terms: COVID-19, Pneumonia, CNN, Deep Learning Techniques, chest X-Ray Images, classification.

I. INTRODUCTION

Image classification involves examining a picture and figuring out which "category" it fits into. This resembles a human version of a virtual machine. Despite of being a straightforward process, classifying photos has proven challenging for computers. A classification system is built, utilizing a database of established trends to identify which group the detected image belongs to. The classification phase involves processing digital data, extracting features, gathering training sets, making decisions, and analysing the outcomes. The virtual camera or another X-ray imaging technology produces digital data to record images. The photos are improved by pre-processing. The matched grayscale picture in

binary compression format is resized by a normalized augmentation of the comparison image in binary format. Feature extraction is the process of measuring, computing, or recognizing features in sample images to extract them. The two better typical methods of extracting features are feature extraction in space and feature extraction in colour. The feature that the best describes the sequence is chosen to serve as the basis for choosing the training data. The input image turns into the output image a week after pre-processing. By contrasting image patterns with attack patterns to determine the most effective tactic, photos are selected and categorized to be assigned to predetermined sets of classes. An outcome will be categorised by using the sample image.

In 2019 Hubei, China detected SARS-CoV-2. Each mammal has a coronavirus. Mammalian viruses are safe. These viruses affected how they spread from animals to people. COVID-19, SARS-CoV-2, entered the body through the nostrils. Coronavirus spreads through touch, handshakes, and face-touching. This makes healthy individuals become sick then 80% of people are acquired mild COVID-19, but this may change. Symptoms vary. In rare situations, the 5-day illness is fatal. At 3 months, SARS-CoV-2 reinfection is possible. Omicron grew rapidly after being discovered in 2021. High-dose vaccines prevent severe disease. COVID-19 causes fever, chills, and breathlessness. Migraines cause headaches, nausea, and odour/taste loss. Rare Symptoms Examine COVID-19. Saliva, nose, or throat swabs can be used to alter test results. If you have COVID-19 and know someone with the virus, evaluate them. COVID-19's side effects demand self-isolation. Follow your doctor's test-and-separation recommendations. If you have a weak immune system or a serious disease, stay home. I recommend day 5 labs. Test availability determines containment length. Expiring MMRs must wait 5 days. False-negative COVID-19 test results may signal that you have the virus, but the test missed SARS-CoV-2. fewer mistakes depending on prognosis, monoclonal injections may help some COVID-19 patients. Antifungal or immunotherapeutic drugs aren't indicated outside the clinic. Medicines reduce infection risk, but not entirely. Even though no vaccination is 100% accurate, outbreaks were estimated as SARS-CoV-2 caused less damage. COVID-19 should clear up in a week.

Pneumonia is caused by bacteria in one or both lungs. About 30 types of pneumonia have various causes. Common ones are bacterial, viral and mycoplasma. TB impacts everyone. Following training is willing: People 65 and older, with major health conditions, and smokers are "seniors." Most of the lung disease patients cough crimson, green, and yellow sputum. Chills, dyspnea, weakness, and weariness are symptoms. A medical record and physical exam identify pneumonia. Blood, sputum, and lungs are tested. Like viruses and bacteria, antibiotics must help many people in the UK and throughout the world get healthy quickly. Most of the viral pneumonia recover without medical intervention. A balanced diet, lots of fluids, enjoyment, inhalers, suffering, sneezing, and flu medications are all remedies. Most kids and teens at risk for pneumococcal bacteria should get vaccinated. Most of the lung disease patients respond to treatment, but those who don't may have complications. You're more critical if you're unwell or have a weakened immune system. Risks include acute respiratory syndrome, chest irritation, and septicemia. Pneumonia strikes anybody, anytime. Children over 2 and seniors over 65 are at-risk. Heart surgery, emergency surgery, ECMO, viruses, breathing Healthcare examines lungs.

A chest X-ray is an imaging procedure that employs X-rays to examine the organs and structures in your chest. It may assist your doctor in determining how well your lungs are working in certain medical disorders that can create abnormalities in the lungs. Certain illnesses can produce anatomical changes in the lungs.

This paper is further comprised as follows: section II is related work, section III elaborates upon the methodology used for the following workflow, Section IV elaborates on the model process, Section V shows the proposed work observations, section VI explores the future goals and section VII deals with the conclusion for better analysis, and classification of viral pneumonia, normal and COVID-19 diseases via CXR images.

II. RELATED WORK

At the end of 2019, China witnessed a COVID-19 pandemic [1]. Medical experts investigated the illness's symptoms, including fever, cough, myalgia, and weariness. Uncommon are permanent diseases. Influenza causes chest discomfort. COVID-19 transmits through particles or aerosols when a patient coughs, talks, or sneezes. COVID-19 differs. It spreads fast and is dangerous when variants breed freaks. Results show abnormalities grow in severity. Fast computing advancements have resulted in the widespread use of digital image processing in medicine, including image segmentation and augmentation. Medical image processing uses Deep Learning technologies like Convolutional Neural Networks [2]. Deep learning models improve forecasting, testing, and categorising.

Sohaib Asif et al. [3] aimed to detect COVID-19 pneumonia patients digitally using X-ray images. This deep learning model identifies COVID-19's special effects, increasing categorization. 864 COVID-19, pneumonia, and normal X-rays. The data was pre-processed and enhanced, even though the system was built on massive data. M.Qjidaa et al. [4] created a clinical decision-support system to detect COVID-19

from chest X-rays. Open sources provided COVID-19, pneumonia, and normal X-rays. 30% of the three-class collection was analysed. Data from two streams were inappropriately obtained and highly processed.

Khasawneh et al. identified CNN's chest X-rays. The first photos were taken at Jordan's King Abdullah University Hospital. 63.15 years old. 31-month-old to 96-year-old. Clinics destroy. After system training and testing, data stores were employed for evaluation. Eventually, CNN, Mobile Nets, and VGG-16 models are used. Model's overfitting photographs and generalised additional details. Pooled data revealed 98.7% detection performance, while maximal techniques were somewhat less effective. COVID-19 was identified by Haiti et al. [6]. -Ray dataset images are reduced to 6400 by 80 x 80. Photo resizing and vectorizing. Reduce inequality by using 135 normal and 135 COVID-19-positive patient images. COVID-19 includes 135 drug-induced blood clots, 135 normal people, and 135 intensive-treatment patients. T2-weighted MRIs are diagnostic. 80x80 MRIs. 1:6400 image vectors X-ray-focused. Categorization strategies failed on all three datasets. The prototype compared DL and ML algorithms.

Alhwaiti, Y. et.al. [7] recommended deep learning to identify coronavirus x-rays. Since COVID-19 was released in December 2019, there was no public science dataset. The hospitals must share multiple data sources. CNN classifier, Google Net, ResNet18, and ResNet50 are pre-trained models. Also, grid search. This approach is global. CNN's training was changed. ILR, L2 regularisation, momentum, and minibatch size are coming. Precision, accuracy, sensitivity, and F1-score are estimated. Using various performance indicators, the prototype's ability to predict COVID-19 occurrences from records was objectively evaluated. GS and ResNet50 prototypes made breakthroughs. COVID-19 and CNN were created by Abiyev et al. Input image processing procedures include normal pneumonia and X-ray image database analysis, image splitting into training, validation, and testing sets, size, feature extraction, and information resampling. Comparing the newest responses to the target classes yields the error rate. The error function and learning algorithm later affect CNN signals. Images are categorised as upcoming, scaling down, feature extraction, and picture restoration. The intended modelling is a fraction of the network model that identifies if X-rays reveal COVID-19, pneumonia, or a normal case. The learning algorithm refreshes CNN's models.

Umar Ibrahim et al. [9] developed assays for viral chest infections and COVID-19. The collection contains 5856 positive and negative X-rays. 1-5-year-olds with various health issues are involved. Training, validation, and testing files. The image database is 30% of proposal testing. Training the prototype involved 50:50, 60:40, 70:30, 80:20, and 90:10. Using an 80/20 training/testing dataset, they analysed split ratios. An algorithm trained with 5740 intercepts, 20 epochs, and a 0.0001 learning rate. Later, a CNN-based model identified viral pneumonia in x-rays. Convolutional layers comprise Alex Net. Convolution, max pooling, and normalising are CONV layer processes. Two layers are joined, and one is SoftMax. In categorization training, 70:30 worked effectively. 99.84% specificity, 98.59% sensitivity.

Elshennawy et al. [10] used chest X-rays for deep-learning pneumonia models. Pneumonia Detection offered a chest X-ray dataset for training and testing. 712*439 to 2338*2025 pixels are in the image dataset. 6.5% were under 20, 26.4% were aged 20-40, and 24.3% were over 60. Next, training and validation photos are split 70/30. Photos were randomly divided into training and validation. CNN RNN, LDTM, ResNet 152v2, Mobile Net v2, and Deep Pneumonia are recommended. The recommended concepts were evaluated by using accuracy, precision, F1-score, recall, and AUC. ResNet152V2 accuracy was 99.22%, 99.43%, and 99.75%.

Shah S. et al. [11] used Convolutional Neural Networks and Kaggle's photographic resources to identify pneumonia early. Researchers used Kaggle to design this approach. Shah S. designed and built the system. Each diagnosis is generated from a publicly available chest X-ray dataset and public dataset. The American College of Radiology made this dataset public. These are all grayscale X-rays. No photo is coloured. Then, a CNN-based recommendation is made. Cengil E. et al. [12] provided a method for detecting COVID-19 as a system for deep feature concatenation in classification. This procedure detects the illness. Hypothetical occurrence order before COVID-19 diagnosis, Pipeline processes normal, COVID-19, and pneumonia data sets. Normal data is first then created a new set of attributes by applying distinct algorithms to each dataset. Various classification techniques were used to classify the components.

Deep-COVID-19 identifies COVID-19 in X-rays [13]. The COVID-19 X-ray pictures were analysed using six commercial convolutional neural networks. Picture analysis was possible. These steps were needed to analyse the study findings. VGG16, VGG19, and Mobile Nets are dependable, according to the trial. B, M., S., and others [14] classified pneumonia using chest X-rays and a CNN model. Researchers did this with CNNs (CNN). Each file contains 5840 chest x-ray images. Name for the data set. "Normal" and "pneumonia" subfolders are in each folder. The Image Data Generator class will change the dataset for training. This increases model accuracy. Our method leverages a CNN-like Xception model.

[15] CNN and deep learning were used to identify COVID-19 in thoracic X-rays. This step came first. CNN's models can now discern between classes and categorise data. After searching Kaggle, 112 pneumonia images and 112 chest X-ray photos were picked for analysis. When determining a person's performance, accuracy, precision, memory, and F1 score are considered. The final dataset is a composite of two available datasets. Deep categorization of COVID-19 radiological pictures was researched and suggested by Baseer, A., and colleagues [16], who are also advised employing neural networks. Researchers developed an innovative method for classifying chest X-ray images and made it accessible to the public on the internet. Transfer learning is utilised to provide an extract from deep neural networks that have been trained and kept up to date. This demonstrates the capability of the technique. In addition to having a classification accuracy of 97.36% overall, it has a COVID-19 classification accuracy of 99.29%.

Guefrechi et al. [17] recommended deep learning to detect COVID-19 in chest x-rays. The author employed two datasets: one with thousands of normal chest X-ray scans and another

with 224*224-pixel pictures. Randomize rotation, noise, and 10-degree horizontal flips. Deep-learning techniques pre-process X-rays. Resnet50, InceptionV3, and VGG16 score 97.20, 98.10, and 98.30%. Akter et al. [18] used chest x-rays to discover COVID-19. Below may have updated images. 80:20 test/training split. The dataset uses VGG16, VGG19, MobileNetV2, InceptionV3, NFNNet, ResNet50, ResNet101, Dense Net, EfficientNetB7, Alex Net, and Google Net. ResNet101 is 95% correct. MobileNetV2's accuracy is 98%. First, they computerised COVID-19 detection in chest X-rays. 959 X-rays, 250 cases of bacterial and viral pneumonia. Dataset-2 covers bacterial and viral pneumonia. Pre-processing lowered photo sizes so all pretrained models had the same resolution. Photos are 1102 to 2280 pixels wide. The image has been pre-processed to enhance certain aspects while hiding other details. ResNet50, InceptionV3, NASNetMobile, and VGG16 are some of the CNN transfer learning models. MobileNetv2, one of the usable models, was shown to be 81% as accurate as DenseNet121 [19].

III. METHODOLOGY

The goal of this project is to identify several methods for quickly identifying a disease from X-ray chest images and then to reliably classify the diagnostic images into COVID-19 or normal, viral pneumonia using multiclass classification.

A deep learning model often entails various workflow processes.

- a). Data collection
- b). Data Pre-processing and Augmentation
- c). Select the model.
- d). Prepare your model
- e). Assess the model.

Finding relevant data and gathering data to be sent as input to the network are the first steps in this study. Several image processing techniques are used to pre-process the data. Pre-processing is a technique for performing operations on low-quality photos to enhance the image quality or to extract relevant data from the images, including feature extractions. The next stage is to choose a deep learning model that operates well and produces cutting-edge outcomes. The most crucial stage in the process flow is then training the model, where the best model is chosen to train the data and the entire evaluation is based on how the model is trained. The training model is a dataset used to train the model, which compares the input and output data against a sample output and modifies the model as needed. This is referred to as "Model fitting." The model that has been trained must be evaluated as the last stage. In this step, the model will be evaluated using the training and validation datasets. The general process flowchart for our deep-learning survey is shown in Fig. 1.

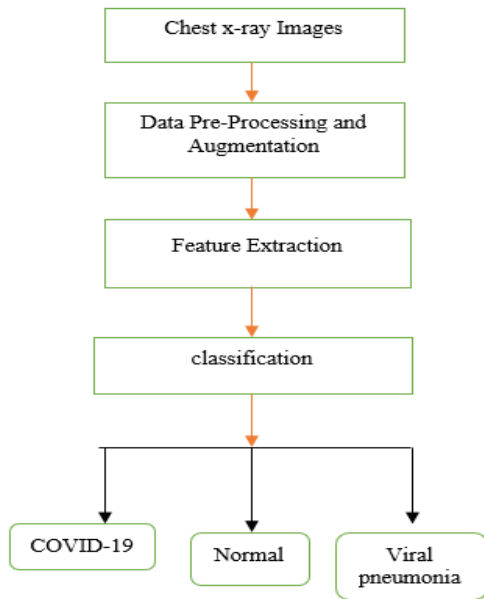


Figure 1. Generic Process Flowchart

A. Data Set

In general, the dataset will be collected from kaggle.com [20] which is under open access, where the dataset consists of CXR images along with the 4 classes covid-19, normal, viral pneumonia and bacterial pneumonia with different input shapes like 224*224 pixels and the colour format of the CXR scan images is grayscale. It has 317 total images, 317 of which are normal chest X-rays and 317 of which are cleaned COVID-19 images organized into the test and training directories.

TABLE I.
CHEST X-RAY DATASET

	Total
COVID-19	137
Normal	90
Viral pneumonia	90

B. Training, Testing

The dataset was divided into 70% training and 30% testing for each class as shown in table 2.

TABLE II.
CHEST X-RAY DATASET DISTRIBUTION DURING TRAINING AND TESTING

	Training	Testing
COVID-19	111	26
Normal	70	20
Viral pneumonia	70	20

C. Data Pre-Processing

The initial steps in the deep learning workflow are to prepare the raw image data into formatted data. The steps present in the image data pre-processing are reading the image, resizing the image, removing the noise and making the

images into a Denoising format. In the case of this proposed dataset images had high a resolution but the possible solution is to resize images to smaller dimensions to simplify the model training process. We have chosen 224 * 224 * 3 as our image tensor input to our network input.

D. Data Augmentation

A big dataset is often necessary for DL algorithms to overcome issues like overfitting. As a result, algorithms used in practical applications face a general obstacle. The task of collecting and analysing data can be time-consuming, which is why the task of labelling could also require domain experts. An augmentation technique is commonly used to expand existing datasets. In this study, the considered traditional augmentation methods to study how COVID-19, normal and pneumonia(viral pneumonia) diseases are detected, which have proven effective in numerous studies worldwide. As part of these processes, simple image processing changes like rotations, noise reduction, or blurring are implemented at the pixel level to introduce distortions to images. Our data has been subjected to various rotations by various angles, and perspectives, as well as affine, shearing, shifting, and mirroring procedures that preserve the dimensions of our training data.

E. Deep Models Selection, Training and Validation

The various deep learning models had been selected as shown in fig 3. The hyper matters that are used during the training of the model are shown in table 4.

TABLE III.
THE DEEP LEARNING HYPERPARAMETER

Parameters	Values
Batch size	32
Number of Epochs	150
Optimizer	Adam
The activation function of the last classifier layer	SoftMax
Leaming Rate	0.0001
Dropout	0.6

TABLE IV.
4 X 4 CONFUSION MATRIX

PREDICTED LABELS			
ACTUAL LABELS	TN	FN	TN
	FP	TP	FP
	TN	FN	TN

F. Deep Learning Image Classifiers

Using chest X-ray scans, deep-learning image classifiers can identify COVID-19, normal, and pneumonia diseases. The process of our methodology is depicted in Figure 2 and includes 13 different pre-trained CNN models, including the VGG16, VGG19, Xception, Densenet121, Densenet169, and densenet201.

IV. MODEL PROCESS

In this process, the models developed for one task are used as the foundation for another model. The enormous amount of computing power and time required to develop neural network models for these problems makes using pre-trained models a common approach in deep learning for obtaining skill jumps on related problems. The model process as shown below in fig 2.

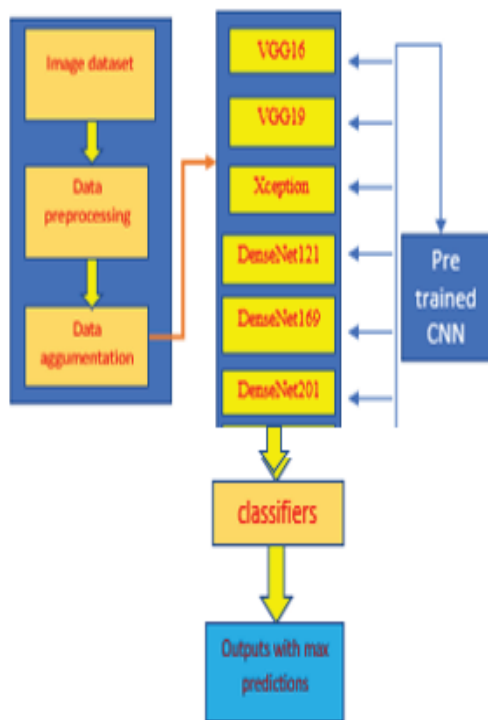


Figure 2. Model Process

VGG16: The 16 in VGG16 denotes the fact that there are 16 layers with weights. This network has roughly 138 million parameters, making it a sizable network. It has a faster training speed, fewer training samples per time, and higher accuracy. If there is not enough data or if the model is too big, then it can't get the good accuracy rate needed.

The VGG16 pre-trained CNN model has some experience with the data from ImageNet. The VGG16 model receives input from images that have a resolution of 224x224x3 pixels. Following that is a pooling layer, which brings the height and breadth of the image down to 112 x 112 x 64, and then there are two convolutional layers, each of which has a size of 224 224 x 64. After that, the image is cut up into two conv128 layers, each of which is 112 by 112 by 128 pixels. This is followed by a pooling layer, which brings the height and width of the image back down to 56 by 56 by 128. The size

of the image is then decreased to 28x28x256 by using a pooling layer, and this is followed by three conv256 layers, each of which measures 56x56x256. After that, there are three conv512 layers, and each one has a size of 28x28x512 pixels. Finally, there is a pooling layer that brings the image down to 14x14x512 pixels. The next layer is a pooling layer, which contains 7x7x521 layers, followed by three conv512 layers, each of which contains 14x14x521 levels, and ultimately, two dense or fully connected layers, each of which contains 4096, 4096, and 4096 nodes. The last layer is a dense layer, which is also called an output layer as shown in fig 3. It has a thousand nodes and can put an image network into one of three groups.



Figure 3. VGG16 Architecture

VGG19: A convolutional neural network with 19 layers is called VGG-19. It is an image recognition model. This survey made use of the pre-trained CNN network. In ResNet50V2, a modification was made in the propagation formulation of the connections between blocks. The deep networks are hard to train because of the vanishing gradient problem. The complexity of the architecture is more.

The VGG19 network contains two completely connected layers with a total of 4096 channels in each, followed by a third fully connected layer that predicts three different labels using 512, 256, and 128 channels, respectively. When it comes to classification, the SoftMax layer is the very last fully connected layer that is employed. Convolutional layers with 3*3 filters make up the first two layers of this image. Because the first two layers each utilise the same 64 filters, the total volume of the effect is 224*224*64. This is because the convolutions used are the same. Each of the filters always consists of a 3 x 3 step. The height and width of the volume were then reduced from 224 by 224 by 64 units to 112 by 112 by 64 units with the use of a pooling layer that had a maximum pool size of 2 by 2 and a stride of 2. The subsequent two convolutional layers, each of which has 128 filters, are identical. The result is a new dimension of 112 x 112 x 128. As soon as the pooling layer is utilized, the volume is reduced to 56 by 56 by 128. Down sampling brings the size down to 28*28*256 after the addition of two further convolutional layers, each of which has 256 filters. Following that will be two further stacks, each one consists of three convolutional layers and being separated by a max-pool layer. The last layer of pooling, which is a 7*7*512 volume, is flattened to an FC

layer, which has a set number of channels and a soft maximum output of three classes.

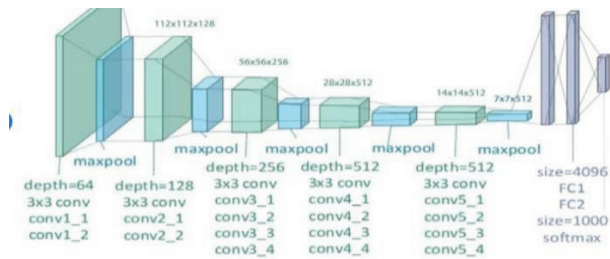


Figure 4. VGG19 Model

Xception: It is an extreme improvisation of Inception that serves as a different pre-trained model in many ways. This model consists of 3 blocks entry flow, middle flow, and exit flow as shown in fig 5. The implication of greater computational efficiency is the advantage. It is still computationally inefficient because of convolutions.

In the xception model, the entry flow consists of the input image with a size of 299x299x3, then conv32 followed by 3x3 and with a stride of 2x2. Then conv64, followed by a 3x3 size of the convoluted image size. Then it adds three conv of 1x1 followed by the stride of 2x2. Internally, it consists of separable conv128,256,728 and max pooling of 3x3 with a stride of 2x2. Then it adds 19x19x728 feature maps. The middle flow consists of separable conv728 with a 3x3 convoluted image size, and the same step repeats 8 times. Then later moves to the exit flow by adding the 19x19x728 feature maps to one conv1x1 followed by the stride of 2x2 internally consisting of separable conv728,1024 and max pooling of 3x3 with a stride of 2x2. Finally, the exit flow is separable from 1536 and 2048 with a 3x3 convoluted image size. All layers are made up of Relu and global average pooling, then 2048 dimensional layers and fully connected layers that can be turned on or off.

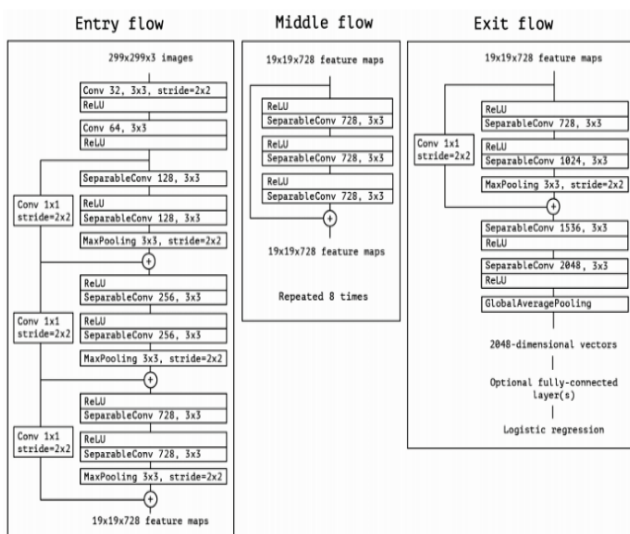


Figure 5. Xception Blocks

DenseNet121: It is a CNN that connects to the deeper layers of the network, with the first layer connecting to the second,

third, and fourth layers, and the second layer connecting to the third, fourth, and fifth layers, etc. Therefore, in this survey, this was chosen as the pre-trained model. they alleviate the vanishing gradient problem, strengthen feature propagation, and encourage feature reuse. substantially reduce the number of parameters. The class imbalance is the major challenge while training the model as shown below in fig 6.

The DenseNet121 consists of input with the size of 224x224x3. The DenseNet-121 has [6,12,24,16] layers in the four dense blocks consisting of Conv(7x7,1x1,3x3), with an average pooling of stride 2 and maximum pooling of 3x3 and global average pooling of 7x7 then finally the fully connected layer with SoftMax activation function then finally classifies the output.

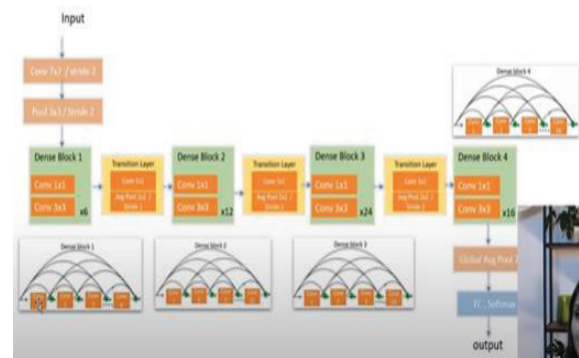


Figure 6. DenseNet121 Blocks

DenseNet169: The Dense Net -169 model is one of the models in the Dense Net family designed for image classification. The main variations are in the Dense Net -121 model's size and accuracy. The Dense Net -169 is larger at just over 55MB compared to the Dense Net -121 model's roughly 31MB size. The strong gradient flow, High parameters and high computational efficiency. Maintains low complexity features.

The DenseNet169 pretrained model consists of an input image with a size of 224x224x3. Then it consists of the convolution layer. In DenseNet-169, it has 3 dense blocks. Each dense block has [6, 12, 32, 32] layers. In between each block, there is a conv, pooling layers where the pooling layers are used to reduce the feature map size. The feature map sizes match each block. Finally, it consists of a pooling layer and FC as linear. Then it displays the output as depicted in fig 7.

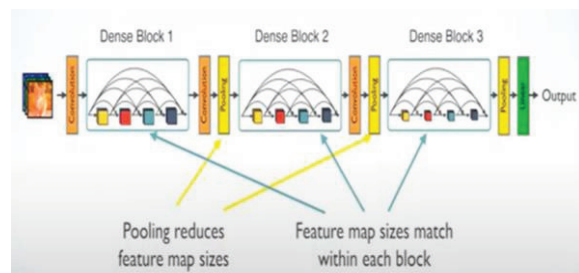


Figure 7. DenseNet169 Architecture

DenseNet201: A convolutional neural network with 201 layers is called DenseNet-201. A version of the network that

has already been trained on more than a million images is stored in the ImageNet database. They alleviate the vanishing-gradient problem, strengthen feature propagation, encourage feature reuse and substantially reduce the number of parameters. The disadvantage of the classifier is more prone to overfitting.

The pretrained DenseNet201 consists of an input with a size of 224x224x3, DenseNet-201 model optimization, where the number of hidden layers is 512, 128, 64, 32. In this model, each dense block consists of 16 convolutional layers. In batch normalization, the transition layer is used as a connector between every block. Relu activation function and a SoftMax activation function are used as shown in fig 8.

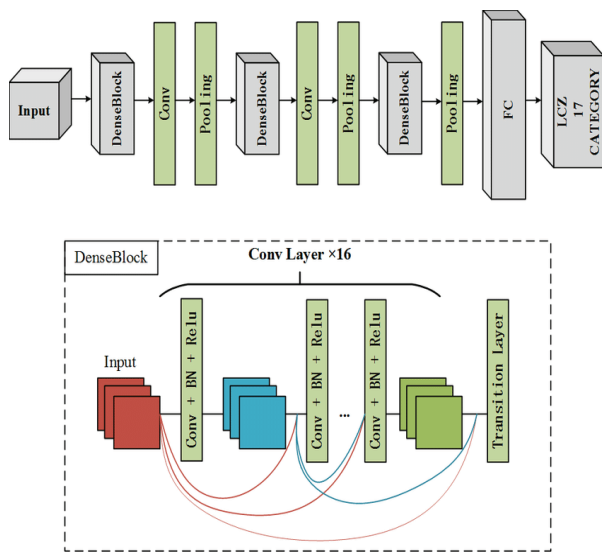


Figure 8. DenseNet201 Blocks

Experimental Setup

To implement the proposed work deep learning techniques the following hardware and software support shown below: Processor: 11th Gen Intel(R) Core (TM) i5-1135G7 @ 2.40GHz 2.42 GHz, RAM: 8.00 GB, Storage: 476 GB, Nvidia GPU. OS: Windows, Python: 3.10.5 version, TensorFlow: 2.8.2 version, Open CV2 python: 4.6.0 version, other necessary modules.

V. OBSERVATIONS

The proposed models are trained for 150 epochs using the Adam optimizer, learning rate and the momentum to 0.0001, Loss is employed here as the loss criterion and is used as the output of the procedure to correct any existing labels.

The models were trained by using an augmented dataset that included images from augmentation and actual images. A validation test was then performed to assess its generalizability. The training and validation phases of the proposed network show good convergence showed in Figure 16 illustrates the training loss and validation loss distributions based on the number of epochs in both phases. The curve shows the number of images that were correctly identified during validation as shown in fig 9.

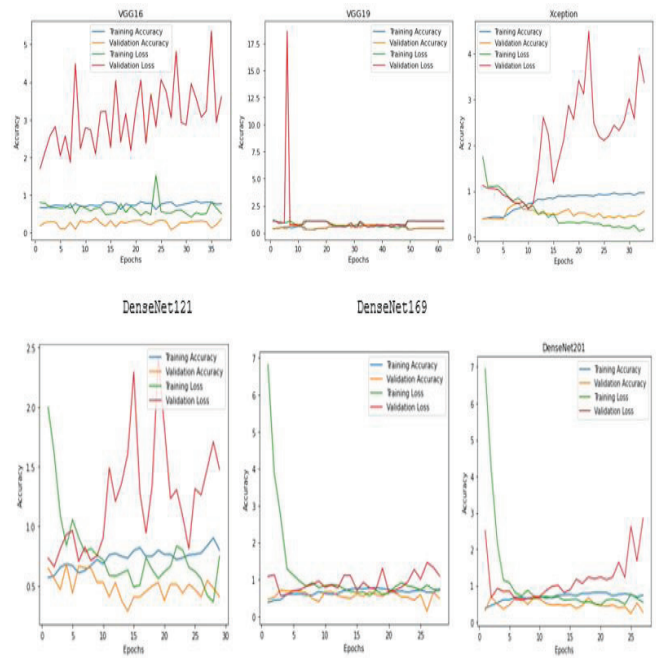


Figure 9. Corresponding Accuracy and Loss Curves

In a confusion matrix, the numerical values of test data for which the true values are known are used to rate the performance of a classification model. Fig.18 shows the confusion matrix on the detection dataset. The matrix shows the misclassified and correctly classified images. As shown in the matrix y-axis represents the true labels and the x-axis shows the predicted/detected labels., Class predictions are of two types: yes or no. In our example, positive results would indicate the presence of a disease, and negative results would indicate the absence of the disease.

Further, The evaluated classifiers using the following metrics: Accuracy, Precision, Recall, and F1-score metrics as shown in fig 10.

Accuracy: The accuracy of data classification refers to the percentage of correct classifications over total instances.

$$\text{accuracy} = \frac{TN + TP}{TP + TN + FP + FN}$$

Precision: For a good classification system, the precision should be as high as 1. $TP = TP + FP$ and FP is equal to zero when $TP = TP + FP$ which means that precision is 1 when the numerator and denominator are equal. Due to the increase in FP , the denominator's value becomes larger than the numerator's value, and when this happens, precision will decrease.

$$\text{Precision} = \frac{TP}{FP + TP}$$

Recall: For a classifier to be effective, the recall should be high. A classifier is effective only when both the denominator and the numerator match; $TP = TP + FN$, which also implies FN is zero. As FN increases, the numerator increases, and the denominator decreases. The recall rate is also referred to as the sensitivity rate or true positive rate, and it is calculated in the following way:

$$\text{Recall} = \frac{TP}{TP + FN}$$

F1-Score: This would like ideally for both precision and recall to be a weighted sum of ones within a good classifier, which also means that FP and FN count for nothing. As a consequence, they developed a metric that takes precision as well as recall into account. In the F1-score measurement system, accuracy and recall are both taken into account, and what is defined as follows:

$$\text{F1 score} = 2 \times \frac{\text{Precision} \times \text{Recall}}{\text{Precision} + \text{Recall}}$$

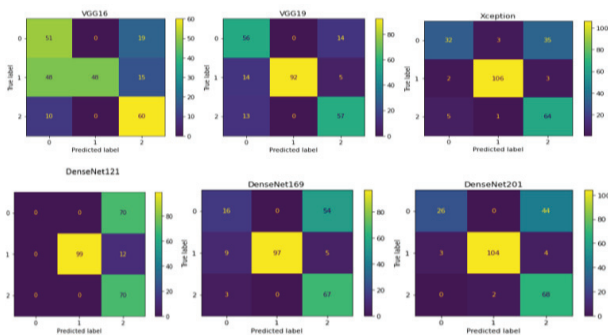


Figure 10. Corresponding Results of The Confusion Matrix

The statistics of accuracy, precision, recognition, F1 score and AUC are shown in Table 5 to illustrate the performance validation of the different models. Of all the classification methods, A classification accuracy of 100% was achieved by densenet121net, densenet201 had the highest percentage of correct classifications (89.66%). The VGG19 highest recall score is 80.00%. For general classification purposes, VGG19 performed best compared to all other methods with an F1 score of 73.20%. Overall, densenet201's AUC for classification is the highest at 97%.

TABLE V.

OVERALL COVID-19 CLASS ACCURACY, PRECISION, RECALL, F1-SCORE, AND AUC VALUES FOR COVID-19

COVID-19					
Models	Accur acy	Precisi on	Recall	F1- score	Accu racy
VGG16	72.85	46.79	72.86	56.98	87
VGG19	80.00	67.47	80.00	73.20	94
Xception	50.00	82.05	45.71	58.72	94
DenseNet121	1.00	00.00	00.00	00.00	92
DenseNet169	77.14	57.14	22.86	32.65	91
DenseNet201	62.85	89.66	37.14	52.53	97

Table 6 shows performance validation statistics for various models, including accuracy, precision, recall rates, F1 values, and area under the curves. Mobilenetv3large achieved the highest accuracy of 95.49% among the categorization approaches. Densenet121, VGG16, and densenet169

achieved a perfect precision classification rate of 100%. The highest rate of correct recall classification (95.50%) was achieved by Xception and an unprecedented F1 of 97.72%, making it the most effective approach for general categorization. Overall, the best AUC for classification is achieved by densenet201, and mobile Net, all of which achieve a value of 100%.

TABLE VI.
OVERALL NORMAL CLASS ACCURACY, PRECISION, RECALL,

Normal					
Models	Accuracy	Precision	Recall	F1- score	Auc
VGG16	43.24	1.00	43.24	60.38	99
VGG19	82.88	1.00	82.88	90.64	98
Xception	95.49	96.36	95.50	95.93	99
DenseNet121	89.19	1.00	89.19	94.29	99
DenseNet169	87.38	1.00	87.39	93.27	99
DenseNet201	93.69	98.11	93.69	95.85	100

In Table 7, the accuracy, precision, area under the curves, F1 values, and recall rates along with the performance validation information for a variety of models. The different classification strategies of densenet201 achieved the highest accuracy of 97.14%. VGG19 classified the precision as 75%. Densenet121 was classified with a recall value of 100%. VGG19 was found to be the most effective method for broad-based classification with an F1 score of 78.08%.

TABLE VII.

OVERALL ACCURACY, PRECISION, RECALL, F1-SCORE, AND AUC VALUES FOR PNEUMONIA (VIRAL PNEUMONIA)

Pneumonia (Viral pneumonia)					
Models	Accuracy	Precision	Recall	F1- score	Auc
VGG16	85.71	63.38	85.71	73.17	93
VGG19	81.42	75.00	81.43	78.08	95
Xception	91.42	62.75	91.43	74.42	88
DenseNet121	1.00	46.05	1.00	63.06	97
DenseNet169	95.71	53.17	95.71	68.37	94
DenseNet201	97.14	58.62	97.14	73.12	99

VI. FUTURE SCOPE

The possible future directions for developing this research is consisting of multiple models are used and their predictions combined, an ensemble approach is employed, which can improve results. Image classification and the identification of

COVID-19, normal and pneumonia illnesses can be improved using various deep learning algorithms, such as Deep CNN and hybrid models. The Adam optimizer and other optimization methods can be used because they are efficient and have low memory traces. Efficient Net is the latest version of the Efficient Net family network that was developed in 2021. Efficient Net improves accuracy by introducing several architectural reforms.

VII. CONCLUSIONS

This study shows that CXR images with a variety of deep learning algorithms can be used to sort images into three groups: pneumonia (viral pneumonia), normal, and COVID-19. In the above study, an automated prediction model based on CXR scan image processing and classification approaches was built to detect and classify COVID -19, normal, and pneumonia disease from real-time chest radiographs. Model performance and graphs of many other transfer learning models were compared. For a deeper CNN model, more image data are needed to generalize it effectively. Therefore, the dataset was enlarged after pre-processing. The last step was to apply transfer learning to known pre-trained models. The proposed model and dataset were both perfected through several tests. When comparing the VGG, Dense Net, and Xception families with different versions of the COVID -19 image dataset, densenet121 achieved the highest model classification accuracy for COVID-19 at 100%, xception of the normal class achieved 95.49% and densenet201 achieved the highest for the viral pneumonia class is 97.14%. Doctors and researchers use the model for computer-aided diagnosis of COVID -19, normal and pneumonia (viral pneumonia) including cancer and diabetic retinopathy. The model was developed using medical imaging techniques for healthcare applications.

REFERENCES

- [1] B. Prabhu Christopher, S. Udhaya Kumar, D. Thirumal Kumar, "The rise and Impact of COVID-19 in India" 22 May 2020, *Frontier in Medicine*.
- [2] Vibhor Jain, Anju Mishra, Neha Sharma, "An Analysis of Convolutional Neural Networks for Image Classification" Volume 132, 2018, pages 377-384.
- [3] Si Jinhai, Sohaib Asif, Yi Wenhui, Hou Jin, "Classification of COVID-19 from Chest X-ray images using Deep Convolutional Neural Networks", *IEEE*, 12 Feb 2020.
- [4] Y. Mechbal, A. Ben-fares, M. Qjidaa, et al. "Early detection of COVID-19 by deep learning transfer model for populations in isolated rural areas" *IEEE*, 2020.
- [5] Khasawneh, N., Fraiwan, M., Fraiwan, L., Khassawneh, B., & Ibranian, A. (2021), Detection of COVID-19 from chest X-ray images using deep convolutional neural networks. *Sensors*, 21, 17, 5940.
- [6] Alhwaiti, Y., Siddiqi, M. H., Alruwaili, M., Alrashdi, I., Alanazi, S., & Jamal, M. H. (2021). Diagnosis of COVID-19 using a deep learning model in various radiology domains. *Complexity*, 21, 3.
- [7] Ozcan, T. A deep learning framework for coronavirus disease detection in X-ray images, 4, 3, (2020).
- [8] Abiyev, R. H., & Ismail, A. (2021), COVID-19 and pneumonia diagnosis in X-ray images using Convolutional neural networks. *Mathematical Problems in Engineering*, 32, 14, 1-14.
- [9] Umar Ibrahim, A., Ozsoz, M. Salete, S., Al-Turjman, F., Habeeb Kolapo, S. (2021). Convolutional neural network for diagnosis of viral pneumonia and COVID-19 alike & diseases. *Expert Systems*, 13, (7).
- [10] Elshennawy, N. M., & Ibrahim, D. M. (2020), Deep-pneumonia framework using deep learning models based on chest X-ray images. *Diagnostics*, 10, (9), 649.
- [11] Shah, S., Mehta, H., & Sonawane, P. Pneumonia detection using Convolutional neural networks. 2020 Third International Conference on Smart Systems and Inventive Technology (ICSSIT), 43, (12).
- [12] Cengil, E., & Çınar, A. (2021). The effect of deep feature concatenation in the classification problem: An approach on COVID-19 disease detection. *International Journal of Imaging Systems and Technology*, 32, (6), 26-40.
- [13] EFiky, A. H (2021), Deep COVID-19: Deep learning for COVID-19 detection from X-ray images. *International Journal of Innovative Technology and Exploring Engineering*, 11, (7), 1-6.
- [14] B, M., S, S., T, V., K, S. S., R, S. S., & A R, S. (2021). Pre-trained Convolutional neural network model-based pneumonia classification from chest X-ray images. *SSRN Electronic Journal*, 5(4), 1-8.
- [15] Makris, A., Kontopoulos, I., & Tserpes, K. (2020). COVID-19 detection from chest X-ray images using deep learning and Convolutional neural networks. *SETN*, 12(3), 17.
- [16] Baseer, A., & Bhatti, N. (2020). Deep networks-based classification of COVID-19 chest X-ray images. 2020 14th International Conference on Open-Source Systems and Technologies (ICOSST), 4(3), 1-6.
- [17] Guefrechi, S., Jabra, M. B., Ammar, A., Koubaa, A., & Hamam, H. (2021). Deep learning-based detection of COVID-19 from chest X-ray images. *Multimedia Tools and Applications*, 80(21-23), 3180331820.
- [18] Akter, S., Shamrat, F. M., Chakraborty, S., Karim, A., & Azam, S. (2021). COVID-19 detection using deep learning algorithm on chest X-ray images. *Biology*, 10(11), 1174.
- [19] Aggarwal, S., Gupta, S., Alhudhaif, A., Koundal, D., Gupta, R., & Polat, K. (2021). Automated COVID-19 detection in chest X-ray images using fine-tuned deep learning architectures. *Expert Systems*, 39(3).
- [20] <https://www.kaggle.com/datasets/pranavraikokte/covid19-image-dataset>.

Comparative Analysis and Ranking of Selected Bio-Fuels

Manjeet Kharub

Assoc. Prof., CVR College of Engineering/Mechanical Engg. Department, Hyderabad, India

Email: manjeetkharub@gmail.com

Abstract: As public awareness of environmental issues increases, the need to investigate alternative energy sources becomes crucial. Numerous alternative energy sources, such as nuclear, solar, wind, and biofuels, are well-known worldwide. Biofuel is a process that generates energy from organic materials that can replace fossil fuels. Transesterification, the process of animal and vegetable oils into usable fuels, causes a substantial amount of energy. This paper analyses the mechanical properties of an internal combustion (IC) engine operating on conventional diesel and biofuels, including power, torque, and efficiency. Biodiesel, among others, is a formidable competitor to traditional diesel. It was discovered that biodiesel produces a significant amount of energy. In addition, research articles have demonstrated that the torque produced by biofuels will be distributed as follows: Diesel fuel vs biodiesel vs methanol vs pine oil. Biofuel, fossil fuels, trans-esterification, and animal and vegetable oils are included in the index.

Index Terms: first term, second term, third term, fourth term, fifth term, sixth term

I. INTRODUCTION

Biofuels are considered the best alternative fuel and are produced via transesterification [1]. Among others, vegetable oils, ethanol, or animal fat are used to make biofuel fuels, which are then combined with alcohol to form ethyl esters and glycerol [2]. The use of biofuels has resulted in a decrease in the consumption of gasoline and diesel. These oils have found their applications in the transportation system after being blended with diesel or in their pure form as crude oil. Numerous studies have demonstrated that using biofuels reduces harmful gas emissions such as carbon monoxide (CO), unsaturated hydrocarbons (UHC), sulphur dioxide (SO₂), nitric polycyclic aromatic hydrocarbons (NPAHC), and particulate matter (PM) [3]. But even though these studies showed that biofuels cut down on harmful gas emissions, they have one problem in the same area: Nitrogen Oxides (NO_x) are observed to be increased in the case of biofuels when compared to diesel fuel [4]. Table 1 summarises the available biofuels.

The table depicts that biofuels such as pine oil, methanol, and biodiesel have very similar properties to diesel in terms of kinematic viscosity (mm²/s), calorific value (KJ/kg), density (Kg/m³), flash point (°C), and boiling point (°C) [5]. Also, it is observed that biodiesel is superior to diesel in every way that makes the diesel engine run smoothly [6].

However, when it comes to pine oil, a few areas must be improved, such as viscosity. As per the findings [7], if viscosity needs to be increased, the temperature properties of the fluid may decrease. When the temperature of a diesel engine falls below the required temperature, mechanical

properties reduce. While methanol is deficient in every way, it is a renewable resource. Through research and increased use of methanol as a fuel, it is possible to improve its properties [8]. Because biofuels are renewable, they help to reduce our reliance on fossil fuels [9]. This also contributes to reducing emissions, making it more environmentally friendly [10].

TABLE I.
VARIOUS PROPERTIES OF BIO-FUELS AND DIES

Property/Fuel Names	Pine oil	Methanol	Bio-Diesel	Diesel
Kinematic viscosity (mm ² /s)	1.3	0.4	5.6	3.5
Calorific Value (KJ/Kg)	41500	22700	37270	43500
Density (Kg/m ³)	875	760	875	850
Flash Point (°C)	55	9	150	62-65
Boiling Point (°C)	160	65	340-375	160

In contrast, they have some disadvantages, such as biofuels do not produce as much power as diesel or petrol [11], and they are not as efficient as diesel and gasoline in terms of thermal efficiency. There are, however, numerous other alternatives, such as retrofitting vehicles with hybrid technology. These alternative modes of transportation are efficient but not renewable, whereas biofuels are renewable but less efficient than conventional fuels [12]. Although the researches on biofuels are still in progress, they are considered potential alternative in the face of critical environmental condition and to meet future demands of sustainable development.

II. DESIRABLE MECHANICAL PROPERTIES

The following section discusses the desirable mechanical properties of a typical diesel engine:

- A. Torque
- B. Speed
- C. Dimensions (length, diameter)
- D. Power
- E. Efficiency

A. Torque

Torque is a twisting force that refers to the engine's rotational power and indicates how much of that rotational force is available when the engine is exerted. While horsepower is expressed as a single number, torque is typically expressed in pounds-feet. Calculating the magnitude of the torque is practical by first determining the lever arm and then multiplying it by the applied force. The lever arm is the perpendicular distance between the rotational axis and the force's line of action.

B. Speed

The term "speed" refers to spinning the crankshaft in piston engines and rotating compressors, turbines, and electric motor rotors, and it is quantified in terms of revolutions per minute (RPM).

C. Power

A four-stroke engine is an internal combustion (IC) engine in which the piston travels through four distinct strokes as the crankshaft is turned. A stroke is a total distance travelled by the piston in either direction along the cylinder.

D Efficiency

Mechanical efficiency is a metric that indicates how effectively an automated system works. It is often defined as the ratio of the power produced by an automatic system to the power given to it, and this efficiency is always less than one due to friction.

E Brake Power

An IC engine's braking power equals the power available at the crankshaft. This power is typically determined using a brake mechanism, the force produced by a machine at the output shaft.

F. Indicated Power

It is generated by the gases expanding in the cylinders, ignoring any friction, heat losses, or entropy inside the system. The force produced by an engine cylinder is calculated using an indication diagram and some primary engine data.

G. Actual Mean Effective Pressure

The mean adequate pressure is a parameter associated with the functioning of a reciprocating engine. It is a valuable indicator of an engine's ability to do work independently of its displacement.

H. Brake Mean Effective Pressure

The brake means adequate pressure (BMEP) is derived from the dynamometer power (Torque). This is the engine's actual output at the crankshaft.

I. Engine Dimensions (Bore & Stroke)

The bore of the cylinder is the diameter, while the stroke is the distance travelled by the piston from the top dead centre (TDC) to the bottom dead centre (BDC). The stroke used to be larger than the bore in older engines, but the trend in recent years has been toward a shorter piston stroke. The faster the piston stroke, the less power is lost through friction. Additionally, the bearings' inertia and centrifugal load are decreased. The square engine, the most advanced technology available, has an equal bore and stroke.

III. EXPERIMENTATION

Transesterification is used in the experiment. Any vegetable oil and alcohols are used in the transesterification process, transforming mixed reactions into ethyl esters and glycerol. Transesterification is described scientifically as a

chemical reaction in which one-mole triglycerides (the scientific term for vegetable oils or animal fats) interact with three moles of alcohol to form three moles of alkyl esters or ethyl esters and one-mole glycerol. Glycerol is a by-product or a co-product of a chemical reaction. In this instance, the reactants react in the presence of a catalyst, primarily potassium hydroxide and sodium hydroxide. Triglyceride is a term that refers to a molecule composed of three fatty acids linked to a glycerol backbone. Each molecule's three fatty acids functioning as triglycerides may be identical or distinct. The fatty acid compositions of the oil or fat contribute to many of the resulting biofuels' characteristics. Transesterification begins rapidly and gradually slows down until it approaches equilibrium. At this stage, some unreacted glycerides remain unchanged in the biofuel. It is possible to enhance the quality by removing the settled glycerides and running another reaction, thus shifting the equilibrium point closer to the products. This is the scientific process by which the reactants create the intended outcome, which in this case, is biofuel.

The apparatus required for the experiment are:

- i. *Pine oil, methanol, and Bio-diesel act as the triglycerides in this process. The mentioned bio-fuel individually consists of 3 fatty acids*
- ii. *Ethanol acts as the alcohol,*
- iii. *Two flasks containing 125 ml and 250 ml, all with stoppers, (iv) A 250 ml separatory funnel,*
- iv. *A stirring hot plate,*
- v. *Magnetic Stir bar*
- vi. *Thermometer,*
- vii. *Aluminium foil,*
- viii. *A weighing scale,*
- ix. *Potassium Hydroxide,*
- x. *A 4-stroke single-cylinder diesel engine.*

3.1. Pine Oil

The process of making biofuels from pine oil is as follows:

- a) Firstly, weigh 1 gram of potassium hydroxide into a 125 ml flask. Into the same flask, add 20 ml of ethanol.
- b) Add a stir bar and cover the flask with aluminium foil. Place the flask on a stirring hot plate.
- c) Continue the process until potassium hydroxide is completely dissolved.
- d) Now, add 80 ml of pine oil to a 250 ml flask. Add a magnetic stir bar and put the flask on a stirring hot plate.
- e) Start heating the oil to around 600 C, which the thermometer can measure.
- f) Once the temperature reaches 600C, add the alcoholic-catalyst mixture to the oil in the flask. Cover the flask with aluminium foil to keep the alcohol vapours from escaping.
- g) Stir the mixture at a moderate speed for up to 60 minutes while maintaining the temperature at 600C.
- h) After 60 minutes, stop heating and stir the mixture in the flask. Now, transfer the mixture into a 250 ml separatory funnel and allow it to cool for about 20-30 minutes.

- i) After the cooling process, the glycerol and biofuel will be separated. The top end of the flask will be bio-fuel, and the bottom end will be glycerol. Due to their weight, they are separated at their respective places.
- j) Finally, take the glycerol present in the funnel, and thus 100% of bio-fuel is obtained.

3.2. Methanol

The process of making biofuels from methanol is as follows:

- a) Firstly, weigh 1 gram of potassium hydroxide into a 125 ml flask. Into the same flask, add 20 ml of ethanol.
- b) Add a stir bar and cover the flask with aluminium foil. Place the flask on a stirring hot plate.
- c) Continue the process until potassium hydroxide is completely dissolved.
- d) Now, add 80 ml of methanol to a 250 ml flask. Add a magnetic stir bar and put the flask on a stirring hot plate.
- e) Start heating the oil to around 600 C, which the thermometer can measure.
- f) Once the temperature reaches 600C, add the alcoholic-catalyst mixture to the oil in the flask. Cover the flask with aluminium foil to keep the alcohol vapours from escaping.
- g) Stir the mixture at a moderate speed for up to 60 minutes while maintaining the temperature at 600C.
- h) After 60 minutes, stop heating and stir the mixture in the flask. Now, transfer the mixture into a 250 ml separatory funnel and allow it to cool for about 20-30 minutes.
- i) After the cooling process, the glycerol and biofuel will be separated. The top end of the flask will be bio-fuel, and the bottom end will be glycerol. Due to their weight, they are separated at their respective places.
- j) Finally, take the glycerol present in the funnel, and thus 100% of bio-fuel is obtained.

3.3. Vegetable Oil (Bio-Diesel)

The process of making biofuels from Vegetable oil is as follows:

- a) Firstly, weigh 1 gram of potassium hydroxide into a 125 ml flask. Into the same flask, add 20 ml of ethanol.
- b) Add a stir bar and cover the flask with aluminium foil. Place the flask on a stirring hot plate.
- c) Continue the process until potassium hydroxide is completely dissolved.
- d) Now, add 80 ml of Vegetable oil to a 250 ml flask. Add a magnetic stir bar and put the flask on a stirring hot plate.
- e) Start heating the oil to around 600 C, which the thermometer can measure.
- f) Once the temperature reaches 600C, add the alcoholic-catalyst mixture to the oil in the flask. Cover the flask with aluminium foil to keep the alcohol vapours from escaping.
- g) Stir the mixture at a moderate speed for up to 60 minutes while maintaining the temperature at 600C.

- h) After 60 minutes, stop heating and stir the mixture in the flask. Now, transfer the mixture into a 250 ml separatory funnel and allow it to cool for about 20-30 minutes.
- i) After the cooling process, the glycerol and biofuel will be separated. The top end of the flask will be bio-fuel, and the bottom end will be glycerol. Due to their weight, they are separated at their respective places.
- j) Finally, take the glycerol present in the funnel, and thus 100% of bio-fuel is obtained.

3.4. Engine Performance

Purified biofuel is then utilised to evaluate the engine's performance characteristics in a four-stroke single-cylinder diesel engine [13]. As we all know, a four-stroke engine is a kind of internal combustion engine in which the piston completes four distinct strokes as the crankshaft is turned. Suction, Compression, Expansion, and Exhaust are the four different strokes. The piston's stroke changes from TDC to BDC during the suction stroke. The cylinder's valve opens to allow the air-fuel combination to enter the engine.

Usually, the piston travels from BDC to TDC during a compression stroke, compressing the air-fuel mixture and initiating the ignition. Diesel has a higher flash point than biodiesel, which results in a shorter ignition delay during the compression stroke [14]. The crankshaft has now completed a complete 360-degree rotation. While the piston is at TDC, a spark plug or the heat produced by high compression ignites the compressed air-fuel combination, forcing the piston back to BDC [15]. This stroke causes the engine to generate mechanical work to spin the crankshaft. The piston travels from BDC to TDC during the exhaust stroke [16]. While the exhaust valve is open, the piston returns from BDC to TDC. During this stroke, the exhaust valve discharges the lean air-fuel mixture [17]. We get the necessary data throughout this period, such as engine speed, engine torque, and actual, and brake mean effective pressures.

IV. RESULTS AND DISCUSSION

A. Diesel

Figure 1 illustrates the performance characteristics of an IC engine in terms of Power, Torque, and Efficiency [18, 19, 20,23].

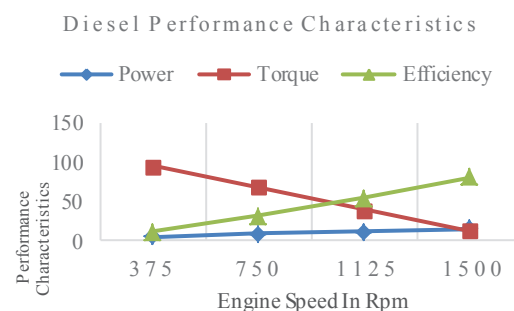


Figure 1. Performance characteristics of an IC engine like Power, Torque & Efficiency using diesel

As many academics have studied and shown that diesel provides superior performance to all other fuels, we obtained the same level of performance via testing. While the mechanical characteristics of diesel in a diesel engine are a benefit, there are a few drawbacks. The emission characteristics of diesel in a diesel engine continue to be a source of contention. There are two reasons to be looking for biofuels [21]. They are renewable energy sources and greenhouse gas emissions. Though diesel produces 33% fewer pollutants than gasoline, it is a factor to consider when attempting to reduce emissions. Carbon Monoxide (CO), Unsaturated Hydrocarbons (UHC), Sulphur Dioxide (SO₂), Nitric Polycyclic Aromatic Hydrocarbons (NPAHC), and Particulate matter (PM) are some of the pollutants released.

B. Pine Oil

The chart below, i.e., figure 2, illustrates the performance characteristics of an internal combustion engine (IC) in terms of Power, Torque, and Efficiency [20, 22, 23] while utilising Pine oil.

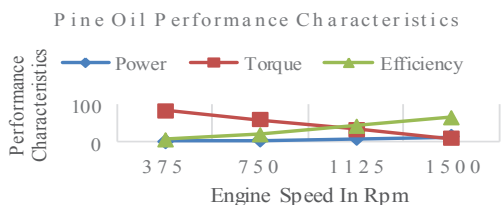


Figure 2. Performance characteristics of an IC engine like Power, Torque & Efficiency using Pine Oil

Through extensive study and testing, it has been determined that pine oil performs somewhat less well than diesel but produces fewer pollutants. B5 is utilised in these biofuels (5 percent pine oil and 95 percent Diesel). Initially, the emission rate for pine oil is likewise very high, although less so than diesel, but the emission rate progressively lowers. Carbon Monoxide (CO), Unsaturated Hydrocarbons (UHC), Sulphur Dioxide (SO₂), Nitric Polycyclic Aromatic Hydrocarbons (NPAHC), and Particulate matter (PM) were all released in much lower amounts.

Further study and testing on different compositions such as B10-B100 (10% pine oil & 90% diesel – 100% pine oil) may enhance the performance characteristics and get them closer to those of diesel. When compared to diesel, pine oil consumes more fuel. Because pine oil is renewable, this is not an issue in these instances.

C. Methanol

Figure 3 illustrates the performance characteristics of an internal combustion engine (IC) in terms of Power, Torque, and Efficiency [23, 24]. It was determined through extensive study and testing that methanol's mechanical performance characteristics are nowhere near those of diesel or the next biofuel. Carbon Monoxide (CO), unsaturated hydrocarbons (UHC), sulphur dioxide (SO₂), nitric polycyclic aromatic hydrocarbons (NPAHC), nitrogen oxides (NO_x), and

particulate matter (PM) emissions are very low in comparison to other biofuels or diesel.

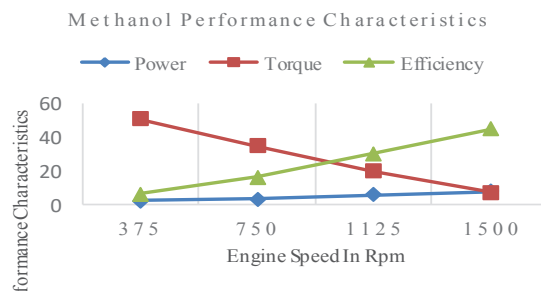


Figure 3. Performance characteristics of an IC engine like Power, Torque & Efficiency using methanol

The emissions are much lower than with biodiesel. Methanol has an extremely high fuel consumption due to its low viscosity, calorific value, flash point, boiling temperature, and density. Essentially, all characteristics necessary for a vehicle to operate normally are fuel economy and mechanical performance. Methanol has the same chemical makeup as pine oil B5 (5 percent methanol & 95 percent Diesel).

D. Bio-Diesel

The chart below, i.e., figure 4, demonstrates the performance characteristics of an internal combustion engine (IC) utilising biodiesel in terms of Power, Torque, and Efficiency [5, 6, 11, 20, 23].

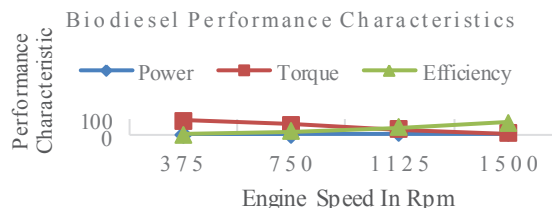


Figure 4. Performance characteristics of an IC engine like Power, Torque & Efficiency using Bio-Diesel

Following extensive study and testing, it was determined that the mechanical performance characteristics of bio-diesel are equivalent to those of conventional diesel. Additionally, the emission characteristics of biodiesel are improved. Carbon Monoxide (CO), unsaturated hydrocarbons (UHC), sulphur dioxide (SO₂), nitric polycyclic aromatic hydrocarbons (NPAHC), and particulate matter (PM) emissions are very low in comparison to other biofuels or diesel. Except for Nitrogen Oxides (NO_x), which are somewhat increased due to their more unique flash point, which results in a much quicker combustion process. The higher the rate of combustion, the greater the NO_x emissions since there is no additional combustion within. When compared to conventional diesel, biodiesel consumes more fuel.

E. Power

Figure 5 illustrates the performance characteristics of an internal combustion engine (IC engine), such as power [25], while utilising Pine oil, methanol, and Bio-Diesel.

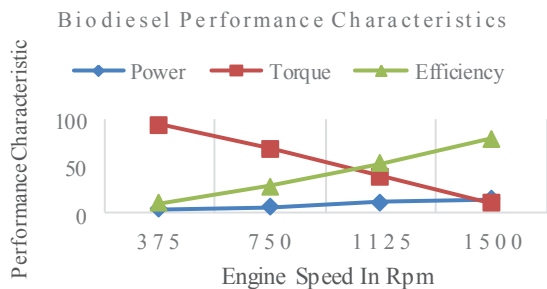


Figure 5. Analysis of Performance characteristics of an IC engine like power using Pine oil, Bio-Diesel & Methanol

The study of these three fuels is based on the measurements taken during the testing and the conversion of the measured values to their corresponding formulas. The engine's torque and speed determine the performance of power. Pine oil, methanol, and biodiesel have performed better in testing than in the study. According to a few study articles, fuel produced from pine oil cannot surpass 8KW, methanol cannot exceed 5KW, biodiesel cannot exceed 10KW, and all other biofuels exceed theoretical limits. As a result, the following sequence applies to biofuels: Biodiesel>Pine oil>Methanol. When the composition is just B5, this power value is obtained. By increasing the design, the performance is improved further, and it may be used as a substitute fuel.

F. Torque

The chart below, i.e., figure 6, illustrates the performance parameters of an internal combustion engine (IC), such as torque [25], while utilising Pine oil, methanol, and Bio-Diesel. The study of these three fuels is based on data taken during testing with a dynamometer to determine the torque at the specified speed [26].

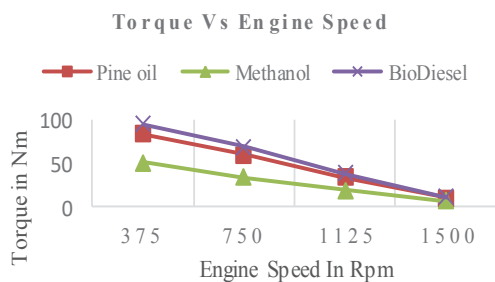


Figure 6. Analysis of Performance characteristics of an IC engine like torque using Pine oil, Bio-Diesel & Methanol

Pine oil, methanol, and bio-diesel perform better in testing. According to a few study articles, the fuel produced from pine oil cannot exceed 70Nm, methanol cannot exceed 50Nm, biodiesel cannot exceed 80Nm, and all of the bio-fuels surpassed the theoretical limits. As a result, the following sequence applies to biofuels: Biodiesel>Pine oil>Methanol. When the composition is just B5, this power value is obtained. By increasing the design, the performance is improved further, and it may be used as a substitute fuel.

G. Efficiency

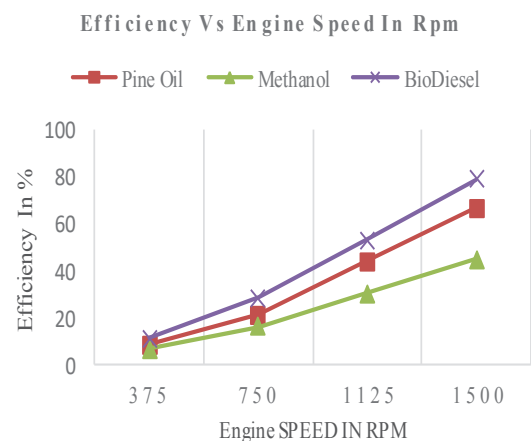


Figure 7. Analysis of Performance characteristics of an IC engine like efficiency using Pine oil, Methanol & Bio-Diesel

The above chart, i.e., figure 7, illustrates the performance characteristics of an internal combustion engine, such as its efficiency while running on pine oil, methanol, or biodiesel. The study of these three fuels is based on the measurements taken during the testing and the conversion of the measured values to their corresponding formulas. Efficiency performance depends on the engine's brake and indicated power [27]. Brake and implied control are proportional to brake and mean adequate pressure. Pine oil, methanol, and biodiesel have performed better in testing than in the study. According to a few study articles, the fuel produced from pine oil cannot surpass 50%, methanol cannot exceed 30%, bio-diesel cannot exceed 70%, and all other bio-fuels exceed the theoretical limits. As a result, the following sequence applies to biofuels: Biodiesel>Pine oil>Methanol. When the composition is just B5, this power value is obtained. By increasing the document, the performance is improved further, and it may be used as a substitute fuel.

V. CONCLUSIONS

All fuels are compared to conventional diesel, and biodiesel, among others, is found to be a close rival. The amount of power produced by biodiesel is highly significant. Torque comparisons revealed similar findings, with biodiesel providing the highest torque, followed by pine oil

and methanol. Initially, in literature was seen that the power produced by all biofuels would be much less than diesel. Additionally, it has been shown in study articles that the torque produced by biofuels will be in the following sequence: Diesel fuel vs biodiesel vs methanol vs pine oil.

However, it was discovered via testing and research that the sequence is conventional diesel > biodiesel > pine oil > methanol. We obtained the power value by noting the gained torque value and putting it into the appropriate power equations. As a result, the Power order is identical to that of Torque: Diesel fuel > Biodiesel fuel > Pine oil > Methanol. We get the efficiency value by determining the IMEP and BMEP values of the fuel in the engine and inserting them into their corresponding formulas, i.e., indicated power and brake power. Efficiency is prioritised: Diesel fuel > Biodiesel fuel > Pine oil > Methanol. The primary drawback of utilising biodiesel is its slow start-up time. The following is a ranking of biofuels: Power, Torque, and Efficiency: Methanol > Biodiesel > Pine oil.

The primary goal of this project was to highlight the need for alternative fuel(s) as demand continues to grow. The primary issue with alternative fuels is their performance compared to conventional fuels such as diesel, gasoline, and so on. The performance and emissions of alternative biofuels in internal combustion engines are measured and analysed in this research. Another issue with biofuel(s) is carbon monoxide, carbon dioxide, hydrocarbon, and nitrogen oxide emissions. Despite their relatively high performance, biofuels are assessed for their environmental effect. Carbon monoxide and carbon dioxide emissions are low in biofuels; however, NOx emissions vary depending on the alternative.

In comparison to traditional fuels, biofuels and mixes produce less smoke. The study identified key variables affecting the future of combustion engine fuels. Natural availability, environmental effect, economic feasibility, and mass manufacturing are all variables to consider. Biofuels are both economically effective and environmentally beneficial. It is strongly suggested that pentanol be utilised directly in the CI engine without modification. Pentanol, methanol, neem-oil biofuel, 15% di-ethyl ester mix, jatropha biofuel blend, and vegetable oils are all recommended biofuels for optimal performance and decreased emissions. Numerous studies have shown that increasing the bio-diesel percentage in blends improves performance while lowering emissions. Certain compounds have been shown to reduce hazardous emissions substantially. Metal-based additives such as copper (II) oxide result in a modest performance boost.

REFERENCES

- [1] Murugesan, A., C. Umarani, R. Subramanian, and N. Nedunchezian. "Bio-diesel as an alternative fuel for diesel engines—a review." *Renewable and sustainable energy reviews* 13, no. 3 (2009): 653-662.
- [2] Paul, Gaurav, Ambarish Datta, and Bijan Kumar Mandal. "An experimental and numerical investigation of the performance, combustion and emission characteristics of a diesel engine fueled with jatropha biodiesel." *Energy Procedia* 54 (2014): 455-467.
- [3] Alagumalai, Avinash. "Combustion characteristics of lemongrass (*Cymbopogon flexuosus*) oil in a partial premixed charge compression ignition engine." *Alexandria Engineering Journal* 54, no. 3 (2015): 405-413.
- [4] Rakopoulos, C. D., K. A. Antonopoulos, D. C. Rakopoulos, D. T. Hountalas, and E. G. Giakoumis. "Comparative performance and emissions study of a direct injection diesel engine using blends of diesel fuel with vegetable oils or biodiesels of various origins." *Energy conversion and management* 47, no. 18-19 (2006): 3272-3287.
- [5] Haşimoğlu, Can, Murat Ciniviz, İbrahim Özsert, Yakup İçingür, Adnan Parlak, and M. Sahir Salman. "Performance characteristics of a low heat rejection diesel engine operating with biodiesel." *Renewable energy* 33, no. 7 (2008): 1709-1715.
- [6] Agarwal, Deepak, Lokesh Kumar, and Avinash Kumar Agarwal. "Performance evaluation of a vegetable oil fuelled compression ignition engine." *Renewable energy* 33, no. 6 (2008): 1147-1156.
- [7] Paul, Gaurav, Ambarish Datta, and Bijan Kumar Mandal. "An experimental and numerical investigation of the performance, combustion and emission characteristics of a diesel engine fueled with jatropha biodiesel." *Energy Procedia* 54 (2014): 455-467.
- [8] Rakopoulos, Dimitrios C., Constantine D. Rakopoulos, and Evangelos G. Giakoumis. "Impact of properties of vegetable oil, bio-diesel, ethanol and n-butanol on the combustion and emissions of turbocharged HDDI diesel engine operating under steady and transient conditions." *Fuel* 156 (2015): 1-19.
- [9] Varuvel, Edwin Geo, Nadia Mrad, Mohand Tazerout, and Fethi Aloui. "Experimental analysis of biofuel as an alternative fuel for diesel engines." *Applied Energy* 94 (2012): 224-231.
- [10] Özener, Orkun, Levent Yüksek, Alp Tekin Ergenç, and Muammer Özkan. "Effects of soybean biodiesel on a DI diesel engine performance, emission and combustion characteristics." *Fuel* 115 (2014): 875-883.
- [11] Atadashi, I. M., Mohamed Kheireddine Aroua, and A. Abdul Aziz. "High quality biodiesel and its diesel engine application: a review." *Renewable and sustainable energy reviews* 14, no. 7 (2010): 1999-2008.
- [12] Sadhik Basha, J., and R. B. Anand. "The influence of nano additive blended biodiesel fuels on the working characteristics of a diesel engine." *Journal of the Brazilian Society of Mechanical Sciences and Engineering* 35, no. 3 (2013): 257-264.
- [13] Li, Ruina, Zhong Wang, Peiyong Ni, Yang Zhao, Mingdi Li, and Lilin Li. "Effects of cetane number improvers on the performance of diesel engine fuelled with methanol/biodiesel blend." *Fuel* 128 (2014): 180-187.
- [14] Kumar, M. Senthil, Jérôme Bellettre, and Mohand Tazerout. "The use of biofuel emulsions as fuel for diesel engines: a review." (2009): 729-742.
- [15] Nabi, Md Nurun, Md Shamim Akhter, and Mhia Md Zaglul Shahadat. "Improvement of engine emissions with conventional diesel fuel and diesel–biodiesel blends." *Bioresource Technology* 97, no. 3 (2006): 372-378.
- [16] Mirzajanzadeh, Mehrdad, Meisam Tabatabaei, Mehdi Ardjmand, Alimorad Rashidi, Barat Ghoobadian, Mohammad Barkhi, and Mohammad Pazouki. "A novel soluble nanocatalysts in diesel–biodiesel fuel blends to improve diesel engines performance and reduce exhaust emissions." *Fuel* 139 (2015): 374-382.
- [17] Aghbashlo, Mortaza, Meisam Tabatabaei, Pouya Mohammadi, Mehrdad Mirzajanzadeh, Mehdi Ardjmand,

- and Alimorad Rashidi. "Effect of an emission-reducing soluble hybrid nanocatalyst in diesel/biodiesel blends on exergetic performance of a DI diesel engine." *Renewable Energy* 93 (2016): 353-368.
- [18] Aghbashlo, Mortaza, Meisam Tabatabaei, Pouya Mohammadi, Navid Pourvosoughi, Ali M. Nikbakht, and Sayed Amir Hossein Goli. "Improving energetic and sustainability parameters of a DI diesel engine using polymer waste dissolved in biodiesel as a novel diesel additive." *Energy Conversion and Management* 105 (2015): 328-337.
- [19] Karabektas, Murat. "The effects of turbocharger on the performance and exhaust emissions of a diesel engine fuelled with biodiesel." *Renewable Energy* 34, no. 4 (2009): 989-993.
- [20] Bhale, Purnanand Vishwanathrao, Nishikant V. Deshpande, and Shashikant B. Thombre. "Improving the low-temperature properties of biodiesel fuel." *Renewable energy* 34, no. 3 (2009): 794-800.
- [21] Vallinayagam, R., S. Vedharaj, W. M. Yang, C. G. Saravanan, P. S. Lee, K. J. E. Chua, and S. K. Chou. "Emission reduction from a diesel engine fueled by pine oil biofuel using SCR and catalytic converter." *Atmospheric Environment* 80 (2013): 190-197.
- [22] Crookes, R. J. "Comparative bio-fuel performance in internal combustion engines." *Biomass and Bioenergy* 30, no. 5 (2006): 461-468.
- [23] Behçet, Rasim. "Performance and emission study of waste anchovy fish biodiesel in a diesel engine." *Fuel Processing Technology* 92, no. 6 (2011): 1187-1194.
- [24] Huang, Wei-Dong, and YH Percival Zhang. "Energy efficiency analysis: biomass-to-wheel efficiency related with biofuels production, fuel distribution, and powertrain systems." *PLoS One* 6, no. 7 (2011): e22113.
- [25] Hasan, M. M., and Md Mustafizur Rahman. "Performance and emission characteristics of biodiesel–diesel blend and environmental and economic impacts of biodiesel production: A review." *Renewable and Sustainable Energy Reviews* 74 (2017): 938-948.
- [26] Kumar, Rajesh, and Lokeshwar Reddy Ch. "Performance Analysis of Rooftop Solar Plants in CVR College of Engineering: A Case Study." *CVR Journal of Science and Technology* 11 (2016): 41-46.
- [27] Striker, K. "Investigation of wear characteristics of Fe-Cr-C hardfacing alloy on AISI-304 steel." *CVR Journal of Science and Technology* 11 (2016): 47-50.

Analysis of a Feasible Gate Location in Injection Mold for Plastic Cloth Peg: New Product Development

Neeraj Kumar Jha

Assoc. Professor, CVR College of Engineering/ Mechanical Engg. Department, Hyderabad, India

Email: neerajjha.me@gmail.com

Abstract: Product design is the most important and invaluable factor to determine success of a product. Its role changes consistently throughout the life cycle of a product. It is well known that the ultimate design of a product is dependent on various influencing factors right from material and process selection to the end use as well as re-use of the product. These factors put challenges in front of designers and manufacturers of consumer goods. Judicious utilization of material and other resources along with optimized profit are the constraints to control. It is achievable only if the design concepts and the manufacturing experience is used in the correct combination. This article aims at illustrating a new product development process for a plastic part and analyzing it on the parameters of few process constraints related to its manufacturing process viz. gate location. The product considered for the study is clothe peg, which is individually made up of plastic, unlike existing similar products made in combination of plastic and metal parts. This part is analyzed by considering its manufacturing by injection molding process. A model mold was also prepared for validation of the research findings.

Index Terms: product design, injection molding, gate location, distortion, parting line, shrinkage.

I. INTRODUCTION

Plastic is an engineering material with multiple engineering applications and advantages. The reusable grades of plastics become soft when they are heated. By applying pressure, they change shape at this softness to come to a usable form. This is the basic principle behind the processing of plastic. Injection molding process is one of the processes of processing thermoplastics with which 80% of the plastic products are manufactured. The process utilizes a plastic injection machine along with a permanent mold. The machine plasticizes the polymer granules by heating them and pressurizes them to fill the mold. The mold consists of cavity as the shape of the required product along with flow path to fill the cavity. The mold additionally consists of provision of cooling the injected polymer in its cavities. These cooling channels help in fast solidification and improve cycle time of the process. The process seems simple and controlled, but uncontrolled process parameters lead to defects in part produced, wastage of material, cost, and time in injection molding process. injection pressure, injection temperature, mold temperature etc. along with the processing material properties, are some process parameters which must be analyzed properly to ensure defect free components obtained by injection molding process. Not just process parameters but process planning also plays a great role in successful

production of a product. At macro level process planning controls resource utilization to increase profit margin but micro level process planning controls all the steps with which overall efficiency of production can be maintained. One such tool is the injection molding die (mold) which is used in the injection molding process. Design of this mold is one of the crucial parts of the entire production process. A properly designed mold will be easy to manufacture and easy to operate. It will have least possible inserts or other parts so that it can last long with negligible maintenance. We must understand that such molds are made to improve the production efficiency and productivity while their cost must be kept as low as possible. Design of such mold will be based on the part which it has to shape, and its observation done by the mold designer. A designer must analyze the part, to make a durable mold at optimum cost and can shape defect-free products. Analyzing the product and modifying it for ease of its manufacturing is part of product design. Providing adequate fillet on corners and draft on vertical faces are few attributes of the product design process for injection molding. Out of many design constraints in a mold design, the gate location has its own importance. Gate is the last element of the flow path of a mold. It connects runner with mold cavity and through the gate only material enters the mold cavity. They are with the least cross-section compared to other elements of the flow path so that back flow of material can be prevented, and directional solidification can be ensured. There are many types of gates in mold making practice. They are used as per specific need. Edge gate with circular cross-section is more frequently used for ease of cutting. They leave a mark on the product. Thus, their position and type are considered specifically as per the use of the product.

The product considered in this work is clothes peg. It is not the same conventional clothes peg used for gripping the clothes on a rope while the clothes are getting dried. It is a new product to serve the same purpose, but it is different in shape, elements and appearance compared with the conventional cloth pegs. The existing pegs are mainly made of plastic, and they implement metal spring to serve their purpose. Usually, they don't last long due to non-parallel characteristics of metal parts and plastic parts. This work aims at making the entire peg from a single piece of plastic. This work innovatively utilizes shrinkage occurring in a plastic part blended with shape transformation to replace metal spring from a plastic clothes peg. The design of the proposed clothes peg is influenced with the existing clothes peg but it is new of its kind. It is considered as new product development because the steps involved for a new product development

process are followed [1]. From past research it is evident that there are seven most shouted steps in new product development. Many researchers utilize twelve steps of new product development. Thus, it is evident that as per the product complicity and application, few of the stages can be obsolete or combined.

The article is structured in the following sections: Section II explains the product design process by considering stages of the new product development process in background. Section III explains process simulation by considering material and process parameter selection. Section IV is about die trials and Section V is the conclusion of this research work.

II. PRODUCT DESIGN

There are seven main steps in the new product development process. They are, idea discovery, idea screening, content development and test, business analysis, development of mix between product and marketing, market test and product launch. This work discovered the idea based on the drawback of existing clothe peg. Over a period of use, plastic degrades while the metal spring remains stronger in the existing clothes pegs. Further use of such pegs leads to fracture of plastic part against metal spring and the part can no longer be used. Thus, there was a need for a durable peg. The idea screening is important and challenging at the same time. In this step there is a need to analyze the need or problem statement deeply. Here it is observable that durability issues are coming into picture due to incompatible combinations between metal and plastic parts. Metal spring was needed for stiffness and plastic part is needed due to its own advantages. In order to enhance durability, thicker plastic parts cannot be used as that will affect the cost of the product. Thus, durability can be aimed by plastic part alone which will limit product cost also [2]. But obtaining stiffness like a metal spring was another hurdle. Under content development, this work decides to utilize camber curve profile as solution for stiffness in plastic parts. The designed peg is shown in Fig. 1. Once molded as in figure, it will shrink in negative camber form. The gap between elongated parts will compress the cloth and rope together. Circular recess in the camber region is for receiving the diameter of hanging wire or rope.

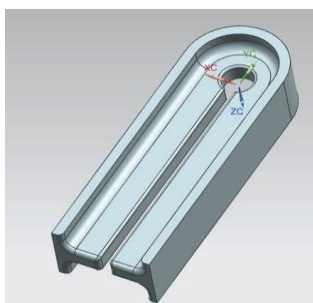


Figure 1. New Cloth Peg Solid Model

The finalized cross-section was T-section. Apart from these other feasible sections can be I and trapezoidal. Solid trapezoidal section cannot be a good choice as it will lead to a lot of shrinkage and thereby distortion of the molded

product. Symmetric I-section cannot serve the purpose of cambering due to its symmetry. Modified I-section can be considered as alternate of trapezoidal section. But as per the application of the product we need high tensile stress on the outer surface and high compressive stress at the inner surface. It can be managed by varying material accumulation on inner and outer surfaces. Modified I-section will decrease intensity of compressive stress on the inner surface. This can be justified from calculation by considering the camber region as a curved beam or by stress analysis using convenient software. Stress analysis for T-section is shown in Fig. 2.

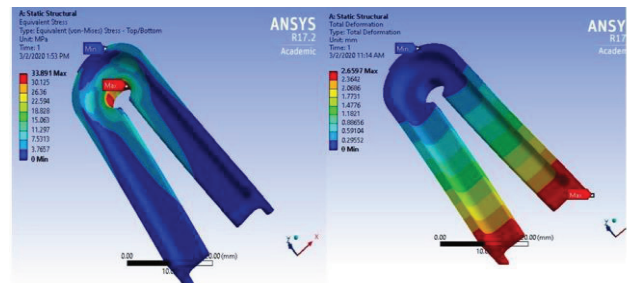


Figure 2. Equivalent Stress (L) and Total Deformation (R)

In Fig. 2, the left side image represents equivalent stress analysis while the right side image represents total deformation analysis performed by ANSYS R17.2. The maximum load implemented was 16.38 KN. This is the amount of load required to stretch a conventional clothe peg. This load value is obtained by experiment performed on a conventional clothe peg. It is observable from Fig. 2 that maximum stress was acting at circular recess and its magnitude is 33.89 MPa. Maximum deformation observed was nearly 3 mm at the free end. Both the values are in the agreement of design as it is not taking the part to ultimate failure against applied load and major volume of part material is receiving minimum stress as indicated in blue color. This can be considered as justification for another phase of product development process, content development and test. Hence, we can observe that the provided solution is an alternative to existing clothe pegs. It has an additional advantage for business analysis point of view over the conventional pegs. It can be observed that the existing pegs are made of minimum three number of parts ie. Two plastic parts and one metal spring. While the provided solution is constituted in a single piece. This adds direct benefit for business point of view. We know that for making more parts more time requirement will be there as well as to process plastic and metal parts separate machinery and equipment will be needed. Thus, it can be qualitatively estimated that the provided design solution can be developed in less investment as compared with the conventional pegs. Further, development of mix between product and marketing, market test and product launch are beyond the scope of this work as this work is dedicated to the initial phase of product development. The remaining phases are based on pushing the product in the market, getting feedback, and further analyzing the outcomes with different tools. Hence that broader scope of work is not included in this research work. The proposed peg was developed by

considering its manufacturing by injection molding process, thus all the design considerations for the design was considered accordingly. Not just the strength criteria but application and appearance also were considered while finalizing the design. At the free end of the peg fillet is provided for the smooth engagement of peg against rope. Flat surfaces are mostly dominating and additionally curvatures are not added to keep machining cost of the mold on the lower side. The web and flange regions are given with different thickness to avoid thick mass accumulation and thereby distortion and shrinking during the molding process. The drawing of the proposed cloth peg is shown in Fig. 3.

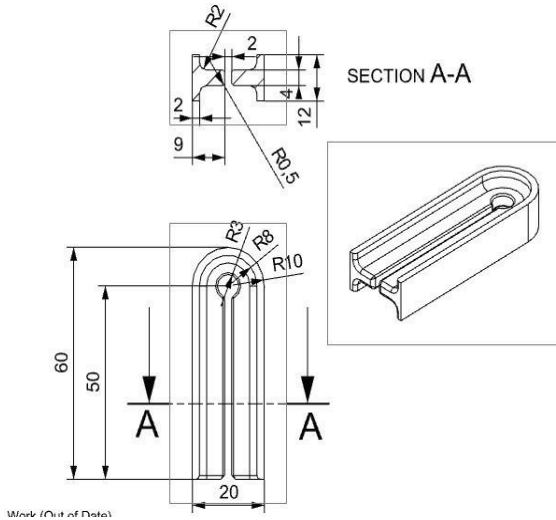


Figure 3. Drawing of New Cloth Peg (All dimensions are in mm)

III. PROCESS SIMULATION

This section will attempt to justify that the designed part is manufacturable. Suitable material selection, proper control on process parameters and process constraints will contribute to process simulation of the part. The same will be evaluated from the trial after manufacturing of the die.

A. Material Selection

The conventionally available cloth pegs are available in metal, wood and combination of plastic and metal. But this work aimed at making peg from plastic. There are a wide range of plastic materials suitable for the purpose, but this work proceeded with Polypropylene (PP) due to its own advantages.

TABLE I.
MATERIAL SPECIFICATION
POLYPROPYLENE (PP)

Density	946 kg/m ³
Melting Point	160 °C
Formula	(C ₃ H ₆) _n
Type	Thermoplastic
Flexural Strength	40 N/mm ²
Shrinkage	1-2.5% mm/mm
Tensile Strength	32 N/mm ²
Injection Temperature	32-36 °C
Heat Deflection Temperature	100 °C
Specific Gravity	0.91

Few of the properties of PP are enlisted in Table I. Adequate flexural strength with low rate of shrinkage, compared with other thermoplastics makes PP suitable for this application. Additionally, PP has the least per unit cost among all polymers after polyethylene.

B. Process Parameter Selection

Selection of adequate process parameters is a very important phase of process design. Adequate injection pressure, shot volume, heating capacity of machine etc. are few important factors before starting the manufacturing activity [3]. As this work decided to make a model die for the trial of the part, a suitable machine was identified with adequate capacity for manufacturing of the part. Table II represents machine specifications of semi-automatic injection molding machines available for the trial.

TABLE II.
MACHINE SPECIFICATION
(TEXPLASST 1HD, MP LAB, CVRCE)

Shot Capacity	2 – 45 gms / shot
Plunger Diameter	25 mm
Stroke Length	450mm
Clamping Capacity	6.0 Tons
Injection Pressure	80 kg/cm ²
Heating Capacity	1.5 kw
Total Installed Power	3.7 kw
Total Shut Height	100 - 450mm

Apart from these process parameters few other aspects are also important to consider. One such aspect is the gate position of the part in the mold. By definition gate position is the part of flow path through which material enters into the mold cavity in the shaping process. But the decision of gating position is influenced by many factors. An inadequate gate position may lead to complicated and difficult to manufacture dies. Various defects may also appear in the components due to improper gating position. Gates are usually arranged along a parting line. But this decision mainly depends on the thickness of the part. The proposed part can have two convincing gate positions and the same is indicated in Fig. 4. Parting plane is indicated in red color in Fig. 4. It is passing through half of the thickness of the part. Probable gate position 1 (GP1) is indicated with a dark red arrow while probable gate position 2 (GP2) is indicated with purple color arrow. Both the positions have their own advantages and limitations. GP1 has the advantage that it is at an axis of symmetry, but die will be bigger while if GP2 is preferred, die size will be smaller and cost saving is possible but part quality is to be evaluated. This work further compared outcomes of each gate position through simulation.

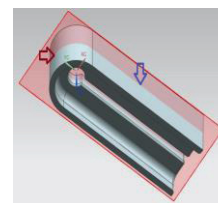


Figure 4. Probable Gate Positions and Parting Plane

C. Simulation Results

Molded part quality is important to be observed before going for die manufacturing [4]. Thus, this work analyzes part quality for both the gate positions. Autodesk Mold Flow Adviser 2019 is utilized for this purpose. Such tools are conveniently utilized in manufacturing industries. It helps in a lot of time and cost saving in product design and development process. Fig. 5 represents confidence of filling the cavity, under common filling pressure. It can be seen that if filling is done from GP1, 100% high chance of filling is predicted while that of GP2 is 71%. The reason behind this result is that from GP1 feeding is uniform in both the arms while filling from GP2 one arm is getting filled easily and another arm fills later by residual pressure.

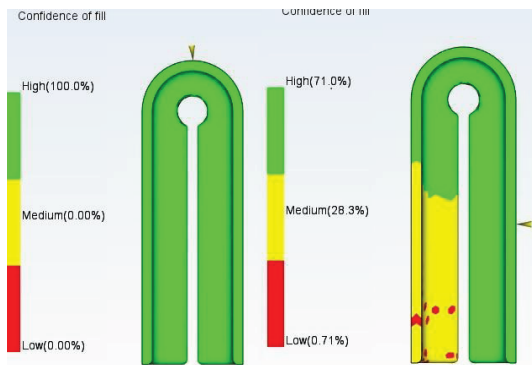


Figure 5. Confidence of Fill Results, GP1 (L), GP2(R)

Further quality prediction tests indicate 84.6% high quality for GP1 while it is coming 50.4% high for GP2. This analysis is done for analyzing the quality of molded part [5]. This analysis is shown in Fig. 6.

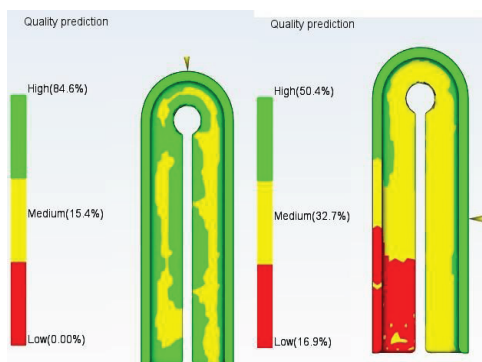


Figure 6. Quality Prediction Results, GP1 (L), GP2(R)

In the similar manner the analysis for fill time indicates that it is taking 4 seconds for filling of the mold cavity from GP1 while it is taking 12 seconds to fill from GP2 under the same amount of pressure. Fig. 7 is representing the filling of the cavity at 3 seconds. The reason behind quick filling from GP1 can be splitting of stream in camber region and filling of both arms simultaneously while in case of GP2 flow stream diverts to fill one arm first and back pressure causes proper filling of second arm. In general practice longer fill time affects overall

cycle time of the part molding. Usually keeping small cycle time is desirable for any manufacturing process.



Figure 7. Fill Results in 3 Seconds, GP1 (L), GP2 (R)

Further this work analyzes the cooling quality of the parts. This analysis predicts the way heat will be liberated from the hot part naturally and flow towards outer boundaries of the mold [6]. Fig. 8 represents cooling quality results for both the filling situations. We can clearly observe that the cooling quality is 94.8% high for GP2 filling while it is only 54.3% high for GP1 filling. This is an advantage for GP2 filling which is quite in agreement with previous results. As the cavity is filling with back pressure and taking much time to fill the mold cavity, it is getting cooler at a higher rate than in GP1 filling.

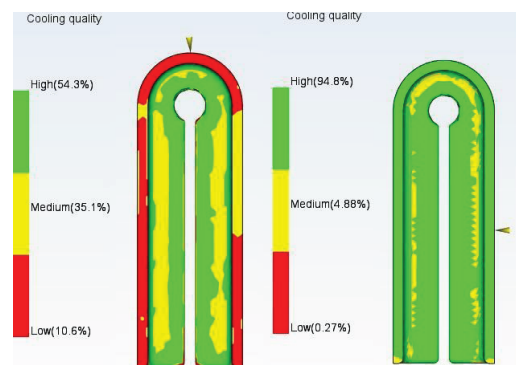


Figure 8. Cooling Quality Results, GP1 (L), GP2 (R)

From all these results it was observed that though there are some advantages with GP2, GP1 is more beneficial in order to obtain good quality components. Cooling quality can be improved in GP1 filling by providing suitable cooling channels. Thus, the work proceeded with GP1 filling.

IV. DIE TRIAL

Based on the consideration in the product design section and outcomes of the simulation, a sample die was machined. Gate position 1 was provided. From the opposite direction of the gate position, vents were provided to ensure proper filling of the mold and no air entrapment into the mold cavity. The machined cope half and drag half of a model mold is shown in Fig. 9. The same is representing all the elements of flow path including air vents. This mold was aligned at a semi

automatic injection molding machine, specifications of which are mentioned in Table II. Trial was taken after opening one half of the mold, part obtained after 1st trial is shown in Fig. 10. the output was as per the simulation results.

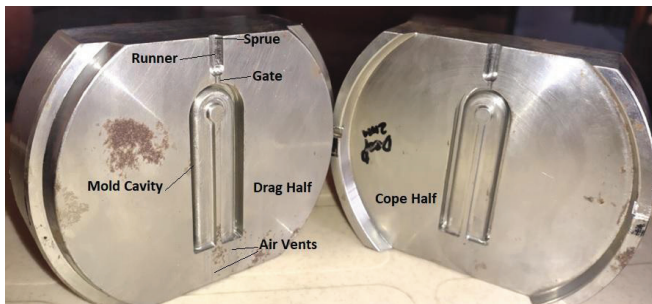


Figure 9. Cope and Drag Half of Model Mold



Figure 10. First Trial (Drag Half Removed)

Parts after trial were observed for camber due to shrinkage behavior. It was expected and the same was discussed in the product design section. Fig 11 indicates two parts adjacent to each other. The left side part is immediately taken out of mold thus it is undergoing solid shrinkage. Here the arms are straight as per mold cavity. But the right-side part is cooled to room temperature and hence it has undergone camber due to shrinkage [7].



Figure 11. Camber, After Cooling to Room Temperature

The main reason behind camber is the solidification pattern in the last to solidify region. Metal accumulation at outer regions easily liberates temperature to become solid while the material remains in liquid form at core. Due to this change of phase in a cross section, camber occurs as an outcome of shrinkage. Fig. 12 is representing final parts after removal from flow path elements and its application.



Figure 12. Manufactured Parts (L) and Application (R)

V. CONCLUSIONS

This research work was dedicated to analyzing an existing problem and obtaining a creative solution for that. A designer must analyze the manufacturability of his design. At the same time, he cannot ignore the cost efficiency of his provided solution. For the plastic part considered in this work, simplicity of the design and cost effectiveness are the most shouted benefits. The considerations and the standards followed in this work can be utilized by upcoming researchers for their work in the field of tooling. This work has not done cost analysis and market research to analyze success or failure of the product as it can be part of further extended research. But the work has considered and provided enough justification for representing this part as one feasible solution which is durable and manufacturable at less cost.

Based on the outcome of this research work a proper injection molding die can be manufactured with multiple cavities, cooling provision and mechanism of ejection. This work doesn't claim that the provided solution is the only solution for the problems occurring in the existing clothes pegs. Based on further analysis and expertise in the field of product development, more feasible solutions are also possible. As per the feedback provided after using the part produced, a few possible improvements can be, 1. providing a bigger fillet at the end of the arm and 2. providing a depression at the outer surface of the arms for a better grip.

REFERENCES

- [1] Kim, Y.-H., Park, S.-W. and Sawng, Y.-W. (2016), "Improving new product development (NPD) process by analyzing failure cases", *Asia Pacific Journal of Innovation and Entrepreneurship*, Vol. 10 No. 1, pp. 134-150. <https://doi.org/10.1108/APJIE-12-2016-002>
- [2] J. Bouquet, D. Van Camp, O. Malek, P. Ten Haaf, K. Vanmeensel, B. Lauwers, Aiming for Improved Lifetime of Die and Mold Components through an Integrated Laser Hardening Operation, Combining Machining and a Selective

- Heat Treatment in One Setup, *Procedia CIRP*, Vol. 46, 2016, pp. 541-544, ISSN 2212-8271, <https://doi.org/10.1016/j.procir.2016.04.018>.
- [3] Rupendra, Ch & Vivek, D & Sai, Yuva & Raju, Sudhakar & Jogarao, Bikkavolu. (2020). Design, Analysis and Fabrication of Safe Holder and Cam Dies in Injection Molding. *International Journal of Recent Technology and Engineering (IJRTE)*. 8. 2277-3878. 10.35940/ijrte.F9707.038620.
- [4] Youmin Wang, and Guoqing Wang, (2022), “Research on the Injection Mold Design and Molding Process Parameter Optimization of a Car Door Inner Panel”, *Advanced Composite Materials and Their Applications* <https://doi.org/10.1155/2022/7280643>
- [5] Hongbo Fu, Hong Xu, Ying Liu, Zhaogang Yang, S. Kormakov, Daming Wu and Jingyao Sun, “Overview of Injection Molding Technology for Processing Polymers and Their Composites”, *ES Mater. Manuf.*, 2020, Vol. 8, pp. 3–23
- [6] Neeraj Kumar Jha and Bhavya Sri Tadiparthi, (2019) “Design and Analysis of the Sleeve Ejection System in Injection Molding Die for Trolley Wheel”, *CVR Journal of Science and Technology*, Vol 17 No 1.
- [7] Wu, Y., Gong, Y., Cha, K.J. et al. Effect of microstructures on the shrinkage of injection molding product. *J Mech Sci Technol* 33, 1357–1363 (2019). <https://doi.org/10.1007/s12206-019-0236-y>

Mechanical Characterization and Evaluation of Effects of Epoxy in Lamination for Kevlar Composites

A. Suresh

Asst. Professor, CVR College of Engineering/Mechanical Engg. Department, Hyderabad, India
Email: suri0341@gmail.com

Abstract: Hybrid type of composites have considerable budding for certain specific strength and stiffness, efficacious in industries such as submarines, aerospace, and medium duty automotives. The macroscopic and microscopic properties of the hybrid composites can be enhanced by making the various layers of the epoxy and Kevlar in various directions. The lay up using the epoxy in various combinations can lead to promote the mechanical properties. Each of the constituent present in the Kevlar composite can make the difference in the tensile strength, bonding strength. The experiments with various combinations of the resin and hardener are always there in the researchers mind to find the effects of each individual over the other properties of the composite. In this voyage the optimal mix of that particular element in this instance the epoxy usage influence will be found out. The mechanical properties such as the tensile strength, binding strength in between the fabric and matrix will be found. 3 unique sheets, namely P (3:2), Q (4:1) and R (2:3) are fixed by the hand layup procedure to make a conglomerate composite. Experimental analysis in accordance with the ASTM standards of 3039, are exhibited to paramount the mechanical properties. Delamination tests are then performed as per ASTM standard to find out the inter layer laminar strength in between the Kevlar fiber and glass layers. The outcomes archived indicate that sample of glass/Kevlar fiber-based hybrid composite in the mix of 3:2 in lamination is best with respect to mechanical properties and it has also shown the least swelling ratio, in addition to it material system composed of 4:1 mix details the optimal adhesion capabilities and inter laminar properties.

Index Terms: Mechanical characterization, Evaluation, epoxy, Lamination, Kevlar, Composites.

I. INTRODUCTION

Composite materials usually made by different distinct process few of them are metal matrix composites and fiber-based composites [1]. In any composite the main constituent property that holds the major role is the binding strength in between the inter laminar layers. The strength depends on the quantity and quality of the resin, fiber and hardener used. It also depends upon the orientation of the fiber and also the no of layers of the ply [2]. Likewise, since ages the interest to explore the various facets of the composite material that improves the mechanical strength, binding energy and inter laminar holding ability. The idea to make the composite has come due to the search for the high strength and temperature resistant materials [3]. It has started from the metals then it went to alloys phase then after the search has stopped at the composite materials. The reason for it lies upon the properties that composite material possesses [4]. Even though the composite material is made by the different materials of

different properties as a whole it has started showing the best properties that no one has shown individually. If each constituent is considered separately for the fabrication of a new composite material, it has shown the most adorable result. That is each of the constituent material has some distinct properties for example some of brittle in nature some are ductile in nature, but such distinct materials together have produced a composite material that has both good properties of the parent materials [5]. Usually, it can be experienced in the material world that the materials which strong in tensile strength ate week in compressive strength and vice versa. But a composite material is the one which has the best tensile strength and compressive strength together [6]. It is because of the fact that all original materials possess the isotropic properties and the composite material is anisotropic material. In any distinct position its properties are not same [7].

This feature is obtained to the composite material due the multi-layer foundation it has and also these layers are been bound together by the epoxy resin combined with the silicon powder and hardener. Along with the time the evaluation of the composites is also changed and they broadly divided into MMC, PMC and CMC. MMC is Metal Matric Composite in which the main constituent or dominant material is metal. In the PMC i.e., Polymer Matric Composites the base materials are the polymer and the last one is CMC means Ceramic Matrix Composites these are been fabricated by ceramic materials as the base materials. In the present work the Kevlar epoxy reinforced composite material is used for the determination of the mechanical properties and also to find the effects of the epoxy are been analyzed. The main reason behind selecting the Kevlar composite is due its light weight, high strength, high wear resisting ability. The Kevlar fiber materials are used vividly in the aerospace applications to make the air crafts and space crafts and also it is used in novel marine structural applications [8,9,10]. With respect to strength comparison the Kevlar composites are about five times better than steel. High strength to weight ratio, low wear ability and light weight have made arena towards the popular utilization in the aero space applications. The inter atomic bonding present in the Kevlar composite is much stronger than the conventional van der walls intermolecular connection. But to make the usage of these materials more in terms of cost criterion and hybrid composites came into existence [11,12]. Since the fabrication of the hybrid composites have started the making cost is reduced and the wide spread usability of the Kevlar/ e-glass composites has increased [13]. There are numerous applications that has begun since after glass fiber hybrid composites have made

particularly in the electronic applications, printed wire boards, circuit boards etc [14,15,16]. The lay direction, Kevlar fibre angle, no of plies, resin to hardener ratio, volume fraction etc. are the key parameters in deciding the strength and other mechanical properties of the Kevlar / e-glass hybrid composites. Out of all the binding ability of the adhesive material and the resin, hardener majorly make the matrix phase that influence the overall competency of the composite.

II. EXPERIMENT

A. Preparation of the Specimen

In making the E-glass based composite with Kevlar-49 every layer is prepared with a thickness of about 0.5 mm coupled with the hardener and epoxy resin in a of industrial grade for strong adhesive quality for the preparation of the hybrid composites [17,18]. The fabrication begins with the sandwich manner in which the Kevlar-49 fiber is kept in the middle and the e-glass is covered from the top and bottom. In present experimental analysis the laminates of hybrid composites (P, Q, and R) are prepared as shown in Figure 1. During the fabrication the quantities of the epoxy resin & hardener are made with hand layup procedure. It is tabulated in Table I. The properties of materials viz E-glass, epoxy, and Kevlar are detailed in Table II [19,20].

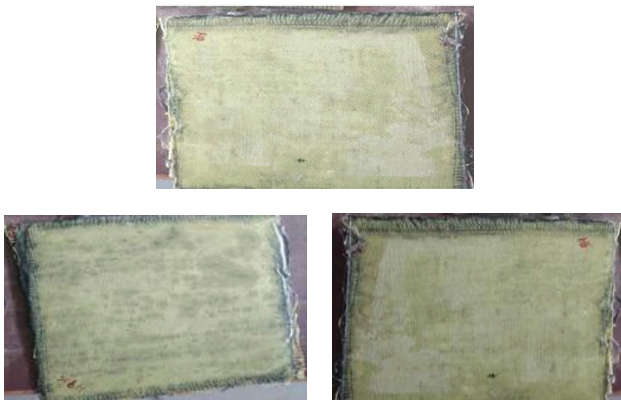


Figure 1. Fabricated Specimens using various ratios of resins

TABLE I.
LAYUP PROCEDURE OF FIBERS

Layer details	P	Q	R
No of layers	3	3	3
E-glass	2	2	2
Kevlar-49 fiber	1	1	1
epoxy/ resin	2	3	4
Hardener	3	2	1

TABLE II.
PROPERTIES OF MATERIALS

Parameter	E-glass	Kevlar	Epoxy
Strength of Fiber	340	2761	-
Strength of Laminate	1510	1445	13-41
Laminate Density (g/cc)	2.596	1.48	1-1.13
Strength to Weight ratio	559	989	27

B. Mechanical Testing-Tensile Test

It is a test intended to know the tensile strength of the given specimen. At first the specimens are shaped into the following shown Figure 2. and Figure 3. to insert them in the tensile testing machine. Usually there is no specific tensile testing machine but on the Universal testing machine only the tensile testing will be performed. The testing is performed as per the ASTM standards.



Figure 2. Test specimen for tensile testing in Universal testing machine



Figure 3. Tensile Test UTM machine

The 3 specimens are of dimensions thickness = 5mm, width = 24mm and length = 150mm are used for the tensile testing. The applied load will start from 0kN to and reach up to 5kN. For the three samples P,Q and R tensile strength, strain rate, ultimate load, ultimate stress and associated parameters will be found [21,22].

C. Removal (Peel) Test

The peel removal test is one of the important test that shows the ability of the plies of the composite material that bind together. There were many ways to perform this test out of which most commonly used tests are 90° and 180° [23,24]. Here in the present work the 90° peel removal test is used in this the plies are forcefully removed one after another gently perpendicular to the workpiece. See Figure 4.

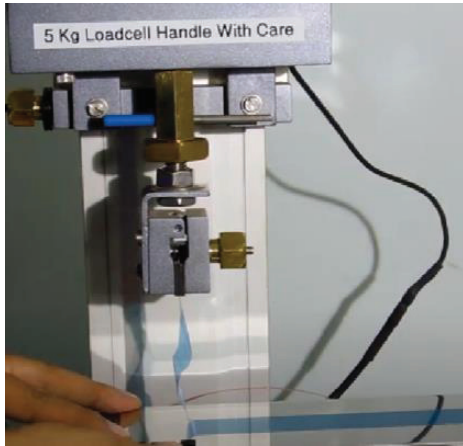


Figure 4. Peel removal test

For the 90° peel removal test. The more is the force required to peel off the strong is the material and its internal bonding, it is as simple as this and vice versa. The measurement of this peel removing is done as force required for unit length. That means N/mm. The results pertaining to the peel removal test are given in the results and conclusions section [25,26].

III. MECHANICAL TESTING

A. Testing of *HARDNESS*

Hardness of the composite material is one of the significant parameters to be considered while defining its strength. Here in the present work the hardness of the composite material is been tested on the Rockwell hardness test machine that can show the C number based on that its hardness characteristics can be defined. As shown in the Figure 5, the prepared composite material sample is kept on the pan and an indenter will apply force on the surface of the material and based on the impression made by the indenter the hardness value will be computed, in other words hardness is the ability of the material to withstand the load against failure. The results of the hardness test are given in the results and discussion section [27,28,29].

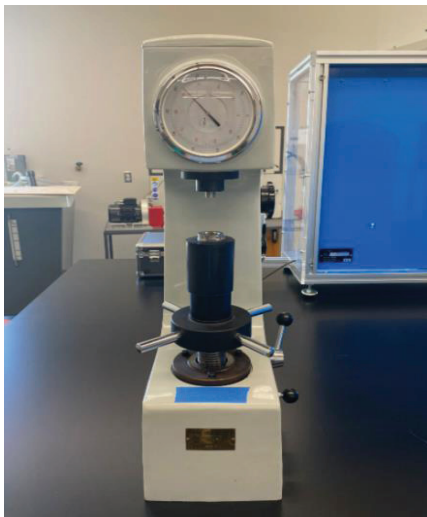


Figure 5. Rockwell hardness testing

B. Testing of *Density*

This is one of the fundamental and important tests to ascertain the packing of the material in the given volume. It will lay an arena to understand the material dispersity and uniformity of packing within the given volume. The dimensions of prepared composite specimen considered for testing of the density is length = 24 mm, width = 24 mm and thickness = 0.2 mm. The density of the sample is found by keeping the sample in the cuboid channel closely such that no gaps will be found and based on the weight of the material that has occupied for unit volume its density will be assessed and can be expressed in $\frac{N}{mm^2}$ [30,31].

C. Water Absorption Test

This is the test performed to assess the ability of the composite material to show its intendedness to absorb the water. This quality of the material to absorb the water when immersed in the water containing vessel signifies the quality of the material [32,33]. To perform the test at first the sample is weighed and then it is immersed completely in distilled water for about 24 hours at room temperature i.e., 30°C as shown in Figure 6. After the time got lapsed then the sample is been taken out and then its weight will be tested based on the difference in the weights the composite material strength will be assessed.



Figure 6. Test set up for water absorption

IV. RESULTS AND DISCUSSIONS

A. Tensile Test

The results of the tensile test are given in the below Figure 7., Figure 8. and Figure 9. As the 3 samples are prepared from 3 different compositions the variations in the tensile strength are clearly distinguished. From the Figure 7. For the sample P it can be evident that at the strain of 3 mm the tensile strength has changed the slope and increased steeply. The highest tensile strength is observed as 1987 MPa at strain of 5.87mm.

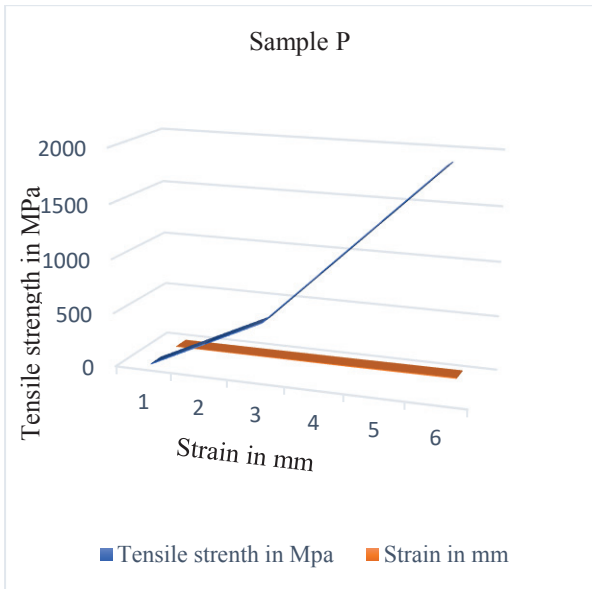


Figure 7. Sample P

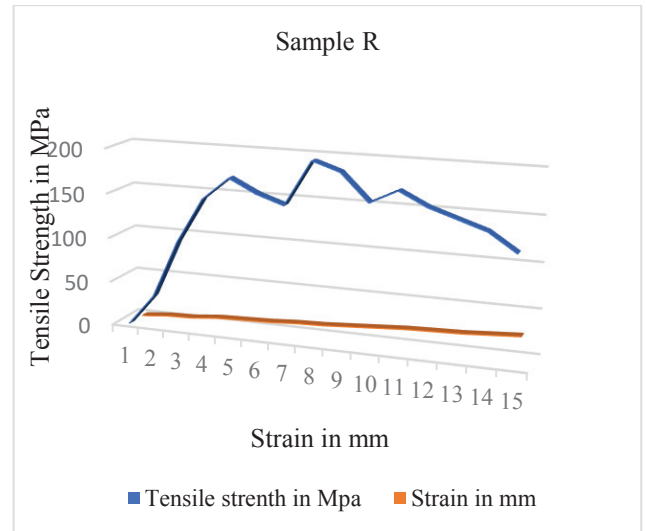


Figure 9. Sample R

From the Figure 9 For the sample R the strength vs strain curve is quite similar to the mild steel. That is the test results have yielded similar properties of isotropic material such as mild steel or aluminum even though the material used is an anisotropic (composite material). The tensile strength is increased till 3.5mm of strain and its value has reached 145 MPa and then it reached to local peak of 160 MPa at 4.5 mm. Then it fell down to a value of 142 MPa at 6.7 mm of strain. In similar fashion it has attained to a peak of 175 MPa for the strain of 7.8mm. Then it went on declining and reached to least value of 105 MPa for the strain of 14.8mm.

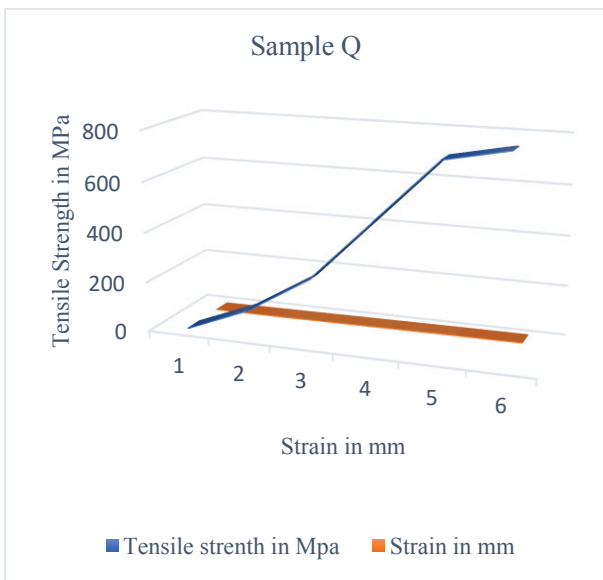


Figure 8. Sample Q

From the Figure 8. For the sample Q it can be evident that at the strain of 3 mm the tensile strength has changed the slope and increased steeply again at the strain of 5 mm the tensile strength has changed its slope and shown a steady downfall. However, the net tensile strength is increased to the end and its value is found to be maximum at 6 mm of strain and corresponding tensile strength is 779 MPa.

B. Peel off Test

Peel off test results shows the significant outcomes in terms of binding strength of the composite material. From Figure 10, Figure 11 and Figure 12 it can be seen that for the sample Q there is a steady and uniform range in peel force is observed. For the sample P and sample R the peel off force has shown more variations in the considered range. As the three samples were made from three different sources of materials hence the peel off force required is also altered accordingly. But as a whole the sample P, Q have resulted in similar outcomes and sample R has shown quite less peel off force.

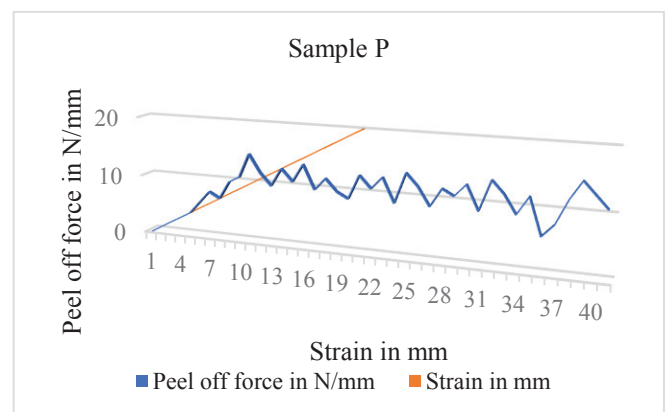


Figure 10. Sample P

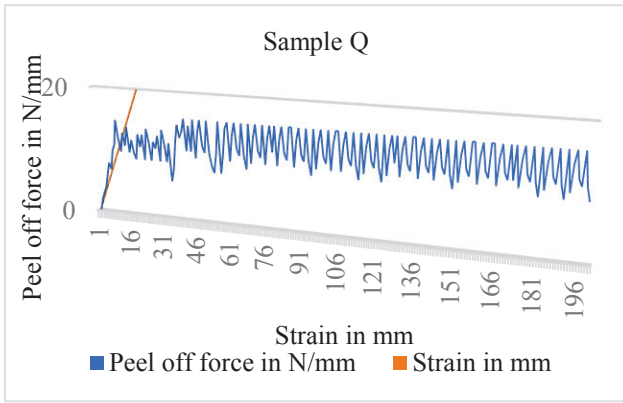


Figure 11. Sample Q

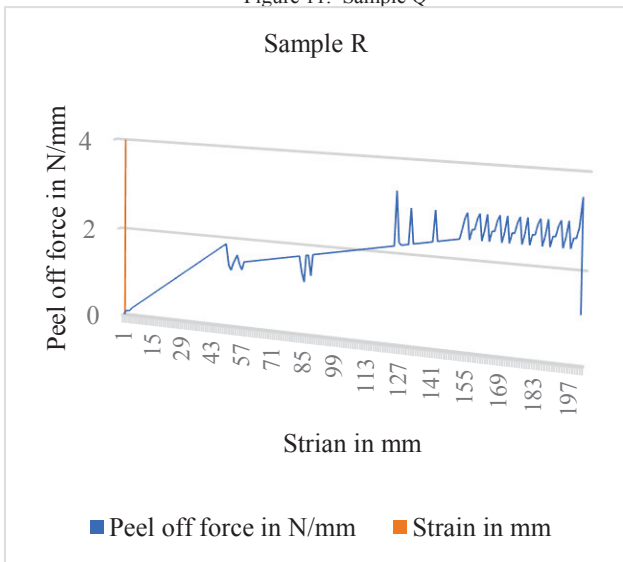


Figure 12. Sample R

C. Hardness Test

The hardness for the samples P,Q and R have resulted in different outcomes as it can be seen in Figure 13. Sample P has obtained the hardness value of 94.887 and sample Q has observed 91.66 and sample R has observed 83.67. From this outcomes it can be witnessed that sample P is harder among the three samples and sample R is least in hardness.

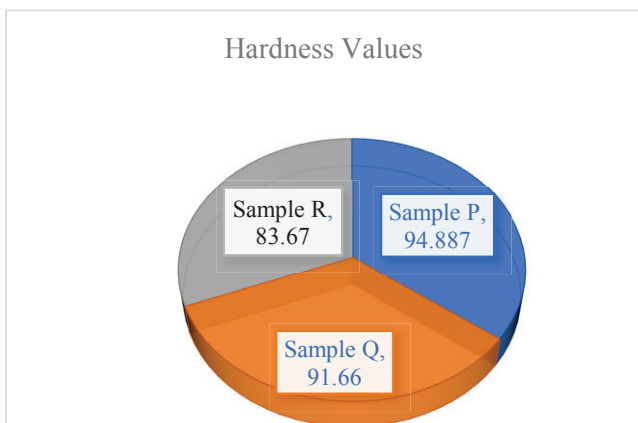


Figure 13. Hardness test results

D. Density Test

The outcomes of the density test are given below in Figure 14. In the graph three parameters are interpreted and they have shown the sample P density is higher than other samples and the density is found least for sample R. However, sample Q and R density are nearer compared P and Q. The weights and Mean values are also obtained in similar fashion.

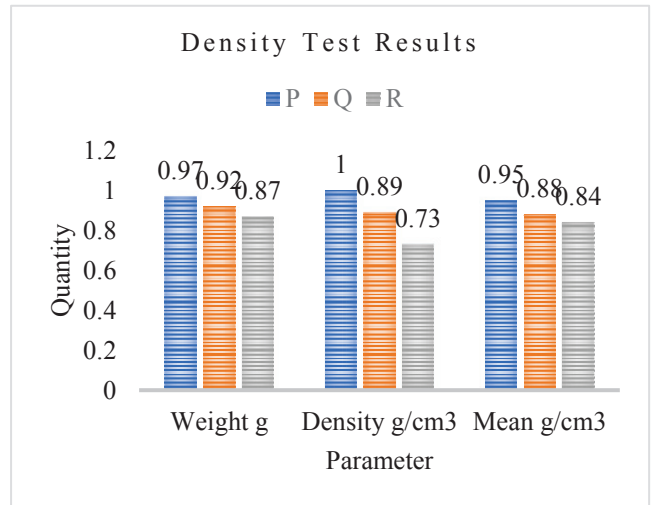


Figure 14. Density test results

E. Water Absorption Test

The water absorption test has yielded the result of material strength with respect to swelling ratio. The swelling ratio can be calculated using below equation no 1.

$$\text{Swelling ratio \%} = \left(\frac{\text{Wet laminate} - \text{Dry Laminate}}{\text{Dry laminate}} \right) * 100 \quad (1)$$

Out of the three samples analyzed the sample B has got more swollen and its swelling ratio is 1.31 followed by A 1.23 and least swelling ratio is for sample C i.e., 1.19. Usually, the materials with less swelling ratio are preferable for all practical purposes.

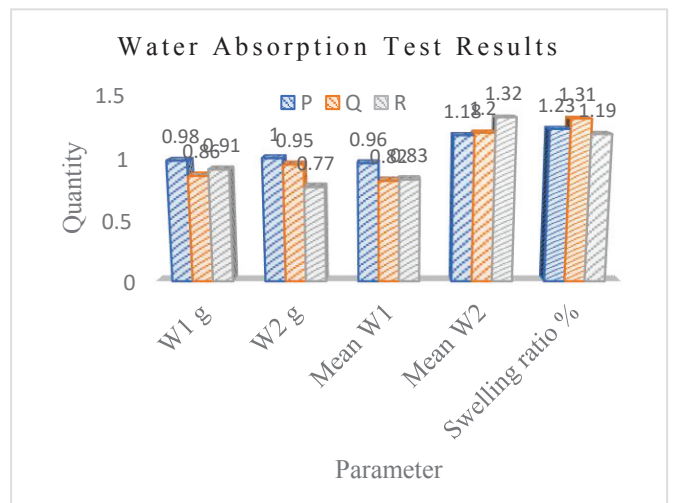


Figure 15. Water absorption test results

V. CONCLUSIONS

From the above experimental analysis, it can be concluded that the samples three have shown the significant outcomes with respect to the mechanical properties. However, the following observatory conclusions are arrived by the end of the experimental and testing work.

- Tensile test has shown that P is stronger than other two.
- Peel off test has shown that sample P and Q are moderate and sample R is stronger.
- According to hardness test sample P is harder among all.
- As per density test sample P is denser than all other samples.
- As per water absorption test Q and P are stronger followed by R.

As a whole sample P is preparatory method and composition is suggested for further analytical investigations.

REFERENCES

- [1] P V Sai Swaroop, A. Suresh, Effects of Fiber Orientation on Mechanical Properties and Analysis of Failures for Kevlar Epoxy Reinforced Composites, CVR Journal of Science and Technology, June 2021, 142-146, DOI: 10.32377/cvrjst2022.
- [2] Ms. B Reetha, Mr. B. Nikhil, P. Mamatha, A. Suresh, Evaluation of Mechanical Properties and Simulation of Kevlar Epoxy Reinforced Composite with Silicon Carbide filler, International Journal of Advances in Engineering and Management, Volume 3, Issue 5 May 2021, pp: 33-42, DOI: 10.35629/5252-03053342.
- [3] Kashif, M.; Ngaini, Z.; Harry, A.V.; Vekariya, R.L.; Ahmad, A.; Zuo, Z.; Alarifi, A. An experimental and DFT study on novel dyes incorporated with natural dyes on titanium dioxide (TiO₂) towards solar cell application. *Appl. Phys. A* 2020, 126, 1–13.
- [4] A Suresh, P Bhargavi, M Kiran Kumar, Simulation and Mechanical Characterization on Kevlar epoxy reinforced composite with silicon carbide filler, *Materials Today: Proceedings*, June 2020, Volume 38, Part 5, 2021, Pages 2988-2995, <https://doi.org/10.1016/j.matpr.2020.09.321>
- [5] Zhang, X.Z.; Xu, P.H.; Liu, G.W.; Ahmad, A.; Chen, X.H.; Zhu, Y.L.; Qiao, G.J. Synthesis, characterization and wettability of Cu-Sn alloy on the Si-implanted 6H-SiC. *Coatings* 2020, 10, 906.
- [6] Aravind, M.; Ahmad, A.; Ahmad, I.; Amalanathan, M.; Naseem, K.; Mary, S.M.M.; Zubair, M. Critical green routing synthesis of silver NPs using jasmine flower extract for biological activities and photocatalytic degradation of methylene blue. *J. Environ. Chem. Eng.* 2020, 9, 104877.
- [7] Hussain, S.; Khan, A.J.; Arshad, M.; Javed, M.S.; Ahmad, A.; Shah, S.S.A.; Khan, M.R.; Akram, S.; Zulfqar, Ali, S.; et al. Charge storage in binder-free 2D-hexagonal CoMoO₄ nanosheets as a redox active material for pseudocapacitors. *Ceram. Int.* 2020.
- [8] Saleem, M.; Irfan, M.; Tabassum, S.; Alotman, Z.; Javed, M.S.; Hussain, S.; Zubair, M. Experimental and theoretical study of highly porous lignocellulose assisted metal oxide photoelectrodes for dye-sensitized solar cells. *Arab. J. Chem.* 2020, 14, 102937.
- [9] Mr. A. Suresh, Ms. B. Vidhya Darshini, C. Laxmi Sruthi, Madhusudhan Reddy, Mechanical Characterization and Failure analysis of Kevlar epoxy reinforced composites with alterations in fiber orientations, 2021, National Conference on Recent Innovations in Science and Technology, CVR College of Engineering, Hyderabad.
- [10] Madkour, L.H. *Nanoelectronic Materials: Fundamentals and Applications*; Springer: Berlin/Heidelberg, Germany, 2019; Volume 116.
- [11] Zhan, M.; Hussain, S.; AlGarni, T.S.; Shah, S.; Liu, J.; Zhang, X.; Liu, G. Facet controlled polyhedral ZIF-8 MOF nanostructures for excellent NO₂ gas-sensing applications. *Mater. Res. Bull.* 2021, 136, 111133.
- [12] Kashif, M.; Jaafar, E.; Bhadja, P.; Low, F.W.; Sahari, S.K.; Hussain, S.; Al-Tamrah, S.A. Effect of potassium permanganate on morphological, structural and electro-optical properties of graphene oxide thin films. *Arab. J. Chem.* 2020, 14, 102953.
- [13] Tang, L.; Dang, J.; He, M.; Li, J.; Kong, J.; Tang, Y.; Gu, J. Preparation and properties of cyanate-based wave-transparent laminated composites reinforced by dopamine/POSS functionalized Kevlar cloth. *Compos. Sci. Technol.* 2019, 169, 120–126.
- [14] Pandey, J.; Nagarajan, V.; Mohanty, A.K.; Misra, M. Commercial potential and competitiveness of natural fiber composites. In *Biocomposites*; Elsevier: Amsterdam, The Netherlands, 2015; pp. 1–15.
- [15] Ahmad, A.; Mubharak, N.M.; Naseem, K.; Tabassum, H.; Rizwan, M.; Najda, A.; Hussain, S. Recent advancement and development of chitin and chitosan-based nanocomposite for drug delivery: Critical approach to clinical research. *Arab. J. Chem.* 2020, 13, 8935–8964.
- [16] Reis, P.N.; Neto, M.A.; Amaro, A.M. Effect of the extreme conditions on the tensile impact strength of GFRP composites. *Compos. Struct.* 2018, 188, 48–54.
- [17] Mustafa, E.H.B.; Dyadyura, K.; Jan, V.; Harničárová, M.; Zajac, J.; Modrák, V.; Pandová, I.; Vrábek, P.; Nováková-Marcinčinová, E.; Pavelek, Z. *Manufacturing Technology of Composite Material Structure*; Sudan University of Science and Technology: Khartoum, Sudan, 2017.
- [18] Xiong, J.; Du, Y.; Mousanezhad, D.; Asl, M.E.; Norato, J.; Vaziri, A. Sandwich structures with prismatic and foam cores: A review. *Adv. Eng. Mater.* 2019, 21, 1800036.
- [19] Kwonpongsagoon, S.; Jareemit, S.; Kanchanapiya, P. Environmental impacts of recycled nonmetallic fraction from waste printed circuit board. *Int. J. Geomate* 2017, 12, 8–14. [CrossRef]
- [20] Qi, L.; Ju, L.; Zhou, J.; Li, S.; Zhang, T.; Tian, W. Tensile and fatigue behavior of carbon fiber reinforced magnesium composite fabricated by liquid-solid extrusion following vacuum pressure infiltration. *J. Alloys Compd.* 2017, 721, 55–63.
- [21] Pervaiz, M.; Ahmad, I.; Yousaf, M.; Kim, S.; Munawar, A.; Saeed, Z.; Rashid, A. Synthesis, spectral and antimicrobial studies of amino acid derivative Schiff base metal (Co, Mn, Cu, and Cd) complexes. *Spectrochim. Acta Part A Mol. Biomol. Spectrosc.* 2019, 206, 642–649.
- [22] Rajesh Kumar, G.; Hariharan, V.; Saravanakumar, S.S. Enhancing the free vibration characteristics of epoxy polymers using sustainable phoenix Sp. fibers and nano-clay for machine tool applications. *J. Nat. Fibers* 2019, 1–8.
- [23] Kabir, S.M.F.; Mathur, K.; Seyam, A.M. A critical review on 3D printed continuous fiber-reinforced composites: History, mechanism, materials and properties. *Compos. Struct.* 2020, 232, 111476.
- [24] Anjum, N.; Suresha, B.; Prasad, S.L.A. Influence of Water ageing on mechanical properties of CaCO₃ filler filled epoxy resin and sansevieria/carbon fiber reinforced composites. *Open J. Compos. Mater.* 2019, 9, 1–20.
- [25] Liu, M.; Rohde, B.J.; Krishnamoorti, R.; Robertson, M.L.; Dawood, M. Bond behavior of epoxy resin–

- polydicyclopentadiene phase separated interpenetrating networks for adhering carbon fiber reinforced polymer to steel. *Polym. Eng. Sci.* 2019, 60, 104–112.
- [26] de Souza, L.C.; Rodrigues, N.S.; Cunha, D.A.; Feitosa, V.P.; Santiago, S.L.; Reis, A.; Loguercio, A.D.; Paris, T.; Saboia, V.d.A.; Perdigao, J. Two-year clinical evaluation of proanthocyanidins added to a two-step etch-and-rinse adhesive. *J. Dent.* 2019, 81, 7–16.
- [27] Braga, R.; Magalhaes, P., Jr. Analysis of the mechanical and thermal properties of jute and glass fiber as reinforcement epoxy hybrid composites. *Mater. Sci. Eng. C* 2015, 56, 269–273.
- [28] A. Suresh, A. Sai Kiran Goud, R. Srilekha, A. Praneeth, Testing and analysis of Kevlar epoxy reinforced composites made from 3D printing process, 2021, National Conference on Recent Innovations in Science and Technology, CVR College of Engineering, Hyderabad.
- [29] Xavier, J.; Rodney, K.D.; Prakash, S.J. Mechanical characterisation of epoxy polymer composite reinforced with ramie and synthetic fiber. *SSRN Electron. J.* 2019. [CrossRef]
- [30] Kader, W.B. Physico-mechanical properties of typha angustata (elephant grass) fiber reinforced thermoplastic composites. *IJAR J.* 2019.
- [31] Dolan, G.K.; Cartwright, B.; Bonilla, M.R.; Gidley, M.J.; Stokes, J.R.; Yakubov, G. Probing adhesion between nanoscale cellulose fibres using AFM lateral force spectroscopy: The effect of hemicelluloses on hydrogen bonding. *Carbohydr. Polym.* 2019, 208, 97–107. [CrossRef]
- [32] Dia, A.; Dieng, L.; Gaillet, L.; Gning, P.B. Damage detection of a hybrid composite laminate aluminum/glass under quasi-static and fatigue loadings by acoustic emission technique. *Heliyon* 2019, 5, e01414.
- [33] Phuong, P.T.M.; Won, H.J.; Oh, Y.J.; Lee, H.S.; Lee, K.D.; Park, S.Y. The chemistry and engineering of mussel-inspired glue matrix for tissue adhesive and hemostatic. *J. Ind. Eng. Chem.* 2019, 80, 749–756.

Modelling and Analysis of Domestic Windmill Turbine Blade

Mada Rukmini Sai Rupa Sri

Asst. professor, CVR College of Engineering/Mechanical Engg. Department, Hyderabad, India

Email : mada.rukmini@gmail.com

Abstract: Blade is the key component to capture wind energy. It plays a vital role in the whole wind turbine. The optimum twist of a windmill turbine blade is analyzed on the basis of elementary blade- element theory. Maximum efficiency of power is achieved when the blade is twisted consistently with a program that depends on variation of sectional lift and drag coefficients with angle of attack. For a typical airfoil cross-section, optimum angle of attack decreases from maximum lift coefficient angle of attack at the blade root to greater than 80 percent of this value at the blade tip

The modelling is done in SolidWorks and the static and dynamic analysis is carried out by using ANSYS software. The materials used are stainless steel, e-glass epoxy and grey cast iron. The blade is subjected to FEA studies to demonstrate its ability to withstand the extreme loading conditions as defined in the international offshore wind standards. The results will have acceptable performance with regard to total deformation, directional deformation, equivalent stress, normal and shear stress.

Index Terms: Windmill, efficiency, epoxy resin

I. INTRODUCTION

A turbine is a device that converts the wind's Kinetic Energy into electricity. They are an increasingly important source of intermittent renewable energy and are utilized in many countries to lower energy costs and reduce reliance on fossil fuels. Wind has the lowest relative greenhouse emission, smallest amount water consumption demands and therefore the most favorable social impacts in comparison to photovoltaic, hydro, geothermal, coal and gas [1] [3]. Smaller wind turbines are used for applications like battery charging for auxiliary power for boats or caravans, and to power traffic warning signs. While larger turbines can contribute towards domestic power supply while selling unused power back to the utility supplier via the electrical grid [6].

Wind turbines are manufactured during a wide selection of sizes, with horizontal or vertical axes. It is estimated that thousands of huge turbines, in installations referred to as wind farms, generate over 650 gigawatts of power, with 60 GW added annually. Wind turbines are classified by the wind speed. They are designed for, from class I to class III, with A to C pertaining to the turbulence intensity of the wind [5]. There are two basic sorts of wind turbines: Horizontal-axis turbines and Vertical-axis turbines. There are also sub types of vertical axis wind turbines namely Darrieus wind turbine, Giromill turbines and Savinuous turbines [2] [4].

The size of wind turbines varies widely. The length of the blades determines the quantity of electricity a turbine can generate. Small wind turbines which will power one home may have an electricity generating capacity of 10 kilowatts (kW). The largest wind turbines have electricity generating

capacities of up to kilowatts (10 megawatts), and bigger turbines are in development [8] [9]. Large turbines are often grouped together to make wind generation plants, or wind farms, that provide power to electricity grids.

II. WIND TURBINES AND BLADES

A. Wind turbine working:

According to Betz's law, maximum achievable extraction of wind power by a wind turbine as $16/27$ (59.3%) times the rate at which the kinetic energy of the air arrives at the turbine [7].

Small wind turbines or Domestic wind turbines could also be used for spread of applications including on- grid or off-grid residences, telecom towers, rural schools and clinics, remote monitoring, offshore platforms and other purposes that need energy where there's no electric grid, or where the grid is unstable. Small wind turbines could also be as small as a fifty-watt generator for boat or caravan use [10]. Hybrid solar and wind powered units are increasingly getting used for traffic signage, particularly in rural locations, as they avoid the necessity to get long cables from the closest mains connection point [6].

A turbine turns wind energy into electricity using the force from the rotor blades, which works like an airplane wing or helicopter rotary wing as shown in figure 1. When wind flows across the blade, the atmospheric pressure on one side of the blade decreases. The difference in atmospheric pressure across the two sides of the blade creates both lift and drag. If the force of the lift is stronger than the drag, it causes the rotor to spin. The rotor is connected to the generator, either directly (if it's an immediate drive turbine) or through a shaft and a series of gears (a gearbox) that speed up the rotation and allow for accommodating smaller generator as in figure 1. This translation of force to rotation of a generator creates electricity.

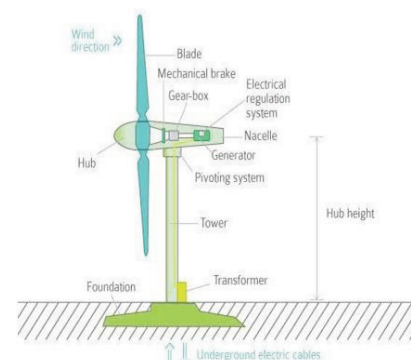


Figure 1. Working of the turbine

B. Windmill Turbine Blades:

Most wind turbines designed for the production of electricity consists of a two or three bladed propeller rotating around a horizontal axis. These propeller like turbine blade designs convert the energy of the wind into usable shaft power called torque. This is achieved by extracting the energy from the wind by slowing it down or decelerating the wind as it passes over the blades. The forces which decelerate the wind are equal and opposite to the thrust type lifting forces which rotates the blades [4].

Just like an aero plane wing, turbine blades work by generating lift through their curve. The side with the foremost curve generates low atmospheric pressure while high air beneath pushes on the opposite side of the blade shaped aerofoil.

This results in a lifting force perpendicular to the direction of flow of the air over the turbines blade. The rotary wing is designed to create the proper amount of rotary wing lift and thrust producing optimum deceleration of the air and therefore better blade efficiency.

If the turbines propeller blades rotate too slowly, it allows an excessive amount of wind to undergo undisturbed, and thus doesn't extract the maximum amount energy because it potentially could. On the opposite hand, if the propeller blade rotates too quickly, it appears to the wind as an oversized flat rotating disc, which creates an oversized amount of drag.

Generally, turbine blades are shaped to get the utmost power from the wind at the minimum construction cost. But turbine blade manufacturers are always looking to develop a more efficient blade design [8]. Constant improvements within the design of wind blades have produced new turbine designs which are more compact, quieter and are capable of generating more power from less wind. It is believed that by slightly curving the turbine blade, they are ready to capture 5 to 10 percent more wind energy and operate more efficiently in areas that have typically lower wind speeds.

Wind turbine blades are of following types as in Fig 2:

1. Flat blades
2. Curved blades
3. Aerofoil blades and
4. Twisted blades

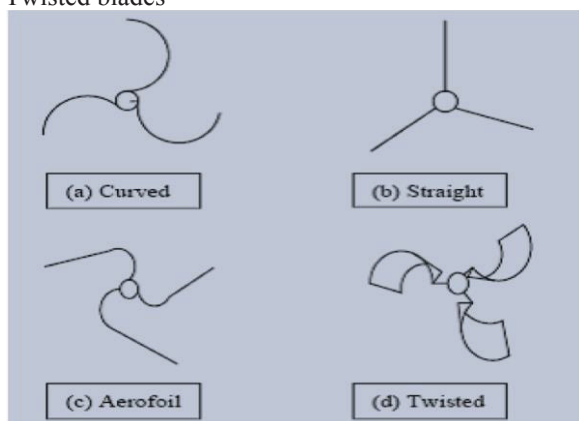


Figure 2. Types of the turbine blade

Flat or straight blade designs offer significant benefits compared to other wind blade designs. Flat rotor blades are easy and cheap to trim from sheets of plywood or metal

ensuring that the blades have a uniform shape and size [1] [4]. They are also the simplest turbines that require less design and construction skills, but their efficiency and therefore the generating electric power is extremely low. Hence the blades of the turbine are designed as straight or flat as shown in figure 3.

III. DESIGN CONSIDERATIONS

A. Modelling of turbine blade

The modelling of turbine blade is done in SOLIDWORKS 2020 SP5 in SLDDRW drawing file and is saved in IGES format. Structural and transient dynamic analysis is carried out in ANSYS 14.5. Fig 3 is the front view; Fig 4 is the side view and Fig 5 is the top view shows the model draft of turbine blades.

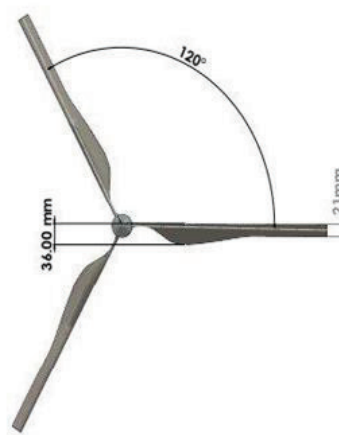


Figure 3. Front View of the turbine

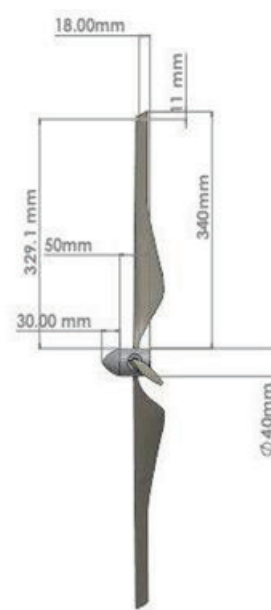


Figure 4. Side View of the turbine

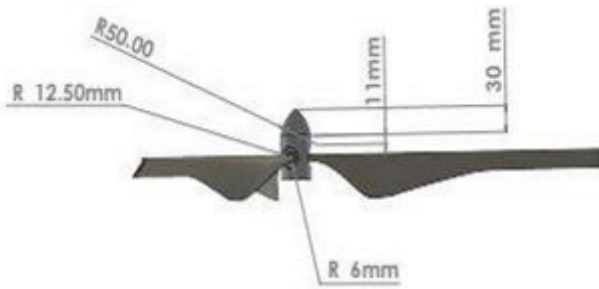


Figure 5. Top View of the turbine

B. Material Considerations

Materials like steel, irons or cast irons, aluminum, fibers, composites and plastics are most widely used in the manufacturing of turbine blades. Considering this stainless steel, grey cast iron and e glass epoxy are used for the design analysis of turbine blade.

Stainless Steel - Grade 304 (UNS S30400) is used for its good corrosion resistance, lower weight, good formability and weld ability. Table I shows properties of stainless steel.

TABLE I.
PROPERTIES OF STAINLESS STEEL

Density	7.85-8.06 mg/m3
Compressive strength	205-310 MPa
Ductility	0.3-0.57
Endurance limit	175-260 MPa
Hardness	1700-2100 MPa
Modulus of rupture	205-310 MPa
Shear modulus	74-81 GPa
Tensile strength	510-620 MPa
Young's modulus	190-203 GPa

JIS G5501 FC200 gray cast iron is used for its density and mechanical properties. Table II shows properties of gray cast iron.

TABLE II.
PROPERTIES OF GREY CAST IRON

Density	7.15 g/cm3
Compressive strength	115-205 MPa
Ductility	0.3-0.57
Endurance limit	175-260 MPa
Hardness	755 MPa
Modulus of rupture	205-310 MPa
Shear modulus	41 GPa
Tensile strength	115-205 MPa
Young's modulus	92.4 GPa

AW 106 Epoxy glass material is used for its toughness, resilience and resistance to dynamic loading. Table III shows properties of epoxy glass.

TABLE III.
PROPERTIES OF EPOXY GLASS

Density	2.6 Kg/Mm ³
Compressive Strength	450 MPa
Ductility	0.8-0.97
Endurance Limit	275 MPa
Hardness	920 MPa
Modulus Of Rupture	350-380 MPa
Shear Modulus	1.7-2.6 GPa
Tensile Strength	900 MPa
Young's Modulus	20 GPa

C. Structural Analysis

Structural analysis on blades is carried out in ANSYS at 750N, 1500N and 2000N for the total deformation, equivalent stress and strain at different loads.

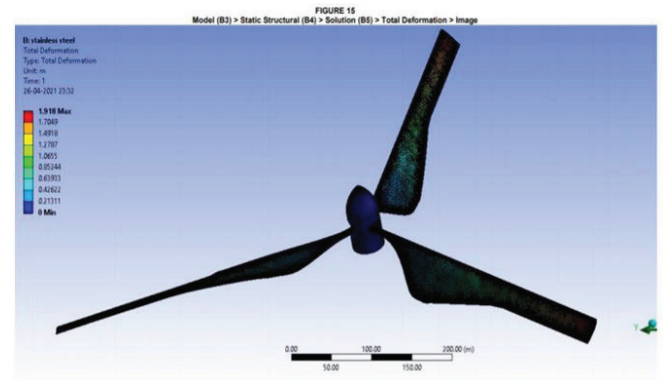


Figure 6. Total deformation of Stainless steel

Fig.6 shows the total deformation in stainless steel and it is observed that the maximum value is 1.198m.

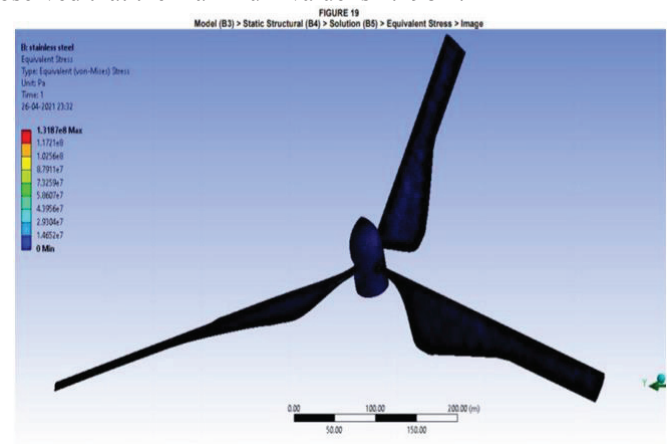


Figure 7. Equivalent Stress of Stainless Steel

Fig.7 shows the equivalent stress in stainless steel, and it is observed that the maximum value of stress is 1.318e8 Pa.

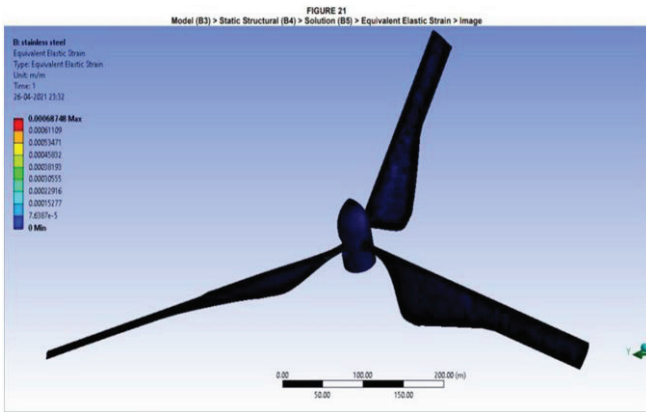


Figure 8. Equivalent Strain of Stainless Steel

Fig.8 shows the equivalent strain in stainless steel and it is observed that the maximum value is 0.000305.

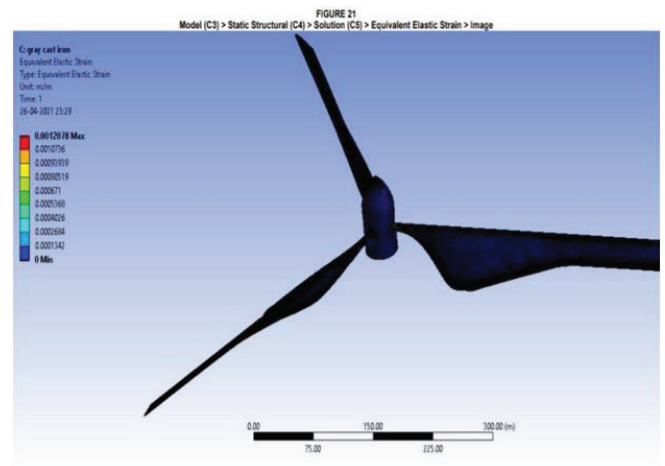


Figure 11. Equivalent Strain of Gray Cast Iron

Fig.11 shows the equivalent strain in gray cast iron and it is observed that the maximum value is 0.005368.

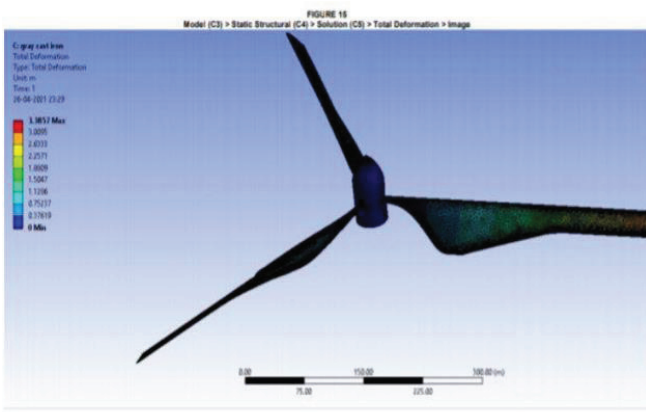


Figure 9. Total deformation of Gray Cast Iron

Fig.9 shows the total deformation in gray cast iron and it is observed that the maximum value is 0.75m.

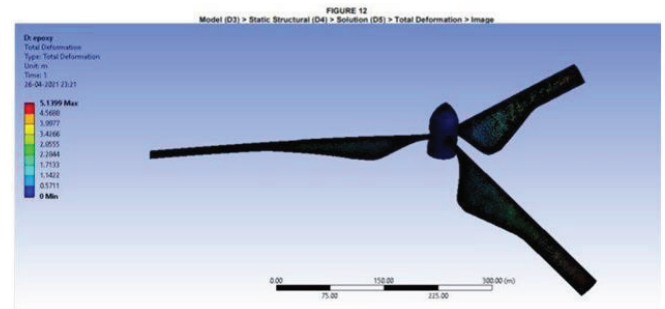


Figure 12. Total deformation of Epoxy Glass

Fig.12 shows the total deformation in epoxy glass and it is observed that the maximum value is 3.42m.

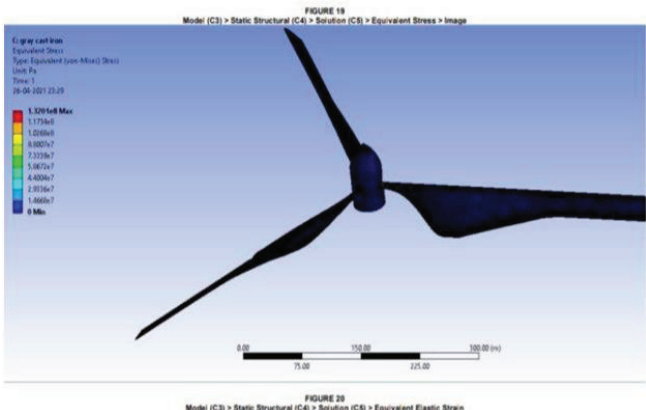


Figure 10. Equivalent Stress of Gray Cast Iron

Fig.10 shows the equivalent stress distribution in gray cast iron, and it is observed that the maximum value is 1.06e8 Pa.

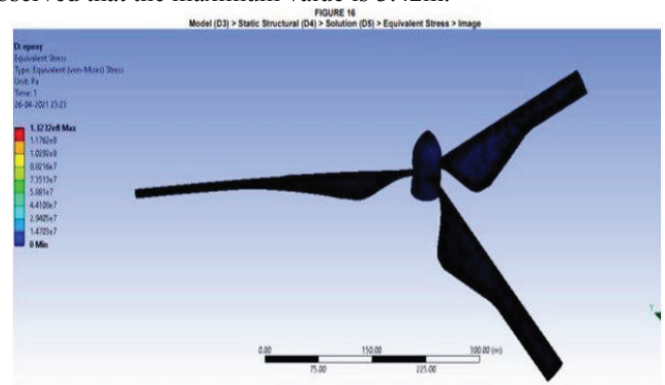


Figure 13. Equivalent Stress of Epoxy Glass

Fig.13 shows the distribution of equivalent stress in epoxy glass, and it is observed that the maximum value is 8.82e7 Pa.

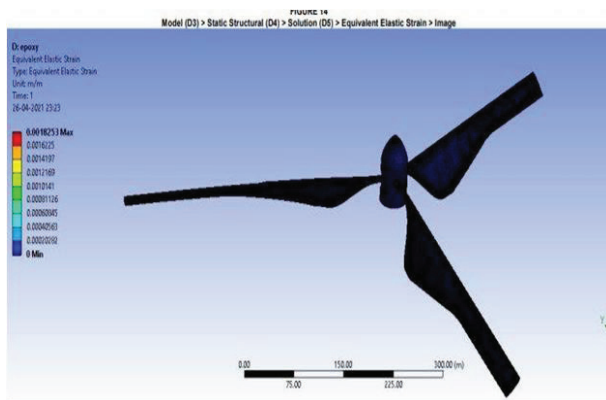


Figure 14. Equivalent Strain of Epoxy Glass

Fig.14 shows the total deformation in stainless steel and it is observed that the maximum value is 0.004256.

IV. RESULTS AND DISCUSSIONS

TABLE IV.

A) RESULTS OF ANALYSIS AT 750 N

Material	Total Deformation (m)	Equivalent Stress (Pa)	Equivalent Strain
Stainless Steel	0.92	6.03e7	0.000305
Gray Cast Iron	0.75	2.93e7	0.0002684
Epoxy Glass	1.14	2.912e7	0.004256

B) RESULTS OF ANALYSIS AT 1500 N

Material	Total Deformation (m)	Equivalent Stress (Pa)	Equivalent Strain
Stainless Steel	1.27	7.36e7	0.00045
Gray Cast Iron	1.12	5.86e7	0.0005368
Epoxy Glass	2.28	5.88e7	0.000603

C) RESULTS OF ANALYSIS AT 2000 N

Material	Total Deformation (m)	Equivalent Stress (Pa)	Equivalent Strain
Stainless Steel	1.918	1.318e8	0.000687
Gray Cast Iron	1.5	1.06e8	0.000805
Epoxy Glass	3.42	8.82e7	0.00121

The Table IV shows the total deformation, equivalent stress and strain for stainless steel, gray cast iron and epoxy glass at 750 N, 1500 N and 2000N. From the analysis results of turbine blade, it is observed that the material STAINLESS STEEL is the preferable material with desirable physical and mechanical properties for turbine blade. Also, it has less deformation under the given loads than the other two materials i.e., grey cast iron and epoxy glass. The analysis carried out on various materials above will make an impressive mark in the field of renewable energy.

REFERENCES

- [1] K. Sunil Kumar, R. Palanisamy, S. Aravindh and G.S. Mohan, "Design and Analysis of Windmill Blades for Domestic Applications," International Journal for Mechanical Engineering and Technology, 8(1), pp.25-36, 2017.
- [2] Gajjala Naresh Kumar Reddy and C Raghunath Reddy, "Design and Analysis Of Domestic Windmill Blades," International Journal of Engineering Science and Computing Volume 7, Issue 7 pp. 13778-13786, 2017.
- [3] J. Schubel and Richard J. Crossley, "Wind Turbine Blade Design," Multidisciplinary Digital Publishing Institute Journal, Volume 5, pp. 3425-3449, 2012.
- [4] Vaibhav R .Pannase, Prof. H. R. Bhagat, and Prof. R. S. Sakarkar, "Optimization Design, Modeling And Dynamic Analysis For Wind turbine Blade," International Journal of Engineering Research and Applications (IJERA), Volume 3, Issue 4, pp. 385-389, 2013.
- [5] Deepak J N, Chandan R, and Doddanna K, "Design and structural analysis of a small windmill turbine blade," International Research Journal of Engineering and Technology, International Research Journal of Engineering and Technology (IRJET), Volume 4, Issue: 11, 2017.
- [6] Hynbum Park, "Design and Evaluation of Glass/epoxy Composite Blade and Composite Tower Applied to Wind Turbine," IOP Conference Series: Materials Science and Engineering, 2018.
- [7] K. Ansal Muhammed, C. Ramesh Kannan, B. Stalin and M. Ravichandran, "Experimental investigation on AW 106 Epoxy/E-Glass fiber/nano clay composite for wind turbine blade," Materials today- proceedings, Volume 21, Part 1, pp.202-205, 2020.
- [8] Jialin Zhang, Zhenggui Zhou and Yansheng Lei, "Design and research of high-performance low-speed wind turbine blades," IEEE, 2009.
- [9] T. Vishnuvardhan and B. Durga Prasad, "Fabrication and Evaluating the Performance of Small Size Wind Turbine Blades with R21 and R22 Profiles," i-scholar- Automation and Autonomous Systems, Volume 3, Issue 7, pp. 327-330, 2011.
- [10] Leon Mishnaevsky Jr., Kim Branner, Helga Nørgaard Petersen, and Justine Beauson, Malcolm McGugan and Bent F. Sørensen, "Materials for Wind Turbine Blades: An Overview," Multidisciplinary Digital Publishing Institute Journal, Volume 10, pp. 1-24, 2017.

Modelling and Fabrication of Hexagonal Turret on Engine Lathe

K. L.N. Murthy

Asst. Professor, Sreyas Institute of Engineering and Technology/Mechanical Engg. Department, Hyderabad, India
Email: klnmurthy1986@gmail.com

Abstract: The aim of this paper is developed from two different lathe machines, i.e. Centre Lathe and Turret Lathe and the main aim of this work is to Model and develop a tool post that can hold six cutting tools, and replace square tool post in center lathe machine. The different tools like a parting tool, turning tool (right hand turning tool or left-hand turning tool), forming tool, thread cutting tool, chamfering tool and knurling tool are enclosed in the turret where it mainly help in reducing the time which is required to change the tool and help in increasing of productivity of the lathe machine. The Modelling and analysis work of this turret is done in SolidWorks 2018. Material used for metal prototype is mild steel and Fabrication process is done by using the milling machine, radial drilling machine and lathe machine.

Index Terms: lathe, Machining, Turret, tools.

I. INTRODUCTION

A lathe is a machine tool that rotates a work piece about an axis of rotation to perform various operations such as cutting, sanding, knurling, drilling facing, and turning, with tools that are applied to the work piece to create an object with symmetry about that axis[1]. The first machine tool developed was around 1300 B.C., earlier was a tree lathe which was a device for rotating and machining a workpiece. The workpiece kept between two adjacent trees and a rope would round the work with its one end attached to a flexible branch of trees and the other end is pulled by a man to rotate the job. Lathes are manufactured in a variety of types and sizes, from very small bench lathes used for precision work to huge lathes used for turning large steel shafts [2]. However, these lathes have been classified into several types in later stages such as Center lathe, capstan Lathe, Turret Lathe, Automatic Lathe, etc.

The main advantage of using lathe machine is that it can be used for various machining operations such as Step and Taper turning, knurling, various forms of treads, Boring, drilling etc., with and without using special cutting tool attachments on it. Metal cutting or machining is the process of producing work piece by removing unwanted material from a block of metal, in the form of chips [3]. For any machining operation the life of a tool is important since considerable time is lost whenever a tool is replaced or reset. Cutting tools lose its sharpness as usage continues and their effectiveness decreases over time. At some point during the life-span of the tool, it is necessary to replace, index or re-sharpen and reset the tool. Tool life is a measure of the length of time a tool will cut effectively. The life of cutting tool depends upon many factors, such as the microstructure of the material being cut, metal removal rate, the rigidity of the setup and effects of cutting fluid (David and Agapiou, 2000; Krar, 1995) [4]. The

correct choice of cutting velocity can enhance tool life but at the same time, the tool should be used to its maximum capacity.

Design of Hexagonal Turret:

The modelling of turret is made in Solid Works 2018 which is a solid modelling computer-aided design (CAD) and computer-aided engineering (CAE). To minimize the modeling time, preprocessor software that helps to create the geometry required for FEA, such as Solid works could be used [5]. Solid modelling is the only Computer Aided Design (CAD) approach that completely and unambiguously represents the 3D geometry of parts and assemblies. It is therefore, the only type of design tool capable of fully supporting today's widely diverse range of engineering applications, from analysis to manufacture and thus enables concurrent engineering. [6]

Fabrication:

The fabrication of Hexagonal turret is made in different steps

Step 1:

Initially the dimensions of the actual square tool post are taken to get the maximum diameter of the tool post that can be fixed on lathe. Then a rough sketch is drawn to prepare a 3D model using SOLIDWORKS 2018.

Step 2: -

3D modelling and drafting

By using Solid Works and the rough sketch prepared earlier, 2D top view of the turret is drawn and developed into 3D by using Solid Works features like extrude, extrude cut, polar array and chamfer. Then the 3d view and cut section is done by using drawing feature (drafting) as shown in the figure.[7][8]

Step 3: -

TABLE I.
ANALYSIS OF THE TURRET UNDER STATIC CONDITIONS

MESH: FINE Entity	Size
Nodes	3985
Elements	15896

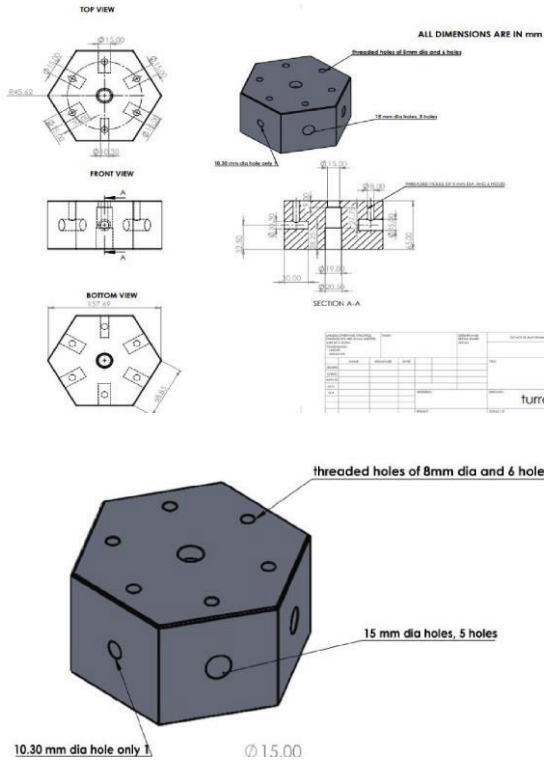


Figure 1. Modelling of turret

The above figure 1 shows modelling of turret using solidworks2018. Meshing was done and the mesh size was kept fine to understand the deformation that takes place at a very small area when the load is applied on the turret. It was fixed and supported at the center stepped holes, and a load of 500N was applied inside the side hole. The material had to withstand the force applied.[9] The result is given below

Result:-

Element Type:

TABLE II.
ELEMENT TYPE

Connectivity	Statistics
TE4	15896 (100.00%)

Element Quality:

T ABLE. III.
ELEMENT QUALITIES

Criterion	Good	Poor
Stretch	15893 (99.98%)	3 (0.02%)
Aspect Ratio	14648 (92.15%)	1241 (7.81%)

Criterion	Bad	Worst	Avg
Stretch	0 (0.00%)	0.270	0.624
Aspect Ratio	7 (0.04%)	5.958	1.916

Material Properties:

TABLE IV.
PROPERTIES OF THE MATERIALS

Material	Mild Steel
Young's modulus	$2e^{+011}$ N-m ²
Poisson's ratio	0.266
Density	7860 kg-m ³
Coefficient of thermal expansion	$1.17e^{-005}$ Kdeg
Yield strength	$2.5e^{+008}$ N-m ²

Static Case Boundary Conditions:

the below figure 2 shows the various boundary conditions of the turret.

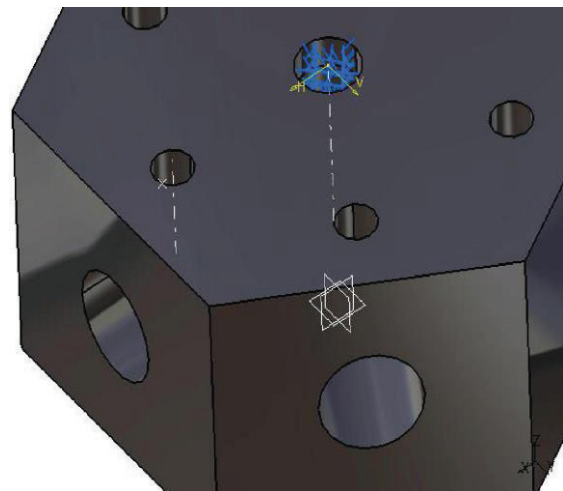


Figure 2. Boundary conditions

Structure Computation:

TABLE V.
STRUCTURE COMPUTATION OF TURRET

Number of nodes	3985
Number of elements	15896
Number of D.O.F.	11955
Number of Contact relations	0
Number of Kinematic relations	0
Linear tetrahedron	15896

Load Computation:

TABLE VI.
APPLIED LOAD RESULTANT

Fx	$-1.000e^{+003}$ N
Fy	$-6.725e^{-021}$ N
Fz	$5.551e^{014}$ N
Mx	$-3.23E^{+001}$ Nm
My	$3.123e^{+001}$ Nm
Mz	$1.435e^{-001}$ Nm

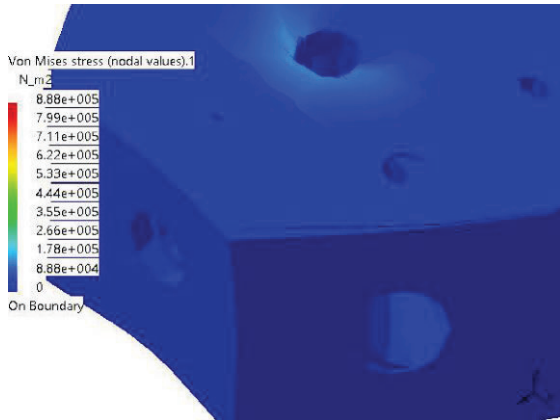


Figure 3. Static case solution vonmises stress

The above figure 3 shows vonmises stress, deformation and the area where the vonmises stress is high. The above chart in the figure shows the maximum stress that can be produced when applying 500N of load is 8, 88000 N/m². The ultimate strength of the mild steel is 350MPa or 350000000 N/m² on comparing the stress developed and ultimate strength we can say that the design is very safe.[10]

Fabrication of Foam Prototype:

As the design is found out to be safe a foam prototype shown in figure 4&5 is made with the help of a 3d model designed in SOLIDWORKS 2018. Machinery like wood cutting band saw and jigsaw are used in making this prototype.

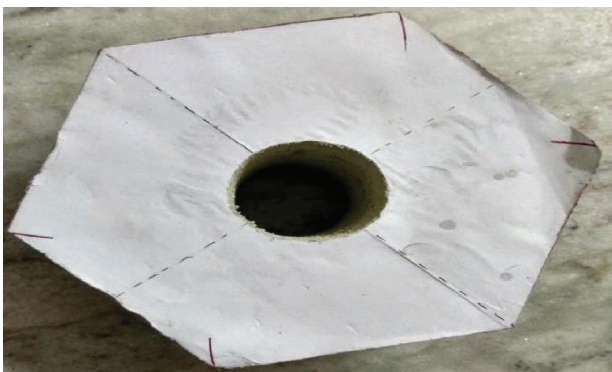


Figure 4 & 5. Prototype of turret made with foam

Step 5:-

Fabrication of Metal Prototype

A Mild steel block is cut with the help of metal cutting band saw according to requirement.[10]
Then the mild steel workpiece is fixed in the lathe chuck, turning and facing operations are performed to remove irregularities if any shown in figure 6.
Dimensions are marked for further operations i.e. milling and drilling.
Milling operation is carried out such that the circular block is shaped into hexagon. To fix the bolts six holes of 8mm diameter are drilled on top portion, five holes of 15mm diameter and one hole of 10.3mm diameter are drilled on each face of the turret for placing the cutting tools. [10][11]
Final output of the tool holder after machining and grinding operations are shown in figure 7,8,9&10 placed at different orientations.



Figure 6. The above figure shows the cutting process of a mild steel block



Figure 7. the above figure shows the block after the turning, facing and boring of MS block in lathe machine

II. EXPERIMENTATION

This is the final stage where the testing of the tool post is done by replacing the square tool post with hexagonal tool post. Testing of the turret is conducted in order to withstand the cutting forces and vibrations. Different machining operations such as turning, forming and drilling are conducted and shown in figures 11,12,13 & 14

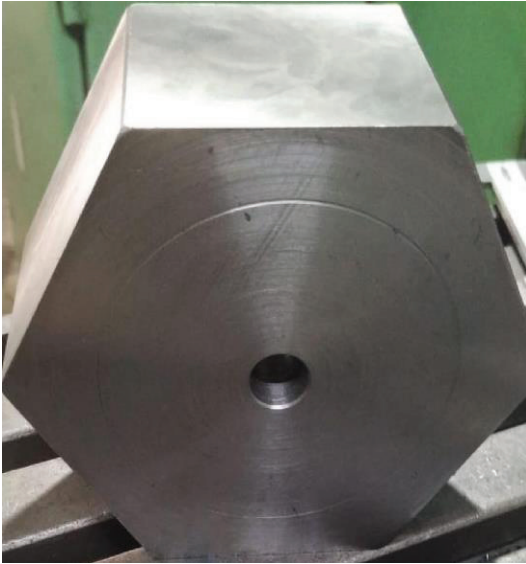


Figure 8. the above figure shows the result after milling.



Figure 11. the above figure show the simple turning operation of a rod of 28mm diameter

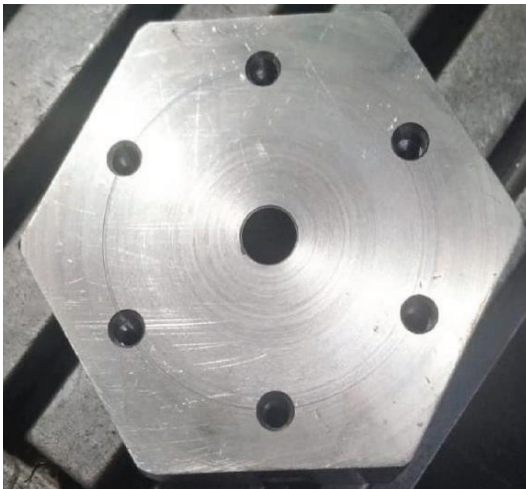


Figure 12 & 13. Forming Operation

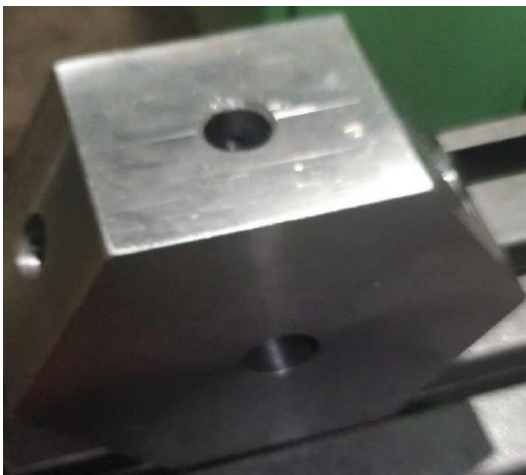


Figure 9 &10. the above figure shows the end product after drilling and tapping operation



Figure 14. turret holding four single point cutting tools, one drill bit of 8mm, one forming tool



Figure 15. the above figure shows the comparison between foam and metal prototype

The above figure 15 shows the final comparison between the foam prototype and metal prototype.

III. CONCLUSIONS

The Hexagonal turret is manufactured and implemented successfully on center lathe machines with six similar and different types of cutting tools and various operations such as turning, facing, taper turning, knurling, thread cutting, and boring operations are performed.

This tool post reduced the time taken for changing of tool (The average time required for replacing the old cutting tool with new and well-grounded is approximately 2 min). Different operations mentioned above are performed on replacing the square tool post with hexagonal tool post.

REFERENCES

- [1] https://en.wikipedia.org/wiki/Lathe#cite_note-1
- [2] Analysis of Single Point Cutting Tool Using ANSYS ISSN: 2321-8169 Volume: 4 Issue: 5 Page 331 – 338
- [3] Finite element analysis of single point cutting tool, Volume: 04 Issue: 09 | Sep -2017, e-ISSN: 2395-0056
- [4] Stress Analysis on Spur Gears Using ANSYS Workbench 16.0, Volume 7–Issue 08,208-213, 2018, ISSN:-2319–7560
- [5] A study on Types of Lathe Machine and Operations: Review, Volume 8 Issue 4 (2020) 286-291, ISSN 2347 – 3258
- [6] The Concept of Solid Modelling in The Plastic Injection Molding Process – Review, ISSN: 2278-0181, Vol. 2 Issue 4, April – 2013
- [7] “*Design Data Book for Machine Elements*,” PSG Tech. Publication.
- [8] “*Design Data for Machine Elements*,” by B. D. Shiwalkar, 2005, Central Techno Publications, Nagpur.
- [9] “*Introduction to Finite Elements in Engineering*,” by Tirupati R. Chandrupatla and Ashok D. Belegundu, 2002. Prentice Hall of India Pvt. Ltd. New Delhi.

- [10] “*A Text Book of Machine Design*,” by R. S. Khurmi & J. K. Gupta, 1997, S. Chand & Company Ltd., New Delhi.
- [11] “*Manufacturing Technology (Volume – II) Metal Cutting & Machine Tools*,” by P. N. Roy, 2008. Tata McGraw Hill Publications, New Delhi.

Synthesis of New Benzothiazole Derivatives as Potential Antimicrobial Agents

Swapna Ponnampalli

Asst. Professor, CVR College of Engineering/ H&S (Chemistry) Department, Hyderabad, India

Email: swapnaponnampalli@gmail.com

Abstract: During the initial efforts to develop novel antibiotics, a new class of benzothiazoles (**3a–n**) were designed and synthesized as potential antibacterial and antimycobacterial agents. Most of the synthesized compounds showed good antibacterial activity against the Gram-positive bacteria tested. The compounds **3i** exhibited excellent *in vitro* activity, with a MIC value of 1 µg/mL against *Mycobacterium tuberculosis* H37Rv. These compounds were also found to have activity against *Candida albicans*, with a MIC value of 4 µg/mL.

Index Terms: Benzothiazole, fused heterocycles, hydrazones, antibacterial, antimycobacterial

I. INTRODUCTION

One of the world's most important public health challenges is antimicrobial resistance [1]. There were an approximate 4.95 million (3.62–6.57) deaths related to bacterial antimicrobial resistance in the year 2019 [2]. *Escherichia coli*, *Staphylococcus aureus*, *Klebsiella pneumoniae*, *Streptococcus pneumoniae*, *Acinetobacter baumannii*, and *Pseudomonas aeruginosa* were major contributors for deaths associated with resistance. The fight against bacterial infection represents one of the high points of modern medicine.

Discovery of antibiotics in the 1940s offered physicians a powerful tool against bacterial infections that has saved the lives of millions of people. Though, because of the widespread and sometimes inappropriate use of antibiotics, strains of bacteria have begun to occur that are antibiotic-resistance [3]. The advent and spread of bacterial resistance pose a major threat to human health across the globe. The number of cases of multi-drug resistant bacterial infections is increasing at an alarming rate. Moreover, the clinicians have become dependent on strong antibiotics such as Vancomycin for serious infections. Therefore, there is an urgent need for the development of novel chemical entities with high safety profiles that are particularly effective against gram-positive pathogens including the resistant strains.

Benzothiazoles are fused heterocycles, which contain a 1,3-thiazole ring that fused to a benzene ring. Since the 1990s, various pharmacological investigations of newly synthesized benzothiazole derivatives demonstrated interesting pharmacological activities and led to the development of new medications for treating human diseases [4,5].

Benzothiazoles comprise a novel class of therapeutic compounds shown to exert a wide range of biological activities such as antimicrobial, anticancer, anthelmintic, antidiabetic, antitubercular, anti-inflammatory, antifungal, antiviral, anti-infective, anti-hypertensive and antipsychotic etc [4-7].

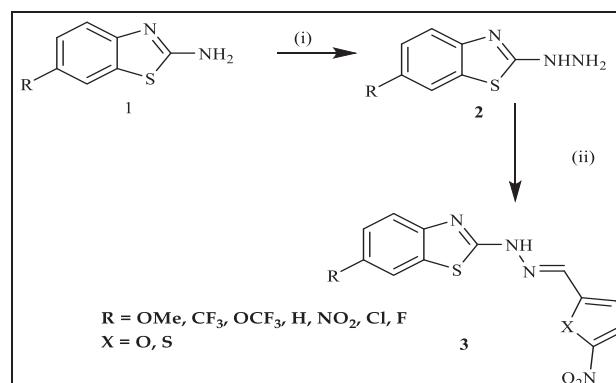
II. CHEMISTRY

As part of antimicrobial research in our laboratory [8-10], a new class of benzothiazoles have been synthesized and evaluated for their biological activity.

Synthesis of Aryl/heterocyclic aldehyde-2-(1,3-benzothiazol-2-yl)hydrazones

The synthesis of benzothiazole hydrazones (**3a–n**) were synthesized by procedure described in Scheme 1. The key intermediates 2-hydrazinobenzothiazoles have been produced by amination of 2-aminobenzothiazole by using hydrazine hydrate. The benzothiazole hydrazines were treated with appropriate aldehydes in presence of acetic acid to afford target benzothiazole hydrazones [11,12]. The details of the structures of **3a–n** were provided in Table 1.

SCHEME I.



Reagents and conditions: (i) Hydrazine hydrate, glycol, 140 °C, 4h; (ii) Aromatic aldehydes, ethanol, cat AcOH, reflux, 2h.

TABLE I.

REPRESENTATIVE COMPOUNDS 3a-m

S.No	Compound	R	X
1	3a	-H	-O
2	3b	-H	-S
3	3c	-OCH ₃	-O
4	3d	-OCH ₃	-S
5	3e	-CF ₃	-O
6	3f	-CF ₃	-S
7	3g	-OCF ₃	-O
8	3h	-OCF ₃	-S
9	3i	-NO ₂	-O
10	3j	-NO ₂	-S
11	3k	-F	-O
12	3l	-F	-S
13	3m	-Cl	-O
14	3n	-Cl	-S

III. BIOLOGICAL ACTIVITY

A. Antibacterial and antifungal activity

Antibacterial activity of compounds **3a-n** were screened for their antibacterial activity against *Staphylococcus aureus*, *Staphylococcus epidermidis*, *Bacillus subtilis*, *Escherichia coli*, *Klebsiella pneumoniae*, and *Pseudomonas aeruginosa* (Table 2) and the antifungal activity was evaluated against yeast *Candida albicans* (MTCC 227). The antimicrobial activities were measured in the inhibitory zones (in mm) and were determined by using agar well method (cup plate method) [13,14]. Antibiotics Streptomycin, Ciprofloxacin and Amphotericin B were used as positive controls against bacteria and fungi respectively. In all determinations, tests were performed in duplicate, and results were reported as the mean of at least three determinations. In Table 2, all compounds exhibited moderate to good antibacterial activity. Compounds **3a-n**

showed significant inhibition against all the bacteria tested. Compounds are more active against gram positive bacteria than gram negative bacteria. Compounds **3b**, **3i**, and **3m** showed good antibacterial activity. In compounds **3a-n**, introduction of thiophen group instead of nitro furan group leads to decrease in the antibacterial activity against gram positive bacteria, this trend reverses in gram negative species. The significant inhibition shown by the compounds **3b**, **3i**, and **3m** might be due to the presence of nitrofurans on the benzothiazole system.

The more active compounds **3i**, and **3m** were further screened for antimicrobial activity in variable concentrations. The antimicrobial activity shown in the zone of inhibition, compound **3m** was found to be the most active compound among the series detailed in Table 3. Compound **3m** exhibited remarkable antibacterial and antifungal activity.

TABLE II.
ANTIBACTERIAL AND ANTIFUNGAL ACTIVITY OF BENZOTHAZOLE ANALOGS (**3a-n**) EXPRESSED IN ZONE OF INHIBITION IN mm

Compounds/Concentrations	<i>Staphylococcus aureus</i>		<i>Staphylococcus epidermidis</i>		<i>Bacillus subtilis</i>		<i>Escherichia coli</i>		<i>Klebsiella pneumoniae</i>		<i>Pseudomonas aeruginosa</i>		<i>Candida albicans</i>	
	50 µg/ml	100 µg/ml	50 µg/ml	100 µg/ml	50 µg/ml	100 µg/ml	50 µg/ml	100 µg/ml	50 µg/ml	100 µg/ml	50 µg/ml	100 µg/ml	50 µg/ml	100 µg/ml
3a	--	13	10	14	--	17	--	12	--	--	--	--	--	23
3b	--	15	15	10	--	14	--	18	--	--	--	--	--	25
3c	--	--	--	12	--	11	--	21	--	15	--	--	--	24
3d	--	--	--	--	--	10	--	25	14	12	14	15	--	20
3e	12	14	17	--	10	15	10	15	--	10	--	17	--	31
3f	--	--	--	--	--	--	09	19	--	10	10	--	--	16
3g	--	14	10	12	10	17	--	21	--	11	--	13	--	28
3h	--	12	--	--	--	13	--	15	--	14	--	12	--	18
3i	1	17	13	23	--	21	--	14	--	10	--	--	--	40
3j	--	--	--	13	--	17	--	16	--	11	--	11	--	--
3k	10	12	10	14	--	17	--	21	--	11	--	12	--	27
3l	--	11	--	--	--	--	--	--	--	--	--	--	11	21
3m	19	26	19	--	17	30	--	34	--	20	--	30	--	30
3n	--	10	--	--	--	15	--	16	--	--	--	--	--	20
STR	22		18		17		21		22		29		--	
CIP	32		35		32		>40		20		30		--	
AT-B	--		--		--		--		--		--		16	

The test were conducted in duplicate and repeated thrice; STP, Streptomycin; CIP, Ciprofloxacin (50 µg/mL); AT-B, Amphotericin (100 units); (--), bacteria are resistant to the compound at the concentrations.

TABLE III.
ANTIBACTERIAL AND ANTI-FUNGAL ACTIVITY OF **3m**, AND **3i** ANALOGS IN DIFFERENT CONCENTRATIONS EXPRESSED IN ZONE OF INHIBITION IN mm

Compounds	3m					3i					CIP	AT-B	Nys
	10	25	50	75	100	10	25	50	75	100			
Concentration in µg/mL	10	25	50	75	100	10	25	50	75	100	50	20	20
<i>Staphylococcus aureus</i>	17	21	24	25	27	9	11	15	17	19	26	NT	NT
<i>Staphylococcus epidermidis</i>	17	22	27	28	29	9	10	12	13	23	34	NT	NT
<i>Bacillus Subtilis</i>	19	22	26	28	28	--	10	14	17	21	32	NT	NT
<i>Escherichia coli</i>	17	21	24	25	27	9	11	15	17	19	38	NT	NT
<i>Pseudomonas aeruginosa</i>	17	22	27	28	29	9	10	12	13		40	NT	NT
<i>Klebsiella pneumoniae</i>	19	22	26	28	28	--	10	14	17	21	21	NT	NT
<i>Candida albicans</i>	NT	18	23	25	28	NT	--	--	--	--	NT	14	--
<i>Aspergillus niger</i>	NT	--	10	24	27	NT	--	--	--	--	NT	23	26
<i>Aspergillus sp</i>	NT	10	10	15	19	NT	--	--	--	--	NT	14	16

The test were performed in duplicate and repeated thrice; CIP, Ciprofloxacin (50 µg/mL); AT-B, Amphotericin (100 units) Nys, Nystatin-I (20 µg/mL); (--), bacteria are resistant to the compound at the concentrations.

TABLE IV.
ANTIMYCOBACTERIAL ACTIVITY OF COMPOUNDS **3a-m** AGAINST *M. TUBERCULOSIS H37Rv* (MIC IN µg/mL)

S. No.	Compound	Molecular Formula	Molecular Weight	CMR (Molar refractivity)	MIC (µg/mL)	C log P (Hydrophobicity)
1	3a	C ₁₂ H ₈ N ₄ O ₃ S	288.28	7.63	>16	3.24
2	3b	C ₁₂ H ₈ N ₄ O ₂ S ₂	304.01	8.23	>16	3.78
3	3c	C ₁₃ H ₁₀ N ₄ O ₄ S	318.31	8.25	>16	3.54
4	3d	C ₁₃ H ₁₀ N ₄ O ₃ S ₂	334.37	8.85	>16	4.07
5	3e	C ₁₃ H ₇ F ₃ N ₄ O ₃ S	356.28	8.14	>16	4.19
6	3f	C ₁₃ H ₇ F ₃ N ₄ O ₂ S ₂	372.35	8.74	>16	4.72
7	3g	C ₁₃ H ₇ F ₃ N ₄ O ₄ S	372.28	8.30	>16	4.65
8	3h	C ₁₃ H ₇ F ₃ N ₄ O ₃ S ₂	388.34	8.89	>16	5.18
9	3i	C ₁₂ H ₇ N ₅ O ₅ S	333.28	8.26	1	3.09
10	3j	C ₁₂ H ₇ N ₅ O ₄ S ₂	349.35	8.84	>16	3.62
11	3k	C ₁₂ H ₇ FN ₄ O ₃ S	306.27	7.65	>16	3.38
12	3l	C ₁₂ H ₇ FN ₄ O ₂ S ₂	322.34	8.24	>16	3.91
13	3m	C ₁₂ H ₇ CIN ₄ O ₃ S	322.73	8.13	>16	3.95
14	3n	C ₁₂ H ₇ CIN ₄ O ₂ S ₂	338.79	8.72	>16	4.48
RMP					0.25	0.5
INH					0.5	-0.7

RMP, Rifampicin; INH, Isoniazid; the Chem Draw Ultra, version 9.0 was used to calculate the values of Molar refractivity and Hydrophobicity of the above compounds.

B. Antimycobacterial activity

All the synthesized compounds were evaluated for the antitubercular activity, and the results are concise in Table 4. The compounds **3a-n** were initially tested against *Mycobacterium tuberculosis H37Rv* at 16 µg/mL as the single concentration. From this screening, the active compounds were selected further to conduct broth microdilution assay to find out Minimum Inhibitory Concentration (MIC) [15,16]. The compounds showing at least 90% inhibition in the initial screen were retested to determine the actual MIC. This has been achieved by serial dilution at lower concentrations against *Mycobacterium tuberculosis H37Rv* using the Nitrate Reductase Assay (NRA). In addition to the NRA reagent to microtiter plate, a change in color to pink indicates the growth of bacteria. The possible lowest concentration of the compound that shows no change in the color relative to controls is defined as MIC. Isoniazid and Rifampicin were used as reference drugs. The compound **3i** has shown good antimycobacterial activity 1 µg/mL (Table 4). Further investigation of other areas of

biological properties of these synthesized compounds (**3a-n**) are going on and the results will be communicated soon.

VI. EXPERIMENTAL DATA

General procedure for the synthesis of heterocyclic aldehyde-2-(1,3-benzothiazol-2-yl)hydrazones (**3a-n**)

2-hydrazeno-benzothiazoles (1 eq) and heterocyclic aldehydes (1 eq) were dissolved in a small amount of ethanol (10 mL). To the above mixture, a catalytic amount of acetic acid was added, and it was stirred for 1 hour. After that period, the reaction has stopped. On filtration, the precipitate was collected washed with cold methanol (3 X 30 mL) followed by cold chloroform (2 X 20 mL). Recrystallization has been done to afford pure respective hydrazones by using hot methanol.

5-Nitrofurane aldehyde-2-(1,3-benzothiazol-2-yl)hydrazone (3a)

The compound **3a** was prepared according to the above-defined method by using 2-hydrazeno-benzothiazole (165 mg, 1 eq) and 5-nitro-2-furancarboxaldehyde (140 mg, 1 eq). Yield: 260 mg (85%).

¹H NMR (DMSO-*d*₆, 200 MHz): δ 6.90 (d, 1H, *J* = 3.7 Hz), 7.22 (d, 1H, *J* = 8.7 Hz), 7.43 (m, 1H, *J* = 2.9, 8.0 Hz), 7.60 (d, 1H), 7.7 (d, 1H, *J* = 3.7 Hz), 7.8 (s, 1H), 7.84 (m, 1H), 12.3 (bs, 1H); ESIMS: *m/z* 289 (M+H)⁺.

5-Nitrothiophene aldehyde-2-(1,3-benzothiazol-2-yl)hydrazone (3b)

The compound **3b** was synthesized as per the above procedure using 2-hydrazino-benzothiazole (165 mg, 1 eq) and 5-nitro-2-thiophenecarboxaldehyde (156 mg, 1 eq). Yield: 256 mg (84 %).

¹H NMR (DMSO-*d*₆, 200 MHz): δ 7.00 (dd, 1H, *J* = 8.0, 2.9 Hz), 7.19-7.15 (m, 3H, *J* = 4.3, 7.1 Hz), 7.35 (d, 1H, *J* = 8.0 Hz), 7.79 (s, 1H), 7.83 (d, 1H, *J* = 4.3 Hz), 12.0 (bs, 1H); ESIMS: *m/z* 305 (M+H)⁺.

5-Nitrofurane aldehyde-2-(6-methoxy-1,3-benzothiazol-2-yl)hydrazone (3c)

The compound **3c** was synthesized as per the above procedure of **3a** using 2-hydrazino-6-methoxy-benzothiazoles (178 mg, 1 eq) and 5-nitro-2-furancarboxaldehyde (140 mg, 1 eq). Yield: 267 mg (89 %).

¹H NMR (DMSO-*d*₆, 200 MHz): δ 3.76 (s, 3H), 6.84 (dd, 1H, *J* = 9.0, 2.25 Hz), 6.96 (d, 1H, *J* = 3.7 Hz), 7.27 (d, 1H, *J* = 2.2 Hz), 7.35 (d, 1H, *J* = 9.0 Hz), 7.58 (d, 1H, *J* = 3.7 Hz), 7.96 (s, 1H), 12.4 (bs, 1H); ESIMS: *m/z* 319 (M+H)⁺.

5-Nitrothiophene aldehyde-2-(6-methoxy-1,3-benzothiazol-2-yl)hydrazone (3d)

The compound **3d** was synthesized as per the above given procedure using 2-hydrazino-6-methoxy-benzothiazoles (165 mg, 1 eq) and 5-Nitro-2-nitrothiophene carboxaldehyde (157 mg, 1 eq). Yield: 281 mg (88 %).

¹H NMR (DMSO-*d*₆, 200 MHz): δ 3.76 (s, 3H), 6.84 (dd, 1H, *J* = 9.0, 2.25 Hz), 7.19 (d, 1H, *J* = 4.7 Hz), 7.27 (d, 1H, *J* = 2.2 Hz), 7.30 (d, 1H, *J* = 9.0 Hz), 7.8 (d, 1H, *J* = 4.7 Hz), 7.96 (s, 1H), 12.4 (bs, 1H); ESIMS: *m/z* 335 (M+H)⁺.

5-Nitrofurane aldehyde-2-(6-trifluoromethyl-1,3-benzothiazol-2-yl)hydrazone (3e)

The compound **3e** was synthesized as per the above given procedure of **3a** using 2-hydrazino-6-trifluoromethyl-benzothiazole (233 mg, 1 eq) and 5-nitrofurane aldehyde (141 mg, 1 eq). Yield: 300 mg (84 %).

¹H NMR (DMSO-*d*₆, 200 MHz): δ 6.9 (d, 1H, *J* = 3.7 Hz), 7.22 (d, 1H, *J* = 8.7 Hz), 7.43 (m, 1H, *J* = 2.9, 8.0 Hz), 7.58 (d, 1H, *J* = 3.7 Hz), 7.60 (d, 1H), 7.84 (m, 1H, *J* = 4.3 Hz), 12.3 (bs, 1H); ESIMS: *m/z* 357 (M+H)⁺.

5-Nitrothiophene aldehyde-2-(6-trifluoromethyl-1,3-benzothiazol-2-yl)hydrazone (3f)

The compound **3f** was synthesized as per the above given procedure of **3a** using 2-hydrazino-6-trifluoromethyl-benzothiazole (233 mg, 1 eq) and 5-nitrothiophene aldehyde (157 mg, 1 eq). Yield: 315 mg (85 %).

¹H NMR (DMSO-*d*₆, 200 MHz): δ 7.19 (d, 1H, *J* = 4.38 Hz), 7.22 (d, 1H, *J* = 8.7 Hz), 7.43 (m, 1H, *J* = 2.9, 8.0 Hz), 7.60 (d, 1H), 7.84-7.82 (m, 2H, *J* = 4.3 Hz), 12.3 (bs, 1H); ESIMS: *m/z* 373 (M+H)⁺.

5-Nitrofurane aldehyde-2-(6-trifluoromethoxy-1,3-benzothiazol-2-yl)hydrazone (3g)

The compound **3g** was synthesized according to the procedure described for **3a** by using 5-nitrofurane aldehyde (141 mg, 1 eq) and 2-hydrazino-6-trifluoromethoxy-benzothiazole (249 mg, 1 eq) (yield 316 mg, 85 %).

¹H NMR (DMSO-*d*₆, 200 MHz): δ 8.42 (bs, 1H), 7.44-7.41 (m, 2H), 7.36 (d, 1H), 7.27 (d, 1H, *J* = 2.4 Hz), 7.30 (d, 1H, *J* = 3.9 Hz), 7.14 (d, 1H, *J* = 8.6 Hz), 6.48 (d, 1H, *J* = 3.9 Hz); ESIMS: *m/z* 373 (M+H)⁺.

5-Nitrothiophene aldehyde-2-(6-trifluoromethoxy-1,3-benzothiazol-2-yl)hydrazone (3h)

The compound **3h** was synthesized according to the procedure described for **3a** by using 5-nitrothiophene aldehyde (157 mg, 1 eq) and 2-hydrazino-6-trifluoromethoxy-benzothiazole (249 mg, 1 eq) (yield 329 mg, 85 %).

¹H NMR (DMSO-*d*₆, 200 MHz): δ 12.7 (bs, 1H), 8.14-8.10 (m, 2H, *J* = 7.7, 4.3 Hz), 7.83 (m, 1H), 7.51 (d, 1H, *J* = 4.5 Hz), 7.35-7.30 (m, 2H), 6.93 (dd, 1H, *J* = 2.4, 8.7 Hz), 3.77 (s, 3H); ESIMS: *m/z* 389 (M+H)⁺.

5-Nitrofurane aldehyde-2-(6-nitro-1,3-benzothiazol-2-yl)hydrazone (3i)

The compound **3i** was synthesized as per the method described for the synthesis of **3a** using 2-hydrazino-6-nitro-benzothiazole (210 mg, 1 eq) and 5-nitrofurane aldehyde (141 mg, 1 eq). Yield: 280 mg (84 %).

¹H NMR (DMSO-*d*₆, 200 MHz): δ 7.15-7.12 (m, 2H, *J* = 2.4, 6.8 Hz), 7.30 (m, 1H, *J* = 7.8 Hz), 7.43 (m, 1H), 7.71 (d, 1H, *J* = 3.9 Hz), 8.10 (s, 1H), 12.7 (bs, 1H); ESIMS: *m/z* 334 (M+H)⁺.

5-Nitrothiophene aldehyde-2-(6-nitro-1,3-benzothiazol-2-yl)hydrazone (3j)

The compound **3j** was synthesized as per the method described for the synthesis of **3a** using 5-nitrothiophene aldehyde (157 mg, 1 eq) and 2-hydrazino-6-nitro-benzothiazole (210 mg, 1 eq). Yield: 300 mg (86 %).

¹H NMR (DMSO-*d*₆, 200 MHz): δ 7.15-7.12 (m, 2H, *J* = 2.4, 6.8 Hz), 7.30 (m, 1H, *J* = 7.8 Hz), 7.43 (m, 1H), 8.15-8.09 (m, 2H, *J* = 4.7 Hz), 12.0 (bs, 1H); ESIMS: *m/z* 350 (M)⁺.

5-Nitrofurane aldehyde-2-(6-fluoro-1,3-benzothiazol-2-yl)hydrazone (3k)

The compound **3k** was synthesized as per the method described for the synthesis of **3a** using 2-hydrazino-6-fluoro-benzothiazole (183 mg, 1 eq) and 5-nitrofurane aldehyde (140 mg, 1 eq). Yield: 260 mg (86 %).

¹H NMR (DMSO-*d*₆, 200 MHz): δ 6.84 (dd, 1H, *J* = 9.0, 2.2 Hz), 6.96 (d, 1H, *J* = 3.7 Hz), 7.27 (d, 1H, *J* = 2.2 Hz), 7.35 (d, 1H, *J* = 9.0 Hz), 7.58 (d, 1H, *J* = 3.7 Hz), 7.96 (s, 1H), 12.4 (bs, 1H); ESIMS: *m/z* 307 (M)⁺.

5-Nitrothiophen aldehyde-2-(6-fluoro-1,3-benzothiazole-2-yl)hydrazone (3l)

The compound **3l** was synthesized according to the method given for the synthesis of **3a** using 2-hydrazino-6-fluoro-benzothiazole (183 mg, 1 eq) and 5-nitrothiophen aldehyde (157 mg, 1 eq). Yield: 260 mg (80 %).

¹H NMR (DMSO-*d*₆, 200 MHz): δ 7.18 (d, 1H, *J* = 4.3 Hz), 7.21 (d, 1H, *J* = 8.7 Hz), 7.59 (d, 1H), 7.43 (m, 1H, *J* = 2.9, 8.0 Hz), 7.82-7.84 (m, 2H, *J* = 4.3 Hz), 12.3 (bs, 1H); ESIMS: *m/z* 323 (M+H)⁺.

5-nitro-2-furaldehyde-2-(6-chloro-1,3-benzothiazole 2-yl)hydrazone (3m)

The compound **3m** was synthesized according to the method given for the synthesis of **3a** using 2-hydrazino-6-chloro-benzothiazole (199 mg, 1 eq) and 5-nitrothiophen aldehyde (140 mg, 1 eq). Yield: 261 mg (84 %).

¹H NMR (DMSO-*d*₆, 200 MHz): δ 6.85 (dd, 1H, *J* = 9.1, 2.3 Hz) 6.97 (d, 1H, *J* = 3.6 Hz), 7.27 (d, 1H, *J* = 2.3 Hz), 7.34 (d, 1H, *J* = 9.1 Hz), 7.60 (d, 1H, *J* = 3.6 Hz), 7.88-7.90 (s, 1H), 12.4 (bs, 1H); ESIMS: *m/z* 323 (M)⁺.

5-Nitrothiophen aldehyde-2-(6-chloro-1,3-benzothiazol-2yl)hydrazone (3n)

The compound **3n** was synthesized according to the method given for the synthesis of **3a** using 2-hydrazino-6-chloro-benzothiazole (199 mg, 1 eq) and 5-nitrothiophen aldehyde (157 mg, 1 eq). Yield: 287 mg (85 %).

¹H NMR (DMSO-*d*₆, 200 MHz): δ 7.19 (d, 1H, *J* = 4.3 Hz), 7.22 (d, 1H, *J* = 8.7 Hz), 7.43 (m, 1H, *J* = 2.9, 8.0 Hz), 7.60 (d, 1H), 7.84-7.82 (m, 2H, *J* = 4.3 Hz), 12.3 (bs, 1H); ESIMS: *m/z* 339 (M+H)⁺.

V. CONCLUSIONS

Herein, demonstrate the synthesis and antimicrobial potency of a new class of benzothiazoles against Gram-positive, Gram-negative and *Mycobacterium tuberculosis* bacteria. Amongst the synthesized compounds, **3b** and **3m** have shown potent *in vitro* antibacterial activity. Interestingly, these compounds have also exhibited good antibacterial activity against resistant strains of Gram-positive and Gram-negative. The compound **3i** has shown potent antimycobacterial activity against *Mycobacterium tuberculosis H37Rv*. Further investigations of these new classes of compounds for their potential biological properties are under process.

REFERENCES

- [1] F. Prestinaci, P. Pezzotti, and A. Pantosti, "Antimicrobial resistance: a global multifaceted phenomenon". *Pathog Glob Health*, vol. 109, pp. 309–318, 2015.
- [2] C. J. L. Murray et al. "Global burden of bacterial antimicrobial resistance in 2019: a systematic analysis" *Lancet*, vol. 399, pp. 629–655, January 2022.
- [3] R. I. Aminov, "A brief history of the antibiotic era: lessons learned and challenges for the future", *Front Microbiol*, vol. 1, pp. 134, December 2010.
- [4] A. Kamal, M. A. Syed, and S. M. Mohammed, "Therapeutic potential of benzothiazoles: a patent review (2010-2014)", *Expert Opin. Ther. Pat.*, vol. 25, pp. 335–349.
- [5] P. C. Sharma, A. Sinhmar, A. Sharma, Harish, Rajak and D. P. Pathak, "Medicinal significance of benzothiazole scaffold: an insight view", *Journal of Enzyme Inhibition and Medicinal Chemistry*, vol. 28, pp. 240–266, 2013.
- [6] Y. I. Asiria, A. Alsayari, A. B. Muhsinah, Y. N. Mabkhot and M. Z. Hassan, "Benzothiazoles as potential antiviral agents", *Journal of Pharmacy and Pharmacology*, vol. 72, pp. 1459–1480, 2020.
- [7] R. Ali and N. Siddiqui, "Biological Aspects of Emerging Benzothiazoles: A Short Review" vol. 2013, Article ID 345198, pp. 12, June 2013.
- [8] A. Kamal, P. Swapna, R. V. C. R. N. C. Shetti, A. B. Shaik, M. P. N. Rao, F. Sultana, I. A. Khan, S. Sharma, N. P. Kalia, S. Kumar and B. Chandrakant, "Anti-tubercular agents. Part 7: A new class of diarylpyrrole-oxazolidinone conjugates as antimycobacterial agents", *European Journal of Medicinal Chemistry*, vol. 64, pp. 239-251, 2013.
- [9] A. Kamal, P. Swapna, R. V. C. R. N. C. Shetti, A. B. Shaik, M. P. N. Rao, S. Gupta; Synthesis, biological evaluation of new oxazolidino-sulfonamides as potential antimicrobial agents, *European Journal of Medicinal Chemistry*, vol. 62, 661 2013.
- [10] A. Kamal, S. K. Ahmed, K. S. Reddy, M. N. A. Khan, R. V. C. R. N. C. Shetty, B. Siddhardha, U. S. N. Murty, A. China, and V. Nagaraja, "Synthesis and Biological Evaluation of a New Series of Benzothiazole-Benzothiadiazine Conjugates as Antibacterial Agents", *Letters in Drug Design & Discovery*, 4, 550-556, 2007.
- [11] A. Kamal, R. V. C. R. N. C. Shetti, P. Swapna, S. Azeeza, A. M. Reddy, I. A. Khan, S. T. Abdullah, S. Sharma, and N. T. Kalia, "Synthesis of new benzothiazole derivatives as potential anti-tubercular agents", US2012095021 (A1), April 2012.
- [12] A. Kamal, R. V. C. R. N. C. Shetti, P. Swapna, S. Azeeza, A. M. Reddy, I. A. Khan, S. T. Abdullah, S. Sharma, and N. T. Kalia, "Synthesis of new benzothiazole derivatives as potential anti-tubercular agents", US 2016/0175303 A1, June 2016.
- [13] Villanova, 1982. National Committee for Clinical Laboratory Standards (NCCLS), Standard methods for dilution antimicrobial susceptibility tests for bacteria, which grows aerobically, p. 242.
- [14] National Committee for Clinical Laboratory Standards (NCCLS), Standard methods for dilution antimicrobial susceptibility tests for bacteria, which grows aerobically; approved standard-5th edition. Approved standard NCCLS document M7-A5. NCCLS: Wayne, PA, 2003.
- [15] F. Dornbiewski, "Antimicrobial susceptibility testing of *Mycobacterium tuberculosis*", *Eucast discussion document E.DIS 8.1 DECEMBER 2001*. vol. 8, ISSUE 10, P1-10, October 01, 2002.
- [16] K. S. Goh, and N. Rastogi "Simple and rapid method for detection of nitrate reductase activity of *Mycobacterium tuberculosis* and *Mycobacterium canettii* grown in the Bactec MGIT960 system", *J Microbiol Methods*, vol. 81, pp. 208-210, May 2010.

In the next issue (Vol. 24, June 2023)

- 1. Extensive Content Feature Based Image Classification and Retrieval using SVM* *Dr. A. Srinivasa Reddy*
- 2. Student Location Reporting System using Arduino Uno* *Mr. G. Naga Sai Manoj*
Dr. Rameshwar Rao
- 3. Design and ASIC Implementation of Modified Shift-and-Add Algorithm using Redundant Arithmetic Integrator Adder and Subtractor* *Mrs. T. Subha Sri Lakshmi*

Template for the Preparation of Papers for Publication in CVR Journal of Science and Technology

First A. Author¹ and Second B. Author²

¹Designation, Name of Institution/Department, City, Country
Email: first.author@hostname1.org

²Designation, Name of Institution/Department, City, Country
Email: second.author@hostname2.org

Abstract: These instructions give you basic guidelines for preparing camera-ready papers for CVR College journal Publications. Your cooperation in this matter will help in producing a high-quality journal.

Index Terms: first term, second term, third term, fourth term, fifth term, sixth term

I. INTRODUCTION

Your goal is to simulate the usual appearance of papers in a Journal Publication of the CVR College. We are requesting that you follow these guidelines as closely as possible. It should be original work. Format must be done as per the template specified. Diagrams with good clarity with relevant reference within the text are to be given. References are to be cited within the body of the paper. Number of pages must not be less than five with minimum number of 4000 words and not exceeding eight pages. The journal is published in colour. Colours used for headings, subheadings and other captions must be strictly as per the template given in colour.

A. Full-Sized Camera-Ready (CR) Copy

Prepare your CR paper in full-size format, on A4 paper (210 x 297 mm or 8.27 x 11.69 in). No header or footer, no page number.

Type sizes and typefaces: Follow the type sizes specified in Table I. As an aid in gauging type size, 1 point is about 0.35 mm. The size of the lowercase letter “j” will give the point size. Times New Roman has to be the font for main text. Paper should be single spaced.

Margins: Top and Bottom = 24.9mm (0.98 in), Left and Right = 16 mm (0.63 in). The column width is 86mm (3.39 in). The space between the two columns is 6mm (0.24 in). Paragraph indentation is 3.7 mm (0.15 in).

Left- and right-justify your columns. Use tables and figures to adjust column length. On the last page of your paper, adjust the lengths of the columns so that they are equal. Use automatic hyphenation and check spelling. Digitize or paste down figures.

For the Title use 24-point Times New Roman font, an initial capital letter for each word. Its paragraph description should be set so that the line spacing is single with 6-point spacing before and 6-point spacing after. Use two additional line spacings of 10 points before the beginning of the double column section, as shown above.

TABLE I.
TYPE SIZES FOR CAMERA-READY PAPERS

Type size (pts.)	Appearance		
	Regular	Bold	Italic
6	Table caption, table superscripts		
8	Tables, table names, first letters in table captions, figure captions, footnotes, text subscripts, and superscripts		
9	References, authors' biographies	Abstract	
10	Section titles, Authors' affiliations, main text, equations, first letters in section titles		Subheading
11	Authors' names		
24	Paper title		

Each major section begins with a Heading in 10 point Times New Roman font centered within the column and numbered using Roman numerals (except for REFERENCES), followed by a period, two spaces, and the title using an initial capital letter for each word. The remaining letters are in SMALL CAPITALS (8 point). The paragraph description of the section heading line should be set for 12 points before and 6 points after.

Subheadings should be 10 point, italic, left justified, and numbered with letters (A, B, ...), followed by a period, two spaces, and the title using an initial capital letter for each word. The paragraph description of the subheading line should be set for 6 points before and 3 points after.

For main text, paragraph spacing should be single spaced, no space between paragraphs. Paragraph indentation should be 3.7mm/0.21in, but no indentation for abstract & index terms.

II. HELPFUL HINTS

A. Figures And Tables

Position figures and tables at the tops and bottoms of columns. Avoid placing them in the middle of columns. Large figures and tables may span across both columns. Leave sufficient room between the figures/tables and the main text. Figure captions should be centered below the figures; table captions should be centered above. Avoid placing figures and tables before their first mention in the

text. Use the abbreviation “Fig. 1,” even at the beginning of a sentence.

To figure axis labels, use words rather than symbols. Do not label axes only with units. Do not label axes with a ratio

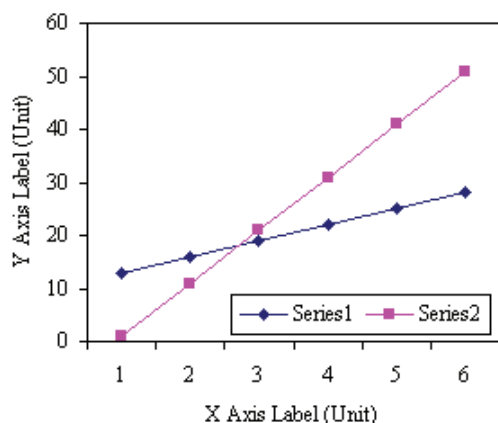


Figure 2. Note how the caption is centered in the column.

of quantities and units. Figure labels should be legible, about 8-point type.

All figures, tables and references must be cited in the text.

Please indicate the broad area/specializations into which the research paper falls, in the covering letter/mail to the Editor, so that reviewers with those specializations may be identified.

B. References

Number citations consecutively in square brackets [1]. Punctuation follows the bracket [2]. Use “Ref. [3]” or “Reference [3]” at the beginning of a sentence:

Give all authors’ names; use “et al.” if there are six authors or more. Papers that have not been published, even if they have been submitted for publication, should be cited as “unpublished” [4]. Papers that have been accepted for publication should be cited as “in press” [5]. In a paper title, capitalize the first word and all other words except for conjunctions, prepositions less than seven letters, and prepositional phrases. Good number of references must be given.

Latest references in the area must be included and every refence must be cited in the text of the research article.

C. Footnotes

Number footnotes separately in superscripts ^{1, 2, ...}. Place the actual footnote at the bottom of the column in which it was cited, as in this column. See first page footnote as an example.

D. Abbreviations and Acronyms

Define abbreviations and acronyms the first time they are used in the text, even after they have been defined in the

abstract. Do not use abbreviations in the title unless they are unavoidable.

E. Equations

Equations should be left justified in the column. The paragraph description of the line containing the equation should be set for 6 points before and 6 points after. Number equations consecutively with equation numbers in parentheses flush with the right margin, as in (1). Italicize Roman symbols for quantities and variables, but not Greek symbols. Punctuate equations with commas or periods when they are part of a sentence, as in

$$a + b = c . \tag{1}$$

Symbols in your equation should be defined before the equation appears or immediately following. Use “(1),” not “Eq. (1)” or “equation (1),” except at the beginning of a sentence: “Equation (1) is ...”

F. Other Recommendations

Use either SI (MKS) or CGS as primary units. (SI units are encouraged.) If your native language is not English, try to get a native English-speaking colleague to proofread your paper. Do not add page numbers.

III. CONCLUSIONS

The authors can conclude on the topic discussed and proposed, future enhancement of research work can also be briefed here.

REFERENCES

- [1] G. Eason, B. Noble, and I. N. Sneddon, “On certain integrals of Lipschitz-Hankel type involving products of Bessel functions,” *Phil. Trans. Roy. Soc. London*, vol. A247, pp. 529–551, April 1955.
- [2] J. Clerk Maxwell, *A Treatise on Electricity and Magnetism*, 3rd ed., vol. 2. Oxford: Clarendon, 1892, pp.68–73.
- [3] I. S. Jacobs and C. P. Bean, “Fine particles, thin films and exchange anisotropy,” in *Magnetism*, vol. III, G. T. Rado and H. Suhl, Eds. New York: Academic, 1963, pp. 271–350.
- [4] K. Elissa, “Title of paper if known,” unpublished.
- [5] R. Nicole, “Title of paper with only first word capitalized”, *J. Name Stand. Abbrev.*, in press.
- [6] Y. Yorozu, M. Hirano, K. Oka, and Y. Tagawa, “Electron spectroscopy studies on magneto-optical media and plastic substrate interface,” *IEEE Transl. J. Magn. Japan*, vol. 2, pp. 740–741, August 1987 [Digests 9th Annual Conf. Magnetism Japan, p. 301, 1982].
- [7] M. Young, *The Technical Writer's Handbook*. Mill Valley, CA: University Science, 1989.
- [8] T. Ali, B.K. Subhash and R.C. Biradar, “A Miniaturized Decagonal Sierpinski UWB Fractal Antenna”, *PIERS C*, vol. 84, pp. 161-174, 2018.

ABOUT THE COLLEGE

CVR College of Engineering, an autonomous institution under the UGC, was established in the Year 2001, the first college in Telangana to be promoted by NRI technology professionals resident in the USA. The NRI promoters are associated with cutting-edge technologies of the computer and electronics industry. They also have strong associations with other leading NRI professionals working for world-renowned companies like IBM, Intel, Cisco, Facebook, AT & T, Google, and Apple who have agreed to associate with the College with a vision and passion to make the College a state-of-the-art engineering institution.

All B. Tech Programmes are accredited three or four times by the NBA since 2007. As of now, all 7 eligible B. Tech Programmes are accredited. NAAC reaccredited the college for five years with grade A with effect from 2022.

As formulated by the IQAC, many FDPs are organized by departments. College has MoUs with organizations such as Virtusa, Mitsubishi, NRSC, COMSAT, CADENCE, IIIT. Under innovation activities faculty have published 32 patents so far. Projects from NRSC under the RESPOND programme of ISRO, AICTE-RPS, TEQIP-III from JNTU, MODROBS-AICTE worth Rs.71 Lakhs are some of the recent projects funded by central agencies. Total funds received are Rs. 160 lakhs. Newgen IEDC of Government of India (DST) has sanctioned Rs.287 Lakhs for a period for five years in 2018-19, for Innovative Entrepreneurship Development Programmes by students and staff. 10 Projects were completed in 2019-20, 16 in 2020-21, 20 in 2021-22. An exclusive Innovation Centre of 5000 Sqft. has been created for practical work and counseling.

The AICTE sanctioned Rs. 2 lakhs to students and faculty of CE and ME for a study tour of ATAL tunnel and Rs. 1 lakh towards activities under Scheme for Promoting Interests, Creativity and Ethics among Students (SPICES).

The college has been creating records year after year. With more than 100 companies visiting CVRCE and 1600+ placements for the 2022 - 2023 academic year, it is the highest among the peer group of colleges. The highest offer is **47 Lakhs** at Microsoft and next being **44 Lakhs** by 3 students at AMAZON and several students received offers higher than **Rs. 25 Lakhs**. More than **75 students** received offers higher than **Rs. 10 Lakhs**. About **300 offers** are higher than **Rs. 7 Lakhs** (a record). With this, CVRCE becomes one of the leading colleges in the state in terms of offers with higher salaries. The placement percentage continues to be 100% since 5 years. The college has made huge progress in a short span of time and is preferred by the students and parents during the EAMCET counseling this year and is among the **top 3 colleges** in the state.

In keeping with the current global emphasis on green and eco-friendly energy generation, 360KW Solar PV plant has been installed on the campus to meet the power requirements of the college to a significant extent.

CALL FOR PAPERS:

Papers in Engineering, Science and Management disciplines are invited for Publication in our Journal. Authors are requested to mail their contributions to Editor, CVR Journal of Science and Technology (Email Id: journal@cvr.ac.in). Authors can also submit their papers through our online open journal system (OJS) www.ojs.cvr.ac.in or www.cvr.ac.in/ojs. Papers are to be written using a Standard Template, which may be obtained on request from the Editor. It is also available on the college website www.cvr.ac.in



CVR JOURNAL OF SCIENCE AND TECHNOLOGY



CVR COLLEGE OF ENGINEERING

(UGC Autonomous- Affiliated to JNTU Hyderabad)

Mangalpalli (V), Ibrahimpatnam (M),

R.R. District, Telangana - 501510

<http://cvr.ac.in>